

AD \_\_\_\_\_

AWARD NUMBER DAMD17-94-J-4444

TITLE: Spatial Distribution of the EGF Receptor in Regulation of Breast Epithelial Cell Growth and Organization

PRINCIPAL INVESTIGATOR: H. Steven Wiley

CONTRACTING ORGANIZATION: University of Utah  
Salt Lake City, Utah 84132

REPORT DATE: December 1998

TYPE OF REPORT: Final

PREPARED FOR: U.S. Army Medical Research and Materiel Command  
Fort Detrick, Maryland 21702-5012

DISTRIBUTION STATEMENT: Approved for public release;  
distribution unlimited

The views, opinions and/or findings contained in this report are those of the author(s) and should not be construed as an official Department of the Army position, policy or decision unless so designated by other documentation.

19990901 032

REPORT DOCUMENTATION PAGE			Form Approved OMB No. 0704-0188	
<small>Public reporting burden for this collection of information is estimated to average 1 hour per response, including the time for reviewing instructions, searching existing data sources, gathering and maintaining the data needed, and completing and reviewing the collection of information. Send comments regarding this burden estimate or any other aspect of this collection of information, including suggestions for reducing this burden, to Washington Headquarters Service, Directorate for Information Operations and Reports, 1215 Jefferson Davis Highway, Suite 1204, Arlington, VA 22202-4302, and to the Office of Management and Budget, Paperwork Reduction Project (0704-0188), Washington, DC 20503.</small>				
1. AGENCY USE ONLY (Leave blank)	2. REPORT DATE December 1998	3. REPORT TYPE AND DATES COVERED Final (1 Sep 94 - 1 Sep 98)		
4. TITLE AND SUBTITLE Spatial Distribution of the EGF Receptor in Regulation of Breast Epithelial Cell Growth and Organization		5. FUNDING NUMBERS DAMD17-94-J-4444		
6. AUTHOR(S)  H. Steven Wiley				
7. PERFORMING ORGANIZATION NAME(S) AND ADDRESS(ES) University of Utah Salt Lake City, Utah 84102		8. PERFORMING ORGANIZATION REPORT NUMBER		
9. SPONSORING/MONITORING AGENCY NAME(S) AND ADDRESS(ES) U.S. Army Medical Research and Materiel Command Fort Detrick, Frederick, MD 21702-5012		10. SPONSORING/MONITORING AGENCY REPORT NUMBER		
11. SUPPLEMENTARY NOTES				
12a. DISTRIBUTION / AVAILABILITY STATEMENT  Approved for public release; distribution unlimited		12b. DISTRIBUTION CODE		
13. ABSTRACT (Maximum 200 words)  The epidermal growth factor receptor (EGFR) system is particularly important in the growth and development of mammary epithelial cells. Disruption in normal EGFR signaling is frequently observed in breast cancers. We tested the hypothesis that EGFR and its ligands must be in the correct cellular location to initiate correct signaling. We tested this by altering the EGFR and its cognate ligand using techniques of molecular biology. The altered genes were then expressed in noncancerous cells to see how they affected cell behavior. We made several significant findings. First, we found that the EGF-R system acts as "cell sonar" in telling the cells about their environment. <u>Where</u> a receptor is triggered specifies the signals that are transmitted. Receptors in the wrong place transmit wrong signals. Second, normal cells can apparently determine when their receptors are defective and can stop growing as a result. Because defective receptors are commonly found in cancer, the normal "proofreading" functions of cells probably becomes inactivated in cancer. Our finding are important because they suggest several novel sensing mechanisms that are probably defective in cancer cells. In addition, by preventing ligand release one can prevent EGFR-mediated cell growth.				
14. SUBJECT TERMS EGF Receptors, Polarity, Growth Factors, Epithelium, Differentiation, Membranes, Sorting, TGF-Alpha		15. NUMBER OF PAGES 144		
		16. PRICE CODE		
17. SECURITY CLASSIFICATION OF REPORT Unclassified	18. SECURITY CLASSIFICATION OF THIS PAGE Unclassified	19. SECURITY CLASSIFICATION OF ABSTRACT Unclassified	20. LIMITATION OF ABSTRACT Unlimited	

NSN 7540-01-280-5500

Standard Form 298 (Rev. 2-89)  
Prescribed by ANSI Std. Z39-18  
298-102

FOREWORD

Opinions, interpretations, conclusions and recommendations are those of the author and are not necessarily endorsed by the U.S. Army.

*HW* Where copyrighted material is quoted, permission has been obtained to use such material.

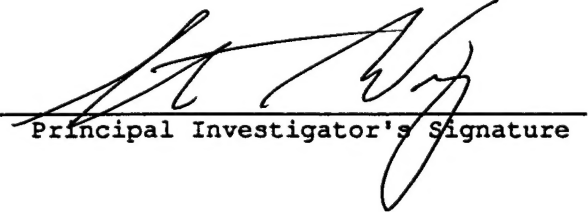
*HW* Where material from documents designated for limited distribution is quoted, permission has been obtained to use the material.

*HW* Citations of commercial organizations and trade names in this report do not constitute an official Department of the Army endorsement or approval of the products or services of these organizations.

*NA HW* In conducting research using animals, the investigator(s) adhered to the "Guide for the Care and Use of Laboratory Animals," prepared by the Committee on Care and Use of Laboratory Animals of the Institute of Laboratory Animal Resources, National Research Council (NIH Publication No. 86-23, Revised 1985).

*NA HW* For the protection of human subjects, the investigator(s) have adhered to policies of applicable Federal Law 32 CFR 219 and 45 CFR 46.

*HW* In conducting research utilizing recombinant DNA technology, the investigator(s) adhered to current guidelines promulgated by the National Institutes of Health.

  
Principal Investigator's Signature

12/1/98  
Date

## TABLE OF CONTENTS

Foreword.....	3
Introduction.....	5
Body .....	8
Conclusions .....	55
Figure Legends.....	57
References .....	67
Figures.....	80
List of Publications.....	143
Personnel.....	144



## INTRODUCTION

An important goal of current breast cancer research is to develop an in vitro system that can define the mechanisms involved in the progression of human mammary epithelial cells (HMEC) towards a transformed phenotype. In this project, we have focused on an aspect of HMEC behavior that is likely to be involved in this progression, namely, the correct spatial sorting of growth factors and their receptors to discrete cellular locations. We chose this research focus for two important reasons: 1) recent evidence indicates that defects in receptor/ligand trafficking is hallmark of proliferative disorders in epithelial cells (1,2), and 2) since receptor trafficking is primarily a negative regulatory process defects in this pathway are likely to amplify receptor signaling (3,4). Because correct receptor trafficking depends on the function of many intracellular regulatory systems, it provides a sensitive readout of their status. The EGF receptor system is used as the primary experimental model because it plays a central role in the growth, motility and proliferation of normal HMEC as well as many breast cancers (5-8). Therefore any significant alterations in growth factor regulation in HMEC is likely to perturb the EGF receptor system.

The functions of growth factors extend far beyond simple growth regulation. They are involved in cell differentiation, chemotaxis, morphogenesis, wound healing and gastric acid secretion (9). Originally, growth factors were thought to be products secreted by cells, but in fact, many are produced as membrane-associated precursors. For example, EGF is initially produced as a 170 kDa membrane protein (10) and transforming growth factor alpha (TGF- $\alpha$ ) is produced as a 20-22 kDa MW precursor (11). In the case of TGF- $\alpha$ , release from the cell surface occurs through regulated proteolysis (12). The multiple levels at which availability of growth factors can be regulated provide many opportunities for fine control of tissue functions.

Three main routes of growth factor signaling are currently recognized: autocrine, paracrine and juxtacrine (13). In autocrine signaling, cells make both the growth factor and the complementary receptors. In general, the factors must be transported to the cell surface to be functional. In paracrine signaling, different cells make the ligand and receptors. The factor must be transported from the site of production to the site of binding, usually by diffusion. Finally, juxtacrine signaling occurs when receptors on one cell bind directly to the membrane-associated ligand on another cell. All of these types of signaling can be regulated by controlled synthesis, rate of ligand release, and by competition for ligand capture either between different cells or by extracellular matrix proteins (13). Growth factor signaling is also regulated by the physical separation of the ligand and receptor at the cell surface or within the endocytic pathway. This spatial regulation is mediated by sorting components which bind to receptor cytoplasmic domains (14). Growth factors may also be synthesized initially as transmembrane proteins, presumably allowing cells to physically segregate them from receptors.

Epithelial cells display a high degree of spatial organization as evidenced by their polarized phenotype. Kidney, breast and intestinal epithelial cells all show similar features; all are associated through tight junctions and have distinct basolateral and apical surfaces (15). In-vivo, breast epithelium is organized into ducts, ductules and alveoli consisting of a basement membrane, a discontinuous layer of myoepithelial cells, a layer of basal epithelial cells and a layer of luminal cells (16). Both basal and luminal cells display a polarized distribution of integrins and EGFR (17-19). Integrins mediate interactions with the basement membrane and appear essential for controlling specific gene expression and maintaining polarization and differentiated functions (20,21). EGFR are important in regulating epithelial cell growth, and in the breast, are expressed at high levels in myoepithelial cells, basal cells and at the basolateral surface of luminal epithelial cells (19). The functional significance of the basolateral

distribution of these receptors is not understood, but could be involved in maintaining the correct organization of epithelial cells within tissues.

Three ligands are thought to be produced in mature breast alveoli which can bind to the EGFR: EGF, TGF- $\alpha$  and amphiregulin (5,22,23). The best studied of these, TGF- $\alpha$ , is produced by epithelial cells and at least in the mouse, is localized at their basolateral surface (24). Because the basolateral surface contains the EGFR, the space between this surface and the basement membrane comprises the "microenvironment" in which signaling through the EGFR occurs. Although EGF is found at high concentrations in the ductal lumen of both mouse and human, little TGF- $\alpha$  is found in breast milk or nipple aspirates of humans (approximately 0.8 ng/ml and 5 ng/ml respectively), indicating a polarized secretion of EGF to the apical surface and TGF- $\alpha$  to the basolateral surface of luminal cells (25). Nothing is known regarding the distribution of amphiregulin in HMEC, but in intestinal cells it displays a luminal distribution (26). Significantly, an extremely high concentration of EGF is found in breast fluids of non-lactating (>200ng/ml) or lactating (100-140 ng/ml) women (25). These concentrations are 2 orders of magnitude higher than the  $K_d$  of the EGFR in HMEC. Therefore, the polarized organization of HMEC segregates their EGFR from a large reservoir of active hormone.

Ligand activation of EGFR leads to heterodimer formation between EGFR and erbB-2, which is thought to result in activation of erbB-2 by transphosphorylation (27,28). Transactivation of erbB-2 also occurs upon the addition of heregulin, a ligand for erbB-3 and erbB-4 (29-32). As observed for EGF, heregulin induces the formation of heterodimers between erbB-3 or erbB-4 with erbB-2, resulting in erbB-2 becoming tyrosine phosphorylated (30,33-36). There is also evidence to suggest that EGFR interacts with erbB-3 and erbB-4 (37). Thus, activation of any member of the EGFR family results in signaling through multiple receptor types. Understanding how these receptors interact with each other is therefore essential to knowing how they work.

The pattern of tyrosine phosphorylation of EGFR and erbB-2 is important in signal transduction. Specific phosphorylated tyrosines residues serve as docking sites for proteins containing SH2 domains, such as the PI3 kinase p85 subunit and GRB2 (38). The assembly of signaling complexes dictates the subsequent pattern of signal transduction. Intracellular trafficking of the activated EGFR also regulates receptor activity by controlling the availability of substrates and signaling partners (39). Although ligand binding induces rapid internalization and subsequent lysosomal targeting of EGFR, it is uncertain whether erbB-2 trafficking is influenced by the EGFR. It has been suggested that all members of the erbB family are "internalization defective" except for the EGFR (40), but those studies were done by direct activation of erbB family members or by using chimeric receptors. It has been reported that EGF treatment can stimulate the degradation of erbB-2 in some epithelial cells, but the mechanism of this transmodulation is unclear (41). If EGFR activation does alter the trafficking of erbB-2, this could be an important mechanism for regulating both the activity and distribution of these signaling molecules in cells. However, the degree of spatial overlap between the members of the EGFR family in mammary epithelial cells is unknown.

The correct distribution of the EGFR within a cell is also very important in regulating signal transduction. Receptors that are mutated to remove sequences that specify receptor internalization can be transforming (4). This is presumably due to an inability to down regulate and thus attenuate signaling from the mutant receptor. However, these mutant receptors may also have access to inappropriate substrates which may contribute to the transformed phenotype.

A great many studies have investigated the relationship between EGFR and breast cancer (8,19,42,43). In general, overexpression of the EGFR in breast tumors indicates poor prognosis,

but other members of the EGFR family, such as erbB-2, also appear to be linked to breast cancer (8). The incidence of overexpression of the EGFR is more common than overexpression of erbB-2 (45% versus 20% respectively; (8)). Significantly, less than 20% of the tumors that display overexpression of the EGFR also show amplification of the EGFR gene, whereas all incidents of erbB-2 overexpression appear to be due to gene amplification (44). This indicates that the EGFR is subject to multiple levels of control that can be independently altered during transformation.

Tight control on the EGFR system is probably necessary because it appears to be the major regulator of HMEC proliferation in vivo. EGF-containing pellets can stimulate normal ductal growth in regressed mammary glands of ovariectomized mice (24). Estrogens appear to regulate the proliferation of HMEC in vivo and in vitro in part through an EGFR autocrine loop (45,46). Blocking EGFR occupancy in vitro using a monoclonal antibody causes HMEC to reversibly enter G<sub>0</sub> (6). EGF is essential for the motility and assembly of HMEC into organized alveolar structures in vitro. EGF also has a dual effect of promoting growth and chemotaxis/motility of keratinocytes (47) and intestinal epithelial cells (48), suggesting that it has a general role in both establishing and maintaining the structure of epithelial tissues. Recently, rearrangements of the EGFR have been found in 78% of breast carcinomas (49), again implicating the activity of this receptor in transformation of breast epithelial cells.

Because of the importance of the EGFR in HMEC regulation, it appears likely that genetic alterations that give HMEC a growth advantage will operate either directly or indirectly through this receptor system. Despite the numerous studies on EGFR and breast cancer, this idea has not been critically tested. Studies that document the presence or absence of EGFR (or their overexpression) are not particularly informative in this regard. For example, the MCF-7 breast cancer cell line displays very low levels of EGFR expression compared to normal HMEC, but estrogen can induce proliferation in these cells in part through an EGFR/TGF- $\alpha$  autocrine pathway (50). In rapidly proliferating HMEC, there is a positive relationship between TGF- $\alpha$  levels and proliferation, apparently due to a positive feedback loop operating through the EGFR (5). Amphiregulin and EGFR levels are also high in proliferating HMEC, but not in intact organoid structures (5,23). Control of receptor number could regulate other aspects of HMEC function, such as directional sensing of ligands. In addition, genetic lesions that operate downstream of the EGFR itself would not necessarily affect receptor expression. The present uncertainty regarding the role, if any, of the EGFR in breast cancer reflects our general lack of understanding of its role in normal epithelial cell function, an issue directly addressed by our studies.

Over the last four years, we have made excellent progress in our efforts to understand the role of the EGFR distribution in both tissue organization and cancer. We have caused mislocalization of EGFR in polarized epithelial cells and found that regulation and down regulation of the EGFR are distinct from apical and basolateral surfaces. Furthermore, substrate phosphorylation is distinct from the two cell surfaces. We have altered the structure of the EGFR ligands that are expressed by these cells and have discovered that the membrane-anchoring domain of EGFR ligands serve an important role in restricting the site of receptor activation. Significantly, we found that inhibiting the proteolytic release of EGFR ligands will block proliferation of these cells, providing a novel approach to breast cancer therapy. We have also extended our studies to the transmodulation of the erbB-2 gene product by the EGFR. We found that overexpression inhibits down regulation of erbB-2 triggered by EGFR activation. In addition, overexpression of erbB-2 also inhibits normal downregulation of the EGFR, apparently by inhibiting lysosomal targeting. Finally, we have improved our methodologies for expressing mutant forms of EGFR and its ligands in nontransformed

HMEC, providing a basis for further studies on the role of EGFR trafficking in HMEC physiology.

## **BODY**

The tasks in the statement of work are:

Task 1: Determine the normal pattern of compartmentation and regulation of EGFR and its ligands in nontransformed mammary epithelial cells. Define the extent to which this is similar to the pattern described for other cell types and define conditions under which these cells form organized alveolar structures. (Months 1-24)

Task2: Determine whether oncogenic forms of the EGF receptor found in breast cancer display the same pattern of spatial regulation and biological activity as activated, wild type EGF receptors (Months 12-36)

Task3: Express genetically altered EGF receptors and ligands in mammary epithelial cells (Months 12-36)

Task 4: Demonstrate that mis-sorting or inappropriate expression of the EGFR or its ligands provides a growth advantage to HMEC or inhibit normal organization (Months 24-48)

Task 5: Determine how the pattern of spatial regulation of the EGFR affects its ability to transactivate and transmodulate erbB-2 (Months 12-36)

TASK 1: Determine the normal pattern of compartmentation and regulation of EGFR and its ligands in nontransformed mammary epithelial cells. Define the extent to which this is similar to the pattern described for other cell types and define conditions under which these cells form organized alveolar structures.

We have examined the properties of both basal and luminal HMEC and determined conditions that foster their organization. To establish how these results compare with other cell types, we also conducted a study of the effect of high receptor expression on another epithelial cell type; LLCPK1 cells. Because this cell type forms tight junctions on transwell filters, it is possible to determine the effect of receptor overexpression on apical/basolateral signaling.

In all cell types that have been studied to date, most EGFR are found on the cell surface (51-54). Additionally, ligand-induced lysosomal targeting and down-regulation of EGFR has always been observed to be preceded by rapid occupancy-dependent internalization (55). Because of the close association of the two trafficking processes, it has been assumed that they are functionally linked. This is clearly not the case with all receptors, such as the  $\beta$ -adrenergic receptors, where internalization ("sequestration") and lysosomal targeting ("down-regulation") have been viewed as separate events (56). Recently, the structural domains of the EGFR that are associated with endocytosis and lysosomal targeting have been mapped and have been shown to be distinct (57). Additionally, the biochemical requirements for endocytosis and lysosomal targeting are also different. It has been shown that clathrin, GTP hydrolysis, unidentified cytoplasmic proteins, and the intrinsic kinase activity of the receptor are required for ligand induced internalization (54,58). In contrast, lysosomal targeting relies



upon the vesicular trafficking machinery, such as the protein snx-1, but does not require receptor kinase activity (57,59,60).

Default trafficking of EGFR and the biochemical steps involved in endocytosis and lysosomal targeting have been defined using transformed cell lines, such as A431, or fibroblasts engineered to express high levels of specific EGFR mutants (4,52,58,61-65). In these cells, it has been observed that EGFR are primarily cell surface receptors. It has also been observed that several steps in receptor trafficking are saturable, presumably because the mechanisms rely upon limiting amounts of specific components (52,65). Although useful, these EGFR experimental systems do not provide an ideal context for understanding receptor regulation. Fibroblasts express few EGFR and their growth *in vivo* does not depend upon EGFR activity (66). The A431 cell line is derived from a highly aggressive neoplastic transformation and its growth is inhibited by EGFR stimulation (67). Nontransformed HMEC are an ideal cell type in which to investigate the function of the EGFR. Not only due to the involvement of the EGFR in breast cancer, but also they normally expresses high numbers of receptors and also depend upon EGFR for a variety of cell functions.

Because normal, non-transformed HMECs express high numbers of EGFR, we expected to find a corresponding increase in the capacity of these cells to negatively regulate these receptors. To an extent, this expectation was met. However, we also found that in the absence of ligand the default, steady-state, trafficking pattern of the EGFR was quite distinct between basal and luminal cells. For example, consistent with observations from other cells types, the luminal HB2 cells expressed almost all EGFR at the cell surface. In contrast, 30-50% of empty EGFR in 184A1 cells was found in intracellular pools. We found that redistribution of empty EGFR was the result of the specific and rapid endocytosis of the empty EGFR. We also observed this phenotype in cell lines derived from primary tissue explants, suggesting that rapid constitutive internalization of EGFR and that the establishment of internal pools of EGFR may be a general characteristic of basal, EGFR responsive HMEC. This trafficking paradigm may represent an important form of EGFR regulation and signal coordination.

Since several polarized human epithelial tissues express predominantly basolateral EGFR, we also asked whether EGFR regulation and specific EGFR-mediated responses were compartmentalized as well. To explore this, we caused the mislocalization of EGFR to the apical cell membrane by overexpressing them in polarizing kidney epithelial cells that normally express predominantly basolateral EGFR. The formation of highly electrically resistant monolayers on permeable filters, allowed us to independently stimulate apical or basolateral EGFR with epidermal growth factor (EGF). We found significant differences in EGFR down-regulation, endocytosis, tyrosine kinase activity, and signaling between basolateral and apical EGFR. We conclude that certain substrates involved in EGFR regulation and signaling are compartmentalized in polarized epithelial cells.

## Materials and Methods

*General* - Reconstituted extracellular matrix derived from Englebreth-Holmes-Swarm fibrosarcoma (Matrigel) was purchased from Collaborative Research (Cambridge, MA). Human EGF was purchased from PreProTech, Inc. Human transferrin was purchased from Sigma. Polyclonal rabbit antibodies specific for phosphotyrosine were generated and affinity-purified as described (68). Monoclonal antibodies 528 and 225 against the EGFR (69) were purified from hybridomas obtained from American Type Culture Collection. Monoclonal antibody 13A9 against the human EGFR was a generous gift from Genentech. Polyclonal rabbit antibody N-13 directed against a peptide corresponding to residues 1-13 in human EGFR was a gift of Dr. Debora Cadena. Secondary antibodies labeled with either Texas-Red or fluorescein were obtained from Molecular Probes (Eugene, OR). The cell lines 184, 184A1, 161,

48R and 231 were provided by Dr. Martha Stampfer and were cultured in medium DFCI-1 as described (70) supplemented with 12.5 ng/ml EGF. HB2 cells were obtained from Dr. Joyce Taylor-Papadimitriou and were cultured as described (71). Eighteen hours prior to EGFR internalization experiments, cells were transferred to a 37°C tabletop incubator in either DFCI-1 without bicarbonate (1% serum), for 184A1, or serum-free and bicarbonate-free DMEM (72), for HB2. Several independent experiments were performed with cells removed directly from normal culture. The two protocols produced similar results.

Matrigel was equilibrated by dialysis against MCDB 170 basal medium at 4°C. Cells are plated at a density of 200,000 cells/well of a 12 well plate, with each well coated with 0.7 ml of Matrigel. After plating, the cells are examined daily and photographed. Wells contained medium without EGF, with 12.5 ng/ml EGF, or with 10 µg/ml 225 anti-EGFR antibody. Histologic sections were prepared by digesting cultures with collagenase - dispase. Intact colonies were then fixed in Bouin's fixative, embedded in paraffin, sectioned, and stained with hematoxylin and eosin.

EGF, human transferrin, and monoclonal anti-human EGFR antibodies 528 IgG, 225 IgG, were iodinated with <sup>125</sup>I (ICN) using IODOBEADS (Pierce) according to the manufacturer's recommendations. Free iodine was separated from the radiolabeled ligands by passing the mixture over a 0.8 x 20 cm column of Sephadex G-10 equilibrated with phosphate buffered saline. The specific activity of <sup>125</sup>I-labelled EGF was generally between 0.9 - 1.8 X 10<sup>3</sup> cpm/fmol; the specific activity of <sup>125</sup>I-labeled monoclonal antibodies was between 0.5 - 2.3 X 10<sup>3</sup> cpm/fmol and the specific activity of transferrin was between 0.4 - 1.0 X 10<sup>3</sup> cpm/fmol.

EGFR numbers were determined by Scatchard analysis. 184A1 and HB2 cells were brought to 0°C by rinsing in ice-cold PBS. <sup>125</sup>I-EGF concentrations between 0.16 nM to 50.0 nM were added in DMEM lacking bicarbonate but containing 20 mM HEPES pH 7.6 and 0.1 mg/ml BSA. Samples were allowed to come to equilibrium (18 hr. incubation on ice) before rinsing and acid-stripping the cells at 0°C using stripping buffer (50mM glycine-HCl, 100mM NaCl, 2M Urea, pH 3.0 (72)). The amount of surface-associated (stripped) ligand was then determined using a gamma counter. Cell numbers were determined with a Coulter counter and the specific activity of the ligand was corrected prior to analysis. The data were plotted according to the method of Scatchard (73).

*Overexpression of EGFR in LLCPK1 Cells.* The full-length human EGFR gene was cloned into the vector RC/CMV which was then used to transfect a clone (Cl4) of the LLCPK1 cell line using the calcium phosphate method and 1.8mg/ml G418 for selection. The stably transfected Cl4 (LLCPK1) cells were called K2 cells. Transepithelial resistance was measured and only wells measuring 350 ohms-cm<sup>2</sup> or higher were used for experiments.

To measure receptor number, cells were plated at 50,000 cells per well onto polycarbonate filters (0.45µm Transwell; Costar) in a-MEM (ICN) with 10% fetal calf serum (Hyclone), penicillin, streptomycin, and glutamine. At 14 days in culture, the medium was changed to cold α-MEM-HB (1gm/L bovine serum albumin and 20mM HEPES buffer) for 30 min. EGF was labeled with <sup>125</sup>iodine to approximately 150,000 cpm/ng as described above. 408,000 K2 cells per Transwell filter were incubated to equilibrium at 0°C with serial half-dilutions of <sup>125</sup>I-EGF (12 nM) in DV-HB that were applied to either the apical or basolateral sides of the monolayers. Nonspecific binding was measured in the presence of a 100-fold excess of unlabeled EGF. The cells were incubated at 4°C for 24 hours. The cells were washed 5 times with ice-cold WHIPS-saline (20mM HEPES (pH7.4), 130mM NaCl, 5 mM KCl, 0.5 mM MgCl<sub>2</sub>, 1mM CaCl<sub>2</sub>, 1mg/ml PVP) and stripped in 1 ml of stripping buffer ( 50mM glycine- HCl, 2M urea (pH3), 100mM NaCl, 2mg/ml PVP) for 1 minute. The stripping buffer was collected and counted in a gamma counter. EGFR affinity and number per cell were determined by

Scatchard analysis. Parameters were estimated by non-linear regression using the Levenberg-Marquardt algorithm and were fit using the Profit program (Quantum Soft).

*Internalization and recycling measurements* - Internalization of  $^{125}\text{I}$ -EGF and  $^{125}\text{I}$ -mAb 225 was measured by changing to medium containing the indicated concentrations of ligands at  $37^\circ\text{C}$ . The rinsing of the cells with ice-cold saline was performed using a semiautomatic apparatus previously described (53). The relative amounts of ligand associated with the surface and interior of the cells were determined by acid-stripping at  $0^\circ\text{C}$  using stripping buffer (53). Nonspecific binding of EGF and mAb 225 was measured in the presence of 100X unlabeled ligand. All data were corrected for inside-surface spillover. The value of the specific internalization rate of EGF, mAb 225 or Tf receptors ( $k_e$ ) was determined by the internalization plot method (74-76). The integral of surface binding that this method requires was determined by numeric integration of the surface data. Computer templates for the correction of all data and the automatic calculation of the integral surface binding, average receptor occupancy, and  $k_e$  were created for Microsoft Excel.

Endocytosis of antagonistic mAb 528 was measured after prebinding of ligands to cells at  $0^\circ\text{C}$ . Cells were incubated at  $0^\circ\text{C}$  in the presence of either  $1.7\text{ nM}$   $^{125}\text{I}$ -EGF or  $6.7\text{ nM}$   $^{125}\text{I}$ -mAb 528 for 3 hours. Media containing ligands were aspirated, the cells were washed with ice cold PBS and then the cells were warmed to  $37^\circ\text{C}$  in the absence of ligands. Loss of EGF and 528 from the surface and accumulation of ligands on the inside of cells was determined over a 23 minute time course. Surface counts were collected with stripping buffer above and inside counts were those solubilized in 2% SDS after surface stripping. Each point is plotted as a percent of total cpm at that time point.

*Time-lapse videomicroscopy* - Time-lapse photography as performed using a Sony video camera attached to a Wild dissection microscope through a video camera adaptor. A Panasonic commercial VHS time-lapse tape deck was used to acquire images. The recorder was triggered through a TTL relay (Alpha Electronics) attached to a Macintosh computer through its serial port. A BASIC program was written to acquire individual frames at the appropriate time intervals.

*Fluorescence microscopy* - Cells were plated on fibronectin-coated coverslips 48 hrs before the experiment. Cells were fixed 10 min in 4% paraformaldehyde and permeabilized 5 min in 0.1% Triton X-100 in PBS. All intermediate washes were done with ice cold PBS. All non-specific binding was blocked by including 1% RIA-grade BSA in all antibody solutions. EGFR was detected by incubating cells for 60 min in the presence of a mix of anti-EGFR antibodies mAb 225 and mAb 13A9 ( $10\mu\text{g/ml}$  and  $1\mu\text{g/ml}$  respectively). Alternatively, cells were incubated at  $37^\circ\text{C}$  with mAb 225 prior to fixation and permeabilization. Antibodies were visualized by staining with FITC-labeled goat anti-mouse at 1:300 (Molecular Probes, Inc.) for 45 min. Phosphotyrosine was detected using of affinity-purified antiphosphotyrosine polyclonal antibody (1:1000) (68) followed by Texas-Red conjugated goat anti-rabbit at 1:300 (Molecular Probes, Inc.) for 45 min. When phosphotyrosine was being detected,  $500\mu\text{M}$  orthovanadate was included in all washes, and all incubations were done on ice. The coverslips were mounted in ProLong antifade medium (Molecular Probes, Inc.) and viewed with a Nikon inverted fluorescence microscope with a 100X oil immersion objective. Images were acquired using a Photometrics cooled CCD camera and a Macintosh workstation running OpenLab software (Improvision, Inc.). Images were scaled and normalized to 256 levels of grey using Adobe Photoshop.

*EGFR half-life measurements* - 184A1 and HB2 cells were labeled to steady state (24 hours) with cysteine and methionine free Dulbecco's modified Eagle's medium (ICN) supplemented with 10% FCS (Hyclone, Logan UT),  $60\mu\text{g/ml}$  penicillin,  $100\mu\text{g/ml}$  streptomycin,  $100\mu\text{M}$

glutamate, 5  $\mu$ g/ml insulin, 5% normal media and 100  $\mu$ Ci/ml of EXPRE<sup>35</sup>S<sup>35</sup>S (NEN). Cultures were rinsed 6 times with normal culture medium and chased in complete DMEM media with 100X excess methionine and cysteine (15  $\mu$ g/ml) with or without 17 nM EGF. At 0, 1, 3, 5 and 7 hours post-chase, EGFR was extracted on ice for 10 min in 10% glycerol, 1% Triton X-100, 20 mM HEPES pH 7.0, 2 mM EDTA, 0.02% azide containing 1  $\mu$ g/ml each of pepstatin, chymostatin, leupeptin, and aprotinin. Samples were centrifuged at 14,000g for 10 min at 4°C. Equal amounts of protein from the supernatant were subjected to immunoprecipitation with 4  $\mu$ g/ml 13A9 antibody overnight at 4°C. Samples were washed 5 X in 300mM NaCl, 10 mM Tris pH 8.3, 0.1% SDS, 0.05% NP-40. Samples were then separated on 5-15% SDS-acrylamide gel and dried onto 3MM paper. EGFR bands were quantified using the Bio-Rad G250 Molecular Imager.

*Tyrosine phosphorylation of the EGFR* – K2 cells or HB2 and 184A1 cells were incubated in the presence or absence of the specified amounts of EGF or mAb 225 for 10 min at 37°C. The cells were rapidly rinsed at 0°C, extracted in the 100 mm plate with RIPA (150 mM NaCl, 1% NP-40, 0.5% SDS, 0.5% DOC, 50 mM Tris pH 7.2, containing 1  $\mu$ g/ml pepstatin, chymostatin, leupeptin, aprotinin, and 0.1 mM orthovanadate) (68). After 10 min at 0°C, cell debris was removed by centrifugation for 10 min at 14,000g. Samples were normalized for protein using the BCA Assay (Pierce), and equal amount of protein from each sample were denatured at 100°C in 1% SDS, 1%  $\beta$ -mercaptoethanol, 10 mM Tris-HCl pH 6.8, 5% glycerol and separated on a 7.5% SDS-PAGE gel. Samples were transferred to nitrocellulose in the presence of 1.0 mM orthovanadate and blocked with 2.5% BSA, 1.0 mM orthovanadate and 0.005% Tween 20. EGFR was detected with rabbit polyclonal anti-EGFR antibody N13 followed by an HRP-conjugated goat anti-rabbit secondary antibody. Parallel samples were developed with HRP-conjugated anti-phosphotyrosine antibody RC-20 (Transduction Labs). Bands were visualized using enhanced chemiluminescence (NEN-Renaissance) and detected on film. Alternatively, EGFR was detected with rabbit polyclonal anti-EGFR antibody N13 and phosphotyrosine was detected with an affinity-purified antiphosphotyrosine polyclonal antibody. Bands were visualized with <sup>125</sup>I-Protein A and detected on film.

*Hypotonic shock and potassium depletion* - Cells were grown on 35 mm tissue culture plates in standard media in the absence of EGF for 24 hours prior to the start of the experiment. Cells were washed 4 times in 2 mls Buffer A (50 mM HEPES pH 7.4, 100 mM NaCl) at 23°C, then incubated in 1 ml DFCI-1:dH<sub>2</sub>O (1:1) 5 min at 37°C. Control samples were washed 4 times in 2 mls Buffer A plus 10mM KCl then incubated in 2mls of the same buffer plus 1% BSA for 30 min at 37°C. Experimental samples were washed 4 times in 2 mls Buffer A and then incubated in 2mls Buffer A plus 1% BSA for 30 min at 37°C. Finally, control cells were washed 4 times in 2 mls Buffer A plus 10mM KCl, and experimental samples were washed 4 times in 2 mls Buffer A. All washes were at 23°C. Immediately following these treatments the endocytosis of EGF, mAb 225 and transferrin were measured as described above.

*Mitogenic response of polarized K2 cells.* - Polarized and confluent (14-days in culture) monolayers of K2 cells in culture on Transwell filters (24mm), were treated with 20ng/ml EGF in complete media (a-MEM + 2mM L-glutamine, 10% fetal calf serum, 1.8mg/ml G418) that was added to the apical or basolateral compartments. Control cells received no EGF. After 18 hours, the media in the apical and basolateral compartments was replaced with Hank's Balanced Salt Solution containing 2  $\mu$ Ci/ml of [<sup>3</sup>H]-thymidine. After 2 h at 37°C, the solution was replaced with 10% trichloroacetic acid and the acid insoluble radioactivity measured. In some cases, 10  $\mu$ g/ml of anti-EGFR antagonistic monoclonal antibody (mAb 225) was added ipsilateral or contralateral to the compartment containing EGF to demonstrate the specificity of EGFR activation and the integrity of the cell monolayers. In addition, cell counts were used to corroborate the changes in thymidine incorporation: K2 cells were plated at 2x10<sup>4</sup> cells per



24mm Transwell filter and cultured for 14 days at which time 20ng/ml EGF was added to either the apical or basolateral compartments. Control cells received no EGF. The cells were cultured for another 5 days, then dispersed with trypsin and counted using a hemocytometer.

*Down-regulation of EGFR from apical and basolateral surfaces* - Polarized monolayers of K2 cells on 12mm Transwell filters (approximately  $5 \times 10^5$  cells per Transwell) were incubated with 100 ng/ml unlabeled EGF added to either the apical or basolateral chamber at 37°C for the indicated periods of time. Cells were rinsed twice with phosphate-buffered saline and then incubated 2 hr on ice with 100 ng/ml of  $^{125}\text{I}$ -EGF added to the same chamber as the unlabeled EGF. Membranes were then rinsed 6 times with ice-cold phosphate buffered saline, removed with a #4 cork borer and solubilized in 2% SDS prior to counting. The results were calculated as the amount of radiolabeled EGF bound as a percent of that bound to untreated cells.

*Internalization of EGFR from apical and basolateral surfaces* - Polarized monolayers of K2 cells on 12mm Transwell inserts (approximately  $5 \times 10^5$  cells per Transwell) were incubated with 10 ng/ml of  $^{125}\text{I}$ -EGF ( $1.5 \times 10^5$  cpm/ng) added to either the apical or basolateral chamber for up to 5 min at 37°C. At 1 min intervals, the inserts were rinsed in ice-cold phosphate-buffered saline 6 times and the membranes removed using a #4 cork borer. Surface radioactivity was removed by placing the membranes in 1.5 ml acid strip solution (50 mM glycine/HCl (pH 2.5), 150 mM NaCl, 2 M urea) for 8 minutes. Internalized radioactivity was solubilized using 2.5 ml 1N NaOH. The relative amount of internalized and surface associated EGF was converted to internalization plots as previously described (76). Nonspecific EGF binding was determined in parallel using a 1000-fold excess of unlabeled EGF. LLC PK1 cells were transfected with the pRC-CMV vector containing the c'973 EGFR and a G418 resistance gene by the calcium phosphate method. Polarized monolayers were evaluated for internalization from the apical versus basolateral surfaces as described above.

*Differential phosphorylation of EGFR substrates* - Polarized monolayers of K2 cells on Transwell filters (24mm) were treated with or without 100ng/ml of EGF added to either the apical or basolateral chambers for 15 minutes. Triplicate groups of cells were lysed in ice-cold lysis buffer, sonicated for 10 seconds, then clarified at 14,000 rpm at 4°C for 15 minutes. The pellets were stored at -70°C until further use. 2 $\mu$ g of SHC mAb (Transduction Laboratories) or 4 $\mu$ g of anti focal adhesion kinase (FAK) mAb (Transduction Laboratories) were added to the supernatants and incubated on a rocker at 4°C overnight. Then, 50 $\mu$ l of a 50% slurry of Protein A/G-Sepharose Immunopure beads (Pierce) were added to each lysate and incubated on a rocker at 4°C for 2 hours. The beads were washed three times in 1ml of lysis buffer then boiled in SDS-reducing sample buffer. The samples were divided in half and resolved on SDS-7% acrylamide gels and transferred to nitrocellulose. The blots were blocked in 1% TTBS (100mM Tris-Cl, 0.9% NaCl, 0.1% Tween, 1% BSA) overnight, then probed with either a 1:2500 dilution of antiphosphotyrosine mAb PY20 (Transduction Laboratories), a 1:5,000 dilution of mAb's to SHC (Transduction Laboratories) or a 1:2000 dilution of FAK (Transduction Laboratories) in 1% TTBS for 2 hours. The blots were washed twice for 20 minutes each, then incubated with a 1:5000 dilution of rabbit-anti-mouse mAb (Zymed). The blots were washed twice, then detected with 50ng/ml  $^{125}\text{I}$ -protein A. The blots were washed twice, then scanned and quantified using a Molecular Imager storage phosphor device (Bio-Rad Laboratories).

For beta-catenin: 2 $\mu$ g of E-cadherin mAb (Transduction Laboratories) were used to coprecipitate beta-catenin from the Triton X-soluble fraction using the same immunoprecipitation method above. 2 $\mu$ g of beta-catenin mAb (Transduction Laboratories) were then used to immunoprecipitate beta-catenin from the Triton X-soluble fractions after immunodepletion of E-cadherin. 2 $\mu$ g of beta-catenin mAb (Transduction Laboratories) were used to immunoprecipitate beta-catenin from the Triton X-insoluble pellet fractions after

solubilization in 0.1% SDS in lysis buffer (pellets were boiled for 3 minutes and sonicated prior to immunoprecipitation). Phosphotyrosine and beta-catenin were detected by the western blot protocol described above.

*Confocal immunofluorescence imaging:* K2 cells grown on 12 mm Transwell filters until a transepithelial resistance reading of greater than 350 ohms-cm<sup>2</sup> (about 8-9 days) was obtained. The media was aspirated, the monolayers rinsed twice with PBS, and the cell monolayers were fixed in 4% paraformaldehyde-PBS for 20 minutes at room temperature. The monolayers were washed twice with PBS then incubated in a blocking buffer (1% bovine serum albumin (Bio-Rad) in PBS, pH 7.4) for 30 minutes. The monolayers were then incubated with a 1:500 dilution of beta-catenin mAb (Transduction) in blocking buffer for 30 minutes. The cells were washed twice with blocking buffer and then incubated with a 1:1000 dilution of FITC-rabbit-anti-mouse (Jackson ImmunoResearch) in blocking buffer for 30 minutes. The monolayers were washed twice with blocking buffer, then the filters were cut out of their plastic inserts, mounted on glass slides in 4μl of antifade solution (Vector Laboratories), and covered with a square coverslip which were sealed using a clear nail polish. XY-plane images were collected using a 60X objective microscope (Zeiss) fitted with a MRC-1024ES confocal laser scanning system (Bio-Rad). Serial images were obtained at 0.5μm spacing which were then reconstructed with the LaserSharp program (Bio-Rad) into X-Z plane interpolated images.

## Results and Discussion

Organization of HMEC on Matrigel - Human mammary epithelial cells (HMEC) strain 184 form a contact inhibited simple monolayer when grown under standard conditions on plastic tissue culture surfaces (Fig. 1A). When plated on extracellular matrix derived from Englebreth-Holmes-Swarth fibrosarcoma (Matrigel), however, 184 cells rapidly assemble into epithelial cords to form complex three dimensional structures. Colonies mature over 6 to 10 days to form a complex tubular - branched network with multiple end buds that superficially resemble alveolar complexes *in vivo* (Fig. 1B). Sections of mature structures revealed histologic features of adenosquamous differentiation (Fig. 2). More pronounced squamous differentiation was seen after prolonged incubation, consistent with terminal squamous differentiation of senescent epithelial cells.

Video time lapse photography revealed a dynamic process in which structures mature through several distinct phases. Single cells rapidly migrate across the matrix surface during the first 24 hours after plating on Matrigel. Cell - cell contact induced cell spreading and proliferation in small aggregates, and cell movement across the matrix surface ceased as small aggregates formed. Large, macroscopic aggregates appeared during the next several days in a process that apparently involves remodeling of the extracellular matrix. Time lapse photography revealed *en bloc* movement of cellular aggregates and contraction of the extracellular matrix around stable structures. All cellular movement within the matrix stopped after several days as the relatively simple tubular - branched structures stabilized. The epithelial structures achieved their final form as large buds (approximately 40 to 50μm) grew over 5 to 7 days without further evidence of aggregate movement (see below).

Because EGFR occupancy is important for the growth of HMEC, we were interested in determining its role in HMEC organization on Matrigel. Because 184 cells produce transforming growth factor-α and other ligands for the EGFR, we inhibited autocrine receptor activation by removing EGF from the culture medium and blocking autocrine ligand binding with a blocking antibody (225) against the EGFR. Interrupting the EGFR autocrine loop inhibited all phases of HMEC organization on Matrigel (Fig. 3). HMEC remained as small groups of cells when plated on Matrigel in the absence of EGF and the presence of 225

antibody. There was no evidence of epithelial organization during prolonged incubation of these cultures.

We examined the effect of both EGF and antagonistic 225 antibody on the early phases of organization by using thin layers of Matrigel. Cells were plated at a low density and then examined 18 h later. As shown in Fig. 4 individual cells adhered to the layer of Matrigel in the absence of EGF, but did not spread. When two or more cells were in contact during plating, they spread, underwent rapid migration and recruited cells into a growing cell mass (Fig. 4, left panel). In the presence of exogenous EGF, all cells spread and migrated when plated on Matrigel (middle panel). In the presence of 225 mAb, no cells were able to spread or migrate (right panel). We conclude that EGF promotes spreading and cell migration on Matrigel. Interestingly, in the absence of exogenous EGF, only cells contacting a neighboring cell are able to respond to autocrine growth factors.

Organization of 184A1 HMEC was dependent on both time and cell density. Increasing numbers of 184A1 cells were plated on Matrigel in either the presence or absence of exogenous EGF. As shown in Fig. 5, within 24 h the cells were able to form simple branching structures. Because the doubling time of these cells is 18-24 h (77), cell proliferation is unlikely to play a major role in formation of the initial structures. In the absence of exogenous EGF, a cell density of at least  $1 \times 10^5$  cells/cm<sup>2</sup> was required for organization. In the presence of EGF, a density of only  $2 \times 10^4$  cells/cm<sup>2</sup> was necessary. In the absence of exogenous EGF, the cells primarily formed branching structures that were stable over time (Fig. 5, left panels). The addition of exogenous EGF stimulated formation of endbud-like structures (Fig. 5, right panels), most likely by stimulating cell proliferation. The addition of anti-EGFR mAb 225 completely blocked organization of the cells at all time points (data not shown; also see below).

There was also a time window of approximately 12-24 h during which exogenous EGF facilitated organization of 184A1 cells. Visual observations suggested that this was related to invasion of the Matrigel by the cells. Thus, if EGF was provided to cells while they were still on the surface of the extracellular matrix, the cells could organize, but EGF had little effect once the cells entered the matrix. As indicated in Fig. 5 by the arrows, cells not included in a structure by 24 h remained as isolated colonies. The addition of EGF greatly increased the fraction of cells that joined organized structures, suggesting that cell migration and cell-cell contact were important aspects of EGF-stimulated organization.

From these studies, we conclude that normal organization of HMEC on a basement membrane requires activation of the EGFR. The process of organization is complex and involves cell movement, proliferation and differentiation. Because blocking the EGFR stops many different cell processes, it was not possible to determine the level at which EGF exerted its effect. The results of this study encouraged us to take a more subtle approach in disrupting EGFR activation. In particular, we initiated a series of studies to determine whether the spatial pattern of EGFR ligand production was important in specifying the spatial pattern of cell organization (see task 3 below).

EGFR are Localized within Endocytic Vesicles in HMECs - It has been previously reported that HMEC express high numbers of EGFR (78). As shown in Fig. 6A, both 184A1 and HB2 cells express high levels of EGFR. Scatchard plot analysis indicates that 184A1 cells express approximately  $4 \times 10^4$  high affinity and  $1.7 \times 10^5$  low affinity receptors per cell whereas HB2 cells express approximately  $1.2 \times 10^5$  and  $6 \times 10^5$  high and low affinity receptors respectively. EGFR expression in HMECs is intermediate relative to the expression observed in the common experimental cell systems of fibroblasts and A431 cells,  $2 \times 10^4$  and  $3 \times 10^6$  receptors per cell, respectively (79,80). Total expression levels of  $1 - 5 \times 10^5$  are often achieved in transfected cells engineered to express wild type and mutant forms of the EGFR (81,82).

Although both cell lines are immortalized, non-tumorigenic HMEC, their response to exogenous and endogenous EGF is quite distinct. As shown in Fig. 6B, the proliferation of 184A1 cells is stimulated by the addition of exogenous EGF and inhibited by the addition of antagonistic, anti-EGFR mAb 225. In contrast, the proliferation of HB2 cells is not significantly affected by either the addition of EGF or mAb 225. Similar results were obtained with respect to cell motility as assessed by time-lapse video microscopy (data not shown). This data is consistent with that reported by other investigators (83) and indicates that although 184A1 and HB2 cells possess similar numbers of EGFR, their response to EGFR activation is dissimilar.

We and other investigators have reported that the EGFR is primarily, if not exclusively, found on the cell surface in the absence of exogenous ligand (51-54). When we began our studies, we tested whether or not this was also true for HMECs. To determine the steady state distribution of EGFR in HMECs we used indirect immunofluorescence microscopy (Fig. 7A and B). The distribution of EGFR was established using anti-EGFR antibodies. As shown in Fig. 7A, HB2 cells display the typical EGFR surface staining pattern, with receptors being localized along cell borders and diffusely across the entire cell surface. Unexpectedly, in 184A1 cells (Fig. 7B), we not only observed surface localization but we also observed significant EGFR staining in punctuate structures evenly distributed throughout the cells. The size, shape and distribution of the brightly staining structures suggested to us that they were endocytic vesicles. To determine if this was the case, we preincubated 184A1 cells at 37°C in the presence of mAb 225. Following fixation, we visualized the mAb 225 with a fluorescent secondary antibody. If the internal pool of receptors was derived from the cell surface then the antibody should be found within endocytic vesicles. Both HB2 and 184A1 cells were incubated with either EGF or mAb 225 for 2 hours at 37°C (Fig. 7C-F). As shown in Fig. 7D, we again found strong EGFR localization in peripheral, punctuate structures in 184A1 cells. HB2 cells displayed little or no staining because most surface-bound mAb 225 disassociated during the fixation/permeabilization protocol (data not shown) and little had been endocytosed. As noted in other cell types, treating cells with EGF prior to fixation and visualizing the distribution of the EGFR resulted in their redistribution into large, perinuclear structures, probably lysosomes (Fig. 7E and F). These results indicate that the 184A1 cells, unlike cells previously studied, have significant pools of intracellular EGFR, and that these pools are derived from internalized receptors.

At Steady State, 30-50% of all empty EGFR in 184A1 are Intracellular - The intensity of immunofluorescence associated with the EGFR in endocytic vesicles in Fig. 7 indicated that a large number of receptors were localized there. We wanted to determine what fraction of the entire receptor population was intracellular. To do this, we measured inside/surface ratio of radiolabeled mAb 225 at 37°C over a time course of 2-3 hours. The results of a typical experiment are shown in Fig. 8. Because mAb 225 is an antagonistic EGFR antibody, it only binds an empty EGFR, and it allows us to follow the trafficking of receptors populations in the absence of receptor activation. The trafficking pattern of the mAb 225 should thus indicate the steady state, default trafficking pattern of the EGFR. The results from Fig. 8 indicate that 38% of all EGFR expressed in 184A1 are localized intracellularly. In contrast, only 8-9% of EGFR could be detected within HB2 cells. Results from multiple experiments show that 30-50% and 5-10% of EGFR were detected in an intracellular compartment in 184A1 and HB2 cells, respectively. Consistently, as a percentage, there are a 4-10 fold more internal receptors in 184A1 cells.

Although 184A1 cells are non-tumorigenic, they are an immortalized, clonal cell line that displays defined chromosomal abnormalities (84). Thus it seemed possible that the intracellular distribution of EGFR that we observed in these cells was a nonphysiological consequence of their derivation. To evaluate this possibility, we measured the EGFR



inside/surface ratio using a normal population of basal HMEC derived from primary tissue explants (cell line 48R). Although the EGFR inside/surface ratio was lower in the 48R cell line, it much more closely resembles 184A1 than HB2, and it is consistently, as a percentage, 3-5 fold greater in 48R than HB2. We also cultured the cells in serum-free medium MCDB-170 and obtained similar results, thus ruling out the effect of specific growth conditions (data not shown). It appears that in the more basal 184A1 cell line, a significant fraction of the total receptor population is intracellular at steady state.

184A1 Cells Rapidly Internalize Empty EGFR - The rate at which HB2 and 184A1 cells reached steady state in Fig. 8 suggested that the empty EGFR was being rapidly endocytosed. The inside/surface ratio is a function of internalization, recycling and degradation. The rate at which the inside/surface ratio reaches a steady state is proportional to the rate of degradation plus recycling. Because recycling of the empty EGFR is typically much more rapid than receptor degradation, the rate at which steady state is reached will largely be a function  $k_x$  (recycling rate constant) and the steady state inside/surface ratios will approximate the ratio of  $k_e$  (endocytic rate constant) and  $k_x$  (85)). Since it required approximately the same amount of time for 184A1 and HB2 cells to achieve steady state (Fig. 8) their  $k_x$  values should be similar. Consequently, because their inside/surface ratios were different, their  $k_e$  values were probably dissimilar.

To test this hypothesis, we directly measured the internalization rate of radiolabeled anti-EGFR mAb 225 in both HMEC lines. As a control we also measured the rate of endocytosis of occupied, activated EGFR in both cell types by using radiolabeled EGF. We found that in HB2 cells (Fig. 9, upper panel), the specific internalization rate of  $^{125}\text{I}$ -labeled mAb 225 was about  $0.03 \text{ min}^{-1}$ , very similar to that observed in transfected fibroblasts and other cell types (58). The rate of  $^{125}\text{I}$ -EGF internalization (Fig. 9, lower panel) was significantly greater at  $0.15 \text{ min}^{-1}$ , and was again similar to the values observed in other cell types (58). The 5-fold difference in the specific internalization rate of empty and occupied EGFR observed in HB2 cells, is consistent with rapid, occupancy-induced endocytosis. However, in 184A1 cells, the specific internalization rate of  $^{125}\text{I}$ -labeled mAb 225 was approximately  $0.16 \text{ min}^{-1}$ , and was not significantly different than the rate of  $0.17 \text{ min}^{-1}$  observed for  $^{125}\text{I}$ -EGF ( $p > 0.95$ ). This not only indicates that internalization of empty EGFR is rapid in 184A1 cells, but also suggests that receptor occupancy does not stimulate receptor internalization. Thus it appears that rapid internalization of EGFR is constitutive in 184A1.

We performed the same experiment using several normal populations of basal HMEC derived from primary tissue explants (lines 48R, 161 and 184). Although the specific internalization rate of mAb 225 in these cells was lower than the rate observed in 184A1 cells and it was lower than the rate of EGF endocytosis, the two ligands showed the same pattern of variation within each cell type and the rate of mAb 225 internalization in these cell types was always four to eight fold higher relative to HB2 cells. It appears that a rapid constitutive EGFR internalization rate is a general feature of basal HMEC.

To determine whether the rapid internalization of mAb 225 was simply a property of mAb 225 ( $\text{IgG}_1$ ), we examined the internalization of the unrelated mAb 528 ( $\text{IgG}_{2a}$ ). 184A1 cells were incubated with either  $^{125}\text{I}$ -EGF or  $^{125}\text{I}$ -labeled 528 mAb for 3 h at  $0^\circ\text{C}$ . The ligands were removed and the cells rapidly warmed to  $37^\circ\text{C}$ . The transfer of radiolabeled ligand from the surface to the inside of the cells was then followed by acid stripping. As shown in Fig. 10, both EGF and 528 mAb were internalized equally fast by the cells, indicating that our previous results were not biased by the use of a specific monoclonal antibody.

Ligand Induced Internalization is Not Saturable in HMEC - Because normal, non-transformed HMECs express high numbers of EGFR, we expected to find a corresponding increase in the

capacity of these cells to negatively regulate these receptors. We did not expect that either receptor endocytosis or lysosomal targeting would saturate and become rate limiting. This prediction would certainly be true of EGFR endocytosis in 184A1 cells if receptor internalization is constitutive and rapid. To test this prediction, the specific internalization rate,  $k_e$ , of the EGFR was determined in both 184A1 and HB2 cells as a function of receptor occupancy using concentrations of EGF ranging from 0.08 to 70 nM. As a control, the value of  $k_e$  for the overexpressing cell line A431 was also measured. If internalization of occupied EGFR is saturable, the value for  $k_e$  will decrease at high occupancy levels (52). As shown in Fig. 11, however, specific internalization rates of the EGFR did not decrease in either HB2 or 184A1 cells until approximately  $3 \times 10^5$  receptors were occupied. In agreement with previous findings, the specific internalization rate of EGFR in A431 cells decreased at relatively low levels of receptor occupancy (52). This level of occupancy was approximately 10-fold lower than that necessary to saturate internalization in HMEC. These results are consistent with the hypothesis that saturation of EGFR internalization is due to overexpression of the EGFR without a concomitant increase in components that mediate rapid internalization. These observations are also consistent with the suggestion that 184A1 cells rapidly and constitutively endocytose EGFR.

EGFR are rapidly recycled in HMEC - If the empty EGFR in 184A1 cells undergo rapid constitutive internalization, then they must either be quickly recycled or rapidly degraded and resynthesized. To determine which of these two possibilities was occurring, we first determined the half life of the EGFR in both the presence and absence of EGF. Both HB2 and 184A1 cells were incubated with  $^{35}\text{S}$ -amino acids and then chased in the presence or absence of EGF. The EGFR were immunoprecipitated, separated by gel electrophoresis and quantified using storage phosphor plates. As shown in Fig. 12, the half life of the empty EGFR was very similar in HB2 and 184A1 cells (14h and 11h respectively) and similar to the half life reported for other cells, such as fibroblasts (61). The addition of EGF accelerated the degradation of the EGFR to a similar extent in both cells ( $t_{1/2}$  of 1.6 versus 2 h for HB2 and 184A1 cells respectively). Because the degradation rate of the empty EGFR is relatively slow in both HB2 and 184A1 cells, it appears that the receptors in 184A1 cells must undergo rapid recycling.

The rate at which the inside/surface ratio reaches a steady state is proportional to the rate of degradation plus recycling. For example, if the EGFR is only degraded following internalization (no recycling) at a rate  $k_{\text{deg}}$ , then the time necessary to reach 1/2 of the steady state inside/surface ratio would be approximately  $\ln 2/k_{\text{deg}}$  (86). The fastest rate of EGFR degradation observed in the presence of EGF is 1.6 h (Fig. 12). If all internalized receptors were degraded, then the time necessary to reach half steady state would have been approximately 100 minutes. However, both HB2 and 184A1 cells reach half steady state by 10 minutes (Fig. 8), indicating that the receptors are lost from inside of the cells far more rapidly than can be accounted by degradation. The rapid process is most likely receptor recycling and the assumption that  $k_x \gg k_{\text{deg}}$  is therefore true. Therefore in this case, the inside/surface ratio of EGFR in these cells approximates the ratio of  $k_e$  and  $k_x$ . The data from Fig. 8 and Fig. 12 indicate that the recycling rate constant,  $k_x$ , is about  $0.2 \text{ min}^{-1}$  and  $0.3 \text{ min}^{-1}$  for HB2 and 184A1 cells respectively. This translates into a halflife of recycling of about 3 minutes.

Receptor activation is not necessary for rapid constitutive internalization of the EGFR - Mammary epithelial cells are autocrine in that they express at least one if not several ligands for the EGFR (87). Although the mAb 225 will not bind to occupied EGFR, it seemed possible that transactivation of EGFR in the 184A1 cells was responsible for their high constitutive internalization rate. We found that in the case of HB2 cells, addition of high concentrations of EGF did not alter the internalization rate of mAb 225 (data not shown). In addition, immunofluorescence experiments demonstrated that the internal pool of receptors in 184A1

Cell Line	TfR <sup>1</sup> ( $k_e$ (min <sup>-1</sup> ))	Fluid Phase Endocytosis <sup>2</sup> (fmol/10 <sup>6</sup> hour)	
		-EGF	+EGF <sup>3</sup>
184A1	0.412 +/- 0.037	14.3 +/- 2.7	13.8 +/- 3.6
HB2	0.437 +/- 0.044	10.7 +/- 2.5	15.5 +/- 5.3

<sup>1</sup> Transferrin concentration was 4.0 nM. Half the cell samples were grown in the presence of 75mM Desferol for 2 days prior to the endocytic assay to increase the expression of TfR. There was no effect of desferol upon the endocytosis of TfR. Both sets of numbers were used to calculate the average  $k_e$  value shown. The measurement of  $k_e$  was determined as described in the materials and methods section.

<sup>2</sup> Fluid phase endocytosis was measured as previously described (Wiley and McKinley, 1987). HRP concentration was 2.5 - 5 mg/ml and added to cells in the presence of 5 mg/ml yeast mannan. Cells were solubilized in 0.5% Triton X-100, 15mM HEPES pH 7.5. The values shown are in units of nl/hr X10<sup>6</sup> cells and consistent with previously reported values (McKinley and Wiley, 1988; Wiley and Cunningham, 1982).

<sup>3</sup> EGF concentration was 16.5 nM

cells is not activated. Cells were examined with anti-PY and anti-EGFR in the presence and absence of EGF. In the absence of additional EGF, a significant population of EGFR can be detected in vesicular structures in 184A1 cells, yet little or no anti-PY signal is colocalized to these structures (Fig. 13E and F). A similar result was obtained using an antibody to anti-activated EGFR (results not shown). Addition of EGF resulted a large pool of activated receptors in both HB2 and 184A1 cells. In this case, there was significant colocalization of the EGFR and anti-PY signal in intracellular vesicles (Fig. 13G and H).

Western blot analysis also demonstrated that the fraction of activated EGFR in either HB2 or 184A1 cells was quite low in the absence of exogenous EGF and that the addition of large amount of mAb 225 does not activate the EGFR to any measurable extent (Fig. 14, A and B). Following EGF addition, however, there was a large, dose dependent and comparable increase in the phosphotyrosine content in both cell types. These findings suggest that internalized, empty receptors are not activated, and that the intrinsic tyrosine kinase activity of the EGFR is not required during the process of constitutive endocytosis.

Fluid Phase Endocytosis is Similar in HB2 and 184A1 Cells - The differences between the constitutive internalization rate of the EGFR in HB2 and 184A1 cells could be due to differences in a specific component that mediates rapid internalization of empty EGFR. Alternately, nonspecific plasma membrane internalization rates, or the number of coated pits, could be much greater in 184A1 versus HB2 cells. To test these possibilities, we first measured fluid phase uptake of horseradish peroxidase (HRP) as an indication of nonspecific membrane endocytosis (88). Because the surface/volume ratio of endocytic vesicles is relatively constant, rates of fluid phase endocytosis reflect nonspecific membrane endocytosis (89). As shown in Table 1, rates of fluid phase endocytosis in 184A1 and HB2 cells were similar. These values, 14.3 and 10.7 nl/hr per 10<sup>6</sup> cell respectively, are similar to those reported for other cell types, such as fibroblasts (89,90). Addition of EGF stimulated fluid phase endocytosis in HB2 cells, but had little effect upon HRP uptake in 184A1 cells. These results show that the overall membrane internalization rate in 184A1 cells could not explain the higher endocytic rate of empty EGFR.

*Table 2. Endocytosis of both the occupied and unoccupied EGFR and the transferrin receptor is blocked in HMECs by hypotonic shock followed by depletion of potassium*

<u>Cell Line</u>	<u>Ligand</u>	<u>Endocytic Block</u>	<u>k<sub>e</sub> (min<sup>-1</sup>)</u>
<u>184A1</u>	EGF	-	0.22
		+	0.01
	Tf	-	0.91
		+	0.08
	mAb225	-	0.13
		+	0.01
<u>HB2</u>	EGF	-	0.16
		+	0.04
	Tf	-	3.48
		+	0.30
	mAb225	-	0.07
		+	0.03

184A1 and HB2 were subjected to hypertonic shock and potassium-depletion. The endocytosis of <sup>125</sup>I-EGF, <sup>125</sup>I-mAb 225 and <sup>125</sup>I-transferrin was followed as described in the material and methods. Control values were determined by treating the cell samples with a hypotonic shock, but incubating them in a potassium replete version of the second buffer before making an endocytic measurement.

To determine whether 184A1 cells displayed a higher rate of coated pit endocytosis relative to other cell types, we measured the internalization rate of transferrin receptors (TfR), which are known to enter cells through the coated pit pathway. As shown in Table 1, the specific internalization rate of TfR was equal in HB2 and 184A1 cells. Thus, the rapid constitutive internalization rate of EGFR in 184A1 cells could not be directly attributed to a higher rate of either nonspecific membrane endocytosis or coated pit formation.

Empty EGFR appear to be Internalized by Coated-Pits - Although a high rate of coated pit formation (or internalization) in 184A1 cells could not explain the high constitutive



internalization rate of the EGFR, it seemed possible that a previously undescribed endocytic mechanism could explain our results. To explore this possibility, we inhibited coated pit internalization by either hypotonic shock coupled with potassium depletion or by cytoplasm acidification. We then compared the relative effects of these treatments on internalization of the TfR and the EGFR. If a novel mechanism was responsible for EGFR internalization, we would expect to see a differential effect on EGFR and TfR endocytosis. However, as shown in Table 2, the specific internalization rate of both TfR and EGFR were affected the same by hypotonic shock followed by potassium depletion. Cytoplasmic acidification inhibited endocytosis of the TfR and EGFR similarly, 51% and 46% respectively (data not shown). This suggests that constitutive endocytosis of empty EGFR is mediated by coated pits.

Polarized distribution of EGFR in epithelial cells - It is well appreciated that polarized epithelial cells display distinct sets of membrane proteins on their apical versus basolateral surfaces. This distribution is due to differential sorting of newly synthesized as well as recycling proteins. Signals for apical or basolateral targeting reside within the proteins themselves and are recognized by as yet poorly defined cellular mechanisms that operate at several different steps in the membrane trafficking process. It is clear that the correct localization of a number of membrane transporters is essential for the function of most polarized epithelium (15). Abnormal localization of ion transporters is known to be associated with a number of disorders, such as polycystic kidney disease (PKD) (91) and the loss of normal membrane polarity is frequently found in cancer and as a consequence of oncogene expression (15,92,93). Far less understood, however, is the role that loss of cell polarity plays in disease itself. Is mislocalization of membrane proteins a symptom or a causal element?

Receptors for growth factors and cytokines, such as EGF also display a polarized distribution in epithelial cells as do the autocrine ligands which activate these receptors (94-96). An assumption underlying models relating abnormal receptor distribution with diseases is that there is a functional consequence of specific receptor mislocalization. Although it is clearly necessary to have receptors colocalized with their activating ligand, the ability of receptors to signal could also depend on their coincidence with substrates (97). In addition, the ability of regulatory molecules to modulate receptor signaling could also depend on their colocalization. To date, however, no studies have addressed the consequences of receptor mislocalization on their regulation and signaling.

Overexpression of EGFR causes missorting of EGFR to the apical cell surface - To determine the effect of EGFR mislocalization on its activity, we needed to express the EGFR in an epithelial cell that could be grown as a polarized monolayer. Extensive work on HMEC showed that they would not form tight junctions on transwells. Thus we could not use this cell type to look at the role of EGF localization on its biological activity. Note that this is a methodological problem. It is quite likely that EGFR display a polarized distribution in vivo. Due to the limitations of current experimental protocols, however, cells that are useful for in vitro studies must form electrically tight junctions when grown on transwells. This restricts the cell types that can be used for these studies. After extensive consultations with other scientists, we settled on using the LLC PK1 epithelial cell line.

For our studies, EGFR were overexpressed in a clone (Cl4) of the LLC PK1 polarized porcine kidney epithelial cell line. The parental Cl4 cells expressed approximately  $3 \times 10^4$  EGFR per cell ( $\sim 2.2 \times 10^4$  basolateral and  $\sim 5 \times 10^3$  apical EGFR per cell) as determined by  $^{125}\text{I}$ -EGF binding studies at  $0^\circ\text{C}$  (Fig. 15). Transfection of Cl4 cells with a vector containing the full-length human EGFR cDNA resulted in stable transfectants (K2 cells) expressing approximately  $1.4 \times 10^6$  EGFR per cell basolaterally and  $5 \times 10^5$  apically, as determined by ligand binding analysis at  $0^\circ\text{C}$  (Fig. 15). Thus, K2 cells expressed many more EGFR apically than the total receptor

complement of the parental cell line. EGFR overexpression did not diminish the formation of highly electrically resistant monolayers. The measured transepithelial resistance of confluent K2 monolayers was typically greater than 600 ohms-cm<sup>2</sup>. Since the ratio of apical to basolateral EGFR for K2 cells (1:3) was greater than the parental cell line (1:4.4), the overexpression of EGFR in K2 cells resulted in mislocalization of receptors to the apical cell surface. The apical and basolateral EGFR expressed by the parental C14 and transfected K2 cells were comprised of both low ( $K_d = 10^{-7}M$ ) and high ( $K_d = 10^{-9}M$ ) affinity classes of receptors.

Activation of apical or basolateral EGFR causes cell proliferation - To determine whether the EGFR expressed on the apical or basolateral cell surfaces possessed biological activity, we examined cell proliferation in confluent cell monolayers following the addition of EGF to the apical or basolateral compartment. Similar levels of <sup>3</sup>H-thymidine incorporation were observed in response to either apical or basolateral EGFR activation over an 18 hour period (Fig. 16A). The simultaneous addition of EGF and an antagonistic anti-EGFR antibody to the ipsilateral side of the monolayer resulted in a significantly diminished mitogenic response. Addition of anti-EGFR antibody contralaterally to EGF had no effect. This demonstrated the specificity of EGFR-mediated proliferation and that there was no significant leakage of EGF through the polarized epithelial monolayer.

The addition of EGF to the apical or basolateral compartments of K2 cell monolayers, increased cell numbers as well (Fig. 16B). There was a 1.6-fold increase in cell number above control following apical EGF and a 1.4-fold increase following basolateral EGF. This corroborated the increased thymidine incorporation by K2 cells following either apical or basolateral EGF addition with an actual increase in cell numbers.

EGFR down-regulation is more efficient from the basolateral cell surface - Previous studies have shown that a major mechanism for attenuating EGFR-mediated cell proliferative signaling is through internalization of the EGFR. In fact, kinase-active EGFR mutants incapable of internalization caused unregulated growth that ultimately resulted in cell transformation. Furthermore, angiotensin II receptors at the apical and basolateral cell surfaces of polarized renal epithelial cells demonstrated different rates of down-regulation and endocytosis, suggesting that the machinery for receptor downregulation may differ between the apical and basolateral membrane surfaces. This led us to examine the efficiency of EGF-induced down-regulation of apical and basolateral EGFR.

K2 cells were incubated with high concentrations of EGF and the number of receptors remaining on the cell surface as a function of time was determined by <sup>125</sup>I-EGF binding at 0°C. Basolateral EGFR showed a continuous decrease in numbers for the entire incubation period, reaching approximately 20% of initial numbers (Fig. 17). In contrast, the apical EGFR displayed an initial drop, but then remained constant at 60% of the initial receptor levels. These data suggest that EGFR down-regulation is less efficient from the apical than basolateral cell surface. This inefficiency of down-regulation of apical EGFR might be due to a decreased rate of ligand-induced disappearance of EGFR from the apical cell surface. We tested this by examining the rates of ligand-induced endocytosis of apical and basolateral EGFR. Endocytosis of the EGFR was significantly faster at the basolateral than apical cell surface (Fig. 18A). Previous studies have demonstrated that ligand-induced endocytosis of the EGFR is dependent on a specific cytoplasmic domain of the EGFR. To ensure that the faster rate at the basolateral surface did not simply reflect a different net rate of endocytosis from the two surfaces, a mutated EGFR, c'973, was expressed in C14 cells. This receptor mutant possesses intrinsic tyrosine kinase activity, but lacks the domains necessary for ligand-induced endocytosis (3,4). There were no differences in apical versus basolateral endocytosis of c'973 receptors (Fig. 18B).

EGFR tyrosine kinase activity differs between the apical and basolateral surfaces - Since there were spatial and temporal differences between apical and basolateral EGFR regulation, we wondered whether apical EGF would cause greater EGFR tyrosine kinase activity than basolateral EGF. Confluent monolayers of K2 cells grown on permeable filter inserts were serum-starved for 18 hours after which 50ng/ml of EGF was added at time zero to either the apical or basolateral compartment. At various timepoints during a 20-hour duration following EGF addition, EGFR phosphotyrosine levels were determined by western blot (Fig. 19). EGFR tyrosine phosphorylation was greater in response to basolateral than apical EGF through 60 minutes, which paralleled the greater numbers of basolateral than apical EGFR per cell. However, the attenuation of EGFR tyrosine kinase activity differed between the apical and basolateral cell membrane surfaces starting at 4 hours. There was a significant decline in detectable tyrosine phosphorylated basolateral EGFR by 4 hours and none detected by 20 hours, whereas, tyrosine phosphorylated apical EGFR were still present 20 hours after EGF stimulation. The delayed attenuation of tyrosine phosphorylated apical relative to basolateral EGFR could explain why EGFR-mediated proliferation was stimulated to a similar level 18 hours following apical or basolateral EGF even though there was a nearly 4:1 ratio of basolateral to apical EGFR.

EGF-induced tyrosine phosphorylation of substrates mediating cell proliferation - Since cell proliferation was similarly induced by apical and basolateral EGF, we asked whether activation of EGFR substrates involved in cell proliferation was similar as well.

The signal transduction cascade mediating EGFR-induced mitogenesis has been characterized. The protein SHC (Src-homologous and collagen protein) is a known substrate of the EGFR and is important in EGFR-mediated mitogenesis via activation of the Ras-MAP Kinase pathway (98). The phosphotyrosine content of SHC was determined by western blotting of SHC immunoprecipitates from K2 monolayers on filters following the addition of EGF to the apical or basolateral compartment. SHC tyrosine phosphorylation increased following either apical or basolateral EGFR activation (Fig. 20). In addition, we examined the phosphotyrosine content of ERK1 and ERK2, which are substrates at the downstream end of the EGFR-Ras-MAP Kinase signal transduction pathway. Both ERK1 and ERK2 immunoprecipitates were tyrosine phosphorylated to a similar extent in response to apical or basolateral EGFR activation by western blot analysis (data not shown). These results were consistent with the similar levels of cell proliferation following either apical or basolateral EGFR stimulation, and demonstrated a lack of compartmentation of EGFR substrates involved in EGFR-mediated cell proliferation.

EGF-induced tyrosine phosphorylation of substrates in cell adhesions - Due to previous studies demonstrating differences in apical and basolateral receptor signaling in polarized epithelial cells, we furthered our search for differences in apical and basolateral EGFR signaling. We chose to study EGF-induced tyrosine phosphorylation of substrates in cell adhesion structures since their localization in polarized epithelial cells is well defined. Focal adhesions are localized to the basal cell surface of cells where they provide connections between the extracellular matrix and cytoskeleton. Focal adhesions contain several cytoplasmic proteins, including focal adhesion kinase (FAK) which can be tyrosine phosphorylated in response to various growth factors. Adherens junctions are formed along the lateral cell surfaces of polarized epithelial cells at cell-cell junctions where they mediate cell-cell adhesion. Beta-catenin, a known EGFR substrate, is an important component of adherens junctions. The highly localized distributions of FAK and beta-catenin in polarized epithelial cells made them likely candidates for differential phosphorylation by apical and basolateral EGFR. To test this prediction we examined EGF-induced tyrosine phosphorylation of FAK and beta-catenin.

EGF was added for 15 minutes to either the apical or basolateral compartments of K2 monolayers, after which phosphotyrosine levels of immunoprecipitated FAK and beta-catenin were determined by western blots. An increase in FAK tyrosine phosphorylation above the control (no EGF) was stimulated by basolateral EGFR activation (Fig. 21). Constitutive FAK tyrosine phosphorylation was seen in the absence of EGF, probably reflecting autocrine growth factor production. There was no increase in FAK tyrosine phosphorylation above constitutive levels following apical EGF. Paxillin, another focal adhesion protein, showed only low constitutive levels of tyrosine phosphorylation which failed to increase significantly following either apical or basolateral EGFR stimulation (data not shown).

In striking contrast, beta-catenin immunoprecipitated from total cell lysates was tyrosine phosphorylated to a much greater degree in response to apical than basolateral EGFR activation (Fig. 22A left panel). The loading controls (Fig. 22A right panel) demonstrated two bands immunodetected as beta-catenin. The lower band corresponded exactly to tyrosine phosphorylated beta-catenin on the anti-phosphotyrosine blot and the upper band non-tyrosine phosphorylated beta-catenin. Only the lower (tyrosine phosphorylated) band was seen in any of the lanes on the anti-phosphotyrosine western blot (Fig. 22A left panel). What was apparent from the two western blots was that much more tyrosine phosphorylated beta-catenin was immunoprecipitated following apical than basolateral EGFR stimulation from whole cell lysates. This led us to examine which cell fractions tyrosine phosphorylated beta-catenin was in.

In a separate experiment, EGF was added apically or basolaterally to K2 monolayers for 15 minutes after which they were lysed in a 1% Triton X-100 containing buffer. The pellet fraction was isolated from the supernatant (Triton-soluble) fraction by centrifugation and resolubilized in an SDS-based buffer. Beta-catenin forms complexes with E-cadherin at the adherens junction and in the cytoplasm. Therefore, beta-catenin was coprecipitated with E-cadherin from the Triton X-soluble fraction (Fig. 22B). Equal amounts of E-cadherin were immunoprecipitated from the Triton-soluble fraction (data not shown). Similar levels of beta-catenin coprecipitated with E-cadherin regardless of the degree of beta-catenin tyrosine phosphorylation (compare Fig. 22B left and right panels). However, tyrosine phosphorylation of the coprecipitated beta-catenin was much greater following apical than basolateral EGF (Fig. 22B left panel). No tyrosine phosphorylation of E-cadherin was seen in response to EGF stimulation (data not shown). The same Triton X-soluble fractions that had been immunodepleted of E-cadherin (data not shown), were then used to immunoprecipitate beta-catenin. Again, only apical EGFR stimulation led to tyrosine phosphorylation of beta-catenin (Fig. 22C). This further suggests that not all beta-catenin was complexed with E-cadherin in the Triton-soluble fraction.

Beta-catenin was immunoprecipitated from the Triton-insoluble fraction under denaturing conditions. Again, tyrosine phosphorylation of beta-catenin was greater following apical than basolateral EGFR stimulation (Fig. 22D left panel). Furthermore, more beta-catenin protein was found in the Triton-insoluble fraction following stimulation of apical than basolateral EGFR (Fig. 22D right panel).

In K2 cells, beta-catenin localized to the lateral cell membrane by XZ-plane confocal microscopy (Fig. 23A), but specific cytoplasmic staining was seen as well on XY-plane scans (Fig. 23B). Beta-catenin tyrosine phosphorylation did not change its lateral membrane localization by confocal microscopy in response to apical or basolateral EGFR activation when compared to controls cells (no EGF) (data not shown).

Our studies revealed that EGFR regulation and EGFR-mediated tyrosine phosphorylation of beta-catenin are compartmentalized in polarized epithelial cells. This implies a higher-order



level of regulation of EGFR signaling in polarized epithelial cells based on the spatial compartmentalization of specific substrates. Thus, mislocalization of EGFR in polarized epithelium, through EGFR overexpression or the loss of cell polarity as occurs in certain diseases, may contribute to the pathogenesis of those disorders by resulting in aberrant EGFR signaling.

Task2: Determine whether oncogenic forms of the EGF receptor found in breast cancer display the same pattern of spatial regulation and biological activity as activated, wild type EGF receptors. A naturally occurring EGFR mutant that lacks introns 2-7 ( $\Delta$ EGFR) of the wild type receptor is found in about 20% of glioblastoma multiformae and is also found in 78% of breast carcinomas (49). This molecule, when expressed in a glioblastoma cell line, appears to greatly increase the tumorigenicity of those cells. This receptor has also been reported to transform 3T3 cells. This mutant receptor does not bind EGF but does display a basal level of phosphorylation in the absence of ligand binding. This low level kinase activity has been implicated in the transforming properties of the  $\Delta$ EGFR since elimination of endogenous kinase activity through mutations abrogates its oncogenic activity.

To date, the function of the  $\Delta$ EGFR has been investigated in cells that normally do not require EGF for growth. These studies have resulted in the hypothesis that the  $\Delta$ EGFR functions as a constitutively active EGFR. Such a receptor would not be subject to downregulation, would continuously signal and would thereby cause uncontrolled cell growth. We sought to test this idea by examining the effect of this receptor on cells that require EGF for normal growth and behavior. By selectively blocking the activity of the endogenous receptor it would be possible to determine the contribution of the  $\Delta$ EGFR to the behavior of these cells.

We isolated a series of clones that express different levels of the  $\Delta$ EGFR as well as high levels of the endogenous EGFR. We compared the behavior of these clones to that of the parental cell line HMEC 184 A1L5. We compared the behavior of these cells to those expressing a secreted form of EGF (sEGF). The sEGF molecule lacks both the amino and carboxy-terminal extensions of the naturally occurring EGF precursor and is constitutively secreted into the medium. As a result of the constant presence of the biologically active form of EGF, these cells possess receptors that are chronically signaling.

Examination of these different cell types showed that in mammary epithelial cells, the  $\Delta$ EGFR does not substitute for an occupied EGFR. We found that this receptor, when expressed in cells that are immortalized but not transformed, does not result in transformation. Rather, it renders the cells more sensitive to the absence of EGF and also results in reduced cell migration. It also enables the cells to undergo more crowding and results in an apparent "blindness" to neighboring cells. We hypothesize that this behavior may be due to the mutant receptor interfering with the normal functioning of the endogenous receptor rather than being caused by a unique property of the mutant receptor.

## Materials and Methods

*General* - HMEC 184A1L5 cells grown in medium DFCI-1 were transduced with retrovirus containing the  $\Delta$ EGFR and G418 resistance (a kind gift of H.-J. Su Huang of the Ludwig Cancer Institute). They were selected in medium containing 100  $\mu$ g/ml G418 and examined by flow cytometry for the presence of  $\Delta$ EGFR at the cell surface which was detected using the  $\Delta$ EGFR specific monoclonal antibody D806 followed by FITC-labeled secondary antibody. The levels of fluorescence of the transduced cells were compared to parental cells and indicated that a small population of cells did express the oncogenic receptor. Subsequent to FACS analysis the

cells were diluted to clonal densities and grown in medium containing G418 until enough cells were generated to permit analysis by Western blot.

Matrigel experiments were performed in 12 well plates. Each well was coated with 0.7 ml matrigel (Collaborative Research) prior to seeding with 70,000-100,000 cells. Cells were maintained in either DFCI-1 -EGF, +EGF or + 10  $\mu\text{g}/\text{ml}$  225 mAb; fresh medium was added every 2 days. The cells were photographed on a Nikon inverted microscope using a Nikon 35 mm camera.

*Western blot analysis* - Western blot samples were obtained by scraping cells into a small volume (1 ml) of DMEM medium containing 25 mM Hepes buffer and the protease inhibitors pepstatin, chymostatin, aprotinin, leupeptin and iodoacetic acid followed by centrifugation to pellet the cells. Pelleted cells were extracted in a small volume of 1% Triton X-100, 50 mM Tris pH 7.2, 150 mM NaCl and the protease inhibitors mentioned above (100 $\mu\text{g}/\text{ml}$ ). The clarified cell extracts were boiled in 2% SDS and placed onto 5-15% gradient gels. After electrophoresis the samples were transferred to nitrocellulose and probed with the N13 polyclonal antibody that recognizes both the mutant and wild-type receptor. Anti-phosphotyrosine blots were done using the RC20 genetically engineered anti-PY antibodies from Transduction Laboratories. Anti-SHC antibodies (rabbit) and anti-rabbit IgG-HRP were also from Transduction laboratories. Blots were developed using the ECL reagents from Pierce. A polyclonal anti-phosphotyrosine antibody generated by Chemicon using laboratory-synthesized antigen was also used.

*Proliferation and migration assays* - Growth curves were generated by counting cell samples every 24 hour using a Coulter counter. Prior to starting the measurements, cells were maintained for 48 h in DFCI-1 medium lacking EGF. At time zero a cell sample was taken and either 10  $\mu\text{g}/\text{ml}$  monoclonal antibody 225 or 12.5 ng/ml EGF was added to duplicate plates of cells. Cell counts were taken over a 5 day period.

Clonal growth assays were done by diluting confluent cultures of cells 1:800 into 60 mm dishes and allowing them to grow for three weeks in the presence of control medium (DFCI-1), or with either 10  $\mu\text{g}/\text{ml}$  monoclonal antibody 225 or 12.5 ng/ml EGF. The cells were then stained with crystal violet.

Cell migration assays were performed by scraping cells from 60 mm plates at time zero and then measuring the distance recolonized every 24 h. Measurements were made using a Wild dissecting microscope with an ocular micrometer mounted in the eyepiece. Cells were cultured overnight in the absence of hormone prior to day zero and then placed into fresh medium after scraping.

*Immunoprecipitations* - Both WT and  $\Delta\text{EGFR}$  were immunoprecipitated using Sepharose beads to which were coupled the appropriate antibody. Antibodies were coupled to Protein A Sepharose beads using a rabbit anti-mouse antibody as an intermediate. The antibodies were cross-linked to the beads using dimethyl pimelimidate. After washing the beads they were added directly to cell extracts (made as described above) and the mixture rocked for 1.5 h at 4°C. The beads were washed 5X with a solution containing 300 mM NaCl, 0.1% SDS, 0.05% NP40 and 10 mM Tris pH 8.3 and then boiled in SDS-PAGE sample buffer. SHC was immunoprecipitated from cell extracts using a polyclonal anti-SHC antibody (Transduction Laboratories). Cell extracts were prepared from 100 mm plates of washed cells by scraping the cells into a 1.5 ml volume of PBS containing 25 mM Hepes buffer and 1 mg/ml BSA as well as 10  $\mu\text{g}/\text{ml}$  of the protease inhibitors pepstatin, chymostatin, aprotinin and leupeptin and 1 mM sodium orthovanadate and 10 mM NaF. After centrifugation and resuspension in PBS containing protease and phosphatase inhibitors, cells were recentrifuged and then extracted

with 250ul Triton extract buffer (1% Triton X-100, 150 mM NaCl, 10% glycerol, 10 mM Na pyrophosphate, 1 mM EGTA, 4 mM iodoacetate, 1 mM orthovanadate, 10 mM NaF, 100  $\mu$ g/ml pepstatin, chymostatin, aprotinin and leupeptin 50 mM HEPES, pH 7.0.). After 10 min on ice the extracts were centrifuged at 18,500xg for 10 min at 4°C and the supernatant removed. Protein concentration was determined using the BCA reagent kit (Pierce) and all samples were adjusted to equal protein levels. Extracts were incubated with preimmune rabbit IgG coupled to Protein A Sepharose for 30 min, centrifuged and 2.5  $\mu$ g of anti-SHC antibody was added. After 60 min on ice, Protein A Sepharose was added and the samples rocked for 60 min in a cold room. After centrifugation, the Protein A beads were washed twice in 1% Triton X-100 buffer and then boiled in SDS sample buffer. Samples were electrophoresed on 5-15% gradient gels and transferred to nitrocellulose. The resulting Western blots were probed with RC20 anti-phosphotyrosine antibody (Transduction Laboratories) as described above.

## Results and Discussion

Eighteen G418 resistant clones were generated by transduction with retrovirus. Initial FACS analysis revealed that only a small portion of the cells transduced with virus were positive for the mutant receptor. This result was probably misleading because the antibody directed against the mutant receptor also mildly cross-reacted with the endogenous receptor, resulting in a poor signal to noise ratio. Following generation of clones from the total transduced population, we quantified the expression level of the  $\Delta$ EGFR by Western blot (Fig. 24) The polyclonal antibody N13, which recognizes both the WT and mutant receptor, was used to detect the receptor. The blots revealed that there were 9 positive clones expressing a wide range of mutant receptor mass. Phosphorimager analysis showed that expression of  $\Delta$ EGFR ranged from 15% of the endogenous receptor level to clones in which there was 3-fold more mutant than wild type receptor (see Table 3). For our studies we chose to examine 3 or 4 different clones: #2 in which there are equivalent levels of mutant and WT receptor, #5 in which one quarter of the receptors are mutant, #16 in which one fifth are mutant and #11 in which three quarters of the receptors are mutant. Scatchard analysis of these clones revealed that all but #16 had similar levels of endogenous receptor as the parental cells; clone 16 expresses approximately 55% of the parental level of receptor (data not shown).

**Table 3.** Quantitation of  $\Delta$ EGFR expression in mammary epithelial cells

Clone #	WT EGFR level	$\Delta$ EGFR level	% $\Delta$ EGFR
1	13.9	13.8	50
2	47.6	46.6	49
3	53.9	9.7	15
4	45	12.2	21
5	21.9	7.2	25
6	5.8	ND	--
7	3.7	ND	--
8	4.2	ND	--

9	30.9	ND	--
10	9	2.9	25
11	53.3	167.9	76
12	21.7	ND	--
13	0.6	ND	--
16	16.6	2.7	19
17	93.9	ND	--
19	25.6	19.5	43

Receptor levels are expressed in arbitrary densitometer units.  
ND; not detected.

Since the acquisition of the  $\Delta$ EGFR by cells seems to coincide with a rapid and aggressive tumor growth, we first examined the growth rate of our clones relative to the non-transduced parental cell line. We compared the growth rates of these cells in either complete DFCI-1 medium (containing 12.5 ng/ml EGF) or in DFCI-1 medium lacking EGF and containing 10  $\mu$ g/ml 225 mAb which binds to the WT EGFR and prevents ligand binding. As seen in Fig. 25, both the low expressing clone and the parental cell line grew at similar rates in complete medium. In contrast, the clone expressing the highest amount of  $\Delta$ EGFR grew at a much slower rate. When cells were put into medium containing antagonistic anti-EGFR mAb 225, all the cells grew more slowly but the parental cell displayed the least inhibition. Both the high and low expressing clones displayed negligible growth. The inability of the  $\Delta$ EGFR to support cell growth under these conditions strongly suggests that this receptor does not substitute for an occupied EGFR in these cells.

Results similar to these were obtained from a clonal growth experiment. Cells were split 1:800 and allowed to grow for 3 weeks in DFCI-1 medium either lacking EGF (control), containing 12.5 ng/ml EGF or containing 10  $\mu$ g/ml 225 mAb. Cells expressing sEGF were included for comparison, since these cells have a full complement of activated EGFR (see task 4 below). As can be seen in Fig. 26, the sEGF cells were insensitive to the absence of EGF or the presence of anti-EGFR 225 mAb. In contrast, the parental cells (WT) reached confluence in the presence of EGF, grew slower in the absence of EGF and had essentially no clonal growth in the presence of 225 mAb. Both the high (#11) and low (#16)  $\Delta$ EGFR expressing clones showed lower growth at clonal densities. In particular, these clones were much more affected by the absence of EGF from the medium than was the parental cell. This slower growth was not due to a lowered autocrine capacity in the transductants since RT PCR revealed similar levels of messenger RNA for the EGFR ligands TGF- $\alpha$ , amphiregulin, EGF and HB-EGF in all cell types (data not shown).

It remained possible that the 225 mAb used in the two previous experiments was inhibiting the constitutive activity of the  $\Delta$ EGFR, thus explaining its apparent lack of biological activity. To explore this question, we treated both control cells and cells expressing high levels of  $\Delta$ EGFR with either EGF or 225 mAb. After treatment, we sequentially immunoprecipitated the  $\Delta$ EGFR and WT EGFR, ran the samples on gels and then, following transfer to nitrocellulose, evaluated their phosphotyrosine content by Western blot. As shown in Fig. 27, the anti- $\Delta$ EGFR antibody selectively immunoprecipitated the mutant receptor. The small band seen in the WT cells treated with 225 mAb is due to immunoprecipitation via the prebound 225 mAb. The



anti-phosphotyrosine Western blot shows that the  $\Delta$ EGFR indeed have constitutive kinase activity and that this activity is not affected by 225 mAb treatment. As expected, the WT EGFR only showed significant phosphotyrosine content in the presence of EGF. These results show that 225 mAb does not affect the activity of the  $\Delta$ EGFR and thus the ability of the antibody to block the growth of cells expressing the  $\Delta$ EGFR must be due to its inhibition of the WT EGFR. Therefore, the  $\Delta$ EGFR does not behave like an occupied EGFR.

Despite the fact that the  $\Delta$ EGFR did not support the growth of the cells in the absence of EGF, it remained possible that it could constitutively stimulate other EGFR-mediated cell responses. We chose to examine cell migration initiated in response to a "wound" scraped in a monolayer of cells. This assay was done with cells maintained in the presence or absence of 12.5 ng/ml EGF. Prior to initiating this assay the cells were maintained overnight in the absence of EGF to ensure that all cells started at the same level of growth factor stimulation. Cells were scraped from a line in the plate with a rubber policeman and, after rinsing, the scraped area was marked and measured. After each measurement additional EGF was added to the +EGF plate in a volume of 1  $\mu$ l/ml of medium to ensure that the ligand was not depleted over the course of the experiment.

As shown in Fig. 28 cells expressing sEGF had high rates of migration regardless of the addition of EGF. In contrast, the parental cells exhibited little migration when no EGF was present but displayed a comparable level of motility in the presence of EGF. All of the cells expressing the mutant receptor had low rates of migration in the absence of ligand and also had lower rates of migration in the presence of EGF. Indeed, the ability to migrate was inversely proportional to the level of mutant receptor expression. It thus appears that the  $\Delta$ EGFR inhibits the EGF-stimulated migratory response.

In a recent paper about receptor chimeras, the authors reported that the adaptor protein SHC is required to produce a migration response in their transfected cells. We therefore decided to examine whether there was an alteration in SHC levels in our cells and determine whether SHC is able to interact with either the endogenous or mutant receptor. We did this by immunoprecipitating SHC from extracts of cells maintained in medium lacking EGF or exposed to EGF for 5 min (all extract aliquots were first equalized for protein) or directly visualizing SHC from a portion of these extracts via Western blot. These results are shown in Fig. 29. In the parental cells, there is little SHC phosphorylation in the absence of EGF while the sEGF cells show similar levels of phosphorylation regardless of treatment. The  $\Delta$ EGFR clones also show reduced levels of SHC phosphorylation in the absence of EGF, however they are somewhat higher than that seen in the parental cells. Phosphorylation of SHC permits its functioning as an adaptor protein in signal transduction. However, since we are dealing with a mutant receptor, it is possible that SHC is not participating in the canonical pathway. To determine whether SHC phosphorylated via the mutant receptor is functional, we also probed our SHC immuno-precipitates for the presence of Grb2, a downstream effector of SHC. This Western blot is also shown in Fig. 29. As can be seen, Grb2 is associated with SHC in all samples of the sEGF cells while it is only found in association with SHC in the parental cells when EGF has been added. Similarly, appreciable levels of Grb2 are only associated with SHC in the  $\Delta$ EGFR clone when EGF is present. This indicates that the constitutive phosphorylation activity of the mutant receptor is not sufficient to result in an interaction of both SHC and Grb2 with either the mutant or endogenous receptor. It also suggests that the lack of a migration response in these cells is probably not due to the constitutive association of SHC with the mutant receptor.

Examination of the  $\Delta$ EGFR clones via time lapse photography revealed that these cells lacked more than the ability to move rapidly. When the parental cells touched each other they

responded by membrane ruffling and also by a directed motion away from each other. Such was not the case with the mutants. Rather, these cells did not display any obvious response to touch, appearing to be blind to their neighbors. This type of behavior could be indicative of the beginning of a loss of contact inhibition. To determine whether this was the case, we looked at each cell lines ability to crowd over time. We felt that an inability to respond to neighboring cells would result in a tighter packing of the cells.

Cells were plated out on coverslips and allowed to reach confluence. Duplicate samples were then taken every other day, fixed and stained with DAPI to visualize the nuclei. Three fields were manually counted for each coverslip and the data from the duplicate samples pooled. The results are shown in Fig 30. As can be seen, there is not a major difference in the densities achieved by any of the cells. What is apparent is that the highest density is achieved by the sEGF cells and that the densities of the low expressing  $\Delta$ EGFR cells and the parental cells goes down after reaching a peak value. In contrast, the high expressing clone stays at a constant level throughout the time course of the experiment. It thus appears that cells expressing a high level of  $\Delta$ EGFR reach a greater density than parental cells.

As a final test of the functional consequences of  $\Delta$ EGFR expression, we examined the ability of the high expressing clone to form organized structures on an extracellular matrix (Matrigel). We seeded  $0.7-1 \times 10^5$  cells/well of a 12 well plate on top of a thick layer of matrigel. Cells were seeded and subsequently maintained in medium lacking EGF (control), containing 12.5 ng/ml EGF or 10  $\mu$ g/ml 225 mAb. The cells were allowed to organize over a period of at least 1 week with the medium being changed every 2 days. The results of this experiment are shown in Fig 31. As observed previously, the  $\Delta$ EGFR clone is more sensitive to the absence of EGF than is the parental cell. Similar to the parental, the  $\Delta$ EGFR clone is totally inhibited by the addition of 225 mAb. Even when EGF is added, the  $\Delta$ EGFR clone can not form the large tubular structures seen in the parental cells. In contrast, the sEGF cells show aberrant organization regardless of the type of culture medium.

Expression of high levels of wild-type EGFR does not inhibit cell function – It seemed possible that one reason that the cells grew poorly after expressing the  $\Delta$ EGFR was due to the high levels of EGFR expression. It has previously been shown that occupancy of high levels of normal EGFR can inhibit cell growth. Thus expression of high levels of the constitutively active  $\Delta$ EGFR could have a similar effect. To test for this possibility, cells were transduced with the retrovirus containing the WT EGFR gene and selected in medium containing G418. After about a week in selective medium, individual clones were isolated by limiting dilution. Clones were then evaluated by flow cytometry and Scatchard analysis. The line expressing the highest levels of EGFR (line AXR1) was then used for further analysis.

As shown in Fig. 32, the parental A1-1 cell line expressed approximately  $2.5 \times 10^5$  EGFR per cell. The AXR1 line expressed nearly 10-fold greater receptor number at  $2.5 \times 10^6$ . Both lines displayed biphasic Scatchard plots, indicating multiple affinity classes of receptors (99). Interestingly, the relative fraction of high affinity and low affinity receptors was the same in the two lines, indicating that the high affinity receptor state is not due to saturation of a limiting cellular protein. The overexpression of WT EGFR was confirmed by both flow cytometry and western blot analysis (data not shown).

The growth rates of the AXR1 and parental A1-1 cells were then compared. Cells were incubated in the presence of either no EGF, 1  $\mu$ g/ml EGF or 10  $\mu$ g/ml of the antagonistic anti-EGFR antibody 225. As shown in Fig. 33, the A1-1 and AXR1 cells grew at very similar rates in the absence of EGF. Likewise, the addition of EGF stimulated the growth of both cell lines, although the effect was more pronounced in the case of the A1-1 cells. The addition of the

antagonistic anti-EGFR mAb 225 also inhibited the growth of both cell lines, showing that activation of the EGFR are required for both the parental and overexpressing cell lines.

Several conclusions can be made from this data. The first is that activation of high numbers of EGFR in HMEC is not growth inhibitory. Although the extent of growth stimulation was not as pronounced as in the parental cell line, EGF addition clearly did not inhibit the growth of the HMEC. Thus the pronounced inhibition of cell growth we observed in cells expressing the constitutively active  $\Delta$ EGFR was not simply due to high levels of activated EGFR. This supports our hypothesis that the  $\Delta$ EGFR is a "defective" receptor and generates a qualitatively different signal than a normally activated EGFR.

The second conclusion that can be made is that overexpressing the EGFR does not allow cells to grow in the absence of ligand. Blocking receptor activation by using the antagonistic 225 mAb inhibits growth of receptor overexpressing cells as effectively as the parental cells. It has been known that EGFR overexpression is associated with poor prognosis in breast cancer. It has been assumed that this reflects a degree of growth factor independence that results from receptor overexpression. This is clearly not the case. The AXR1 cells retain their dependence on EGFR ligands. An alternate hypothesis is that overexpression of EGFR results in inappropriate receptor attenuation or regulation. Studies are currently underway to determine whether this is the case with the AXR1 cells.

Even though the  $\Delta$ EGFR has constitutive kinase activity, that activity is only about 10% of the occupied WT receptor. This lowered kinase activity could be the result of a receptor conformation that is different than that of the occupied endogenous receptor. This in turn could permit the  $\Delta$ EGFR to phosphorylate different substrates resulting in altered cell behaviors. While we did not observe any overt change in phosphorylation patterns between our transduced and parental cells it remains possible that there are unique substrates present but in small amounts that are outside the limit of our Western blot detection. Alternately, a different conformation could result in molecular interactions between the phosphorylated receptor and other molecules that are not themselves phosphorylated. While we do not know the exact cause of the alteration in the behavior of these cells it is clear that such behavior can not arise because the mutant receptor is substituting for the wild type receptor in these cells.

### TASK 3: Express genetically altered EGF receptors and ligands in mammary epithelial cells

During this project, we have found that the only workable method for expressing genes in HMEC is to use retrovirus. Therefore, we have successfully mastered the methodology of generating retrovirus in our own laboratory. Previously, the receptor and ligand-containing retrovirus we have used in our experiments have been obtained from other investigators. Because we needed retrovirus encoding a variety of different customized EGFR and EGFR ligand mutants, relying on collaborators was not possible.

We generated a FLAG epitope cassette to allow us to discriminate between mutant receptors (generated by us) and the endogenous EGFR in HMEC. A second approach that we implemented in parallel with the epitope tagging efforts was to use the chicken EGFR (cEGFR) as a mutagenesis target. First, though, we needed an antibody that would react to the cEGFR, but not the human form. This was successfully accomplished by the synthesis of a peptide to sequences 139 to 154 in the cEGFR. This peptide was then coupled to keyhole limpet hemocyanin and used to generate a polyclonal antiserum. We verified by western blot analysis that this antibody would react to cEGFR, but not to the human form of the EGFR. Efforts are currently underway to affinity purify the antibody for use in immunocytochemistry.

## Materials and Methods

Three different promoters - RSV, SV40 and CMV were tested by insertion of the luciferase gene into their respective plasmids (Rep9, pX - a derivative of pBR322 and pcDNA3, respectively). Two different transfection protocols were also employed as well as three different HMEC cell lines. The cells were transiently transfected by either  $\text{CaPO}_4$  precipitation or by use of DoTap lipofectamine reagent (Boehringer Mannheim). Cells were transfected overnight using 20  $\mu\text{g}$  DNA/100 mm plate and then incubated in fresh medium lacking the transfection reagents for 24-48 h. They were then solubilized and the amount of luciferase activity in the supernatant determined using a luminometer.

*Inserting the cEGFR into a retrovirus* - The cEGFR was obtained from Dr. Nita Maihle (Mayo) and placed into Bluescript, generating EGFR/BS. To insert the cEGFR into the MFG retrovirus, the 5' and 3' ends of the gene had to be modified to Nco1 and BglII sites respectively. These compatible cohesive ends were generated by PCR cloning. A BglII site was created at the end of the cEGFR gene by amplifying primers containing the new site, cutting the product with Bcl1 and gel purifying the correct fragment. The cEGFR/BS was cut with HindIII, blunt ended, the a T-overhang was added. It was then cut with Bcl1 and gel purified. The cEGFR/BS fragment was then ligated to the purified PCR product. The correct clone was then picked, amplified and verified by sequencing.

The 5' end of the cEGFR was changed to BspH (compatible with Nco1). The same protocol as above was used, but this time we cut the PCR product with AflIII. The parent plasmid was cut with XbaI, blunt ended, T-overhangs were added and the plasmid was then cut with AflIII. The cut PCR product was then ligated into the parent plasmid. This was cloned, amplified and verified by sequencing.

The MFG retrovirus vector was cut with NcoI and BamHI to remove the stuffer sequence, and gel purified. The modified cEGFR/BS was cut with BspH and BglII, the appropriate fragment was gel purified and ligated into the MFG vector (100). The cEGFR/MFG vector was amplified, purified and used to transform the  $\Psi$ Crip packaging cell line (originally obtained from R. Mulligan) as described (101). Clones of transfectants were isolated and screened for those producing the highest titer. Colonies were isolated from serially diluted plates and grown to confluence in 24 well dishes. The virus-containing supernatants and the cells were frozen until all could be screened at one time.

Screening was done by seeding 184A1 cells into 24 well plates at a density of 10,000/well. When cells were almost confluent, the virus-containing supernatants were rapidly thawed at 37 °C and polybrene was added to a final concentration of 4  $\mu\text{g}/\text{ml}$ . Medium from the screening cells was removed, replaced with the test virus stocks, and cells were incubated for 4 h at 37°C with shaking every 30 min. The test virus stocks were then removed and replaced with fresh medium for an additional 2 days. The cells were then screened for the expression of the cEGFR by immunoperoxidase. Cells were fixed with paraformaldehyde, blocked with 1% BSA and incubated with 10 $\mu\text{g}/\text{ml}$  affinity purified antibody to the cEGFR. Alkaline phosphatase-conjugated secondary antibody was used in conjunction with Chromogen reagent to visualize the positive cells. The 4 producing lines that yielded the highest frequency of positive cells were thawed, expanded and used to produce large quantities of retrovirus for transducing cells.

We are currently using these virus stocks to generate HMEC cell lines that express the cEGFR. Endogenous EGFR will then be inactivated by the addition of antagonistic 225 mAb. Once we have verified that the cEGFR will support the normal biological activities of EGF in



the HMEC, then we will mutagenize the cEGFR by PCR-based mutagenesis and determine the effect of the genetically-altered EGFR in mammary epithelial cells.

*Generation of different mutant of EGFR ligands* - Several of these mutants have been inserted into retrovirus and expressed in both luminal and basal HMEC (see Task 4 below). The basic strategy was to insert an epitope tag (FLAG) at the carboxy terminus of the ligand. This allows us to track the fate of the ligand tail once the core domain of the ligand (which binds to the receptor) is released. We have also inserted a Myc epitope tag at the amino terminus of the ligand to allow us to "capture" the ligand using exogenous anti-epitope antibodies. This approach will allow us to evaluate the fate of different ligand domains following processing and to interfere with autocrine signaling in a meaningful way.

With respect to plasmid vectors, optimal transfection efficiency was achieved with the CMV promoter and HMEC 184A1L5. Owing to these results, we have utilized the pcDNA3.1 plasmid to construct our mutant receptors and have transfected HMEC 184A1L5 with DoTap. We have also inserted the first plasmid of the tetracycline-responsive 2-plasmid system into these cells using our optimized transfection protocol. We have made these cell lines available to other investigators studying breast cancer.

## Results and Discussion

This Task was basically methodological. These methods were used to successfully conduct the experiments presented in the other task sections. Thus the results and discussions on this section are contained in the appropriate sections of the other tasks.

### Task 4: Demonstrate That Mis-sorting or Inappropriate Expression of the EGF Receptor or its Ligands Provides a Growth Advantage to Normally Organized Epithelial Cells

We found that the most fruitful approach to this task was to express chimeric ligands for the EGFR. By changing the membrane-anchoring domain of the ligand, we were able to cause it to be localized to an inappropriate cellular compartment. Aspects of overexpression of the wild type EGFR in HMEC are covered under Task 3 above. Inappropriate expression and missorting of the EGFR in polarized epithelium was covered under Task 1 above.

All the EGFR ligands consist of a conserved receptor-binding core domain flanked on the carboxy side by a membrane-spanning domain and on the amino side by a highly variable extracellular extension (102). These extensions can be proteolytically removed prior to release of the ligand, such as the case with TGF $\alpha$  (103). In other ligands, such as HB-EGF, most of the amino-terminus is retained, which allows binding to extracellular glycosaminoglycans or to other cell surface molecules (104). This extra-receptor binding can have profound effects on cell responsiveness in vitro and presumably in the intact animal (105). The proteolytic release of ligands, such as HB-EGF can change their activity from juxtacrine to paracrine (106). The transmembrane and cytoplasmic domains of the different ligands are also diverse which may regulate cellular transport, localization or proteolytic release (107)). Although the membrane anchoring domain of EGFR ligands may regulate their cellular distribution, it remains to be demonstrated that altered cellular distribution has an impact on their biological activity.

Understanding the role of the membrane-anchoring domain of EGFR ligands is complicated by the fact that most cells making EGFR ligands also express the EGFR. Disruption of the EGFR gene in mice has shown that epithelial cells are most profoundly affected by receptor loss (66,108,109). These cells, such as those found in the gut, the kidneys and epidermis, have all been shown to express one or more EGFR ligands (110-113). Although membrane-anchored growth factors have been shown to be biologically active in a juxtacrine fashion (114,115), these studies have used experimental systems in which the cell type

expressing the ligand is distinct from the cell type expressing the receptor. In this situation, it is relatively simple to envision how spatially restricted juxtacrine signaling could play an important role in tissue organization. If a cell expresses both a receptor and a membrane-anchored growth factor, however, then juxtacrine signaling is unlikely to indicate cellular context. In addition, membrane-anchored EGFR ligands can be converted into soluble forms that are also biologically active (102,103). Thus the function of the membrane-anchoring domain in autocrine signaling is unclear.

To explore the role of the membrane anchoring domain in EGFR ligand function, we constructed two derivatives of EGF: one lacking and one possessing the natural transmembrane domain. These artificial ligands were then expressed in HMEC cells to determine how they affected cell behavior. Surprisingly, we found that removal of the transmembrane domain resulted in a non-interruptible autocrine loop, apparently by an intracrine mechanism. Significantly, these cells could not organize into complex structures when grown on a reconstituted basement membrane. Our results suggest that an important function of the membrane-anchoring domain of EGF is to restrict the cellular location of receptor-ligand binding.

These results also suggested to us that the proteolytic release of the EGFR ligands from their membrane anchor may be involved in regulating their biological activity. All these ligands are made as membrane-spanning prohormones that are processed and released through regulated proteolysis (102). Although the identities of all the proteases involved have not been definitively established, metalloprotease inhibitors, such as TAPI and batimastat, are particularly effective in blocking the release of EGFR ligands from the cell surface (116-118). Recent data suggests that the release of TGF- $\alpha$  involves TACE, a member of the ADAM family of metalloproteases which was originally identified as being responsible for the release of TNF $\alpha$  (119).

Interestingly, knockout of the TACE gene in mice results in a similar phenotype to knockout of the EGFR (120). Although these data have been interpreted to indicate that proteolytic release of EGFR ligands is important in receptor function *in vivo*, this conclusion is contradicted by numerous *in vitro* studies which show that membrane-anchored growth factors are biologically active in a juxtacrine fashion (114,115,121,122). One possible explanation is that the activities of membrane-anchored ligands are distinct from those of the soluble forms. Perhaps juxtacrine ligands mediate short range signaling whereas soluble ligands operate on distal cells. Alternatively, the *in vitro* studies on membrane-anchored ligands may have been misleading. These studies have typically used artificial systems in which the cell expressing the ligand is distinct from the cell expressing the receptor (114,115,121,122). Most EGF-dependent cells, have been shown to express one or more EGFR ligand in an autocrine fashion (110-113). In addition, EGFR ligands stimulate a number of different biological responses in these cells, such as proliferation and migration, which may display different sensitivities to membrane-anchored versus soluble ligands (123). Because of limitations in previous experimental systems, the relative activities of soluble versus membrane-anchored ligands have been difficult to compare.

The release of several EGFR ligands can be blocked by metalloprotease inhibitors (116-118). One of these, batimastat, is a member of a class currently in clinical trials as inhibitors of tumor metastasis (124,125). If proteolytic release of EGFR ligands is important for their activities, then inhibiting this process with batimastat should significantly alter EGFR-mediated cell responses such as proliferation and migration. We found that blocking the proteolytic release of EGFR ligands essentially abolishes their biological activities, suggesting that at least some membrane-anchored forms of EGFR ligands are functionally inactive. In addition, the

efficiency at which batimastat blocks proliferation and migration of epithelial cells suggests that much of its anti-metastatic activity may be mediated by interference with autocrine signaling through the EGFR system.

## Materials and Methods

*General* - Monoclonal antibody 225 (mAb 225) directed against the EGFR (126) was isolated from a hybridoma cell line obtained from the American Type Culture Collection. Monoclonal antibody 13A9, which binds to both occupied and empty EGFR (127) was obtained from Genentech. Monoclonal antibody HA directed against EGF was a kind gift from Katsuzo Nishikawa of the Kanazawa Medical University in Japan (128). Recombinant EGF (QBC, Inc) was conjugated to keyhole limpet hemocyanin (KLH) using sulfo-MBS (Pierce Chemical Co.) after first introducing a sulfhydryl group using Traut's Reagent according to manufacturer's instruction. The KLH-EGF conjugate was used as an antigen to produce rabbit antisera. Polyclonal antibodies against the EGFR were raised in rabbits against affinity purified EGFR (129). Vector pEGF-1 containing the mature sequence of human EGF was a gift from Salil Niyogi (130). LambdaEGF116 containing the entire coding sequence for human EGF was obtained from the ATCC. Human mammary epithelial cells 184 and line 184A1 (substrain L5) (131) were obtained from Dr. Martha Stampfer and cultured in either MCDB 170 (132) or medium DFCI-1 as described (133). Antibodies coupled to Protein A Sepharose beads were cross-linked to the beads using dimethyl pimelimidate and quenched using ethanolamine as described (134). Beads were washed extensively and then directly added to the cell extracts.

*Construction of sEGF and EGF-Ct* - An artificial secreted form of human EGF (sEGF) was constructed using an artificial DNA sequence derived from the amino acid sequence of mature human EGF (130) fused to 200 bp fragment of the 5' untranslated region and adjacent signal sequence of the EGFR. The EGF DNA was removed from pEGF-1 by digesting with *Eag*I, endfilling with Klenow, and digesting with *Eco*RI. The EGF DNA was ligated to pBluescript (Stratagene) that was digested with *Hind*III, endfilled with Klenow and digested with *Eco*RI to create pBluescript-EGF. The 5'-untranslated region and signal sequence of the EGFR were isolated by PCR with primers to the SP6 promoter (5'-GTA TTC TAT AGT GTC ACC TA-3') and the EGFR signal sequence (5'-GCC CGA CTC GCC GGG CAG AG-3') using pLOLB (135) as the template. The PCR product was digested with *Xba*I to remove unwanted vector sequences, resulting in an insert with a 5' *Xba*I end and a single 3' A-overhang left by the Taq polymerase. This insert was ligated into pBluescript-EGF that was first digested with *Eco*RI and endfilled with Klenow followed by addition of T-overhangs with Taq polymerase and digestion with *Xba*I. EGF-Ct was made by inserting the entire membrane anchoring and cytoplasmic domain from lambdaEGF116 into pBluescript-sEGF. Both lambdaEGF116 and pBluescript-sEGF were digested with *Sph*I and *Xho*I. Following gel purification, the 760 bp fragment from pEGF was ligated into pBluescript-sEGF. All constructs were verified by sequencing.

For insertion into the MFG retrovirus vector (100), *Sty*I and *Bgl*II sites were made at the 5' and 3' end of the sEGF construct using the primers 5'-CTT CGG GGA GCA GCC ATG GGA CCC TCC G-3' and 5'-AGA TCT AAC GGA GCT CCC ACC ACT-3'. This set amplified the entire sEGF gene with the appropriate new restriction sites. The product was then ligated into pBluescript following digestion with *Sma*I and addition of T-overhangs with Taq polymerase. The same protocol was followed for the EGF-Ct construct except that a compatible *Nco*I site was used instead of the *Sty*I site using the primer pair 5'-CCA TGG GAC CCT CCG GGA CG-3' and 5'-AGA TCT ACT GAG TCA GCT CC-3'. The PCR reaction mixture included 100pmol of each primer, 20ng of temple, 200 $\mu$ M of each dNTP, 25mM MgCl<sub>2</sub>, and 2.5 U of Taq

polymerase. A DNA thermal cycler (Perkin Elmer Cetus) was used for 25 cycles with an annealing temperature at 50°C. Final products were confirmed by DNA sequencing.

DNA fragments encoding sEGF or EGF-Ct were gel purified and ligated into the Nco1/BamH1 sites of the retrovirus vector MFG as previously described (100). The fidelity of the insert was verified by DNA sequencing. To generate cell lines producing recombinant retrovirus, plasmid DNAs encoding MFG-sEGF and MFG-EGF-Ct were transfected into the  $\Psi$ -CRIP packaging cell line (originally obtained from R. Mulligan) as described (101). Clones of transfectants were isolated and screened for those producing the highest viral titer.

Cells were transfected with retrovirus stock using polybrene and grown for 2 days before plating at clonal density in medium lacking EGF. Individual colonies were isolated using cloning rings and then screened by immunofluorescence and by measuring the medium for the presence of EGF as described below. All experiments were done with several independently isolated colonies and all yielded the same results.

*Organization of HMEC* - Matrigel was brought to 4°C and 0.7 ml was placed in each well of a 12 well plate on ice. The matrix was carefully overlaid with 1 ml of ice-cold MCDB 170 to achieve a flat interface and the plates were transferred to a 37°C incubator for 1 h to solidify the Matrigel. The matrix was allowed to equilibrate overnight with 2 ml of appropriate growth medium before adding cells. The cells were removed from stock plates with trypsin, counted and then 200,000 cells/well were added to the equilibrated Matrigel. After plating, the cells are examined daily and photographed.

*Measurement of EGF and EGFR* - A sandwich ELISA was developed to measure EGF levels in the medium. High binding ELISA plates (Corning) were coated with 50  $\mu$ l of monoclonal antibody HA against EGF (5-10  $\mu$ g/ml) diluted in phosphate-buffered saline pH 7.4 with 0.02% sodium azide (PBSN). The plates were rinsed 4 times with wash buffer (0.05% Tween-20 in PBSN) before each new addition. The plates were then blocked using blocking buffer (10% horse sera in PBSN). Human recombinant EGF was diluted in blocking buffer for a standard curve ranging from 3 to 100 pg. A rabbit polyclonal serum directed against EGF was used as a secondary antibody diluted 1:100 in blocking buffer. Alkaline phosphatase-conjugated goat anti-rabbit antibody (Sigma) was used as the tertiary antibody at a dilution of 1:6000. The ELISA was developed by rinsing the plates twice with 10mM diethanolamine, 0.5 mM  $MgCl_2$ , pH 9.5 and then adding 50  $\mu$ l of 1mg/ml dinitrophenol (Sigma) dissolved in the same buffer. The reaction was allowed to go for 4-10 minutes and then quenched with 0.1M EDTA. The ELISA plates were read at 405nm using a SpectraMax microplate reader.

A sandwich ELISA was developed to measure total EGFR levels in cell extracts. The protocol is the same as for sEGF above, with the substitution of monoclonal antibody 13A9 against the EGFR (10  $\mu$ g/ml) and polyclonal anti-EGFR antiserum #448 at a 1:250. Cells were extracted (250  $\mu$ l per 10 cm dish) in 50 mM HEPES (pH 7.0), 150 mM NaCl, 10% glycerol, 1% Triton X-100, 4 mM sodium iodoacetate, 1 mM EGTA and 10  $\mu$ g/ml each of aprotinin, leupeptin, chymostatin and pepstatin. Cells were removed by scraping, transferred to 1.5 ml microfuge tubes and incubated at 0°C for 10 min. Cell debris was removed by centrifugation at 10,000  $\times$  g for 10 min. Protein concentrations were normalized between all samples before the assay using the BCA assay (Pierce Chemical Co.). A431 cell membranes were used as relative EGFR standards (136). The addition of EGF to the A431 cell membranes confirmed that the EGFR ELISA did not discriminate between empty and occupied receptors.

*Ligand cleavage* - Cells were plated into 6-well plates and grown overnight until near confluence. Cells were then treated with or without 5  $\mu$ M batimastat in the presence of 20  $\mu$ g/ml 225 mAb for 30 minutes. The medium was replaced with 1 ml of fresh medium



containing 225 mAb and batimistat. After 18 hours, the medium was harvested for determination of EGF concentration by ELISA as described (137). Cells were counted and ligand concentration was normalized to nanograms per million cells. Concentrations of TGF- $\alpha$  were determined by radioimmunoassay as described (138). Concentrations of amphiregulin were determined by sandwich ELISA. Capture antibody (anti-AR 6RIC 2.4) was absorbed to wells overnight (0.2  $\mu$ g/well) and blocked with 3% BSA and 0.5% Tween-20. Samples were incubated for 1 h at 37°C and secondary antibody (0.1  $\mu$ g/well biotinylated anti-AR 4.14.18) was added for 1 h at 37° followed by 0.05  $\mu$ g/ml peroxidase-conjugated streptavidin. Substrate (0.5 mg/ml O-phenylenediamine dihydrochloride) was added for 5 min and the reaction product was read in a microplate reader. Standards were recombinant human amphiregulin (R&D systems) diluted in culture medium.

*EGFR phosphorylation* - Cells were plated into 100 mm dishes and grown till near confluence and then treated with or without 10 $\mu$ g/ml mAb 225 or 10 $\mu$ M batimastat for 24 hours. 100ng/ml of EGF was added to one set of plates for 20 minutes. Cell extracts were isolated in RIPA buffer in the presence of 1mM orthovanadate and protease inhibitors (139). Equal amounts of protein were immunoprecipitated with mAb 225, rabbit anti-mouse IgG and protein A-sepharose. The immunoprecipitates were resolved on 5-10% SDS-PAGE gels and transferred to nitrocellulose membrane. The membrane was probed with HRP-conjugated anti-phosphotyrosine antibody (RC-20), followed by ECL detection (Amersham). Band density was determined using a Bio-Rad model GS-670 Imaging Densitometer. After stripping with Tris buffer containing 2% SDS, the blots were reprobed with anti-EGFR mAb C-13 and goat anti-mouse IgG HRP conjugate.

*Cell tracking* - Confluent cultures of cells split at a 1:50 ratio 20 hrs previously, were treated either with or without either EGF or batimastat for 4 hrs and mounted on a 37°C heated stage using DFCI-1 medium lacking bicarbonate but containing 25 mM Hepes. The medium was overlaid with mineral oil to prevent evaporation. Phase contrast images were taken of random fields at 10 min intervals for a total of 15 hrs using a 10X objective and Openlab software (Improvision Ltd). Cells were marked manually in the center of the nucleus at each time point using the Advanced Measurements module. The mean squared displacement of the cells as a function of time was calculated as previously described (140).

*Growth Rates* - To determine the relative growth rates of cells expressing the different EGF constructs, confluent cultures were removed from their plates (6 cm) by trypsin and resuspended in 10 ml of DFCI-1 medium lacking EGF. Aliquots of cells were counted and 15,000 cells were seeded into each 3.5 cm dish. After allowing the cells to attach overnight, the medium was changed to DFCI-1 lacking EGF or that containing either 12.5 ng/ml of EGF or 10  $\mu$ g/ml anti-EGFR mAb 225. Every two days, duplicate plates from each group were harvested and cell number determined with a Coulter counter. Culture medium was changed every two days.

To determine fraction of cycling cells, they were plated on coverslips and grown in complete DFCI-1 medium for one day. Then the cells were switched to control medium, or medium containing the indicated additives for two days. 10 $\mu$ M BrdU was added for the last 18 hours to label any cells in S-phase. Cells were stained with BrdU labeling and detection kit (Boehringer Mannheim Corp.) and counterstained with 15 nM DAPI. Random fields of cells were selected using an automated stage operated with Openlab software (Improvision, Inc.). Images of nuclei were obtained at 470 nm (DAPI) and 520 nm (BrdU) and were counted using the Openlab density slicing and automator modules. At least 20 random fields were counted for each slide. Selected manual counts were done to confirm the accuracy of the software.

To measure clonal growth of cells, confluent cultures of cells were removed from their plates with trypsin, diluted 1:800 with DFCI-1 medium lacking EGF and plated in 6 cm dishes. Approximately 18 hr later, the medium was changed to DFCI-1 lacking EGF or that containing either 12.5 ng/ml of EGF or 10  $\mu$ g/ml anti-EGFR mAb 225. Cultures were allowed to grow for 3 weeks and the media were changed every 3 days. The cells were fixed in 50% methanol and stained with 0.4% Giemsa (Sigma).

*SHC Phosphorylation* - Cells from 100mm plates were removed by scraping, pelleted and extracted for 10 min on ice using 100  $\mu$ l of 1% Triton X-100, 50 mM Tris (pH 7.2), 150 mM NaCl, 10% glycerol, 10 mM Na pyrophosphate, 1 mM EGTA, 10 mM iodoacetic acid, 1 mM sodium orthovanadate, 10 mM NaF, 10  $\mu$ g/ml aprotinin, chymostatin, leupeptin and pepstatin. Following centrifugation to remove debris, protein concentrations of all samples were normalized. Anti-SHC antibodies (Transduction Laboratories) crosslinked to Protein A Sepharose (20-30  $\mu$ l packed beads, approximately 2  $\mu$ g of antibody) were added to each sample which was incubated at 4° with rocking for 1.5 hr. The resulting SHC-anti-SHC bead complex was washed twice in 1% Triton extraction buffer (see above) and then boiled in SDS-PAGE sample buffer prior to electrophoresis on 5-15% gradient gels. Samples were transferred to nitrocellulose and probed with RC20 anti-phosphotyrosine antibody coupled to horseradish peroxidase (Transduction Laboratories). The blots were then developed with Western View ECL reagent (Transduction Laboratories).

*Fluorescence Microscopy* - Cells were plated on fibronectin-coated coverslips 48 hrs before the experiment. Cells were fixed for 10 min with freshly prepared 3.6% paraformaldehyde and 0.024% saponin in  $\text{Ca}^{2+}$ ,  $\text{Mg}^{2+}$ -free phosphate buffered saline. Free aldehyde groups were quenched with 0.1%  $\text{NaBH}_4$  for 5 min. Cells were incubated simultaneously with anti-EGFR mAb 225 (10  $\mu$ g/ml) and anti-EGF rabbit polyclonal Z-12 (Santa Cruz) in 0.012% saponin for 1 h followed by staining with FITC-labeled goat anti-mouse and Texas Red-labeled goat anti-rabbit IgG antibodies (Molecular Probes, Inc.) for 45 min. Alternately, anti-EGFR mAb 13A9 and anti-EGF mAb HA were directly labeled with Alexa 488 and Alexa 594 dyes (Molecular Probes, Inc.) and used at a concentration of 1  $\mu$ g/ml each. Coverslips were mounted in ProLong antifade medium (Molecular Probes, Inc.) and viewed with a Nikon inverted fluorescence microscope with 60x or 100x oil immersion objectives. Images (12 bit, 656 x 517) were acquired using a Photometrics cooled CCD camera with a Macintosh workstation running Openlab 2.0 software (Improvision). For digital confocal microscopy, image triplets were acquired 0.4  $\mu$ m apart centered on the perinuclear endosomes at 520 and 615 nm (for Alexa 488 and Alexa 594 respectively). The image sets were deconvolved using nearest-neighbor subtraction (141). The deconvolved images of both EGF and EGFR distributions were then used to generate binary images using grayscale values between 400 and 4095. A logical "AND" between these images was then used to determine the colocalization between the EGF and the EGFR. The deconvolution routines were calibrated using 15  $\mu$ m FocalCheck beads (Molecular Probes, Inc.).

## Results and Discussion

Expression of Modified EGF Ligands in HMEC - The proteolytic processing of membrane-anchored EGFR ligands can be complex, giving rise to multiple forms of both soluble and membrane-anchored proteins (103). To simplify the interpretation of our experiments, we constructed the two artificial EGF genes diagramed in Fig. 34A. Both lack the amino terminus extension that is frequently proteolytically removed. A signal sequence derived from the EGFR was substituted for the normal amino terminus extension. The sEGF construct terminates at amino acid 1023, which corresponds to the last amino acid in the mature EGF ligand. The EGF-Ct construct retains the entire transmembrane and cytoplasmic carboxy terminus of the EGF

precursor. These artificial EGF genes were inserted into the retrovirus vector MFG which was transfected into the CRIP packaging cell line (101). The resulting recombinant retroviruses were used to transduce the immortalized 184A1 HMEC line. Clonal cell lines were then randomly selected and screened for both EGF mRNA and protein expression.

Conditioned medium from positive cell lines was collected, concentrated and analyzed by gel filtration and western blot analysis. As shown in Fig. 34B, EGF activity from supernatants of cells producing sEGF ran as a single peak, corresponding to a molecular weight of approximately 6.6 kd. This is slightly larger than the 6.2 kd predicted from protein sequence. Western blot analysis demonstrated that protein released from cells producing EGF-Ct ran as two bands, with the predominant lower band corresponding to authentic recombinant human EGF. The sEGF migrated primarily as the higher molecular weight product. Based on the molecular weight values obtained from gel filtration studies, the two bands likely correspond to alternate cleavage sites in the artificial signal sequence. We found that the biological activity of sEGF from conditioned medium was the same as commercially available recombinant EGF as determined by its ability to stimulate EGFR autophosphorylation and cell proliferation (data not shown).

Shown in Fig. 35A are the rates of EGF release from several typical cell lines expressing either sEGF or EGF-Ct. The parental HMEC did not release any measurable amount of EGF into the medium, but clones expressing either sEGF or EGF-Ct released comparable amounts of soluble EGF at rates up to 40ng/10<sup>6</sup> cells per day. Accumulation of EGF in the medium could be substantially increased by adding the receptor blocking antibody 225, indicating that the cells were capable of utilizing a large fraction of the released EGF. Interestingly, if cells produced less than about 10 ng EGF/10<sup>6</sup> cells per day, no EGF was detected in the medium unless the endogenous EGFR were blocked (Fig. 35A). This indicates either that HMEC are able to efficiently capture low levels of autocrine ligands or that the released ligand does not enter the bulk medium prior to receptor binding.

The clonal line secreting high levels of sEGF displayed a 75% reduction in EGFR levels which was not reduced further by the addition of exogenous EGF (Fig. 35B), indicating a maximal level of receptor downregulation. The clonal line expressing lower levels of sEGF displayed a corresponding lower degree of receptor downregulation. A similar situation was observed for lines expressing EGF-Ct (data not shown). If EGF was found in the medium in the absence of antagonistic anti-EGFR antibodies, EGFR downregulation was always complete (compare sEGF clone 1 in Figs 35A and 35B). This suggests autocrine EGF escapes into the medium only when the EGFR are saturated and that at least some of the cell lines make more EGF than they can consume.

The expression of sEGF and EGF-Ct in HMEC was also evaluated by immunofluorescence. Shown in Fig. 36 are cells stained for both the EGFR and for EGF. The EGFR in parental HMEC were predominantly at the cell surface and EGF staining was not above background levels (Fig. 36, upper panels). Cells expressing either sEGF or EGF-Ct displayed greatly reduced levels of EGFR, which were predominantly located lysosomal structures (Fig. 36, middle and lower panels) as shown by staining parallel groups of cells with an antibody to LAMP-2 (data not shown). As expected for a membrane-anchored protein, EGF-Ct was predominantly located at the cell surface (Fig. 36, lower right panel). Some intracellular staining was also observed that colocalized with the EGFR.

The sEGF displayed a very weak staining pattern, consistent with its lack of a membrane-anchoring domain (Fig. 36, middle right panel). The pattern of sEGF staining, however, appeared to be coincident with the distribution of EGFR. To verify this colocalization, we directly labeled anti-EGFR and anti-EGF monoclonals with fluorescent dyes to avoid any

possible cross-reactivity of secondary antibodies. Cells expressing sEGF were then fixed, permeabilized and stained simultaneously with the anti-EGF and anti-EGFR antibodies. The distribution of sEGF and EGFR was then determined using digital confocal microscopy (141). As shown in Fig. 37, both the EGFR and the sEGF were found in small cytoplasmic vesicles. The distribution of sEGF (red) was more restricted than the EGFR (green), most likely due to the loss of soluble sEGF from the permeabilized cells. Virtually all sEGF in the cell was found colocalized with the EGFR, as shown by yellow (Fig. 37, left panel) and by performing a logical AND of the EGFR and EGF images (Fig. 37, right panel). This is in contrast to the situation with EGF-Ct where most of the ligand was found associated with the cell surface (Fig. 36, bottom right panel).

The Transmembrane Domain of the EGF Ligand Allows Interruption of Autocrine Signaling - Some HMEC lines produce more EGF than can be consumed by the endogenous EGFR and display a maximal extent of receptor downregulation (Fig. 35A and 35B). Because receptor downregulation is thought to reduce the sensitivity of cells to subsequent EGF addition (142), we were interested in determining the growth rates of these chronically stimulated cells. The parental 184A1 cells grew in the absence of exogenous EGF, but grew to a higher density when EGF was added (Fig. 38A). Blocking their EGFR with antagonistic mAb 225 strongly inhibited cell growth, as previously reported (131). Although the addition of EGF to cells producing sEGF had no effect on their growth rate, these cells grew at the same rate as parental cells treated with high concentrations of exogenous EGF (Fig. 38A, middle panel). This indicates that downregulation of EGFR does not affect the steady state response of the cells. Surprisingly, addition of high concentrations of antagonistic 225 mAb had no effect on the growth rate of these cells either, indicating that the sEGF-EGFR autocrine loop could not be interrupted. In the case of cells expressing EGF-Ct, growth rates were again similar to those observed for parental cells treated with high concentrations of EGF and addition of exogenous EGF again had little effect (Fig. 38A, right panel). In contrast to the situation with sEGF, however, the addition of 225 mAb effectively inhibited their growth. Thus, interruption of autocrine signaling in HMEC by antagonistic EGFR antibodies appeared to require the membrane anchoring domain of the ligand.

Because cells expressing EGF-Ct produce at least as much ligand as those expressing sEGF (see Fig. 35A), their relative sensitivity to 225 treatment could not be explained simply as an effect of mass action. An alternate explanation could be a clonal variation between cells with respect to their dependence on EGFR activation. We repeated our analysis on several independently isolated clones and observed the same effect; all clonal lines expressing sEGF were resistant to the effect of 225 mAb. To verify that EGFR activation itself was resistant to the effect of 225 mAb in cells expressing sEGF, we examined the phosphorylation of the EGFR substrate SHC in the different cell lines (143). As shown in Fig. 38B, addition of EGF to the parental HMEC line resulted in high levels of SHC tyrosine phosphorylation, but little SHC phosphorylation was observed in either the absence of EGF or in the presence of 225 mAb. In the case of cells expressing either sEGF or EGF-Ct, SHC phosphorylation was significant in the absence or presence of exogenous EGF. Significantly, the addition of 225 mAb had little effect on SHC phosphorylation in cells expressing sEGF, but was strongly inhibitory in cells expressing EGF-Ct. These data demonstrate that sEGF can activate the EGFR even in the presence of antagonistic antibodies. The simplest explanation for this observation is that removal of the membrane-anchoring domain allows EGF to bind to its receptor prior to arrival at the cell surface and thus to operate in an "intracrine" fashion.



In the experiments shown in Fig. 38A and 38B, cells were grown at a relatively high density (between  $0.03$  and  $1 \times 10^5$  per  $\text{cm}^2$ ). As an alternate to the intracrine hypothesis, sEGF could be trapped between cells and thus could bind to EGFR before the antagonistic antibody could diffuse to the cell surface. The more slowly released EGF-Ct would potentially not have such a kinetic advantage. If sEGF was operating in an intracrine manner, then growth of cells producing sEGF should be independent of cell density. If sEGF was simply being trapped between cells, then lowering the cell density should allow the 225 mAb to block receptor activation. To test this idea, cells were plated at clonal densities ( $<100$  per  $\text{cm}^2$ ) and grown for several weeks in the presence or absence of anti-EGFR antibodies. As shown in Fig. 39, 225 mAb was unable to block the growth of cells producing sEGF, but were completely effective in preventing growth of either the parental cell line or cells producing EGF-Ct. These data demonstrate that even at the single cell level, autocrine signaling mediated by sEGF cannot be interrupted.

Spatial Organization of HMEC is Disrupted by Secreted EGF - We examined the effect of non-interruptible autocrine/intracrine signaling on cell organization by observing the ability of HMEC expressing either sEGF or EGF-Ct to form complex structures. Cells were plated on Matrigel at a relatively low density ( $1.3 \times 10^4/\text{cm}^2$ ) so that the effects of different EGF levels could be observed. After 6 days, their state of organization was evaluated. As shown in Fig. 40, parental cells formed small aggregates in the absence of exogenous EGF. As expected, the addition of EGF resulted in the formation of well defined complex structures. Again, addition of anti-EGFR antibody 225 blocked cell organization in the parental HMEC cells.

Cells expressing sEGF formed large aggregates that increased in size over time, but did not make organized structures (Fig. 40). In particular, the ability of these cells to form tubular or duct-like structures was severely affected. The addition of exogenous EGF or antagonistic 225 mAb had no effect on growth or organization of cells expressing sEGF.

In contrast to the effect of sEGF production, expression of EGF-Ct facilitated the formation of structures with clear lobular and ductal aspects (Fig. 40). The addition of exogenous EGF partially inhibited the formation of structures, whereas the addition of antagonistic 225 mAb completely blocked the process. If the cells were cultured for an additional 14 days, the structures formed by the parental HMEC were stable, but those formed by cells expressing EGF-Ct became less defined (data not shown). These observations indicate that the spatial presentation of EGF to receptors is important in its ability to facilitate the organization of HMEC in culture.

Batimastat Inhibits Proliferation of EGF-dependent Cells - To determine whether cleavage of EGFR ligands was necessary for their biological activity, we treated cells either with or without the metalloprotease inhibitor batimastat for 48 hrs. During the final 18 hr, bromodeoxyuridine (BrDu) was added to label cells in S-phase. As shown in Fig. 41A, the addition of batimastat reduced the percentage of BrDu-labeled cells from 40% to 6%. Similarly, blocking endogenous autocrine EGFR signaling with the antagonistic anti-EGFR mAb 225 reduced the percentage of labeled cells to 14%. Addition of soluble EGF stimulated proliferation of the cells. In the presence of both batimastat and EGF, the cell proliferation rate was less than in the presence of EGF alone, but was much greater than displayed by control cells. Thus soluble EGF appeared to reverse most of the inhibitory effects of batimastat.

To verify that batimastat inhibits the proliferation of cells that depend on autocrine signaling through the EGFR, we compared its effect on the colon cancer lines HCA-7 and HCT-116. The growth of HCA-7 cells has previously been shown to be inhibited by blocking the EGFR whereas HCT-116 cells are unresponsive to EGF (144,145). As shown in Fig. 41B, the addition of either batimastat or mAb 225 alone inhibited the growth of HCA-7 cells by about



60%. The addition of both mAb 225 and batimastat completely blocked the growth of these cells. Very similar results were obtained using the autocrine-dependent MDA-468 cell line (data not shown). The addition of EGF reversed the effect of batimastat on HCA-7 cells. The growth of HCT-116 cells, however, was not inhibited by the addition of either mAb 225 or batimastat or a combination of the two reagents. These results indicate that cells that are inhibited by blocking the EGFR are also inhibited by batimastat.

Cells Expressing Soluble EGF are not Inhibited by Batimastat - The EGFR system is "autoinductive" in that EGFR activation can stimulate the synthesis of EGFR ligands (146). It seemed possible that the effect of batimastat on cell proliferation might not be directly due to inhibition of EGFR ligand release, but instead due to an effect on EGFR signaling and a consequent reduction in ligand gene expression. To explore these possibilities, we used cells expressing either sEGF or EGF-Ct. Because these constructs use retroviral promoters, their expression levels are independent of EGFR activity. Proteolytic processing should not be required to produce the mature form of the ligand in the case of sEGF.

In the absence of batimastat, cells expressing either sEGF or EGF-Ct released similar amounts of EGF into the medium (Fig. 42B). This level was very similar to the amount of amphiregulin released (approximately 3.1 ng and 3.5 ng per  $10^6$  cells for EGF and amphiregulin respectively, results not shown). Batimastat reduced the amount of EGF released from cells expressing EGF-Ct by 86% during an 18hr period. In contrast, there was no effect on the release of EGF from cells expressing sEGF. Additional experiments demonstrated that the concentration of batimastat necessary for half-maximum inhibition of EGF release from the cells expressing EGF-Ct was approximately 0.5-1  $\mu$ M. This is the same concentration range of batimastat required to inhibit matrix metalloprotease activity using cell-based assays (Peter D. Brown, British Biotech, Ltd, personal communication, 1998). We conclude that batimastat effectively inhibits the release of membrane-anchored EGF, most likely through its effect on the processing protease. This inhibition is very similar to what has been previously described for the native EGF molecule (118).

To determine whether batimastat can selectively block the growth and proliferation of cells expressing membrane-anchored EGF, we seeded HMEC expressing either sEGF or EGF-Ct, as well as the parental cell line, at clonal density in either the presence or absence of batimastat. After 14 days in culture, the plates were stained to visualize cell colonies. As shown in Fig. 43A, batimastat effectively blocked the clonal growth of both the parental HMEC as well as cells expressing EGF-Ct. Significantly, batimastat had little effect on cells expressing the secreted sEGF. Results from the BrDu labeling studies confirmed these results (Fig. 43B). The addition of batimastat strongly inhibited proliferation of cells expressing EGF-Ct, but had little effect on cells expressing sEGF. The addition of soluble EGF reversed the inhibitory effects of batimastat on cells expressing EGF-Ct. Although batimastat (or soluble EGF) had no effect on the behavior of cells expressing sEGF, these cells were still dependent on EGFR activation. The addition of PD 153035, a specific inhibitor of the EGFR receptor kinase (147), effectively blocked the growth of these cells (data not shown). Together, these results show that batimastat selectively inhibits the proliferation of cells expressing membrane-anchored forms of EGFR ligands.

If batimastat is preventing HMEC proliferation through its effect on EGF release, we should also observe an inhibition of EGFR activation. To directly evaluate this, cells were treated with batimastat, antagonistic mAb 225 or EGF, and the level of EGFR tyrosine phosphorylation was determined by western blots. As shown in Fig. 44, the presence of batimastat inhibited autocrine activation of the EGFR in both parental HMEC and cells expressing EGF-Ct, but had no effect on cells expressing sEGF. The degree of inhibition with

batimastat was similar to that observed for the antagonistic mAb 225. The activation of EGFR by sEGF could not be efficiently inhibited by mAb 225 because sEGF binds to the EGFR prior to receptor arrival at the cell surface (see above). Addition of a bolus of soluble EGF resulted in a high level of EGFR phosphorylation which was not affected by the presence of batimastat. These results show that batimastat has no direct effect on EGFR activation, but appears to work by inhibiting ligand release.

Batimastat Inhibits Migration of Epithelial Cells - Batimastat has been previously shown to inhibit the ability of cells to invade basement membranes, presumably due to its ability to inhibit matrix-degrading enzymes (148,149). Cell invasiveness, however, also requires active migration of the cells into a matrix. Since EGF is known to stimulate the motility a variety of epithelial cells (150,151), we hypothesized that batimastat might also inhibit cell migration by blocking EGFR ligand release. We tested this hypothesis by investigating the movement of cells in either the presence or absence of batimastat. Cell movement was followed by time-lapse video microscopy for 15 h in the presence or absence of batimastat. The position of the cells was then recorded and normalized to their starting position. The tracking data for 8 cells randomly chosen from each group is shown in Fig. 45. It is clear that batimastat strongly inhibited the migration of cells expressing EGF-Ct, but had little effect on cells expressing sEGF. Batimastat also inhibited the migration of parental HMEC (data not shown). As was the case with proliferation, the addition of exogenous EGF reversed the inhibitory effect of batimastat (Fig. 45).

Batimastat reduced the speed of cells expressing EGF-Ct and sEGF by 50% and 18% respectively (from 38 to 19  $\mu\text{m} \times \text{h}^{-1}$  and from 34 to 28  $\mu\text{m} \times \text{h}^{-1}$ ). Reliable values for directional persistence could not be determined in the presence of batimastat. This inhibitor caused the cell migration behavior to become directionally erratic, yielding tracking data that could not be fit to the persistent random walk model used for the analysis (140). Visual observations showed that cells treated with batimastat tended to "oscillate" around their initial location with little net translocation, indicating that batimastat has a strong negative effect on cell persistence. This is supported by inspection of the tracking data (compare the top-left and middle-left panels of figure 45). The net effect of reducing both speed and persistence would be an inability of cells to migrate any significant distance from their origin. Because exogenous or "preprocessed" EGF readily reverses the effect of batimastat (Fig. 45), it appears that batimastat inhibits cell migration by interfering with EGFR ligand release.

Ever since the discovery that EGFR ligands are made as membrane-anchored precursors, the functional role of this ligand form has been debated. The current paradigm is that membrane-anchored growth factors act as juxtacrine regulators of cell-cell signaling (102). This conclusion was based on the demonstration that cells expressing protease-resistant forms of ligands such as TGF $\alpha$ , could activate receptors on neighboring cells (114,115). Although these studies demonstrated clear evidence of cell-cell signaling, several caveats in their interpretation remain. First, cleavage-resistance of the constructs was evaluated by the lack of detectable TGF $\alpha$  in the medium (115). Subsequently, however, it has been shown that released EGFR ligands are not necessarily detectable due to the high capture efficiency of EGFR on the ligand-expressing cells (123,138). We have, in fact, found significant amounts of TGF $\alpha$  released by cells expressing "non-cleavable" TGF $\alpha$  constructs if the endogenous EGFR are first blocked with antagonistic antibodies (unpublished observations). Second, many of the studies on juxtacrine signaling have used cell types that are hypersensitive to EGFR ligands, usually because of EGFR overexpression (114,115,122). Even though these systems can be very useful, they may overestimate the degree of juxtacrine signaling. Finally, most studies have not quantified the relative contribution of soluble versus membrane-anchored ligand to total ligand activities. In those cases where this comparison has been done, soluble ligands have

been found to have much greater activity than their membrane-anchored counterparts (114,152,153).

Our data indicate that in the case of autocrine signaling through the EGFR, conversion of the membrane-anchored to a soluble form is required to observe significant biological activity. Although this appears to be the case for EGF, TGF $\alpha$  and amphiregulin, it may not be true for all EGFR ligands. For example, good evidence exists that HB-EGF can operate efficiently in a juxtacrine mode (153). Nevertheless, TGF $\alpha$  and amphiregulin appear to be the most important ligands in EGFR-dependent tissues, such as the skin, the gut and the mammary epithelium (87,154,155). In these tissues, proteolytic release of the ligand precursors is probably the rate-limiting step in EGFR activation. Membrane-anchored ligands in these cells probably represent a precursor pool for the activating protease. As shown above, the membrane-anchoring domain of EGF serves an important function in restricting the site of ligand access to the EGFR. The requirement for both localization and proteolysis for productive receptor signaling could provide additional points of regulation for the EGFR system.

Metalloprotease inhibitors which prevent EGFR ligand release, such as batimastat, have shown promise in preventing spread of metastatic disease in both animal studies and early clinical trials (124,125). These compounds were originally thought to work by preventing the proteolytic breakdown of the extracellular matrix by invading tumor cells (148). Detailed studies, however, have suggested that their effects may be more complex (149). For example, batimastat inhibits the regrowth of resected human breast cancer cells in nude mice (156). Batamastat also inhibited primary tumor growth in an orthotopic model of colon cancer (124) and of a hemangioma (157) and was synergistic with cisplatin in treatment of ovarian cancer (158). These effects are consistent with an effect of metalloprotease inhibitors on both cell proliferation and migration as well as breakdown of the extracellular matrix.

EGF receptor activation is necessary for the growth of many epithelial tumors and can regulate the synthesis of a number of matrix degrading proteases (159). The inhibitory effect of batimastat on metastasis may be mediated in part through interference with autocrine EGF receptor signaling. Efforts to identify proteases involved in growth factor processing together with rational drug design to selectively inhibit their activity may therefore be a fruitful approach to improve current cancer therapies. In addition, understanding how proteolysis of EGFR ligands is regulated may provide additional insights into how cell behavior is coordinated during development.

#### Task 5: Determine how the pattern of spatial regulation of the EGFR affects its ability to transactivate and transmodulate erbB-2

We investigated the domains of the EGFR which control transmodulation of erbB-2 and have determined how trafficking of the EGFR influences transmodulation of erbB-2. During the final two years of the project, we extended our studies to include an investigation of the affect of overexpression of erbB-2 on its ability to transmodulate the EGFR. The reason for this is that ligand activation of EGFR leads to heterodimer formation between EGFR and erbB-2, which is thought to result in activation of erbB-2 by transphosphorylation (27,28). Transactivation of erbB-2 also occurs upon the addition of heregulin, a ligand for erbB-3 and erbB-4 (29-32). As observed for EGF, heregulin induces the formation of heterodimers between erbB-3 or erbB-4 with erbB-2, resulting in erbB-2 becoming tyrosine phosphorylated (30,33,34,36,38). There is also evidence to suggest that EGFR interacts with erbB-3 and erbB-4 (37). Thus, activation of any member of the EGFR family results in signaling through multiple receptor types. Understanding how these receptors interact with each other is therefore essential to knowing how they work.

The pattern of tyrosine phosphorylation of EGFR and erbB-2 is important in signal transduction. Specific phosphorylated tyrosines residues serve as docking sites for proteins containing SH2 domains, such as the PI3 kinase p85 subunit and GRB2 (160). The assembly of signaling complexes dictates the subsequent pattern of signal transduction. Intracellular trafficking of the activated EGFR also regulates receptor activity by controlling the availability of substrates and signaling partners (39). Although ligand binding induces rapid internalization and subsequent lysosomal targeting of EGFR, it is uncertain whether erbB-2 trafficking is influenced by the EGFR. It has been suggested that all members of the erbB family are "internalization defective" except for the EGFR (40), but those studies were done by direct activation of erbB family members or by using chimeric receptors. It has been reported that EGF treatment can stimulate the degradation of erbB-2 in some epithelial cells, but the mechanism of this transmodulation is unclear (41). If EGFR activation does alter the trafficking of erbB-2, this could be an important mechanism for regulating both the activity and distribution of these signaling molecules in cells.

Ligand binding not only activates the EGF receptor but also initiates negative regulatory processes. In this part of the project, we examined negative regulation by receptor degradation resulting from intracellular trafficking to the lysosomes. While activation of erbB-2, erbB-3 and erbB-4 have been well characterized, the negative regulation of these receptors has not been extensively studied. Conflicting reports have been published regarding the trafficking of erbB-2 following transactivation with EGF. We and others have described effective downregulation of erbB-2 by lysosomal targeting in three different cell types (161,162). In contrast, studies with chimeras composed of the EGFR extracellular domain and the erbB-2 cytoplasmic domain have shown that EGF has no effect on the internalization or degradation rate of the chimeric receptor (40). Another study measured the downregulation of erbB-2 in SKBR-3 cells that contain a 100 fold erbB-2 gene amplification (163). In this project, we found that although erbB-2 was transactivated following EGF treatment, there was no measurable decrease in erbB-2 half-life (163). Instead of interpreting this result to mean that degradation of erbB-2 is not part of its negative regulation, we alternatively suggest that lysosomal targeting is a mechanism of erbB-2 downregulation, but normal regulation was impaired when erbB-2 was overexpressed.

## Materials and Methods

**General** - Polyclonal rabbit antibody N-13 directed against a peptide corresponding to residues 1-13 in human EGFR was a gift of Dr. Debora Cadena. Polyclonal rabbit antibody 1917 to erbB-2 directed against a peptide corresponding to the 18 carboxy terminal residues of human erbB-2, were provided by Dr. Gordon Gill. Rabbit polyclonal antibody C18 against amino acids 1169-1186 of neu/erbB-2 was obtained from Santa Cruz Biotechnology. Ab5 mouse monoclonal antibody against the extracellular domain of erbB-2 was purchased from Oncogene Sciences. Polyclonal rabbit antibodies specific for phosphotyrosine were generated and affinity-purified as described (68). Monoclonal antibodies 528, 579, and 225 against the EGFR (69) were purified from hybridomas obtained from the American Type Culture Collection. RC20 antibody engineered to couple a monoclonal phosphotyrosine antibody directly to horseradish peroxidase enzyme was purchased from Transduction Laboratories. Antibodies 13A9 against the EGFR and 4D5 against human erbB-2 were gifts from Genentech. These were directly labeled with Alexa 488 and Alexa 594 dyes respectively following the manufacturer's protocol (Molecular Probes, Inc.) Secondary antibodies labeled with either Texas Red or fluorescein were obtained from Cappel laboratories.

**Cell Culture** - B82 mouse L cells, which contain no endogenous EGF receptors, and B82 cells transfected with normal (WT) or mutated (M<sup>721</sup>, c'647, c'958, and M<sup>721</sup>c'958) human EGF receptors were a generous gift of Dr. Gordon Gill. Their construction was described previously



(3). B82 cells were grown in Dulbecco's modified Eagle's medium (DME, Flow Laboratories) containing dialyzed 10% calf serum (HyClone). 5  $\mu$ M methotrexate was added to the medium for those cells transfected with human EGF receptor. The human mammary epithelial cell line 184A1L5 (131) was obtained from Dr. Martha Stampfer and was cultured in medium DFCI-1 as described (133). The human mammary epithelial line HB2 was a gift from Joyce Taylor-Papadimitriou and were grown as described (164). The human mammary epithelial cell lines MTSV1-7, ce1 and ce2 have been described previously (165) and were provided as a generous gift from Dr. Joyce Taylor-Papadimitriou. These cells were grown in Dulbecco's modified Eagle's medium (Flow laboratories) containing 10% calf serum (HyClone) supplemented with 1  $\mu$ M insulin and 5  $\mu$ M dexamethasone. Selection for erbB-2 expression was maintained using 500  $\mu$ g/ml G418. SKBR3 cells (163) were obtained from the American Type Culture Collection and grown in McCoy's 5A supplemented with 10% fetal calf serum (HyClone).

*Quantification of EGFR, erbB-2 and phosphotyrosine levels* - Confluent cultures of cells were rinsed and lysed in an NP-40 buffer (150mM NaCl, 1% NP-40, 50mM Tris pH 8) and debris removed by centrifugation. Samples were brought to 2% SDS, 1%  $\beta$ -mercaptoethanol and heated to 100°C for 5 min. Equal amounts of total cellular protein from each sample were separated on 5-7.5% gradient gels and transferred to nitrocellulose. EGFR and erbB-2 were detected by N-13 and 1917 polyclonal antisera respectively using  $^{125}$ I-labeled protein A as described (178). The concentrations of and incubation times with  $^{125}$ I-labeled protein A were chosen to be in the linear range of the protein load of the gels. The blots were analyzed by storage phosphor plates using the Bio-Rad G250 Molecular Imager. The Bio-Rad Molecular Analyst package was used to quantify the amount of radioactivity associated with each band. In some cases, EGFR levels were determined by a sandwich ELISA as previously described (137). In this case, cells were extracted for 10 min at 0°C in 20 mM CHAPS, 10 mM HEPES buffer (pH 7.4), 4 mM iodoacetate and 100  $\mu$ g/ml each of leupeptin, chymostatin, pepstatin and aprotinin. Standard curves were generated using extracts from B82 cells expressing a known level of EGFR protein and using receptor-negative B82 cells as blanks.

To determine the tyrosine phosphosphate content of erbB-2 protein, cells were lysed for 10 min at 0°C in 1% Triton X-100, 150 mM NaCl, 50 mM Hepes (pH 7.2), 10% glycerol, 1 mM Na<sub>3</sub>VO<sub>4</sub>, 4 mM iodoacetate and 10  $\mu$ g/ml each of chymostatin, pepstatin, leupeptin and aprotinin. After centrifugation for 10 min at 10,000  $\times$  g at 0°C, the 1917 anti-erbB-2 polyclonal antiserum was added (1:100) followed by rocking for 3 hr followed by the addition of 100  $\mu$ l of protein A sepharose (50% slurry) for an additional hour. The beads were washed several times in lysis buffer and boiled in SDS sample buffer prior to gel electrophoresis and transfer to nitrocellulose as detailed above. Phosphotyrosine was detected using affinity-purified polyclonal antibodies and erbB-2 protein was quantified in a parallel blot using 1917 antiserum. The Bio-Rad G250 Molecular Imager and the Molecular Analyst package was used to quantify the amount of radioactivity associated with each band.

*Quantification of EGFR mRNA levels* - Total cellular RNA was isolated using Tri-Reagent (Molecular Research Center, Inc.) following the manufacture's directions. cDNA was synthesized using M-MLV Reverse Transcriptase (Promega) and specific products were amplified by PCR using the Idaho Technology air cycler with the following primers and protocols; erbB2 - 5' AACTGCACCCACTCCTGTGT 3' and 5' CAGGGATCCAGATGCCCTTG 3' at 63° annealing, 94° polymerization for 15 s for 30 cycles. G3PDH - 5' GAGCTTGACAAAGTGGTCGTTGAGG 3' and 5' CCACAGTCCATGCCATCACTGCCAC 3' at 63° annealing, 94° polymerization for 15 s for 24 cycles. The number of cycles was chosen empirically to keep product amplification in the linear range. Reaction products were separated on 1.8% agarose gels and stained with ethidium bromide.



*Fluorescence Microscopy* - Cells were plated on fibronectin-coated coverslips 48 hrs before the experiment. Cells treated either without or with EGF were fixed for 10 min with freshly prepared 3.6% paraformaldehyde and 0.024% saponin in  $\text{Ca}^{2+}$ ,  $\text{Mg}^{2+}$ -free phosphate buffered saline. Free aldehyde groups were quenched with 0.1%  $\text{NaBH}_4$  for 10 min. Cells were incubated simultaneously with a mixture of anti-EGFR monoclonals 528, 579, 225 and 13A9 ( $10\mu\text{g}/\text{ml}$  each) and anti-erbB-2 C18 (1:100; Santa Cruz Biotechnology, Inc.) in 0.012% saponin for 45 min followed by staining with FITC-labeled goat anti-mouse and Texas Red-labeled goat anti-rabbit IgG antibodies (1:100) for 45 min. The coverslips were mounted in ProLong antifade medium (Molecular Probes, Inc.) and viewed with a Nikon inverted fluorescence microscope with a 40x oil immersion objective. Images ( $512 \times 512$ ) were acquired using a Photometrics cooled CCD camera with a Macintosh workstation running OncorImage software. For confocal microscopy, samples were viewed with a Bio-Rad MRC 600 laser scanning confocal imaging system attached to a Zeiss Axioplan microscope with a 60X objective. Excitation was achieved with a Krypton/Argon laser using the 488 and 568 nm lines. Paired images ( $384 \times 512$  pixels each) were individually scaled to 256 gray levels using Adobe Photoshop 3.0 on the Macintosh before output to a film recorder.

To follow the transfer of EGFR to lysosomes, the lysosomes were first labeled by incubating cells for 15 min at  $37^\circ\text{C}$  with 5 mg/ml of fluorescein-labeled dextran (10,000 MW, anionic, lysine fixable; Molecular Probes, Inc.), then chased for an additional 2 hours. During the chase period, cells were pulsed for 15 min with  $1.5 \times 10^{-8}$  M EGF-Texas Red streptavidin complex (Molecular Probes, Inc) and chased for time periods between 0-105 min. Total chase time following the initial fluorescein-labeled dextran treatment was 2 hrs for all samples. Cells were fixed with 3.6% paraformaldehyde and mounted in Prolong. Coverslips were viewed with a Nikon inverted fluorescence microscope with a X60, 1.4 N.A. oil immersion objective. Sets of 3 images at 3 different focal planes spaced  $0.5\mu\text{m}$  apart centered on the perinuclear endosomes were acquired at 520 and 615 nm (for fluorescein and Texas Red respectively). The images ( $12\text{ bit}$ ,  $656 \times 517$ ) were acquired using a Princeton Instruments cooled CCD camera attached to a Macintosh workstation running Openlab software (Improvision, Inc). The image triplets were deconvolved using nearest-neighbor subtraction (141). The deconvolved image of the lysosomes (fluorescein) was then used to generate a binary mask using grayscale values between 700 and 4095. This mask was then applied to the deconvolved image of the EGF (Texas Red) to identify all lysosomal "objects" that contained EGF. The integrated intensity of all of these objects was then taken as the amount of EGF within lysosomal structures. A mask of the EGF image was generated in the same way and applied to the EGF image to determine the total integrated intensity of all EGF-containing objects within the cell. The fraction of all EGF colocalized in lysosomes was then calculated. At each time point, four random fields of cells were analyzed which contained between 100-200 vesicles per field.

*Flow cytometry* - Cells were removed from plates by a brief trypsinization, which did not alter the measurable number of either EGFR or erbB-2 at the cell surface. Cells were fixed for 10 min at  $22^\circ\text{C}$  in freshly prepared 3.6% paraformaldehyde, rinsed and incubated for 1 hr in either anti-EGFR mAb 225 or anti-erbB-2 mAb Ab5 followed by FITC-labeled goat-anti-mouse antibody for 1 hr. Samples were analyzed on a FACScan flow cytometry instrument (Becton-Dickinson, Mountain View, CA) and the data analyzed using Cell Quest software.

*Binding analysis* - Number of surface-associated erbB-2 molecules was determined by steady state analysis (166). 4D5 antibody was radioiodinated to a specific activity of  $4.5 \times 10^6$  cpm/pmol and cells were incubated with concentrations from  $6.7 \times 10^{-11}$  to  $2 \times 10^{-8}$  M for 3 hr at  $37^\circ\text{C}$ . The relative amount of antibody associated with the cell surface was determined by acid stripping (167) and the data was analyzed as previously described (166). Scatchard analysis of

EGF binding to cells used  $^{125}\text{I}$ -EGF at a specific activity of  $1.6 \times 10^6$  cpm/pmol and an incubation period of 4.5 hr at  $0^\circ\text{C}$  using ligand concentrations from  $1.7 \times 10^{-11}$  to  $1.7 \times 10^{-8}$  M as described (167). Specific internalization rates for the EGFR were determined as described (167). Measurements were made using a ligand concentration of 10ng/ml, and each rate constant determination was derived from a 5 min incubation period with ligand. Specific internalization rates were determined by plotting the integral surface-associated ligand against the amount internalized, and the slopes were determined by linear regression (167).

*Fractional Recycling* - Cells were grown to confluence in 35 mm dishes and switched to serum-free DME containing 20 mM HEPES (pH 7.4) and no bicarbonate (D/H/B) 12 hours before experiments. The cells were incubated at  $37^\circ\text{C}$  in 0.1 - 30 ng/ml of  $^{125}\text{I}$ -EGF for three hours to allow the sorting process to reach a steady state (58,60). Cells were then washed with acid-strip (50 mM glycine-HCL, 100 mM NaCl, 2 mg/ml PVP, pH 3.0) for 2 min at  $0^\circ\text{C}$  to remove surface-bound ligand (58), rinsed two times with one ml phosphate-buffered saline, and returned to  $37^\circ\text{C}$  in D/H/B containing 1  $\mu\text{g}$ /ml unlabeled ligand to prevent rebinding and reinternalization of recycled ligand. The medium was collected at 10 minutes and an aliquot counted for total radioactivity. Cells were solubilized with 2% sodium dodecyl sulfate and the amount of radioactivity remaining was determined. The medium was loaded on a 15% native polyacrylamide slab gel and the intact and degraded EGF was separated by isotactoelectrophoresis (60). After drying the gel, the relative amount of radioactivity in the bands corresponding to intact and degraded EGF was quantified using a Bio-Rad G250 Molecular Imager. Cell number per plate was determined by counting parallel plates. Fraction of intact ligand was then plotted as a function of ligand in the cells at the start of the chase (lost into the medium + amount remaining) as previously described (65).

*ErbB-2 Half-life Measurements* - Cells were labeled to steady state (24 hours) with cysteine and methionine free Dulbecco's modified Eagle's medium (ICN) supplemented with 250 $\mu\text{Ci}$ /ml of EXPRE $^{35}\text{S}$  from New England Nuclear which contains both radiolabeled methionine and cysteine. Cultures were rinsed 6 times with normal culture medium and chased with medium with or without 100ng/ml EGF. At 0, 1, 3, 5 and 7 hours chase, cells were lysed in RIPA buffer and equal amounts of protein were subjected to immunoprecipitation with 5  $\mu\text{l}$  1917 antibody. Samples were then separated by SDS gel electrophoresis and the gels were then dried on 3MM paper followed by quantitation of erbB-2 bands using a Bio-Rad Molecular Imager as described above.

## Results and Discussion

EGF treatment reduces erbB-2 levels in human mammary epithelial cells - It is known that binding of EGF to its receptor leads to rapid internalization and reduction of EGFR levels as a result of lysosomal targeting (168). It is also well established that activated EGFR can form heterodimers with erbB-2, resulting in erbB-2 transactivation (169). Studies using a normal mouse mammary cell line, HC11, showed that EGF treatment resulted in a loss of erbB-2 cell surface expression due to accelerated degradation (41). Other studies, however, using either Rat-1 cells (27) or transformed human cell lines showed that EGF had no effect on erbB-2 levels (163). Our first goal, therefore, was to determine whether erbB-2 expression or trafficking was affected by EGF in a non-transformed human mammary epithelial cell line, 184A1L5 (131). This line is mitogenically responsive to EGF and expresses both EGFR and erbB-2.

Cells were treated with 100 ng/ml of EGF for 1 hr at  $37^\circ\text{C}$ . The levels of cell surface EGFR and erbB-2 were then measured by flow cytometry. As shown in Fig. 46, EGF treatment reduced the surface expression of EGFR in 184A1L5 cells by approximately 50%. Although cell surface erbB-2 levels were not as high as EGFR levels, EGF treatment resulted in an

approximately 3-fold reduction in their levels. These data demonstrate that activation of the EGFR in mammary epithelial cells not only downregulates the EGFR, but also reduces the surface levels of erbB-2.

To determine whether the reduction of surface erbB-2 levels was accompanied by a reduction in total cellular erbB-2 mass, we treated cells with EGF for varying periods of time and then determined total erbB-2 levels by western blot analysis. EGFR levels were simultaneously measured by using a specific ELISA(137). EGF treatment resulted in a progressive loss of both proteins over a 24 hour time period (Fig. 47, left panel). These data show that EGF can downregulate erbB-2 levels in cells in a similar manner as the EGFR, confirming results previously obtained with mouse mammary epithelial cells (41). The kinetics and extent of loss of both proteins were remarkably similar, suggesting that a similar mechanism may be responsible. If this 'transmodulation' of erbB-2 by the EGFR requires a direct physical interaction between the two molecules, then it should be possible to define the responsible structural features of the EGFR.

Model system for analyzing erbB-2 transmodulation To define the structural features of the EGFR responsible for transmodulation of erbB-2, it is preferable to use a cell type which expressed normal levels of erbB-2, but does not have endogenous EGFR. This allows the use of different mutant forms of the EGFR introduced by gene transfection. A suitable cell type is the mouse B82 cell line which expresses the murine homolog of erbB-2, but lacks endogenous EGFR. To determine whether activated EGFR could alter the levels of erbB-2 in this cell line, we added EGF to B82 cells expressing an introduced human EGFR (3). As shown in Fig. 47 (right panel), EGF treatment caused an approximate 75% loss of both EGFR and erbB-2 protein levels. Again, the kinetics and extent of erbB-2 loss paralleled that observed for the EGFR. We conclude that the ability of the EGFR to affect the cellular levels of erbB-2 in B82 cells appears similar to that observed in human mammary epithelial cells.

The rapidity of the EGF-induced loss of erbB-2 implicates a degradative mechanism. It remained a formal possibility, however, that a reduction in erbB-2 mRNA levels could also be involved. To check for this possibility, both 184A1L5 and B82 cells were treated without or with 100 ng EGF for 4 hrs at 37°C. Total RNA was extracted and the levels of erbB-2 mRNA were determined by RT-PCR. As shown in Fig. 48, treatment of either cell type with EGF had no discernible effect of erbB-2 mRNA levels. This result is consistent with a posttranslational mechanism for the reduction of erbB-2 levels by EGF treatment.

Decreased levels of erbB-2 in response to EGF is due to enhanced lysosomal targeting It is known that the decrease in EGFR protein levels in response to EGF addition is due to enhanced lysosomal targeting. Because of the similar kinetics of the loss of both EGFR and erbB-2, it seemed reasonable that the same mechanism could be responsible. Immunofluorescence visualization is a sensitive method for determining enhanced lysosomal targeting of EGFR. Therefore, we visualized the distribution of both EGFR and erbB-2 in B82 cells incubated either with or without EGF.

As shown in Fig. 49A, EGFR display a predominantly cell surface localization in the absence of EGF. Surprisingly, erbB-2 was primarily localized in small cytoplasmic vesicles, although some was found associated with the cell surface (Fig. 49B). There was little overlap between the EGFR and erbB-2 staining pattern. The addition of peptide specific for the anti-erbB-2 antibody abolished the erbB-2 immunofluorescence, but had no effect on the EGFR staining pattern (Fig. 49C and 49D), indicating the observed localization was specific for erbB-2. The addition of EGF resulted in reduced levels of surface EGFR and a corresponding increase in intracellular EGFR, particularly in perinuclear and lysosomal structures (Fig. 49E). Significantly, EGF also caused a redistribution of erbB-2 into lysosomal structures (Fig. 49F).

Although EGF treatment increased the overlap between intracellular EGFR and erbB-2, there was still a large number of vesicles that contained either EGFR or erbB-2, but not both. We conclude that EGF treatment accelerates lysosomal targeting of both the EGFR and erbB-2, but that the normal cellular distribution of the two proteins is different.

We were surprised at the predominant intracellular localization of erbB-2 because this receptor has previously been described as being cell surface-associated (27). To determine whether the intracellular localization of erbB-2 in B82 cells was atypical, we used confocal microscopy to examine the localization of erbB-2 in various cell lines (Fig. 50). In the case of both B82 cells and the nontransformed human mammary epithelial cell line HB2, there was a high levels of intracellular erbB-2 (top and middle right panels) whereas the EGFR displayed primarily a cell surface distribution (top and middle left panels). The human mammary epithelial cell line 184A1L5 also displayed significant levels of intracellular erbB-2 (data not shown). In contrast, the transformed cell line SKBR3 which overexpresses erbB-2, showed an almost exclusive cell surface localization (bottom panels). This distribution also corresponded to the location of the EGFR (bottom left panel). We conclude that a significant fraction of erbB-2 can exist in an intracellular compartment in nontransformed cells and that in the absence of EGF, the distribution of EGFR and erbB-2 is distinct. The cell surface distribution of erbB-2 previously described may either be a result of cell transformation or overexpression of erbB-2.

Structural aspects of EGFR required for erbB-2 transmodulation Several models could explain the ability of activated EGFR to target erbB-2 to lysosomes. One is that the EGFR activates erbB-2 by direct tyrosine transphosphorylation. The activated erbB-2 would then enter the lysosomal targeting pathway by a similar mechanism as the EGFR. We tested this possibility by determining the effect of EGF on erbB-2 levels using cells expressing kinase inactive EGFR. As shown in Fig. 51, full length kinase inactive EGFR still reduce erbB-2 levels in response to EGF, although not as rapidly as the wild type EGFR (6A versus 6B). This suggests that direct tyrosine phosphorylation of erbB-2 by the EGFR is not necessary for erbB-2 transmodulation.

Heterodimerization between EGFR and erbB-2 is thought to occur through their extracellular domains, but transactivation may also require cytoplasmic sequences of the EGFR (170,171). These sequences fall into three main domains: the regulatory cytoplasmic tail (residues 958-1186), the conserved kinase domain (688-958) and the submembrane region (residues 645-688). In an effort to determine which domain may be involved in transmodulation of erbB-2, we used B82 cells expressing EGFR that lacked various regions. As shown in Fig. 51B, receptors lacking all cytoplasmic sequences (c'647) or sequences distal to the submembrane region (c'688) did not reduce erbB-2 levels following EGF addition. Receptors having the conserved kinase domain (c'958) were able to efficiently reduce erbB-2 levels in response to EGF as effectively as full length receptors (Fig. 51A). Eliminating the intrinsic kinase activity of the c'958 receptor through a point mutation in its ATP binding site (M<sup>721</sup>) also did not eliminate its ability to reduce erbB-2 levels (Fig. 51B). We conclude that although the kinase domain of the EGFR is required for transmodulation of erbB-2, the kinase activity of this domain is not required. This suggests that direct phosphorylation of erbB-2 by the EGFR is not necessary.

The ability of mutant EGFR's to induce tyrosine phosphorylation of erbB-2 correlates with its ability to transmodulate erbB-2 levels - Although direct phosphorylation of erbB-2 by occupied EGFR is clearly not involved in transmodulation, it seemed possible that heterodimerization of kinase-inactive EGFR with erbB-2 could result in activation of erbB-2 through interaction of their cytoplasmic regions. It has been previously shown that EGFR lacking intrinsic kinase activity can activate erbB-2 (172). To test this possibility, we treated cells expressing various EGFR mutants for 15 and 120 minutes with EGF. ErbB-2 was then immunoprecipitated and



probed for phosphotyrosine by western blot analysis. As shown in Fig. 52, both the full length and c'958 mutants were able to induce tyrosine phosphorylation of erbB-2. Phosphorylation was highest at 15 min and fell by 2 hr. The c'958 EGFR mutant was able to induce a higher stimulated level of erbB-2 phosphorylation, although the basal level of erbB-2 phosphorylation was higher as well. Interestingly, kinase-inactive versions of the full length and c'958 EGFR were also able to induce tyrosine phosphorylation of erbB-2, albeit to a lower degree than the kinase active EGFR. The kinetics of erbB-2 phosphorylation were also similar.

In contrast to the results obtained with the full length and c'958 EGFR, receptors truncated to residue 688 were not able to induce tyrosine phosphorylation of erbB-2 (Fig. 53). Thus the ability of EGR-R able to mediate phosphorylation of erbB-2 is correlated with its ability to reduce erbB-2 levels. This is consistent with a model in which erbB-2 is transactivated by heterodimerization with the EGFR. The transactivated erbB-2 would then be targeted to lysosomes in an analogous fashion as ligand-activated EGFR.

The distal region of the EGFR tyrosine kinase domain is required for transmodulation of the EGFR - Although the region between 688 and 958 of the EGFR contains the conserved tyrosine kinase domain, another activity that has been mapped to the distal region of this domain is endosomal retention/lysosomal targeting (between 899 and 958; ref 178). To determine whether this region is required for transmodulation of erbB-2, we prepared an EGFR truncated at residue 899. As shown in Fig. 54, the c'899 EGFR was unable to mediate a reduction of erbB-2 levels in response to EGF. In addition, no tyrosine phosphorylation of erbB-2 was observed. We conclude that the region of the EGFR that contains the endosomal retention/lysosomal targeting sequences also contain the sequences necessary for both transactivation and transmodulation of erbB-2.

Characterization of cells overexpressing erbB-2 Ligand binding not only activates the EGFR but also initiates negative regulatory processes. Overexpression of the EGFR, however, has been shown to inhibit this negative regulation. In addition, overexpression of erbB-2 has been associated with poor prognosis in breast cancer. Since erbB-2 acts as a signaling partner of the EGFR, we wanted to determine whether erbB-2 overexpression affected its own negative regulation, or that of the EGFR. We employed a human mammary epithelial cell line (MTSV) and two derivative lines (ce-1 and ce-2) which have been transfected with the gene for erbB-2 (164,165). The parent cell line, derived from human breast aspirates, was immortalized with SV40 large T antigen, but is not tumorigenic. Transfection with the erbB-2 gene alters the growth characteristics of the ce-1 and ce-2 cells in that the transfectants grow in soft agar, can be propagated as tumors in nude mice, and show disorganized growth on collagen gels (165).

Western blot and a 37°C steady state Scatchard analysis was used to quantify the expression levels of both erbB-2 and EGFR in these epithelial cells. We found that the parental MTSV line expressed  $9.8 \times 10^4$  whereas the ce-2 line expressed  $1.5 \times 10^6$  erbB-2 molecules per cell (Fig. 55A), a 15-fold increase in the transfected cell line. The erbB-2 expression in the ce-1 line varied between 2 to 6 fold higher than the parental cells (data not shown). Western blot analysis indicated a 23-fold increase in erbB-2 mass in the ce2 versus MTSV lines, in good agreement with the values derived from the steady state analysis. This suggests that the radiolabeled antibodies used in the steady state analysis have access to most of the cellular erbB-2 pools. The affinity of the 4D5 antibody for erbB-2 was similar for both the MTSV and ce2 cells at 12 and 10 nM respectively. The percent of 4D5 antibody found internalized at steady state was also similar at 41% ( $\pm 4\%$ ) and 55% ( $\pm 14\%$ ) for MTSV and ce2 cells respectively.

The number of EGFR in these cells was also determined by Scatchard analysis conducted at 0°C to prevent receptor downregulation. As shown in Fig. 55B, both MTSV and ce2 cells



displayed similar numbers of surface EGFR ( $5.7 \times 10^5$  and  $9.2 \times 10^5$  per cell respectively) of predominantly a single affinity class. The affinity of these receptors, 1.4 nM, is similar to what has been described for fibroblasts (173). Western blots of detergent extracts of MTSV, ce1 and ce2 cells confirm that they all express similar number of EGFR (data not shown). Analysis of the western blots using a phosphoimager indicated that relative to cell protein content, ce2 cells express approximately 10% higher EGFR levels whereas the levels of EGFR in ce1 cells was indistinguishable from the parental MTSV cells.

To characterize erbB-2 and EGFR distribution in these cells, sparse cultures were fixed, permeabilized and stained using directly-labeled anti-erbB-2 and anti-EGFR antibodies. As shown in Fig. 56, erbB-2 was found at both the cell surface and in a collection of intracellular vesicles. The EGFR showed a very similar distribution pattern with EGFR and erbB-2 both colocalized at the cell surface and in intracellular vesicles (arrows in Fig. 56). These data suggest that overexpression of erbB-2 is not accompanied by any striking alteration in either its cellular distribution or affinity for antibodies. In addition, the number, distribution and affinity of EGFR do not appear to be greatly altered as a result of erbB-2 overexpression.

Amplification of erbB-2 inhibits the downregulation of erbB-2 - Because the EGFR transactivates erbB-2, changing the ratio of erbB-2 to EGFR may alter EGF-mediated erbB-2 phosphorylation. Both parental MTSV cells and overexpressing ce2 cells were treated with EGF for 5 and 10 minutes. ErbB-2 and EGFR were then immunoprecipitated followed by western blot analysis for phosphotyrosine, as an indicator of receptor activation status. As shown in Fig. 57, the addition of EGF increased the level of phosphotyrosine in both EGFR and erbB-2. In the case of the parental MTSV cells, very little receptor phosphorylation was observed in the absence of EGF addition. Surprisingly, in ce2 cells, there was a substantial amount of phosphorylation of both erbB-2 and the EGFR in the absence of EGF. Although increased basal activation of erbB-2 as a result of overexpression has been documented by other investigators (165,174,175), higher basal activation of the EGFR has not previously been reported. Addition of EGF further increased the level of erbB-2 phosphorylation approximately 3-fold in ce2 cells as compared to 9-fold in the MTSV cells (average of 3 experiments), indicating that the EGFR was capable of transactivating erbB-2 in both cell types.

It seemed possible that constitutive activation of both the EGFR and erbB-2 could be due to autocrine production of EGF-like ligands. We tested this idea by blocking EGFR activation using antagonistic anti-EGFR antibodies 225 and 13A9 (126,176). Neither antibody affected the constitutive activation of either the EGFR or erbB-2 (Fig. 57), suggesting that overexpression of erbB-2 alone was responsible.

To determine whether overexpression of erbB-2 affects its downregulation, we transactivated erbB-2 by treating both MTSV and ce2 cells with 100ng/ml EGF for 24 hours. As a comparison, we also examined a well characterized fibroblast cell line (177). Loss of erbB-2 was assessed by western blot analysis. As shown in Fig. 58A and 58B, fibroblasts and MTSV cells showed a 60% and 72% loss of erbB-2 respectively by 24 hours following EGF treatment. However, the ce2 cell line only displayed a 30% loss in erbB-2 mass. Calculating the net amount of erbB-2 loss following 24 hr EGF treatment showed that the MTSV cells lost a similar amount of erbB-2 mass relative to ce2 cells ( $2.0 \times 10^4$  versus  $2.3 \times 10^4$  arbitrary phosphorimager units). Thus, erbB-2 overexpression affected the relative amount erbB-2 degraded in response to EGF, not the absolute amount.

The kinetics of receptor loss showed that erbB-2 loss in the parental MTSV cells was completed within 6 hours (Fig. 58C). The level of erbB-2 in the overexpressing ce2 line was

only reduced about 5% at the same time. We confirmed that the accelerated loss of erbB-2 protein was due to enhanced degradation by labeling cells with  $^{35}\text{S}$ -amino acids and immunoprecipitation following EGF addition (data not shown). This indicated that EGF decreased the half-life of erbB-2 in MTSV cells from 6 hrs to 1 hr whereas the same treatment of ce2 cells decreased erbB-2 half-life from 6 hrs to 5 hrs. Reverse transcription PCR analysis of mRNA levels indicated that EGF did not affect the erbB-2 mRNA level (data not shown). These data suggest that overexpression of erbB-2 inhibits its downregulation by reducing the degradation rate of the transactivated receptor pool.

ErbB-2 overexpression increases signaling through the EGFR - As previously noted, we observed that overexpression of erbB-2 resulted in the constitutive activation of both the EGFR as well as erbB-2 (Fig. 57). The 6-fold increase in basal EGFR activation was similar to the 7-fold increased basal activity of erbB-2 (Fig. 57). Because erbB-2 acts as a signaling partner to the EGFR, it seemed possible that erbB-2 overexpression may drive heterodimer formation. Activation of the EGFR, however, is normally followed by several negative regulatory processes, such as desensitization and downregulation. To explore the effect of erbB-2 overexpression on both positive and negative regulation of the EGFR, we examined the time course of EGF-induced EGFR activity.

MTSV and ce2 cells were treated with a high concentration of EGF for up to 2 hrs. At different time intervals, cells were solubilized and the EGFR were immunoprecipitated and separated by gel electrophoresis. Receptor levels and phosphorylation states were then determined using western blots. As shown in Fig. 59A, there was no phosphorylation of the EGFR in MTSV cells in the absence of EGF. In contrast, ce2 cells displayed a high constitutive level of EGFR phosphorylation which was not affected by the addition of an antagonistic anti-EGFR antibody. In the case of both MTSV cells and ce2 cells, the addition of EGF caused an increase in EGFR phosphotyrosine (PY) content. However, receptor PY levels rapidly decreased in the case of MTSV cells, but remained elevated in the ce2 cells. A similar pattern was observed for EGFR mass (Fig. 59A). Receptor levels decreased following EGF addition for MTSV cells, but receptor levels remained relatively constant in the case of ce2 cells.

We analyzed the pattern of EGF-induced EGFR phosphorylation in terms of both PY to EGFR ratio and in terms of phosphorylated receptors per cell (Fig. 59B and 59C, respectively). This analysis showed that the amount of PY as a function of receptor mass was actually depressed following EGF addition in cells overexpressing erbB-2. The kinetics of EGFR phosphorylation in parental MTSV cells showed a rapid rise followed by a subsequent decline. This is characteristic of receptor desensitization. However, there was no sign of EGFR desensitization in the ce2 cells.

When analyzed in terms of total phosphorylated receptors per cell, the MTSV cells displayed a rapid loss of activated EGFR such that by 2 hrs following EGF treatment, their levels were similar to the constitutive level of EGFR activation in ce2 cells (Fig. 59C). Addition of EGF to ce2 cells caused a persistently high level of activated EGFR, evidently due to the suppression of receptor loss. We repeated these experiments using cells that express only 6-fold higher levels of erbB-2 (ce1 cells) and found an intermediate result in that the constitutive level of EGFR activation and the degree of receptor loss was between that observed for ce2 and MTSV cells (data not shown).

Our results indicate that the overexpression of erbB-2 inhibits downregulation of the EGFR. To test this idea directly, both MTSV and ce2 cells were treated with 100ng/ml EGF and at various times the cells were solubilized and the EGFR levels were determined by western blot analysis. As shown in Fig. 60, the loss of EGFR mass in both MTSV and ce2 cells was biphasic. The parental MTSV cells lost half their EGFR mass in less than 2 hr, whereas the ce2 cells lost

the same amount in about 10 hr. Thus downregulation of the EGFR is inhibited in cells that overexpress erbB-2.

**ErbB-2 overexpression inhibits EGFR downregulation at multiple levels** - Ligand-induced downregulation of the EGFR is regulated at three distinct levels: endocytosis, endosomal sorting and lysosomal targeting (58,60,178). It has been suggested previously that erbB-2 overexpression inhibits internalization of the EGFR (179). This, in turn, could inhibit EGFR downregulation. To test this possibility, we examined the kinetics of both intracellular and cell surface accumulation of EGF. If overexpression of erbB-2 was inhibiting EGFR internalization, then we should observe an increased amount of EGF at the cell surface and a corresponding decrease in intracellular ligand. MTSV and ce2 cells were incubated with  $^{125}\text{I}$ -labeled EGF at  $37^\circ\text{C}$ . At various times, the relative amount of ligand either inside the cell or at the cell surface was determined. As shown in Fig. 61 (bottom panel), ce2 cells displayed a pronounced increase of  $^{125}\text{I}$ -EGF binding to the cell surface relative to MTSV cells, especially at the longer time points ( $>20$  min). The 3-4 fold elevation in binding could not be explained by the relatively small differences in EGFR levels between MTSV and ce2 cells (see Fig. 55B). Paradoxically, we also observed an increased level of intracellular  $^{125}\text{I}$ -EGF in ce2 cells, but only after about 20 min incubation with ligand (Fig. 61, top panel). The similar amount of internalized ligand in both MTSV and ce2 cells at early time points is inconsistent with an inhibition of internalization. The accumulation of intracellular  $^{125}\text{I}$ -EGF at longer incubation times suggests an inhibition of lysosomal degradation.

Since a change at a single point in the EGFR trafficking pathway could not explain the observed accumulation of both surface-associated and intracellular EGF in ce2 cells, it seemed possible that erbB-2 overexpression could cause multiple alterations in EGFR trafficking. We therefore examined the individual steps. The specific internalization rate was determined by incubating cells with radiolabeled EGF for five minutes, during which time surface-associated and internalized ligand was measured. Fig. 62A shows that overexpression of erbB-2 did not significantly alter the internalization rate constant ( $k_e$ ) for the EGFR ( $0.141 \text{ min}^{-1} \pm 0.01$  versus  $0.116 \text{ min}^{-1} \pm 0.03$  for MTSV and ce2 cells respectively). The kinetics of initial  $^{125}\text{I}$ -EGF binding to both MTSV and ce2 cells was also similar (Fig. 62B), which indicates that the forward rate constant ( $k_a$ ) was the same. To determine the dissociation rate constant ( $k_d$ ), the cells were incubated with EGF for 5, 10 and 15 minutes followed by a chase in a large excess of unlabeled EGF (to prevent rebinding of dissociated  $^{125}\text{I}$ -EGF). The amount of EGF lost from the surface is a combination of ligand internalization and dissociation from the receptor. Thus, the rate of  $^{125}\text{I}$ -EGF loss from the cell surface is equal to  $k_d + k_e$ . Because  $k_e$  is the same in the two cell types (Fig. 61A), differences in loss will reflect  $k_d$ . As shown in Fig. 62C, loss of EGF was substantially slower from the surface of ce2 cells as compared to MTSV cells ( $0.149 \text{ min}^{-1}$  versus  $0.234 \text{ min}^{-1}$  respectively). This did not change appreciably as a function of incubation time. Subtracting the value of  $k_e$  measured in parallel experiments ( $0.135 \text{ min}^{-1}$ ; dashed line in Fig. 62C) yielded a value of  $k_d$  of  $0.013 \text{ min}^{-1}$  in ce2 cells and  $0.10 \text{ min}^{-1}$  in MTSV cells. Thus overexpression of erbB-2 appears to cause a 7-fold reduction in the EGF dissociation rate constant, which could result in increased levels of ligand-bound receptor at the cell surface.

To assess the effect of erbB-2 overexpression on EGFR endosomal sorting, we used a previously described technique that measures the fraction of internalized receptors that are recycled (65). To measure fractional recycling, cells are brought to steady state with different concentrations of  $^{125}\text{I}$ -EGF. Surface-associated EGF is removed with a mild acid strip and the relative amount of intact versus degraded EGF which subsequently appears in the medium is measured. We have previously shown that the ratio of intact versus degraded EGF indicates the fraction of internalized ligand that is recycled versus targeted to lysosomes (65). When we used this technique on MTSV and ce2 cells, we obtained the results shown in Fig. 62D. The

parental MTSV cells showed an increase in fractional ligand recycling from 0.25 to 0.45 as the intracellular ligand increased from  $7 \times 10^3$  to  $4 \times 10^5$  molecules per cell. This "saturation" of endosomal sorting is very similar to what has previously been described in fibroblasts (65). The ce2 cells displayed a very similar fractional recycling pattern, but with a greater degree of recycling at all intracellular ligand concentrations. This suggests that overexpression of erbB-2 inhibits sorting of EGFR from endosomes to the lysosomes, and thus promotes recycling.

To directly test if EGFR transfer to the lysosomes was impaired by erbB-2 overexpression, a kinetic analysis of  $^{125}\text{I}$ -EGF degradation was done. Cells were incubated for 5 minutes with  $^{125}\text{I}$ -EGF followed by a chase in unlabeled medium. The amount of intracellular  $^{125}\text{I}$ -EGF remaining at different times was then determined. Under these conditions, almost all of the  $^{125}\text{I}$ -EGF lost from the cells is degraded ligand (180); also results not shown). As shown in Fig. 63A, there was a lag of approximately 15 minutes in MTSV cells before significant loss of internalized ligand was observed. This lag generally corresponds to the time necessary for internalized EGF to be transferred to lysosomes (181). Thereafter, the  $^{125}\text{I}$ -EGF was lost with a  $T_{1/2}$  of 32 min. In the case of ce2 cells, there was a slightly longer lag before initiation of ligand loss, after which  $^{125}\text{I}$ -EGF was lost with a  $T_{1/2}$  of 53 min. The ce1 cells showed an intermediate rate of ligand loss ( $T_{1/2}$  of 46 min, data not shown). These data indicate that erbB-2 overexpression interferes with EGFR trafficking to the lysosomes.

To confirm that differences in ligand degradation rates were due to differences in intracellular trafficking, we used immunofluorescence to follow the progression of the EGFR from the cell surface to the lysosome. The lysosomes were labeled with a pulse of fluorescently labeled dextran followed by a 2 hour chase. During this chase, the cells were pulsed with Texas Red labeled EGF to label the EGFR. The cells were fixed at different time periods and colocalization of the EGF with the lysosomes was determined using digital confocal imaging. As shown in Fig. 63B, there was little colocalization of the EGF with lysosomes following the initial 15 min pulse. However, there was progressive colocalization of the two fluorescent labels during the 2 hr chase period. Colocalization reached its greatest extent in both MTSV and ce2 cells at 60-80 min (Fig. 63B). The rate at which EGF was transferred to lysosomes was somewhat slower in the ce2 cells as was the extent of transfer (29% versus 35% for ce2 and MTSV cells respectively). Colocalization of EGF in lysosomes in both cell types declined after 80 min and never involved the majority of the ligand. This is probably because our pulse labeling protocol only labels a subpopulation of total cellular lysosomes. The apparent decrease in colocalization is most likely due to EGF being transferred to newly formed lysosomes lacking fluorescein-dextran combined with degradation of previously transferred EGF. Nevertheless, these data confirm that transfer of EGF-containing endosomes to lysosomal structures is slower in ce2 cells relative to MTSV cells. Thus overexpression of erbB-2 results in an inhibition of lysosomal trafficking of EGFR.

## Conclusions

We have successfully completed our project. Growth factors provide important information to the cell regarding its environment. They can also stimulate mitogenesis. Our work has shown that the normal spatial distribution and trafficking of both growth factors and their receptors are necessary for normal cell behavior and physiology. When we initiated these studies, we were primarily focused on the spatial distribution and regulation of the EGF receptor. Our work in the last several years has shown us that the distribution of the ligand and well as receptor subunits (such as erbB-2) are at least as important issues. In fact, ligand distribution seems to play the most important role in regulating EGFR function.

The most important finding of our study was that ligand release is the upstream regulator of EGFR activation. By preventing ligand release (by using protease inhibitors), we can effectively inhibit cell proliferation. This provides a novel opportunity for therapeutic intervention in cancer treatment. The predominant perspective with respect to the EGFR involvement in cancer is that overexpression or derangement in EGFR regulation is a common feature in breast cancer. This may be the case, but the implication of this observation is that one should only attempt to target the dysfunctional EGFR system for therapy. In fact, this is probably the opposite of what one should really consider. If the EGFR is overexpressed in cancer, then it will probably be more difficult to inhibit its activity. Most cancers probably express normal levels of EGFR and the cognate ligands. At their normal levels of expression, they represent an excellent therapeutic target.

Important issues that remain (at least from a therapeutic standpoint) is the role that the EGFR plays in normal physiology and whether targeting the EGFR system *in vivo* will result in significant toxicity to noncancerous tissues. If the EGFR system primarily operates in the context of development, wound healing or tissue regeneration, then targeting this system should cause minimal toxicity to normal tissues. Thus, it could represent an attractive target for anticancer drugs. These types of issues should be addressed with translational studies that attempt to apply the knowledge we have gained to development of new combination therapies for breast cancer.



## Figure Legends

*Figure 1* Organization of HMEC on Matrigel. (A) Cells (line 184) were grown to confluence on plastic or (B) plated on thick layers of Matrigel at a cell density of  $2.5 \times 10^4$  cells/cm<sup>2</sup> in the presence of 2 nM EGF for 10 days.

*Figure 2* Cells organized for 10 days on Matrigel were fixed, embedded in paraffin, sectioned at 10  $\mu$ m and stained with hematoxylin and eosin. "M" designates the Matrigel and "KP" indicates keratin pearls which are indicative of squamous differentiation.

*Figure 3* Organization of HMEC on Matrigel requires activation of EGFR. Cells (line 184) were plated on thick layers of Matrigel at a cell density of  $2.5 \times 10^4$  cells/cm<sup>2</sup> in the presence of 2 nM EGF for the indicated lengths of time. Cells incubated in 225 mAb (lower right panel) were cultured for 2 days in the presence of 10  $\mu$ g/ml of the antibody and in the absence of exogenous EGF. Photos were taken using phase optics. Bars are approximately 200  $\mu$ m length.

*Figure 4* Effect of EGFR activation on spreading of HMEC. Plates were either coated with a thin layer of Matrigel (top panels), or laminin (bottom panels) after which cells were plated in the absence (left) or presence (middle) of 2 nM EGF. Alternately, cells were incubated with 10  $\mu$ g/ml 225 mAb. Photos were taken at 200X approximately 24 h following plating.

*Figure 5* Organization of HMEC in the absence of exogenous EGF is dependent on cell density. The indicated number of cells ( $5 \times 10^4$ ,  $1 \times 10^5$ ,  $2 \times 10^5$ ) were plated on thick layers of Matrigel cast in 6 well culture dishes either in the presence or absence of 2 nM EGF. Photographs were taken of the center of the wells (4X phase objectives) after either 24 h (left panels) or after 72 h (right panels). Arrows indicate individual cells isolated from the main organizing structures.

*Figure 6* Both 184A1 and HB2 cells express high numbers of EGFR, but only the 184A1 cells are responsive to receptor occupancy. (A) 184A1 and HB2 cells were brought to equilibrium overnight at 4 °C with concentrations of <sup>125</sup>I-EGF ranging from 0.16 nM to 50.0 nM. The amount of specifically associated ligand was determined and is presented as a Scatchard plot. (B) At day minus 1 184A1 and HB2 cells were split 1:200 from confluency to 100mm plates into normal growth media. At day zero cells were counted in a coulter counter and medias were changed. Cells were grown in either normal growth media (—■—), with EGF at 3.3 nM (—●—), or with 130 nM mAb 225 (—○—). Cells were counted and the media was changed every other day for 10 days.

*Figure 7* Intracellular distribution of EGFR in HMEC. All cells were serum starved for 24 hrs prior to the start of the experiment. Either mAb 225 at 3.2 nM (C, D) or EGF at 8.2 nM (E, F) or nothing (A, B) was added to the serum free media and all cells were kept at 37°C for 2 hours prior to fixation. In control cells and EGF treated cells, EGFR was visualized with a mix of mAbs 225 and 13A9 at 10  $\mu$ g/ml and 1.0  $\mu$ g/ml, respectively, followed by a FITC-conjugated goat anti-mouse secondary antibody at (1:300). No additional mAb 225 or 13A9 was used to visualize EGFR in the cells already treated with mAb 225 in the media. The pre-bound mAb 225 was visualized with the same FITC-conjugated goat anti-mouse secondary antibody at (1:300). Images were captured with a 40 X Nikon objective and the white bar represents 10  $\mu$ m.

*Figure 8* Rapid endocytosis of empty EGFR in 184A1 cells increases the fraction of EGFR found within the cells. Inside:surface ratio of empty EGFRs in 184A1 (—○—), HB2 (—□—), and 48R

(—△—) cell lines. Cells were incubated in the presence of 0.65 nM  $^{125}\text{I}$ -mAb 225 at 37 °C over the time course 5 - 180 min. Non-specific binding was determined with parallel samples prepared in the presence of 3.0  $\mu\text{M}$  unlabeled  $^{125}\text{I}$ -mAb 225 and subtracted as non-specific binding. The relative distribution of label between surface and inside of the cells was determined and the results were plotted as inside cpm versus surface cpm.

*Figure 9* Ligand induced endocytosis and constitutive endocytosis in HMEC. Statistical summary of the internalization rates of both occupied and empty EGF receptors in different HMEC cell lines. The 184, 161, and 48R cell lines are primary cell lines derived from reduction mammaplasty (182). The 184A1 cell line is an immortal derivative of the 184 line (183). The kinetics of internalization were measured for 5 minutes using either (A)  $^{125}\text{I}$ -mAb 225 or (B)  $^{125}\text{I}$ -EGF at concentrations from 0.20 nM to 0.50 nM to follow the occupied receptor. The relative distribution of label between the surface and the inside of the cells was determined and converted to internalization plots as described (74,75). In both graphs, the *center line* is the median value while *whiskers* enclose all the data values within one standard deviation. Numbers in parentheses indicate the total number of independent experiments. Numbers in parentheses indicate the total number of independent experiments.

*Figure 10* EGF and antagonistic mAb 528 are internalized similarly in 184A1 cells. Endocytosis of occupied and empty receptor EGF (○, □) and antagonistic mAb 528 (●, ■) was measured after prebinding of ligands to cells at 4°C. Cells were pre-incubated at 4°C in the presence of either 1.7 nM  $^{125}\text{I}$ -EGF or 6.5 nM  $^{125}\text{I}$ -mAb 528 for 3 hours and rapidly warmed to 37°C in the absence of ligands. Loss of EGF and mAb 528 from the surface (○, ●) and accumulation of ligands on the inside of cells (□, ■) was then determined. Each point is plotted as a percent of total cpm at that time point.

*Figure 11* Specific internalization of EGFR in 184A1 and HB2 cells as a function of receptor occupancy. The kinetics of  $^{125}\text{I}$ -EGF internalization was measured for 5 min using  $^{125}\text{I}$ -EGF concentrations from 0.017 nM to 50.0 nM in 184A1 (—●—), HB2 (—△—), and A431 (—□—). The relative distribution of label between the surface and the inside of the cells was determined and converted to internalization plots as described (74,75). The specific internalization rates are shown as a function of the average number of receptors occupied during the entire period of uptake.

*Figure 12* Turnover of empty and occupied EGFR in HMEC. Half-life of the EGFR in 184A1 (○, ●) and HB2 (□, ■) cells in the absence (open symbols) and presence (closed symbols) of EGF. 184A1 and HB2 were metabolically labeled with  $^{35}\text{S}$ -amino acids and then chased in unlabeled medium with an excess of methionine and cysteine in the absence or presence of 17 nM EGF. EGFR was immunoprecipitated with 13A9, electrophoretically fractionated on a denaturing and reducing 5-15% polyacrylamide gel (A). The gel was dried, and the amount of label remaining in the receptors was determined at the indicated times using the Bio-Rad Phosphoranalyst hard ware and software. Radioactivity remaining was plotted versus time and a half-life for the EGFR was calculated.

*Figure 13* EGFR contained within internal vesicular compartments of 184A1 cells are not activated. HB2 (A-D) and 184A1 (E-H) cells were grown in the absence of EGF for two days and then either fixed or permeabilized without the addition of EGF (A, B, E, F) or after the addition of 17 nM EGF for 15 minutes (C, D, G, H). All cells were stained for both EGFR and phosphotyrosine content. EGFR was visualized with a mix of mAbs 225 and 13A9 at 10  $\mu\text{g}/\text{ml}$  and 1.0  $\mu\text{g}/\text{ml}$ , respectively, followed by a FITC-conjugated goat anti-mouse secondary

antibody; antiphosphotyrosine was visualized with an affinity purified rabbit polyclonal anti-phosphotyrosine followed by Texas-Red-conjugated goat anti-rabbit. Non-specific staining by secondary antibodies was insignificant (data not shown). Arrows in panels, C and D, and, G and H, indicate colocalization of EGFR and phosphotyrosine. Inset images in panels E and F are enlargements of boxed regions. Images were captured with a 100 X Nikon objective and the white bar represents 5 $\mu$ m.

*Figure 14* Antagonistic mAb 225 does not activate the EGFR. Immunoblot of EGFR and EGFR phosphotyrosine in 184A1 and HB2 cells in the absence and presence of EGF. (A) Cells were grown to near confluency, and then either left untreated or were treated with 17 nM EGF for 10 min at 37°C. (B) Cells were grown to near confluency, and then either left untreated or were treated with either 0.17 nM or 17 nM EGF or 6.5 nM mAb 225 for 10 min at 37°C. All cells were extracted and handled as described in Materials and Methods.

*Figure 15* Scatchard binding analysis of confluent 14-day old parental wildtype (WT) LLCPK1 clone C14, (A), and of C14 cells transfected with a full-length human EGFR construct (K2), (B) Wildtype cells (160,000 cells per filter) expressed approximately 22,000 basolateral and 5,000 apical EGFR per cell. K2 cells (408,000 cells per filter) expressed approximately 1,444,000 basolateral and 474,000 apical EGFR per cell. The apical EGFR expressed by K2 cells were of high ( $K_d = 1.5 \times 10^{-9}$ M) and low affinity ( $2.4 \times 10^{-7}$ M). The basolateral EGFR of K2 cells were of high ( $K_d = 3.6 \times 10^{-8}$ M) and low affinity ( $1.1 \times 10^{-7}$ M) as well.

*Figure 16* (A) [ $^3$ H]-thymidine incorporation, expressed as a percentage over control (incorporation in the absence of EGF), of K2 cell monolayers following the addition of apical or basolateral EGF for 24 hours. As a control, mab 225, an EGFR blocking antibody, was added to the ipsilateral side or contralateral to EGF in order to demonstrate the specificity of apical or basolateral EGFR stimulation. This also demonstrated the lack of significant leakage or translocation of EGF from one side of the monolayer to the other. The results are expressed as the average of triplicate experiments  $\pm$  standard error of the mean (SEM). (B) Cell densities of K2 cell monolayers five days after the addition of apical or basolateral EGF. Cells were plated at equal cell density at time zero and cultured on permeable filters for 14 days at which time EGF (20ng/ml) was added to the monolayers. Cells were counted 5 days after the addition of EGF. Control cells received no EGF. The results expressed are averages of triplicate experiments  $\pm$  SEM

*Figure 17* EGFR down-regulation shown as a percentage of initial  $^{125}$ I-EGF binding to K2 cells. The open circles represent cells pretreated with apical EGF and the solid circles, cells pretreated with basolateral EGF.  $^{125}$ I-EGF binding was observed for 60 minutes.

*Figure 18* EGFR endocytosis plotted as internalized EGF versus the integral surface EGF. The open circles represent cells pretreated with apical EGF and the solid circles, cells pretreated with basolateral EGF. The slope of the lines represents the endocytic rate. (A) A typical plot showing endocytosis of full-length EGFR by K2 cells following apical or basolateral EGF addition. This experiment was performed three times yielding an average endocytic rate constant of  $0.15 \pm 0.022$  (SEM) for cells pretreated with apical EGF and  $0.03 \pm 0.014$  (SEM) for cells pretreated with basolateral EGF. (B) A typical plot showing EGF-induced endocytosis of apical or basolateral c'973 EGFR mutant constructs transfected into the parental cell line (C14). This experiment was performed three times and yielded an average  $K_e$  of  $0.04 \pm 0.007$  (SEM) for cells pretreated with apical EGF and a  $K_e$  of  $0.04 \pm 0.006$  (SEM) for cells pretreated with basolateral EGF.

*Figure 19* Antiphosphotyrosine blot of EGFR at various timepoints following the addition of apical or basolateral EGF (50ng/ml) to confluent K2 cell monolayers. The band representing the EGFR was determined in a parallel western blot (not shown) and is the most prominent tyrosine phosphorylated band seen following EGF stimulation.

*Figure 20* Antiphosphotyrosine blot of SHC protein immunoprecipitated following the addition of apical or basolateral EGF to K2 cell monolayers. Each immunoprecipitation was performed on an equal number of K2 cells. The prominent tyrosine phosphorylated band at the top of the blot is EGFR that coprecipitated with SHC protein. Numbers at the bottom represent the densitometry results, normalized to the control (no EGF), of the bands representing tyrosine phosphorylated SHC.

*Figure 21* Antiphosphotyrosine blot of FAK immunoprecipitated from K2 cell monolayers treated with apical or basolateral EGF. Each immunoprecipitation was performed on an equal number of cells.

*Figure 22* Antiphosphotyrosine (left panels) and beta-catenin immunoblots (right panels) of beta-catenin immunoprecipitated following the addition of apical or basolateral EGF to K2 cell monolayers. All immunoprecipitations were performed on an equal number of cells. (A) Beta-catenin was immunoprecipitated from whole cell lysates and detected with either antiphosphotyrosine (left panel) or beta-catenin antibodies (right panel). Two protein bands were detected on the beta-catenin immunoblots. The upper band represents the unphosphorylated form and the lower band tyrosine phosphorylated beta-catenin. Numbers appearing under the tyrosine phosphorylated bands are densitometry results normalized to the control (no EGF). (B) Beta-catenin was coimmunoprecipitated with an E-cadherin-specific monoclonal antibody from the Triton-soluble cell fraction and probed with antiphosphotyrosine (left panel) or beta-catenin (right panel) monoclonal antibodies. (C) Beta-catenin was immunoprecipitated from the Triton-soluble cell fractions that were immunodepleted of E-cadherin and probed with antiphosphotyrosine (left panel) or beta-catenin (right panel) monoclonal antibodies. (D) Beta-catenin was immunoprecipitated from the Triton-insoluble cell fraction and probed with antiphosphotyrosine (left panel) or beta-catenin (right panel) monoclonal antibodies.

*Figure 23* Confocal laser microscopy of beta-catenin in confluent K2 monolayers in the absence of exogenous EGF. (A) X-Z plane reconstructions of scans of K2 monolayers stained for beta-catenin and detected with a FITC-labeled secondary antibody. Beta-catenin localized to the lateral cell membranes, and, no apical or basolateral staining were seen. (B) X-Y plane scans of the same cells showing phosphotyrosine staining (left panel) as a reference and beta-catenin staining (right panel). Note the presence of specific cytoplasmic staining for beta-catenin.

*Figure 24* Western blot of WT and  $\Delta$ EGFR in mammary epithelial cells. Cells were extracted in 1% Triton buffer and an aliquot from each clone was placed onto a 5-15% polyacrylamide gel. After electrophoresis, the gel was blotted onto nitrocellulose and probed for the presence of receptor using N13 anti-EGFR antibody. The lanes marked WT contained extract from the parental cell line while the lanes marked  $\Delta$ 2-7 contained extracts from U87 glioblastoma cells transfected with the  $\Delta$ EGFR. See Table 3 for quantitation of receptor mass.

*Figure 25* Growth curves of parental cells and cells expressing low and high levels of  $\Delta$ EGFR. Cells were plated at  $2-4 \times 10^5$  cells/ 35 mm plate on day -1 and maintained overnight in



medium lacking EGF. Cells were counted the following day and medium containing either 12.5 ng/ml EGF or 10  $\mu$ g/ml 225 anti-EGFR antibody was added. Cell samples were taken daily and the medium changed on the remaining plates every 2 days.

*Figure 26* Clonal growth of cells. Clones expressing high and low levels of  $\Delta$ EGFR as well as parental cells and cells producing secreted EGF were plated at very low density onto 35 mm plates (1:800 split from confluent plates). They were grown in medium lacking EGF (control), containing 12.5 ng/ml EGF or containing 10  $\mu$ g/ml 225 anti-EGFR antibody. Plates were maintained for 3 weeks until confluence had been reached. After three weeks, the plates were washed and stained with Giemsa.

*Figure 27* Effect of anti-EGFR antibody (225) on  $\Delta$ EGFR activity. Parental cells and the high expressing  $\Delta$ EGFR clone were incubated in medium containing 50 ng/ml EGF, no EGF or 10  $\mu$ g/ml 225 ab for 16 hr. After extraction and protein determination, equal amounts of protein from each sample was reacted with anti- $\Delta$ EGFR antibody coupled to protein A sepharose for 1.5 hr at 4°C. After the antibody beads were removed by centrifugation 528 anti-EGFR antibody coupled to protein A sepharose beads was added to each sample and it was reacted for the same period of time. The resulting antigen-antibody complexes were washed and then electrophoresed onto a 5-15% gradient gel. After transfer the blot was probed with RC20 antiphosphotyrosine antibody coupled to horseradish peroxidase and then stripped and probed with N13 anti-EGFR antibody.

*Figure 28* Wound healing assay. Confluent monolayers of cells were incubated overnight in medium lacking EGF and then a "wound" was made on each plate using a rubber policeman. The "wound" was marked and measured using an ocular micrometer mounted on a Wild dissecting microscope. New medium was added to each plate either containing (12.5 ng/ml) or lacking EGF. Each cell free area was measured daily and a fresh aliquot of EGF (in a 2  $\mu$ l volume) added to each +EGF plate.

*Figure 29* SHC phosphorylation and association of Grb2. SHC immunoprecipitation was performed on extracts of cells maintained in the absence of EGF or exposed to 25 ng/ml EGF for 5 min. The resulting Protein A sepharose-antigen beads were gently washed twice and then boiled in SDS; the samples were divided in half and placed on two 5-15% acrylamide gels. After electrophoresis followed electrophoretic transfer the blots were probed with either anti-phosphotyrosine antibody (RC20) or anti-Grb2 antibody.

*Figure 30* Cell density determinations. Cells were plated onto 1 cm<sup>2</sup> coverslips and allowed to reach confluence in medium containing EGF. Duplicate samples were taken every other day, fixed in paraformaldehyde and stained with DAPI to visualize the nuclei. The coverslips were mounted and 3 fields from each was counted using an inverted fluorescent microscope.

*Figure 31* Organization on Matrigel.  $1 \times 10^5$  cells of each type were plated into a well of a 12 well plate that contained 0.7 ml Matrigel. The cells were then incubated in medium containing no EGF (control), 12.5 ng/ml EGF or 10  $\mu$ g/ml 225 mAb. The medium was changed every two days and the cells were photographed on an inverted microscope.

*Figure 32* Scatchard analysis of parental 184A1 cells and cells transduced with a gene for EGF (AXR1). Cells were brought to equilibrium overnight at 4 °C with concentrations of <sup>125</sup>I-EGF ranging from 0.16 nM to 50.0 nM. The amount of specifically associated ligand was determined and is presented as a Scatchard plot.

*Figure 33* Effect of EGFR overexpression on growth of HMEC. Equal numbers of each cell type were plated into dishes without EGF (—●—) or either with 20 nM EGF (—○—) or 10  $\mu$ g/ml of 225 mAb (—□—). Cell number was determined in duplicate at the indicated times. Shown are the results for the parental 184A1 cells (top panel) and the AXR1 cells which overexpress the EGFR (bottom panel). The medium was changed every other day.

*Figure 34* Modified EGFR ligands in HMEC. (A) Maps of the constructs expressed in HMEC. Top map defines the domains found in native EGF. The core domain binds to the EGFR and is responsible for its biological activity.

(B) Size of the EGF constructs expressed in HMEC. Conditioned medium from cells expressing sEGF was concentrated and applied to a Sephadex G-75 column together with molecular weight markers. Samples were collected and evaluated for EGF levels by ELISA. Elution position of the markers are indicated by arrows. Inset: western blot analysis of concentrated medium from cells expressing either EGF-Ct or sEGF. Antibody used was a polyclonal against human EGF. The standard (rhEGF) was commercial purified recombinant human EGF.

*Figure 35* Expression of modified EGFR ligands in HMEC (A) Rate of EGF production by either parental HMEC (WT) or several lines expressing either sEGF or EGF-Ct. Monolayers of cells were changed to medium lacking EGF and either with (solid bars) or without (hatched bars) 10  $\mu$ g/ml 225 mAb. After 24 h, the conditioned medium was collected and evaluated for EGF levels by ELISA. Cell number was determined at both the initial and collection time points and the average used to correct for the secretion rate. (B) Downregulation of the EGFR in either parental HMEC (WT) or cells expressing either sEGF or EGF-Ct. Cells were incubated in the presence (solid bars) or absence (hatched bars) of 33 nM EGF for 24 h. Cells were then extracted with detergent and the total cellular EGFR content was determined by ELISA. Data was standardized to the receptor content per  $\mu$ g protein in the parental cells.

*Figure 36* Distribution of EGFR and modified ligands in HMEC. Parental cells (WT) and cells expressing either sEGF (clone #1) or EGF-Ct (clone #2) were fixed, permeabilized and simultaneously stained for the EGFR (left panels) or EGF (right panels). Exposure times for visualizing each antigen were identical using the WT cells as the standard for EGFR and the EGF-Ct cells as the standard for EGF.

*Figure 37* Colocalization of sEGF and EGFR in HMEC. Cells expressing sEGF (clone #1) were fixed, permeabilized with saponin and incubated with directly-labeled anti-EGFR antibody 13A9 (green) or anti-EGF antibody HA (red). Image triplets were acquired with a 100X objective and deconvolved using a nearest-neighbor routine (left panel). The red image was converted to a binary image (middle panel) and logically AND'ed with a binary image of the green image to determine colocalization (right panel). The small panels beneath the main images are enlarged sections of the image. The bar is 5  $\mu$ m.

*Figure 38* Autocrine signaling by sEGF cannot be interrupted. (A) Proliferation of HMEC. Equal numbers of each cell type were plated into dishes without EGF (—○—) or either with 20 nM EGF (—●—) or 10  $\mu$ g/ml of 225 mAb (—□—). Cell number was determined in duplicate at the indicated times. The medium was changed every other day. (B) Phosphorylation of the EGFR substrate SHC. Cells treated either with 20 nM EGF for 5 min, or 10  $\mu$ g/ml of 225 mAb for 18 h were extracted and total cellular SHC was immunoprecipitated. After electrophoresis and transfer to nitrocellulose, the blots were probed with anti-phosphotyrosine antibodies. Arrows indicate the 66 kDa SHC-related protein and the 53 kDa and 46 kDa forms of SHC.

*Figure 39* Expression of sEGF allows clonal growth of HMEC in the presence of anti-EGFR antibodies. Parental cells (WT) and cells expressing either sEGF (clone #1) or EGF-Ct (clone #2) were seeded at a density of  $<100$  per  $\text{cm}^2$  into 60 mm dishes and cultured for three weeks in the presence of control medium lacking exogenous EGF, or with either 2 nM EGF or 10  $\mu\text{g}/\text{ml}$  225 mAb. The cells were then stained with crystal violet.

*Figure 40* Expression of sEGF prevents HMEC from organizing into organotypic structures on Matrigel. Parental cells (WT) and cells expressing either sEGF (clone #1) or EGF-Ct (clone #2) were seeded at a density of  $1.3 \times 10^4/\text{cm}^2$  in the absence of EGF (control), in the presence of 2 nM EGF (+EGF) or 10  $\mu\text{g}/\text{ml}$  225 anti-EGFR antibodies (+225). After 6 days, photographs were made using 4X phase objectives.

*Figure 41* Batimastat inhibits proliferation of EGF-dependent cells. (A) Cells plated on coverslips were treated with 225 mAb (67 nM), batimastat (10  $\mu\text{M}$ ) or EGF (50 ng/ml) for 48 hrs. Cells were labeled during the last 18 hr with BrDu. The results are the average of two independent experiments. (B) The indicated cells were grown for 5 days in growth medium alone (control) the presence of mAb 225 (67 nM), batimastat (7.5  $\mu\text{M}$ ), or a combination of mAb 225 and batimastat or batimastat and EGF (4 nM). Media were changed on days 1 and 3.

*Figure 42* Batimastat inhibits release of a membrane-anchored, but not a soluble form of EGF. (A) Map of the artificial EGF genes expressed in HMEC. Top diagram is the native EGF gene from which the two artificial genes were derived. (B) Cells expressing either the EGF-Ct or sEGF constructs were incubated with 67 nM 225 mAb (to prevent ligand uptake) for 18hr either without (□) or with (■) 5  $\mu\text{M}$  batimastat. The medium was analyzed for EGF levels using an ELISA (137). The results are the average of two independent experiments.

*Figure 43* Batimastat inhibits the proliferation of cells expressing a membrane-anchored, but not soluble form of EGF. (A) Parental cells and those expressing the indicated construct were plated at a 1:400 dilution and grown for 2 weeks either with or without 10  $\mu\text{M}$  batimastat. The medium was changed every two days. Cells were then stained with Giemsa. (B) The percent of BrDu-labeled nuclei was determined after an 18 hr BrDu pulse for cells expressing either EGF-Ct (□) or sEGF (■) treated for 48 hrs with the indicated supplement as outlined in the legend of Fig. 1. The results are the average of two independent experiments.

*Figure 44* Batimastat blocks autocrine signaling of cleavage-dependent EGFR ligands. Confluent cultures of either parental HMEC or cells expressing EGF-Ct or sEGF were preincubated for 24 hrs with either 67 nM 225 mAb or 10  $\mu\text{M}$  batimastat. Treatment with EGF (100 ng/ml) was for 20 min. Total EGFR was immunoprecipitated and visualized by western blot using anti-PY antibodies. The blots were then stripped and reprobed with anti-EGFR antibodies. The numbers under the anti-PY lanes are the relative densities of the bands normalized to the untreated controls.

*Figure 45* Inhibition of cell migration by batimastat. Parental HMEC or cells expressing the indicated ligand were followed for 15 hr by time-lapse video microscopy using 10 min intervals. The tracks of 8 random cells from each plate are plotted as flower plots (140) with the origin of each cell set to 0,0. Batimastat was used at 10  $\mu\text{M}$  and EGF was used at 50 ng/ml.

*Figure 46* Effect of EGF on erbB-2 and EGF-R levels in human mammary epithelial cells as evaluated by flow cytometry. HMEC 184A1L5 cells were grown for 48 h in the absence of EGF

and treated for 1 hr at 37°C either without (shaded peaks) or with (light peaks) 100 ng/ml of EGF. Cells were then removed from their plates, fixed and stained with either anti-EGF-R mAb 225 (top panel) or anti-erbB-2 mAb Ab5 (lower panel) as described in Materials and Methods. Secondary antibody alone (FITC-labeled goat anti-mouse) is shown in the top panel (white peak). Data represents FACS results of approximately 5200 cells/profile.

*Figure 47* Kinetics of EGF-mediated down regulation of EGF-R and erbB-2 in human mammary epithelial cells and mouse fibroblasts. Cells were treated for the indicated times with 100 ng/ml of EGF, removed from their plates by scraping and extracted with detergent. EGF-R levels (—●—) were determined using a specific ELISA and erbB-2 levels (—□—) were determined using storage phosphor plates following western blot analysis as described in Material and Methods. Top panel is an image of western blots of erbB-2 at the indicated time after EGF treatment. Data is the average of from 4 to 8 experiments + / - SEM.

*Figure 48* Levels of erbB-2 mRNA do not change after EGF treatment. Monolayers of either 184A1L5 HMEC (left) or B82 mouse fibroblast expressing human EGF-R (right) were treated without or with 100 ng/ml of EGF for 4 hr at 37°C. Total RNA was extracted, reverse transcribed and specific erbB-2 transcripts (top panel) and control G3PDH were amplified by PCR as described in Materials and Methods using the indicated amounts of cDNA. Shown is a scanned image of the reaction products run of 1.8% agarose gels and stained with ethidium bromide.

*Figure 49* Distribution of EGF-R and erbB-2 in mouse B82 fibroblasts. Cells were fixed and permeabilized and the distributions of EGF-R (left panels) and erbB-2 (right panels) were determined by use of mouse monoclonal antibody 528 and rabbit polyclonal antibody C18 respectively. Panels A and B are untreated cells, panels B and C are also untreated cells, but incubation with primary antibodies was done in the presence of competing erbB-2 peptide C18. Panels E and F are cells following treatment for 4 hr at 37°C with 100 ng/ml of EGF. Arrows indicate identical vesicles. Images were acquired with a Photometrics cooled CCD camera as described in Materials and Methods. Exposures times and scaling of all images were identical for each receptor type.

*Figure 50* Distribution of EGF-R and erbB-2 in different cell types as determined by confocal microscopy. Cells grown on coverslips were fixed, permeabilized and simultaneously stained for EGF-R (left panels) and erbB-2 (right panels) using monoclonal and polyclonal antibodies respectively. Optical sections 0.5 microns thick were taken through the lower 1/3 of the cells. The two images were collected separately using barrier filters to prevent spillover between the FITC images (left) and Texas Red images (right). Top panels are mouse B82 fibroblasts. Middle panels are human HB2 mammary epithelial cells and bottom panels are human breast carcinoma line SKBR3.

*Figure 51* Kinetics of EGF-induced downregulation of erbB-2 in cells expressing different mutants of the EGF-R. Mouse B82 cells expressing either kinase-active (panel A) or kinase-inactive (panel B) EGF-R were incubated with 100 ng/ml of EGF for the indicated lengths of time. The cells were extracted with detergent and the remaining erbB-2 mass was determined by quantitative western blot analysis using a Bio-Rad Molecular Imager. The EGF-R types used were wild type (—●—, n= 7), kinase inactive M<sup>721</sup> (—■—, n=5), c'958 (—○—, n=4), c'958 M<sup>721</sup> (—□—, n=3), c'688 (\*, n=2) and c'647 (\*, n=3). The error bars represent the SEM of the indicated number of independent experiments.



*Figure 52* Effect of EGF on tyrosine phosphorylation of erbB-2. Mouse fibroblasts expressing the indicated EGF-R mutants were treated either without (open bars) or with 100 ng/ml of EGF for 15 or 120 minutes (shaded bars) and then extracted with detergent. The erbB-2 was immunoprecipitated from equal amounts of cell extract (corrected for protein) and the samples were split and run on two separate gels. Following transfer to nitrocellulose, they were probed for phosphotyrosine (top panel) or erbB-2 protein (middle panel). The images were acquired using a Bio-Rad Molecular Imager. Bottom panel is the ratio of phosphotyrosine to erbB-2 of the western blots as determined using the Molecular Analyst software package.

*Figure 53* Removal of the kinase domain of the EGF-R eliminates EGF-induced tyrosine phosphorylation of erbB-2. Mouse fibroblasts expressing the indicated EGF-R mutants were treated either without (open bars) or with (shaded bars) 100 ng/ml of EGF for 15 min. Following immunoprecipitation of erbB-2, the levels of phosphotyrosine (top panel), erbB-2 (middle panel) and the PY:erbB-2 ratios (bottom panels) were determined as described in the legend of Fig. 52.

*Figure 54* The ability of EGF to induce down regulation of erbB-2 levels is correlated with tyrosine phosphorylation of erbB-2. Mouse fibroblasts expressing the indicated EGF-R mutants were treated with 100 ng/ml of EGF for 6-8 hr at 37°C. The cells were extracted and the total levels of erbB-2 remaining was determined by quantitative western blots (top panel). The fold increase in phosphotyrosine levels in erbB-2 following 15 min EGF treatment (bottom panel) was determined following immunoprecipitation of erbB-2 in parallel samples as described in the legend of Fig. 52.

*Figure 55* Expression levels of erbB-2 and EGFR in MTSV versus ce2 cells. A. MTSV and ce2 cells were brought to steady state varying concentrations of  $^{125}\text{I}$ -labeled 4D5 antibody as described in Experimental Procedures. The total amount of cell associated ligand associated with either ce2 (—●—) or MTSV (—○—) cells was determined and is presented as a Scatchard plot (ref). Insert is an enlargement of the MTSV data. B. Binding of  $^{125}\text{I}$ -EGF to ce2 (—●—) or MTSV (—○—) cells. Equilibrium binding at 0°C was done as described in Experimental Procedures and is plotted as a Scatchard plot. Lines were generated by nonlinear regression.

*Figure 56* Distribution of erbB-2 and the EGFR at the cell surface is unaffected by erbB-2 overexpression. Cells were fixed and permeabilized and incubated with directly-labeled anti-erbB-2 or anti-EGFR antibodies. Images were then separately acquired in the FITC channel (left panels) corresponding to the EGFR and the Texas Red channel (right panels) corresponding to erbB-2. Arrows indicate corresponding areas of the paired images.

*Figure 57* Activation of erbB-2 and EGF-R in MTSV versus ce2 cells. Cells were treated with or without EGF for 5 and 10 min. Cells were also treated with 10  $\mu\text{g}$ /ml of either mAb 225 or 13A9 for 18 hrs. ErbB-2 was immunoprecipitated from the cell extracts (top panel) followed immunoprecipitation of the EGFR (bottom panel). Phosphotyrosine (PY) levels were then determined by western blot analysis. Shown is a scan from a Bio-Rad Molecular Imager.

*Figure 58* ErbB-2 downregulation is inhibited by erbB-2 overexpression. Levels of erbB-2 were assessed by western blot analysis of extracts of the indicated cell types treated with 17 nM EGF for 24 hours (panel A). The western blot bands were quantified by phosphorimager analysis (panel B). The percentage of erbB-2 remaining after 24 hours EGF treatment is shown as the average with standard deviation from three to six separate experiments. Downregulation kinetics of erbB-2 was also measured over a shorter time course (panel C). Shown is the

average percentage of control erbB-2 levels that remain after EGF treatment from three separate experiments.

*Figure 59* Kinetics of EGFR activation in MTSV and ce2 cells. A. Cells were treated with 100ng/ml of EGF for the indicated time or were treated with 10 $\mu$ g/ml 225 mAb for 18 hr. The immunoprecipitated EGFR was then separated by electrophoresis, transferred to nitrocellulose and probed with anti-PY antibodies (top panel). After visualization of the bands, the blots were stripped and reprobed with anti-EGFR antibodies (bottom panels). B. The density of the bands shown in panel A was determined by densitometry and the ratio of the PY to EGFR bands was then plotted as a function of EGF treatment time for ce2 (—●—) and MTSV (—○—) cells. C. The density of the PY bands shown in panel A as a function of EGF treatment time is shown for ce2 (—●—) and MTSV (—○—) cells.

*Figure 60* EGFR downregulation is inhibited by erbB-2 overexpression. EGFR receptor mass was assessed by western blot analysis of cells treated with EGF for varying times up to 24 hours. Western blot bands were quantified by using a Molecular Imager and averages from three experiments are plotted as a percent of receptor mass in untreated cells.

*Figure 61* Approach of EGF to steady state binding. Cells were incubated with 1.7 nM <sup>125</sup>I-EGF for the time indicated and the relative amount of ligand either inside the cell (top panel) or at the cell surface (bottom panel) was determined for ce2 (—●—) and MTSV (—○—) cells by acid stripping.

*Figure 62* Kinetics of EGF binding and recycling in ce2 and MTSV cells. A. Internalization plot analysis of ce2 (—●—) and MTSV (—○—) cells was done over a 5 minute period using 1.7 nM <sup>125</sup>I-EGF as described in Experimental Procedures. Shown are the average of 4 experiments  $\pm$  standard deviation. B. Surface binding of EGF to ce2 (—●—) and MTSV (—○—) cells using 10 ng/ml <sup>125</sup>I-EGF. Shown is the average of 4 experiments  $\pm$  standard deviation. C. Loss of <sup>125</sup>I-EGF from the surface of ce2 (—●—) and MTSV (—○—) cells. The cells were incubated with 10 ng/ml EGF for 5, 10 and 15 minutes. Cells were rinsed and incubated with 1.7  $\mu$ M unlabeled EGF to prevent rebinding of dissociated ligand. The percent of initially bound ligand remaining on the cell surface at the indicated times was determined by acid stripping. Shown are the average results of all three data sets  $\pm$  the standard deviation. The solid lines were generated by nonlinear regression. The dashed line is loss predicted from the effects of endocytosis alone. D. Fractional recycling of <sup>125</sup>I-EGF from ce2 (—●—) and MTSV (—○—) cells. Cells were brought to steady state with varying concentrations of <sup>125</sup>I-EGF. After removal of surface ligand, the fraction of internalized ligand which recycled back into the medium intact was measured as described in Experimental Procedures. Shown is the fraction of recycled ligand plotted against the amount of internalized ligand at the beginning of the chase period.

*Figure 63* Transport of EGF to lysosomes in MTSV versus ce2 cells. A. Either ce2 (—●—) or MTSV (—○—) cells were pulsed for 5 min with 8 nM <sup>125</sup>I-EGF and then chased with 170 nM unlabeled EGF for the indicated times. The amount of intact ligand remaining in the cells was determined following acid stripping. B. Cells were pulsed for 15 min with fluorescein-dextran to label the lysosomes. The cells were then incubated with Texas Red-labeled EGF for 15 min and chased for the indicated time. Total chase time for the fluorescein-dextran was 120 min for all cells. The amount of EGF colocalized with the dextran-labeled lysosomes was determined by image analysis as described in Experimental Procedures.

## References

1. Momburg, F., Moldenhauer, G., Hammerling, G. J., and Moller, P. (1987) Immunohistochemical study of the expression of a Mr 34,000 human epithelium-specific surface glycoprotein in normal and malignant tissues. *Cancer Res* **47**(11), 2883-2891
2. Simpson, J. F., and Page, D. L. (1992) Altered expression of a structural protein (fodrin) within epithelial proliferative disease of the breast. *Am. J. Pathol.* **141**, 285-289
3. Chen, W. S., Lazar, C. S., Lund, K. A., Welsh, J. B., Chang, C. P., Walton, G. M., Der, C. J., Wiley, H. S., Gill, G. N., and Rosenfeld, M. G. (1989) Functional independence of the epidermal growth factor receptor from a domain required for ligand-induced internalization and calcium regulation. *Cell* **59**, 33-43
4. Wells, A., Welsh, J. B., Lazar, C. S., Wiley, H. S., Gill, G. N., and Rosenfeld, M. G. (1990) Ligand-induced transformation by a noninternalizing EGF receptor. *Science* **247**, 962-964
5. Bates, S. E., Valverius, E. M., Ennis, B. W., Bronzert, D. A., Sheridan, J. P., Stampfer, M. R., Mendelsohn, J., Lippman, M. E., and Dickson, R. B. (1990) Expression of the transforming growth factor- $\alpha$ /epidermal growth factor receptor pathway in normal human breast epithelial cells. *Endocrinology* **126**(1), 596-607
6. Stampfer, M. R., Pan, C. H., Hosoda, J., Bartholomew, J., Mendelsohn, J., and Yaswen, P. (1993) Blockage of EGF receptor signal transduction causes reversible arrest of normal and immortal human mammary epithelial cells with synchronous re-entry into the cell cycle. *Exp. Cell Res.* **208**(1), 175-188
7. Matthay, M. A., Thiery, J. P., Lafont, F., Stampfer, M. F., and Boyer, B. (1993) Transient effect of epidermal growth factor on the motility of an immortalized mammary epithelial cell line. *J. Cell Sci.* **106**, 869-178
8. Klijn, J. G., Berns, P. M., Schmitz, P. I., and Foekens, J. A. (1992) The clinical significance of epidermal growth factor receptor (EGF-R) in human breast cancer: a review on 5232 patients. *Endocr Rev* **13**(1), 3-17
9. Sporn, M. B., and Roberts, A. B. (1988) Peptide growth factors are multifunctional. *Nature* **332**(6161), 217-219
10. Mroczkowski, B., Reich, M., Chen, K., Bell, G. I., and Cohen, S. (1989) Recombinant human epidermal growth factor precursor is a glycosylated membrane protein with biological activity. *Mol Cell Biol* **9**(7), 2771-2778
11. Derynck, R., Roberts, A. B., Winkler, M. E., Chen, E. Y., and Goeddel, D. V. (1984) Human transforming growth factor- $\alpha$ : precursor structure and expression in *E. coli*. *Cell* **38**(1), 287-297
12. Pandiella, A., and Massague, J. (1991) Cleavage of the membrane precursor for transforming growth factor  $\alpha$  is a regulated process. *Proc. Natl. Acad. Sci. USA* **88**, 1726-1730
13. Sporn, M. B., and Roberts, A. B. (1992) Autocrine secretion--10 years later. *Ann Intern Med* **117**(5), 408-414
14. Wiley, H. S. (1992) in *Membrane dynamics and signaling* (Bittar, E. E., ed) Vol. 5A, 1 Ed., pp. 113-142, 8 vols., JAI Press, Inc., Greenwich, Conn.
15. Simons, K., and Fuller, D. F. (1985) Cell surface polarity in epithelia. *Annu. Rev. Cell Biol.* **1**, 243-288

16. Bloom, W., and Fawcett, D. W. (1970) *A textbook of histology*, 9 Ed., W.B. Saunders Co., Philadelphia
17. Koukoulis, G. K., Virtanen, I., Korhonen, M., Laitinen, L., Quaranta, V., and Gould, V. E. (1991) Immunohistochemical localization of integrins in the normal, hyperplastic, and neoplastic breast. Correlations with their functions as receptors and cell adhesion molecules. *Am J Pathol* **139**(4), 787-799
18. Natali, P. G., Nicotra, M. R., Botti, C., Mottolese, M., Bigotti, A., and Segatto, O. (1992) Changes in expression of alpha 6/beta 4 integrin heterodimer in primary and metastatic breast cancer. *Br J Cancer* **66**(2), 318-322
19. Tsutsumi, Y., Naber, S. P., DeLellis, R. A., Wolfe, H. J., Marks, P. J., McKenzie, S.-J., and Yin, S. (1990) neu oncogene protein and epidermal growth factor receptor are independently expressed in benign and malignant breast tissues. *Hum. Pathol.* **21**(7), 750-758
20. Parry, G., Beck, J. C., Moss, L., Bartley, J., and Ojakian, G. K. (1990) Determination of apical membrane polarity in mammary epithelial cell cultures: the role of cell-cell, cell-substratum, and membrane-cytoskeleton interactions. *Exp Cell Res* **188**(2), 302-311
21. Streuli, C. H., Bailey, N., and Bissell, M. J. (1991) Control of mammary epithelial differentiation: basement membrane induces tissue-specific gene expression in the absence of cell-cell interactions and morphological polarity. *J. Cell Biol.* **115**(5), 1383-1395
22. Valverius, E. M., Bates, S. E., Stampfer, M. R., Clark, R., McCormick, F., Salomon, D. S., Lippman, M. E., and Dickson, R. B. (1989) Transforming growth factor alpha production and epidermal growth factor receptor expression in normal and oncogene transformed human mammary epithelial cells. *Mol Endocrinol* **3**(1), 203-214
23. Li, S., Plowman, G. D., Buckley, S. D., and Shipley, G. D. (1992) Heparin inhibition of autonomous growth implicates amphiregulin as an autocrine growth factor for normal human mammary epithelial cells. *J Cell Physiol* **153**(1), 103-111
24. Snedeker, S. M., Brown, C. F., and DiAugustine, R. P. (1991) Expression and functional properties of transforming growth factor  $\alpha$  and epidermal growth factor during mouse mammary gland ductal morphogenesis. *Proc. Natl. Acad. Sci. USA* **88**, 276-280
25. Connolly, J. M., and Rose, D. P. (1988) Epidermal growth factor-like proteins in breast fluid and human milk. *Life Sci* **42**(18), 1751-1756
26. Johnson, G. R., Saeki, T., Gordon, A. W., Shoyab, M., Salomon, D. S., and Stromberg, K. (1992) Autocrine action of amphiregulin in a colon carcinoma cell line and immunocytochemical localization of amphiregulin in human colon. *J Cell Biol* **118**(3), 741-751
27. Stern, D. F., and Kamps, M. P. (1988) EGF stimulated tyrosine phosphorylation of p185<sup>neu</sup>: a potential model for receptor interactions. *EMBO J.* **7**, 995-1001
28. Kokai, Y., Myers, J. N., Wada, T., Brown, V. I., LeVea, C. M., Davis, J. G., Dobashi, K., and Greene, M. I. (1989) Synergistic interaction of p185<sup>c-neu</sup> and the EGF receptor leads to transformation of rodent fibroblasts. *Cell* **58**, 287-292
29. Holmes, W. E., Sliwkowski, M. X., Akita, R. W., Henzel, W. J., Lee, J., Park, J. W., Yansura, D., Abadi, N., Raab, H., Lewis, G. D., Shepard, H. M., Kuang, W. J., Wood, D. V., Goeddel, D. V., and R.L., V. (1992) Identification of Heregulin, A Specific Activator of p185<sup>erbB2</sup>. *Science* **256**(5060), 1205-1210



30. Culouscou, J. M., Plowman, G. D., Carlton, G. W., Green, J. M., and Shoyab, M. (1993) Characterization of a breast cancer cell differentiation factor that specifically activates the HER4/p180erbB4 receptor. *J. Biol. Chem.* **268**(25), 18407-18410
31. Plowman, G. D., Green, J. M., Culouscou, J. M., Carlton, G. W., Rothwell, V. M., and Buckley, S. (1993) Heregulin induces tyrosine phosphorylation of HER4/p180erbB4. *Nature* **366**(6454), 473-475
32. Peles, E., Bacus, S. S., Koski, R. A., Lu, H. S., Wen, D., Ogden, S. G., Levy, R. B., and Yarden, Y. (1992) Isolation of the neu/HER-2 Stimulatory Ligand: a 44 kd Glycoprotein That Induces Differentiation of Mammary Tumor Cells. *Cell* **69**(1), 205-216
33. Dougall, W. C., Qian, X., Peterson, N. C., Miller, M. J., Samanta, A., and Greene, M. I. (1994) The neu-oncogene: signal transduction pathways, transformation mechanisms and evolving therapies. *Oncogene* **9**(8), 2109-2123
34. Plowman, G. D., Culouscou, J. M., Whitney, G. S., Green, J. M., Carlton, G. W., Foy, L., Neubauer, M. G., and Shoyab, M. (1993) Ligand-specific activation of HER4/p180erbB4, a fourth member of the epidermal growth factor receptor family. *Proc. Natl. Acad. Sci. USA* **90**(5), 1746-1750
35. Carraway 3rd, K. L., Sliwkowski, M. X., Akita, R., Platko, J. V., Guy, P. M., Nuijens, A., J., D. A., Vandlen, R. L., Cantley, L. C., and Cerione, R. A. (1994) The erbB3 gene product is a receptor for heregulin. *J. Biol. Chem.* **269**(19), 14303-14306
36. Qian, X. L., Decker, S. J., and Greene, M. I. (1992) p185c-neu and epidermal growth factor receptor associate into a structure composed of activated kinases. *Proc. Natl. Acad. Sci. USA* **89**(4), 1330-1334
37. Cohen, B. D., Green, J. M., Foy, L., and Fell, H. P. (1996) HER2-mediated biological and biochemical properties in NIH 3T3 cells. *J. Biol. Chem.* **271**(9), 4813-4818
38. Carraway, K. L., and Cantley, L. C. (1994) A Neu Acquaintance for ErbB3 and ErbB4: A role for Receptor Heterodimerization in Growth Signaling. *Cell* **78**, 5-8
39. Baass, P. C., Di Guglielmo, G. M., Authier, F., Posner, B. I., and Bergeron, J. J. M. (1995) Compartmentalized signal transduction by receptor tyrosine kinases. *Trends Cell Biol.* **5**(12), 465-470
40. Baulida, J., Kraus, M. H., Alimandi, M., Di Fiore, P. P., and Carpenter, G. (1996) All ErbB receptors other than the epidermal growth factor receptor are endocytosis impaired. *J. Biol. Chem.* **271**, 5251-5257
41. Kornilova, E. S., Taverna, D., Hoeck, W., and Hynes, N. E. (1992) Surface expression of erbB-2 protein is post-transcriptionally regulated in mammary epithelial cells by epidermal growth factor and by the culture density. *Oncogene* **7**, 511-519
42. Tsutsumi, Y., Naber, S. P., DeLellis, R. A., Wolfe, H. J., Marks, P. J., McKenzie, S. J., and Yin, S. (1991) Comparison of EGFR, c-erbB-2 product and ras p21 immunohistochemistry as prognostic markers in primary breast cancer. *Eur J Surg Oncol* **17**(1), 9-15
43. Gabelman, B. M., and Emerman, J. T. (1992) Effects of estrogen, epidermal growth factor, and transforming growth factor-alpha on the growth of human breast epithelial cells in primary culture. *Exp Cell Res* **201**(1), 113-118
44. Klijn, J. G. M., Berns, P. M. J. J., Bontenbal, M., Alexieva-Figusch, J., and Foekens, J. A. (1992) Clinical breast cancer, new developments in selection and endocrine treatment of patients. *J. Steroid Biochem. Mol. Biol.* **43**, 27-43

45. Bates, S. E., Davidson, N. E., Valverius, E. M., Freter, C. E., Dickson, R. B., Tam, J. P., Kudlow, J. E., Lippman, M. E., and Salomon, D. S. (1988) Expression of transforming growth factor alpha and its messenger ribonucleic acid in human breast cancer: its regulation by estrogen and its possible functional significance. *Mol Endocrinol* 2(6), 543-555
46. Colomb, E., Berthon, P., Dussert, C., Calvo, F., and Martin, P. M. (1991) Estradiol and EGF requirements for cell-cycle progression of normal human mammary epithelial cells in culture. *Int J Cancer* 49(6), 932-937
47. Barrandon, Y., and Green, H. (1987) Cell migration is essential for substaisted growth of keratinocyte colonies: the roles of transforming growth factor- $\alpha$  and epidermal growth factor. *Cell* 50, 1131-1137
48. Blay, J., and Brown, K. D. (1985) Epidermal growth factor promotes the chemotactic migration of cultured rat intestinal epithelial cells. *J. Cell. Phys.* 124, 107-112
49. Moscatello, D. K., Holgado-Madruga, M., Godwin, A. K., Ramirez, G., Gunn, G., Zoltick, P. W., Biegel, J. A., Hayes, R. L., and Wong, A. J. (1995) Frequent expression of a mutant epidermal growth factor receptor in multiple human tumors. *Cancer Res* 55(23), 5536-5539
50. Clarke, R., Brunner, N., Katz, D., Glanz, P., Dickson, R. B., Lippman, M. E., and Kern, F. G. (1989) The effects of a constitutive expression of transforming growth factor-alpha on the growth of MCF-7 human breast cancer cells in vitro and in vivo. *Mol Endocrinol* 3(2), 372-380
51. Willingham, M. C., Haigler, H. T., Fitzgerald, D. J., Gallo, M. G., Rutherford, A. V., and Pastan, I. H. (1983) The morphologic pathway of binding and internalization of epidermal growth factor in cultured cells. Studies on A431, KB, and 3T3 cells, using multiple methods of labelling. *Exp. Cell Res.* 146, 163-175
52. Wiley, H. S. (1988) Anomalous binding of epidermal growth factor to A431 cells is due to the effect of high receptor densities and a saturable endocytic system. *J. Cell Biol.* 107, 801-810
53. Wiley, H. S., and Cunningham, D. D. (1982) The endocytotic rate constant: A cellular parameter for quantitating receptor-mediated endocytosis. *J. Biol. Chem.* 257, 4222-4229
54. Lamaze, C., Baba, T., Redelmeier, T. E., and Schmid, S. L. (1993) Recruitment of epidermal growth factor and transferrin receptors into coated pits in vitro: differing biochemical requirements. *Mol. Biol. Cell* 4(7), 715-727
55. Sorkin, A., and Waters, C. M. (1993) Endocytosis of growth factor receptors. *Bioessays* 15(6), 375-382
56. Barak, L. S., and Caron, M. G. (1995) Modeling of sequestration and down regulation in cells containing beta2- adrenergic receptors. *J. Recept. Signal Transduct. Res.* 15(1-4), 677-690
57. Opresko, L. K., Chang, C.-P., Will, B. H., Burke, P. M., Gill, G. N., and Wiley, H. S. (1995) Endocytosis and Lysosomal Targeting of Epidermal Growth Factor Receptors Are Mediated by Distinct Sequences Independent of the Tyrosine Kinase Domain. *J. Biol. Chem.* 270(9), 4325-4333
58. Wiley, H. S., Herbst, J. J., Walsh, B. J., Lauffenburger, D. A., Rosenfeld, M. G., and Gill, G. N. (1991) Role of tyrosine kinase activity in endocytosis, compartmentation and downregulation of the EGF receptor. *J. Biol. Chem.* 266(17), 11083-11094

59. Kurten, R. C., Cadena, D. L., and Gill, G. N. (1996) Enhanced Degradation of EGF Receptors by a Sorting Nexin, SNX1. *Science* **272**, 1008-1010
60. Herbst, J. J., Opresko, L. K., Walsh, B. J., Lauffenburger, D. A., and Wiley, H. S. (1994) Regulation of postendocytic trafficking of the epidermal growth factor receptor through endosomal retention. *J. Biol. Chem.* **269**(17), 12865-12873
61. Stoscheck, C. M., and Carpenter, G. (1984) Down regulation of epidermal growth factor receptors: direct demonstration of receptor degradation in human fibroblasts. *J. Cell Biol.* **98**, 1048-1053
62. Sorkin, A., and Carpenter, G. (1993) Interaction of activated EGF receptors with coated pit adaptins. *Science* **261**(5121), 612-615
63. Sorkin, A., Helin, K., Waters, C. M., Carpenter, G., and Beguinot, L. (1992) Multiple autophosphorylation sites of the epidermal growth factor receptor are essential for receptor kinase activity and internalization. Contrasting significance of tyrosine 992 in the native and truncated receptors. *J. Biol. Chem.* **267**(12), 8672-8678
64. Lin, C. R., Chen, W. S., Lazar, C. S., Carpenter, C. D., Gill, G. N., Evans, R. M., and Rosenfeld, M. G. (1986) Protein kinase C phosphorylation at Thr 654 of the unoccupied EGF receptor and EGF binding regulate functional receptor loss by independent mechanisms. *Cell* **44**, 839-848
65. French, A. R., Sudlow, G. P., Wiley, H. S., and Lauffenburger, D. A. (1994) Postendocytic trafficking of epidermal growth factor-receptor complexes is mediated through saturable and specific endosomal interactions. *J. Biol. Chem.* **269**(22), 15749-15755
66. Miettinen, P. J., Berger, J. E., Meneses, J., Phung, Y., Pedersen, R. A., Werb, Z., and Derynck, R. (1995) Epithelial immaturity and multiorgan failure in mice lacking epidermal growth factor receptor. *Nature* **376**(6538), 337-341
67. Gill, G. N., and Lazar, C. S. (1981) Increased phosphotyrosine content and inhibition of proliferation in EGF-treated A431 cells. *Nature* **293**, 305-307
68. Kamps, M. P., and Sefton, B. M. (1988) Identification of multiple novel polypeptide substrates of the v-src, v-yes, v-fps, v-ros and v-erb-B oncogenic tyrosine protein kinases utilizing antisera against phosphotyrosine. *Oncogene* **2**, 305-315
69. Gill, G. N., Kawamoto, T., Cochet, C., Le, A., Sato, J. D., Masui, H., McLeod, C., and Mendelsohn, J. (1984) Monoclonal anti-epidermal growth factor receptor antibodies which are inhibitors of epidermal growth factor binding and antagonists of epidermal growth factor binding and antagonists of epidermal growth factor-stimulated tyrosine protein kinase activity. *J. Biol. Chem.* **259**(12), 7755-7760
70. Band, V., and Sager, R. (1989) Distinctive traits of normal and tumor-derived human mammary epithelial cells expressed in a medium that supports long-term growth of both cell types. *Proc. Natl. Acad. Sci. USA* **86**(4), 1249-1253
71. Bartek, J., Bartkova, J., Kyprianou, N., Lalani, E.-N., Staskova, Z., Shearer, M., Chang, S., and Taylor-Papadimitriou, J. (1991) Efficient immortalization of luminal epithelial cells from human mammary gland by introduction of simian virus 40 large tumor antigen with a recombinant retrovirus. *Proc. Natl. Acad. Sci. USA* **88**, 3520-3524
72. Knauer, D. J., Wiley, H. S., and Cunningham, D. D. (1984) Relationship between epidermal growth factor receptor occupancy and mitogenic response. Quantitative analysis using a steady state model system. *J. Biol. Chem.* **259**, 5623-5631

73. Scatchard, G. (1949) The attraction of proteins for small molecules and ions. *Ann. N.Y. Acad. Sci.* **51**, 660-672
74. Opresko, L. K., and Wiley, H. S. (1987) Receptor-mediated endocytosis in *Xenopus* oocytes. II. Evidence for two novel mechanisms of hormonal regulation. *J. Biol. Chem.* **262**, 4116-4123
75. Opresko, L. K., and Wiley, H. S. (1987) Receptor-mediated endocytosis in *Xenopus* oocytes. I. Characterization of the vitellogenin receptor system. *J. Biol. Chem.* **262**, 4109-4115
76. Lund, K. A., Opresko, L. K., Starbuck, C., Walsh, B. J., and Wiley, H. S. (1990) Quantitative analysis of the endocytic system involved in hormone-induced receptor internalization. *J. Biol. Chem.* **265**(26), 15713-15723
77. Stampfer, M. R., and Yaswen, P. (1994) Growth, differentiation, and transformation of human mammary epithelial cells in culture. *Cancer Treat Res* **71**, 29-48
78. Valverius, E. M., Bates, S. E., Stampfer, M. R., Clark, R., McCormick, F., Salomon, D. S., Lippman, M. E., and Dickson, R. B. (1989) Transforming growth factor alpha production and epidermal growth factor receptor expression in normal and oncogene transformed human mammary epithelial cells. *Mol. Endocrinol.* **3**(1), 203-214
79. Hollenberg, M. D., and Cuatrecasas, P. (1973) Epidermal growth factor: receptors in human fibroblasts and modulation of action by cholera toxin. *Proc Natl Acad Sci U S A* **70**(10), 2964-2948
80. Kawamoto, T., Mendelsohn, J., Le, A., Sato, G. H., Lazar, C. S., and Gill, G. N. (1984) Relation of epidermal growth factor receptor concentration to growth of human epidermoid carcinoma A431 cells. *J. Biol. Chem.* **259**, 7761-7766
81. Wiley, H. S., Walsh, B. J., and Lund, K. A. (1989) Global modulation of the epidermal growth factor receptor is triggered by occupancy of only a few receptors. Evidence for a binary regulatory system in normal human fibroblasts. *J Biol Chem* **264**(32), 18912-20
82. Countaway, J. L., Girones, N., and Davis, R. J. (1989) Reconstitution of epidermal growth factor receptor transmodulation by platelet-derived growth factor in Chinese hamster ovary cells. *J Biol Chem* **264**(23), 13642-13647
83. Matthay, M. A., Thiery, J. P., Lafont, F., Stampfer, M. F., and Boyer, B. (1993) Transient effect of epidermal growth factor on the motility of an immortalized mammary epithelial cell line. *J. Cell Sci.* **106**(Pt 3), 869-878
84. Walen, K. H., and Stampfer, M. R. (1989) Chromosome analyses of human mammary epithelial cells at stages of chemical-induced transformation progression to immortality. *Cancer Genet. Cytogenet.* **37**(2), 249-261
85. Wiley, H. S., and Cunningham, D. D. (1981) A steady state model for analyzing the cellular binding, internalization and degradation of polypeptide ligands. *Cell* **25**(2), 433-440
86. Berlin, C. M., and Schimke, R. T. (1965) Influence of turnover rates on the responses of enzymes to cortisone. *Mol. Pharmacol.* **1**(2), 149-156
87. Li, S., Plowman, G. D., Buckley, S. D., and Shipley, G. D. (1992) Heparin inhibition of autonomous growth implicates amphiregulin as an autocrine growth factor for normal human mammary epithelial cells. *J. Cell Physiol.* **153**(1), 103-111



88. Wiley, H. S., and McKinley, D. N. (1987) Assay of growth factor stimulation of fluid-phase endocytosis. *Methods Enzymol.* **146**, 402-417
89. McKinley, D. N., and Wiley, H. S. (1988) Reassessment of fluid-phase endocytosis and diacytosis in monolayer cultures of human fibroblasts. *J. Cell Physiol.* **136**, 389-397
90. Wiley, H. S., and Cunningham, D. D. (1982) Epidermal growth factor stimulates fluid phase endocytosis in human fibroblasts through a signal generated at the cell surface. *J. Cell. Biochem.* **19**, 383-394
91. Wilson, P. D., Sherwood, A. C., Palla, K., Du, J., Watson, R., and Norman, J. T. (1991) Reversed polarity of Na(+)-K(+)-ATPase: mislocation to apical plasma membranes in polycystic kidney disease epithelia. *Am J Physiol* **260**, F420-430
92. Pignatelli, M., Cardillo, M. R., Hanby, A., and Stamp, G. W. (1992) Integrins and their accessory adhesion molecules in mammary carcinomas: loss of polarization in poorly differentiated tumors. *Hum Pathol* **23**(10), 1159-1166
93. Schoenenberger, C. A., Zuk, A., Kendall, D., and Matlin, K. S. (1991) Multilayering and loss of apical polarity in MDCK cells transformed with viral K-ras. *J Cell Biol* **112**(5), 873-889
94. Maratos-Flier, E., Kao, C. Y., Verdin, E. M., and King, G. L. (1987) Receptor-mediated vectorial transcytosis of epidermal growth factor by Madin-Darby canine kidney cells. *J Cell Biol* **105**(4), 1595-1601
95. Scheving, L. A., Shiurba, R. A., Nguyen, T. D., and Gray, G. M. (1989) Epidermal growth factor receptor of the intestinal enterocyte. Localization to laterobasal but not brush border membrane. *J Biol Chem* **264**(3), 1735-1741
96. Burwen, S. J., Barker, M. E., Goldman, I. S., Hradek, G. T., Raper, S. E., and Jones, A. L. (1984) Transport of epidermal growth factor by rat liver: evidence for a nonlysosomal pathway. *J Cell Biol* **99**(4 Pt 1), 1259-1265
97. Carraway, K. L., and Carraway, C. A. (1995) Signaling, mitogenesis and the cytoskeleton: where the action is. *Bioessays* **17**(2), 171-175
98. Mansour, S. J., Matten, W. T., Hermann, A. S., Candia, J. M., Rong, S., Fukasawa, K., Vande Woude, G. F., and Ahn, N. G. (1994) Transformation of mammalian cells by constitutively active MAP kinase kinase. *Science* **265**(5174), 966-970
99. Rodbard, D., Munson, P. J., and Thakur, A. K. (1980) Quantitative characterization of hormone receptors. *Cancer* **46**(12 Suppl), 2907-18
100. Eming, S. A., Lee, J., Snow, R. G., Tompkins, R. G., Yarmush, M. L., and Morgan, J. R. (1995) Genetically modified human epidermis overexpressing PDGF-A directs the development of a cellular and vascular connective tissue stroma when transplanted to athymic mice--implications for the use of genetically modified keratinocytes to modulate dermal regeneration. *J Invest Dermatol* **105**(6), 756-763
101. Danos, O., and Mulligan, R. C. (1988) Safe and efficient generation of recombinant retroviruses with amphotropic and ecotropic host ranges. *Proc Natl Acad Sci U S A* **85**(17), 6460-6464
102. Massague, J., and Pandiella, A. (1993) Membrane-anchored growth factors. *Annu Rev Biochem* **62**, 515-541

103. Derynck, R. (1992) The physiology of transforming growth factor- $\alpha$ . *Adv Cancer Res* 58, 27-52
104. Thompson, S. A., Higashiyama, S., Wood, K., Pollitt, N. S., Damm, D., McEnroe, G., Garrick, B., Ashton, N., Lau, K., Hancock, N., and et al. (1994) Characterization of sequences within heparin-binding EGF-like growth factor that mediate interaction with heparin. *J Biol Chem* 269(4), 2541-2549
105. Cook, P. W., Ashton, N. M., Karkaria, C. E., Siess, D. C., and Shipley, G. D. (1995) Differential effects of a heparin antagonist (hexadimethrine) or chlorate on amphiregulin, basic fibroblast growth factor, and heparin-binding EGF-like growth factor activity. *J Cell Physiol* 163(2), 418-429
106. Goishi, K., Higashiyama, S., Klagsbrun, M., Nakano, N., Umata, T., Ishikawa, M., Mekada, E., and Taniguchi, N. (1995) Phorbol ester induces the rapid processing of cell surface heparin-binding EGF-like growth factor: conversion from juxtacrine to paracrine growth factor activity. *Mol Biol Cell* 6(8), 967-980
107. Dempsey, P. J., Meise, K. S., Yoshitake, Y., Nishikawa, K., and Coffey, R. J. (1997) Apical enrichment of human EGF precursor in Madin-Darby canine kidney cells involves preferential basolateral ectodomain cleavage sensitive to a metalloprotease inhibitor. *J Cell Biol* 138(4), 747-758
108. Sibilia, M., and Wagner, E. F. (1995) Strain-dependent epithelial defects in mice lacking the EGF receptor. *Science* 269(5221), 234-238
109. Threadgill, D. W., Dlugosz, A. A., Hansen, L. A., Tennenbaum, T., Lichti, U., Yee, D., LaMantia, C., Mourtou, T., Herrup, K., Harris, R. C., Barnard, J. A., Yuspa, S. H., Coffey, R. J., and Magnuson, T. (1995) Targeted disruption of mouse EGF receptor: effect of genetic background on mutant phenotype. *Science* 269(5221), 230-234
110. Barnard, J. A., Graves-Deal, R., Pittelkow, M. R., DuBois, R., Cook, P., Ramsey, G. W., Bishop, P. R., Damstrup, L., and Coffey, R. J. (1994) Auto- and cross-induction within the mammalian epidermal growth factor-related peptide family. *J Biol Chem* 269(36), 22817-22822
111. Fisher, D. A., Salido, E. C., and Barajas, L. (1989) Epidermal growth factor and the kidney. *Annu Rev Physiol* 51, 67-80
112. Hashimoto, K., Higashiyama, S., Asada, H., Hashimura, E., Kobayashi, T., Sudo, K., Nakagawa, T., Damm, D., Yoshikawa, K., and Taniguchi, N. (1994) Heparin-binding epidermal growth factor-like growth factor is an autocrine growth factor for human keratinocytes. *J Biol Chem* 269(31), 20060-20066
113. Sakurai, H., Tsukamoto, T., Kjelsberg, C. A., Cantley, L. G., and Nigam, S. K. (1997) EGF receptor ligands are a large fraction of in vitro branching morphogens secreted by embryonic kidney. *Am J Physiol* 273(3 Pt 2), F463-472
114. Brachmann, R., Lindquist, P. B., Nagashima, M., Kohr, W., Lipari, T., Napier, M., and Derynck, R. (1989) Transmembrane TGF- $\alpha$  precursors activate EGF/TGF- $\alpha$  receptors. *Cell* 56(4), 691-700
115. Wong, S. T., Winchell, L. F., McCune, B. K., Earp, H. S., Teixido, J., Massague, J., Herman, B., and Lee, D. C. (1989) The TGF- $\alpha$  precursor expressed on the cell surface binds to the EGF receptor on adjacent cells, leading to signal transduction. *Cell* 56(3), 495-506

116. Lanzrein, M., Garred, O., Olsnes, S., and Sandvig, K. (1995) Diphtheria toxin endocytosis and membrane translocation are dependent on the intact membrane-anchored receptor (HB-EGF precursor): studies on the cell-associated receptor cleaved by a metalloprotease in phorbol- ester-treated cells. *Biochem. J.* **310**(Pt 1), 285-289
117. Arribas, J., Coodly, L., Vollmer, P., Kishimoto, T. K., Rose-John, S., and Massague, J. (1996) Diverse cell surface protein ectodomains are shed by a system sensitive to metalloprotease inhibitors. *J. Biol. Chem.* **271**(19), 11376-11382
118. Dempsey, P. J., Meise, K. S., Yoshitake, Y., Nishikawa, K., and Coffey, R. J. (1997) Apical enrichment of human EGF precursor in Madin-Darby canine kidney cells involves preferential basolateral ectodomain cleavage sensitive to a metalloprotease inhibitor. *J. Cell Biol.* **138**(4), 747-758
119. Merlos-Suarez, A., Fernandez-Larrea, J., Reddy, P., Baselga, J., and Arribas, J. (1998) Pro-tumor necrosis factor-alpha processing activity is tightly controlled by a component that does not affect notch processing. *J Biol Chem* **273**(38), 24955-24962
120. Peschon, J. J., Slack, J. L., Reddy, P., Stocking, K. L., Sunnarborg, S. W., Lee, D. C., Russell, W. E., Castner, B. J., Johnson, R. S., Fitzner, J. N., Boyce, R. W., Nelson, N., Kozlosky, C. J., Wolfson, M. F., Rauch, C. T., Cerretti, D. P., Paxton, R. J., March, C. J., and Black, R. A. (1998) An essential role for ectodomain shedding in mammalian development. *Science* **282**(13), 1281-1284
121. Anklesaria, P., Teixido, J., Laiho, M., Pierce, J. H., Greenberger, J. S., and Massague, J. (1990) Cell-cell adhesion mediated by binding of membrane-anchored transforming growth factor alpha to epidermal growth factor receptors promotes cell proliferation. *Proc Natl Acad Sci U S A* **87**(9), 3289-3293
122. Higashiyama, S., Iwamoto, R., Goishi, K., Raab, G., Taniguchi, N., Klagsbrun, M., and Mekada, E. (1995) The membrane protein CD9/DRAP 27 potentiates the juxtacrine growth factor activity of the membrane-anchored heparin-binding EGF-like growth factor. *J Cell Biol* **128**(5), 929-938
123. Wiley, H. S., Woolfe, M. F., Opresko, L. K., Burke, P. M., Will, B. H., Morgan, J. A., and Lauffenburger, D. A. (1998) Removal of the membrane-anchoring domain of EGF leads to intracrine signaling and disruption of mammary epithelial cell organization. *J. Cell Biol.* **143**, 1317-1328
124. Wang, X., Fu, X., Brown, P. D., Crimmin, M. J., and Hoffman, R. M. (1994) Matrix metalloproteinase inhibitor BB-94 (batimastat) inhibits human colon tumor growth and spread in a patient-like orthotopic model in nude mice. *Cancer Res.* **54**(17), 4726-4728
125. Parsons, S. L., Watson, S. A., and Steele, R. J. (1997) Phase I/II trial of batimastat, a matrix metalloproteinase inhibitor, in patients with malignant ascites. *Eur. J. Surg. Oncol.* **23**(6), 526-531
126. Gill, G. N., Kawamoto, T., Cochet, C., Le, A., Sato, J. D., Masui, H., McLeod, C., and Mendelsohn, J. (1984) Monoclonal anti-epidermal growth factor receptor antibodies which are inhibitors of epidermal growth factor binding and antagonists of epidermal growth factor-stimulated tyrosine protein kinase activity. *J. Biol. Chem.* **259**, 7755-7760
127. Winkler, M. E., OConnor, L., Winget, M., and Fendly, B. (1989) Epidermal growth factor and transforming growth factor alpha bind differently to the epidermal growth factor receptor. *Biochemistry* **28**(15), 6373-6378

128. Yoshitake, Y., and Nishikawa, K. (1988) Production of monoclonal antibodies with specificity for different epitopes on the human epidermal growth factor molecule. *Arch Biochem Biophys* **263**(2), 437-446
129. Gill, G. N., and Weber, W. (1987) Purification of functionally active epidermal growth factor receptor protein using a competitive antagonistic monoclonal antibody and a competitive elution with epidermal growth factor. *Meth. Enzymol.* **146**, 82-88
130. Engler, D. A., Matsunami, R. K., Campion, S. R., Stringer, C. D., Stevens, A., and Niyogi, S. K. (1988) Cloning of authentic human epidermal growth factor as a bacterial secretory protein and its initial structure-function analysis by site- directed mutagenesis. *J Biol Chem* **263**(25), 12384-12390
131. Stampfer, M. R., and Yaswen, P. (1993) Culture systems for study of human mammary epithelial cell proliferation, differentiation and transformation. *Cancer Surv* **18**, 7-34
132. Hammond, S. L., Ham, R. G., and Stampfer, M. R. (1984) Serum-free growth of human mammary epithelial cells: rapid clonal growth in defined medium and extended serial passage with pituitary extract. *Proc Natl Acad Sci U S A* **81**(17), 5435-5439
133. Band, V., and Sager, R. (1989) Distinctive traits of normal and tumor-derived human mammary epithelial cells expressed in a medium that supports long-term growth of both cell types. *Proc. Natl. Acad. Sci. USA* **86**, 1249-1253
134. Schneider, C., Newman, R. A., Sutherland, D. R., Asser, U., and Greaves, M. F. (1982) A one-step purification of membrane proteins using a high efficiency immunomatrix. *Journal of Biological Chemistry* **257**(18), 10766-10769
135. Opresko, L. K., and Wiley, H. S. (1990) Functional reconstitution of the human epidermal growth factor receptor system in *Xenopus* oocytes. *J Cell Biol* **111**(4), 1661-1671
136. Wiley, H. S. (1988) Anomalous binding of epidermal growth factor to A431 cells is due to the effect of high receptor densities and a saturable endocytic system. *J Cell Biol* **107**(2), 801-810
137. Will, B. H., Lauffenburger, D. A., and Wiley, H. S. (1995) Studies on engineered autocrine systems: requirements for ligand release from cells producing an artificial growth factor. *Tiss. Engineer.* **1**, 83-96
138. Dempsey, P. J., and Coffey, R. J. (1994) Basolateral targeting and efficient consumption of transforming growth factor- $\alpha$  when expressed in Madin-Darby canine kidney cells. *J. Biol. Chem.* **269**(24), 16878-16889
139. Kamps, M. P., and Sefton, B. M. (1988) Identification of multiple novel polypeptide substrates of the v-src, v- yes, v-fps, v-ros, and v-erb-B oncogenic tyrosine protein kinases utilizing antisera against phosphotyrosine. *Oncogene* **2**(4), 305-315
140. Dickinson, R. B., and Tranquillo, R. T. (1993) Optimal estimation of cell movement indices from the statistical analysis of cell tracking data. *AIChE J.* **39**(12), 1995-2010
141. Agard, D. A., Hiraoka, Y., Shaw, P., and Sedat, J. W. (1989) in *Fluorescence Microscopy of Living Cells in Culture* (Taylor, D. L., and Wang, Y. L., eds) Vol. 30, pp. 353-377, Academic Press, San Diego, CA
142. Wiley, H. S. (1985) Receptors as models for the mechanisms of membrane protein turnover and dynamics. *Curr. Tops. Membr. Trans.* **24**, 369-412



143. Ruff-Jamison, S., McGlade, J., Pawson, T., Chen, K., and Cohen, S. (1993) Epidermal growth factor stimulates the tyrosine phosphorylation of SHC in the mouse. *J Biol Chem* 268(11), 7610-7612
144. Coffey, R. J., Hawkey, C. J., Damstrup, L., Graves-Deal, R., Daniel, V. C., Dempsey, P. J., Chinery, R., Kirkland, S. C., DuBois, R. N., Jetton, T. L., and Morrow, J. D. (1997) Epidermal growth factor receptor activation induces nuclear targeting of cyclooxygenase-2, basolateral release of prostaglandins, and mitogenesis in polarizing colon cancer cells. *Proc. Natl Acad. Sci. USA* 94(2), 657-662
145. Watkins, L. F., and Levine, A. E. (1991) Differential role of transforming growth factor-alpha in two human colon-carcinoma cell lines. *Int. J. Cancer* 47(3), 455-60
146. Barnard, J. A., Graves-Deal, R., Pittelkow, M. R., DuBois, R., Cook, P., Ramsey, G. W., Bishop, P. R., Damstrup, L., and Coffey, R. J. (1994) Auto- and cross-induction within the mammalian epidermal growth factor- related peptide family. *J. Biol. Chem.* 269(36), 22817-22822
147. Fry, D. W., Kraker, A. J., McMichael, A., Ambroso, L. A., Nelson, J. M., Leopold, W. R., Connors, R. W., and Bridges, A. J. (1994) A specific inhibitor of the epidermal growth factor receptor tyrosine kinase. *Science* 265(5175), 1093-1095
148. Rasmussen, H. S., and McCann, P. P. (1997) Matrix metalloproteinase inhibition as a novel anticancer strategy: a review with special focus on batimastat and marimastat. *Pharmacol. Ther.* 75(1), 69-75
149. Chambers, A. F., and Matrisian, L. M. (1997) Changing views of the role of matrix metalloproteinases in metastasis. *J. Natl. Cancer Inst.* 89(17), 1260-1270
150. Barrandon, Y., and Green, H. (1987) Cell migration is essential for sustained growth of keratinocyte colonies: the roles of transforming growth factor-alpha and epidermal growth factor. *Cell* 50(7), 1131-1137
151. Matthay, M. A., Thiery, J. P., Lafont, F., Stampfer, F., and Boyer, B. (1993) Transient effect of epidermal growth factor on the motility of an immortalized mammary epithelial cell line. *J. Cell Sci.* 106(Pt 3), 869-78
152. Ono, M., Raab, G., Lau, K., Abraham, J. A., and Klagsbrun, M. (1994) Purification and characterization of transmembrane forms of heparin- binding EGF-like growth factor. *J Biol Chem* 269(49), 31315-31321
153. Higashiyama, S., Iwamoto, R., Goishi, K., Raab, G., Taniguchi, N., Klagsbrun, M., and Mekada, E. (1995) The membrane protein CD9/DRAP 27 potentiates the juxtacrine growth factor activity of the membrane-anchored heparin-binding EGF-like growth factor. *J. Cell Biol.* 128(5), 929-938
154. Derynck, R. (1992) The physiology of transforming growth factor-alpha. *Adv. Cancer Res.* 58, 27-52
155. Piepkorn, M., Pittelkow, M. R., and Cook, P. W. (1998) Autocrine regulation of keratinocytes: the emerging role of heparin- binding, epidermal growth factor-related growth factors [In Process Citation]. *J Invest Dermatol* 111(5), 715-721
156. Sledge, G. W., Jr., Qulali, M., Goulet, R., Bone, E. A., and Fife, R. (1995) Effect of matrix metalloproteinase inhibitor batimastat on breast cancer regrowth and metastasis in athymic mice. *J Natl Cancer Inst* 87(20), 1546-1550

157. Taraboletti, G., Garofalo, A., Belotti, D., Drudis, T., Borsotti, P., Scanziani, E., Brown, P. D., and Giavazzi, R. (1995) Inhibition of angiogenesis and murine hemangioma growth by batimastat, a synthetic inhibitor of matrix metalloproteinases. *J Natl Cancer Inst* 87(4), 293-298
158. Giavazzi, R., Garofalo, A., Ferri, C., Lucchini, V., Bone, E. A., Chiari, S., Brown, P. D., Nicoletti, M. I., and Taraboletti, G. (1998) Batimastat, a synthetic inhibitor of matrix metalloproteinases, potentiates the antitumor activity of cisplatin in ovarian carcinoma xenografts. *Clin Cancer Res* 4(4), 985-992
159. McDonnell, S. E., Kerr, L. D., and Matrisian, L. M. (1990) Epidermal growth factor stimulation of stromelysin mRNA in rat fibroblasts requires induction of proto-oncogenes c-fos and c-jun and activation of protein kinase C. *Mol. Cell. Biol.* 10(8), 4284-4293
160. Carraway III, K. L., and Cantley, L. C. (1994) A Neu Acquaintance for ErbB3 and ErbB4: A role for Receptor Heterodimerization in Growth Signaling. *Cell* 78, 5-8
161. Worthylake, R., and Wiley, H. S. (1997) Structural aspects of the epidermal growth factor receptor required for transmodulation of erbB-2/neu. *J Biol Chem* 272(13), 8594-8601
162. Marth, C., Marcus, T. L., Cronauer, M. V., Doppler, W., Zeimet, A. G., Bachmair, F., Ullrich, A., and Daxenbichler, G. (1992) Epidermal Growth Factor Reduces HER-2 Protein Level In Human Ovarian Carcinoma Cells. *Int. J. Cancer* 52, 311-316
163. King, C. R., Borrello, I., Bellot, F., Comoglio, P., and Schlessinger, J. (1988) EGF binding to its receptor triggers a rapid tyrosine phosphorylation of the erbB-2 protein in the mammary tumor cell line SK-BR-3. *EMBO J.* 7, 1647-1651
164. Bartek, J., Bartkova, J., Kyprianou, N., Lalani, E. N., Staskova, Z., Shearer, M., Chang, S., and Taylor-Papadimitriou, J. (1991) Efficient immortalization of luminal epithelial cells from human mammary gland by introduction of simian virus 40 large tumor antigen with a recombinant retrovirus. *Proc. Natl. Acad. Sci. USA* 88, 3520-3524
165. D'Souza, B., Berdichevsky, F., Kyprianou, N., and Taylor-Papadimitriou, J. (1993) Collagen-induced morphogenesis and expression of the alpha 2-integrin subunit is inhibited in c-erbB2-transfected human mammary epithelial cells. *Oncogene* 8(7), 1797-1806
166. Wiley, H. S., and Cunningham, D. D. (1981) A steady state model for analyzing the cellular binding, internalization and degradation of polypeptide ligands. *Cell* 25, 433-440
167. Lund, K. A., Opresko, L. K., Starbuck, C., Walsh, B. J., and Wiley, H. S. (1990) Quantitative Analysis of the Endocytic System Involved in Hormone-induced Receptor Internalization. *J. Biol. Chem.* 265(26), 15713-15723
168. Carpenter, G. (1987) Receptors for epidermal growth factor and other polypeptide mitogens. *Annu. Rev. Biochem.* 56, 881-914.
169. Wada, T., Qian, X. L., and Greene, M. I. (1990) Intermolecular association of the p185neu protein and EGF receptor modulates EGF receptor function. *Cell* 61(7), 1339-1347
170. Qian, X., LeVea, C. M., Freeman, J. K., Dougall, W. C., and Greene, M. I. (1994) Heterodimerization of epidermal growth factor receptor and wild-type or kinase-deficient Neu: a mechanism of interreceptor kinase activation and transphosphorylation. *Proc. Natl. Acad. Sci. USA* 91(4), 1500-1504

171. Spivak-Kroizman, T., Rotin, D., Pinchasi, D., Ullrich, A., Schlessinger, J., and Lax, I. (1992) Heterodimerization of c-erbB2 with different epidermal growth factor receptor mutants elicits stimulatory or inhibitory responses. *J. Biol. Chem.* **267**, 8056-8063
172. Wright, J. D., Reuter, C. W. M., and Weber, M. J. (1995) An incomplete program of cellular tyrosine phosphorylations induced by kinase-defective epidermal growth factor receptors. *J. Biol. Chem.* **270**, 12085-12093
173. Wiley, H. S., Walsh, B. J., and Lund, K. A. (1989) Global Modulation of the Epidermal Growth Factor Receptor Is Triggered by Occupancy of Only a Few Receptors. *J. Biol. Chem.* **264**, 18912-18920
174. Samanta, A., LeVea, C. M., Dougall, W. C., Qian, X., and Greene, M. I. (1994) Ligand and p185c-neu density govern receptor interactions and tyrosine kinase activation. *Proc Natl Acad Sci U S A* **91**(5), 1711-1715
175. Ram, T. G., and Ethier, S. P. (1996) Phosphatidylinositol 3-Kinase Recruitment by p185erb-2 and erbB-3 Is Potently Induced by neu Differentiation Factor/Heregulin during Mitogenesis and Is Constitutively Elevated in Growth Factor-independent Breast Carcinoma Cells with c-erbB-2 Gene Amplification. *Cell Growth and Diff.* **7**, 551-567
176. Carraway, K. L. d., and Cerione, R. A. (1993) Inhibition of epidermal growth factor receptor aggregation by an antibody directed against the epidermal growth factor receptor extracellular domain. **268**(32), 23860-23867
177. Worthylake, R., and Wiley, H. (1997) Structural Aspects of the Epidermal Growth Factor Receptor Required for Transmodulation of erbB-2/neu. *J. Biol. Chem.* **272**(13), 8594-8601
178. Opresko, L. K., Chang, C. P., Will, B. H., Burke, P. M., Gill, G. N., and Wiley, H. S. (1995) Endocytosis and Lysosomal Targeting of Epidermal Growth Factor Receptors Are Mediated by Distinct Sequences Independent of the Tyrosine Kinase Domain. *J. Biol. Chem.* **270**(9), 4325-4333
179. Lenferink, A. E., Pinkas-Kramarski, R., van de Poll, M. L., van Vugt, M. J., Klapper, L. N., Tzahar, E., Waterman, H., Sela, M., van Zoelen, E. J., and Yarden, Y. (1998) Differential endocytic routing of homo- and hetero-dimeric ErbB tyrosine kinases confers signaling superiority to receptor heterodimers. *Embo J* **17**(12), 3385-3397
180. Wiley, H. S., VanNostrand, W., McKinley, D. N., and Cunningham, D. D. (1985) Intracellular processing of epidermal growth factor and its effect on ligand-receptor interactions. *J. Biol. Chem.* **260**, 5290-5295
181. Haigler, H. T., Wiley, H. S., Moehring, J. M., and Moehring, T. J. (1985) Altered degradation of epidermal growth factor in a diphtheria toxin-resistant clone of KB cells. *J. Cell. Physiol.* **124**, 322-330
182. Stampfer, M. R. (1985) Isolation and growth of human mammary epithelial cell. *J. Tiss. Cul. Meth.* **9**(2), 107-115
183. Stampfer, M. R., and Bartley, J. C. (1985) Induction of transformation and continuous cell lines from normal human mammary epithelial cells after exposure to benzo[a]pyrene. *Proc. Natl. Acad. Sci. USA* **82**(8), 2394-2398

Figure 1

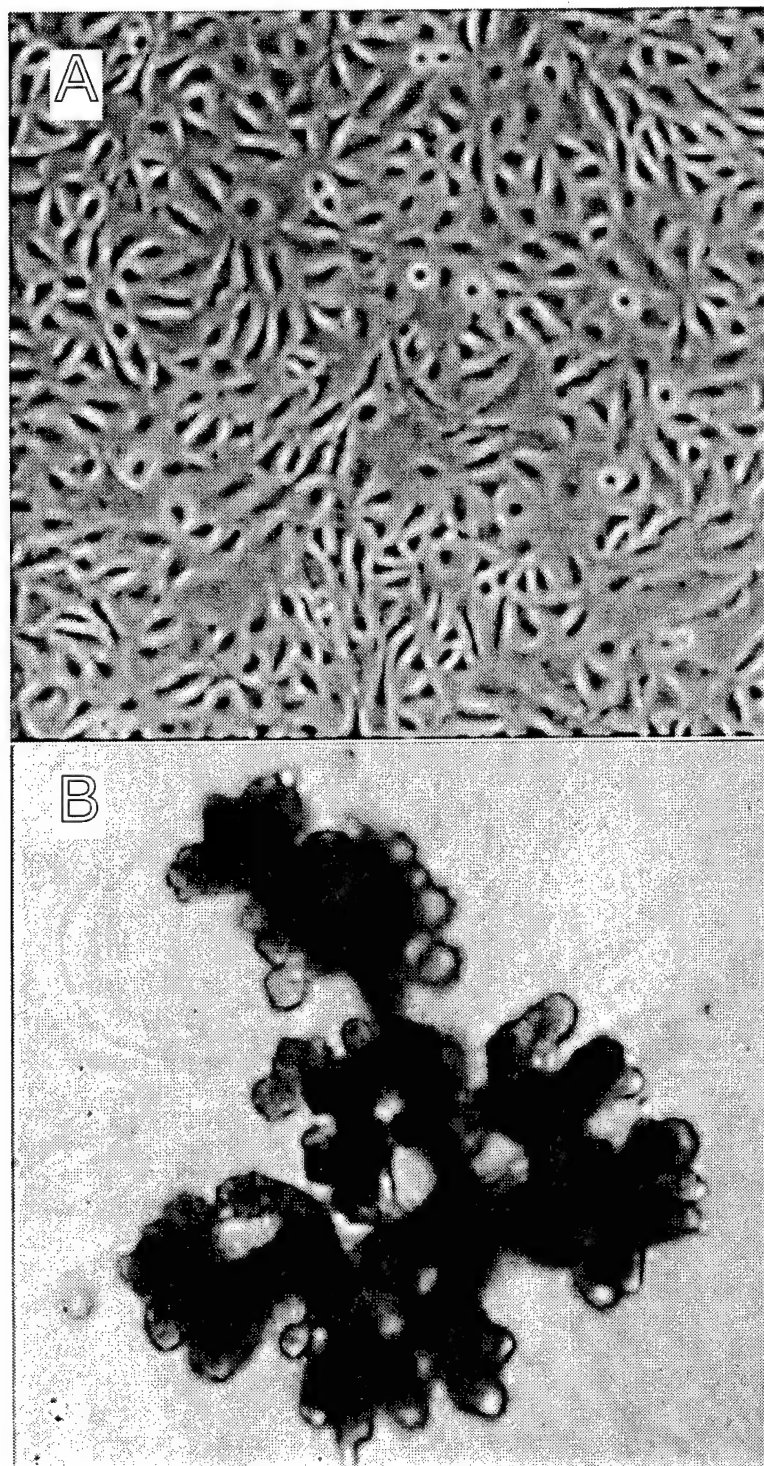




Figure 2

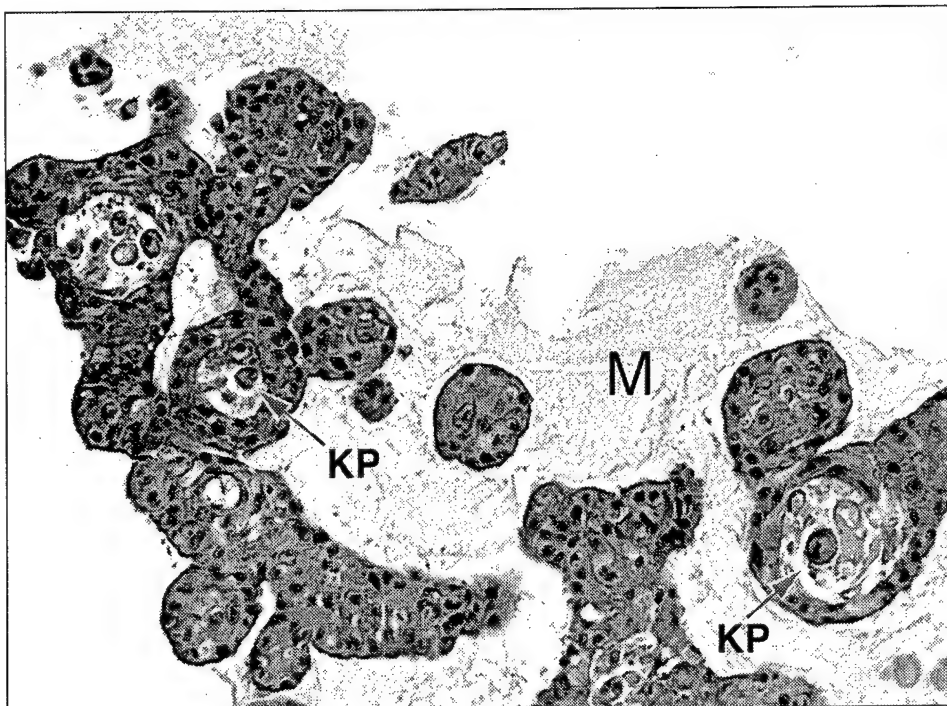


Figure 3

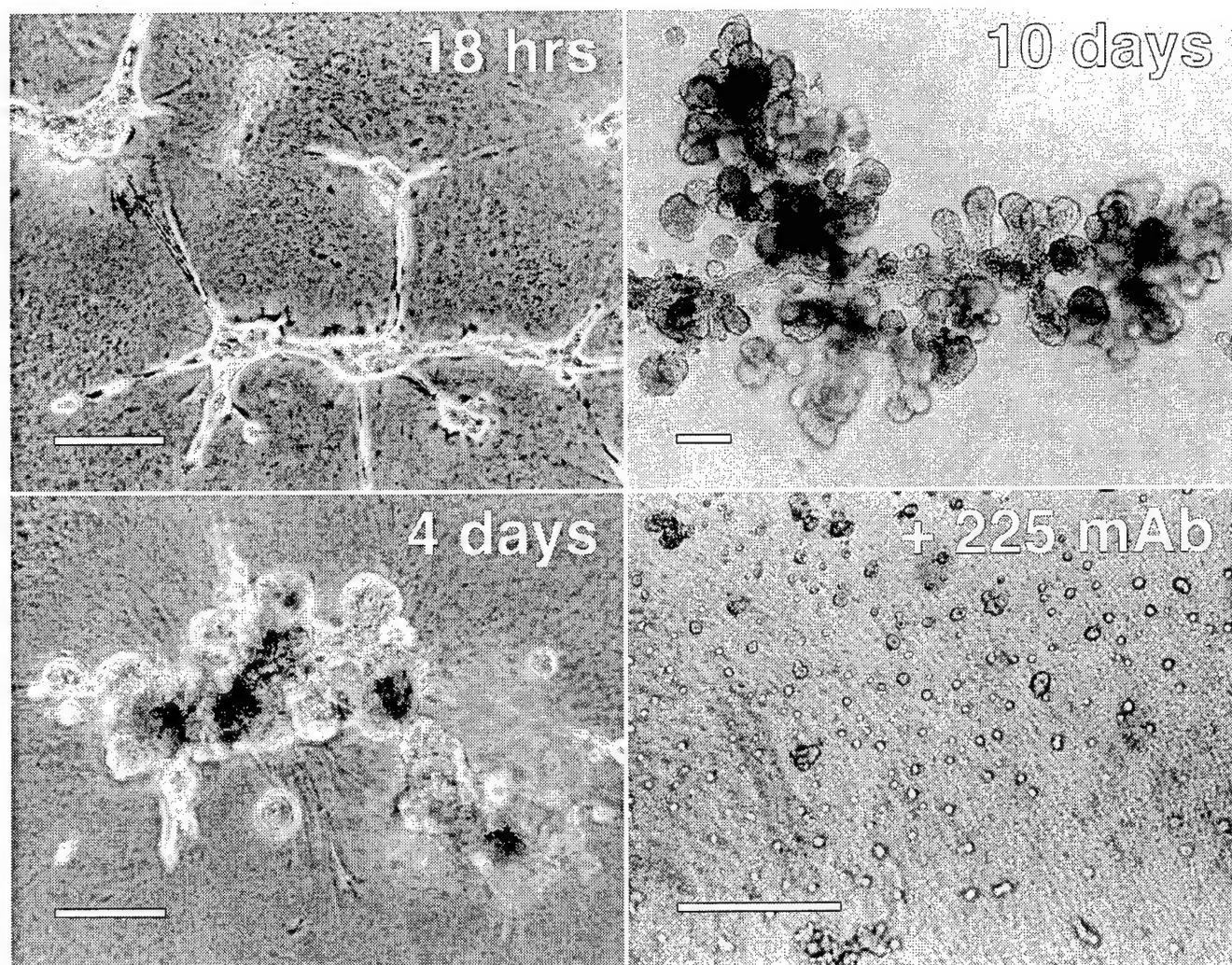


Figure 4

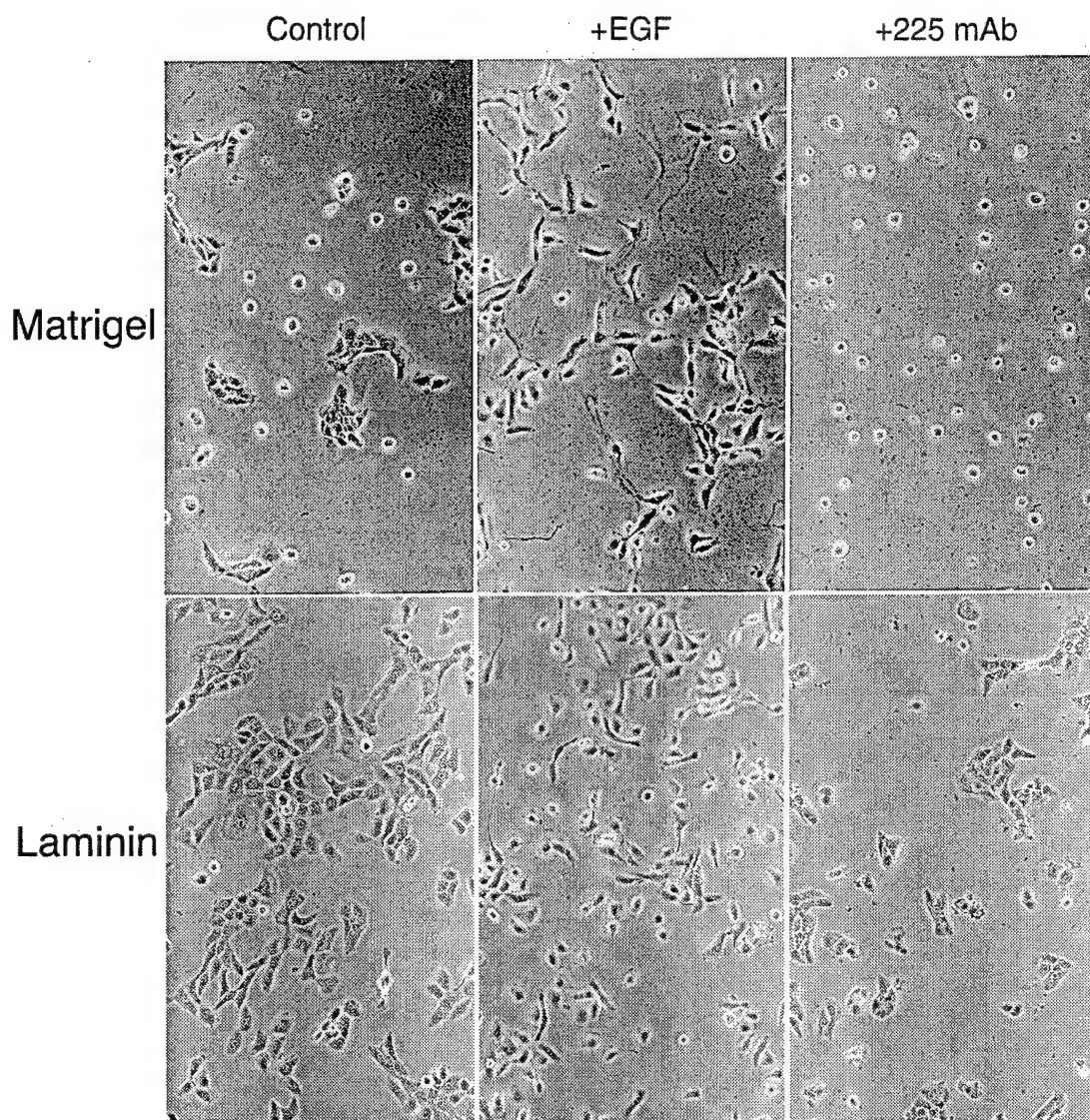


Figure 5

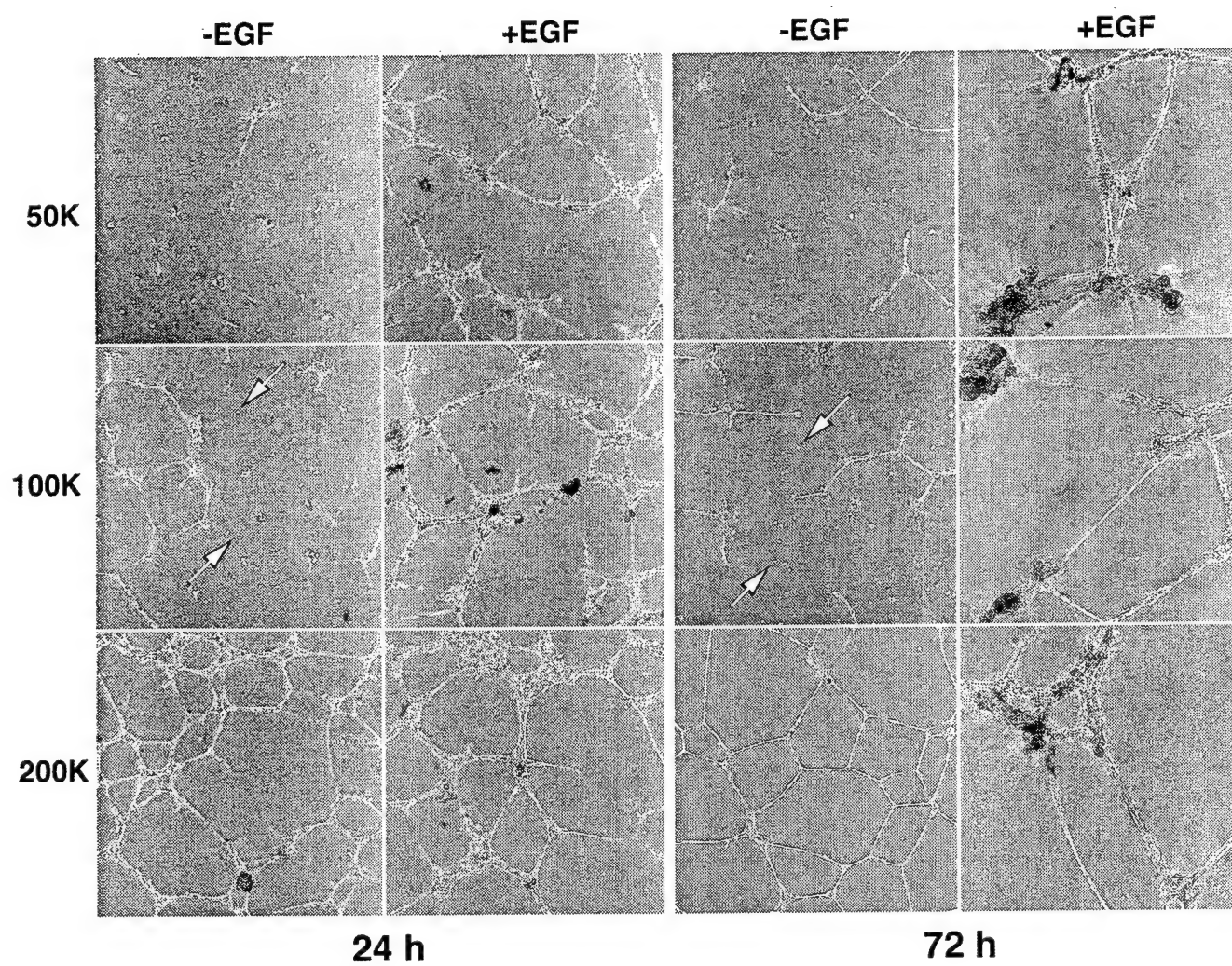




Figure 6

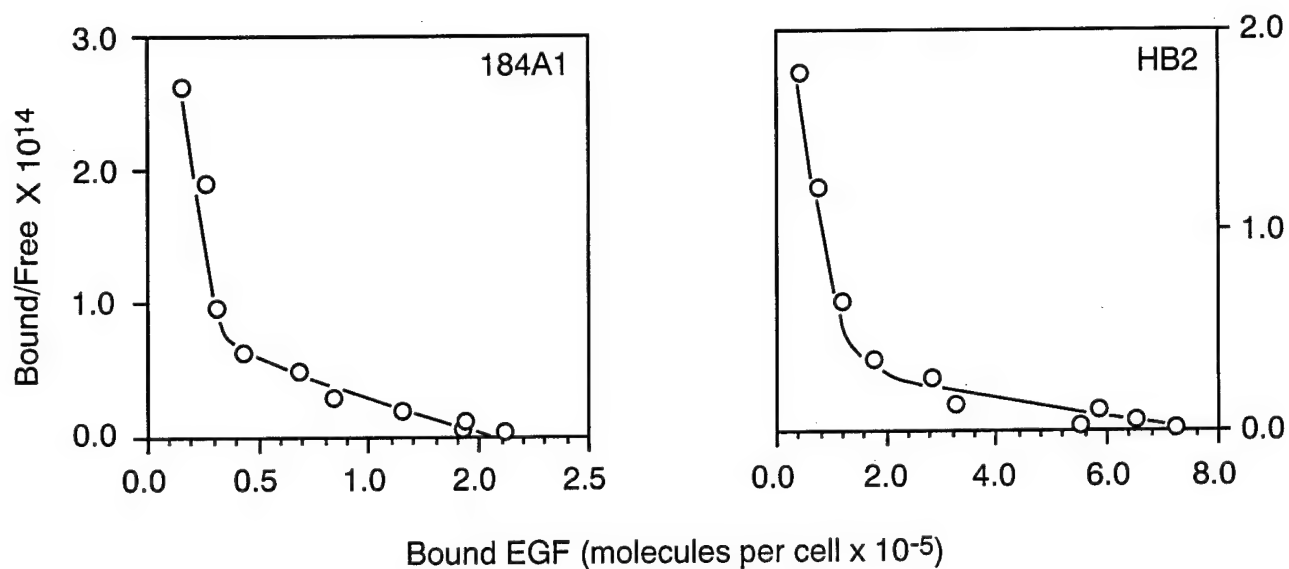
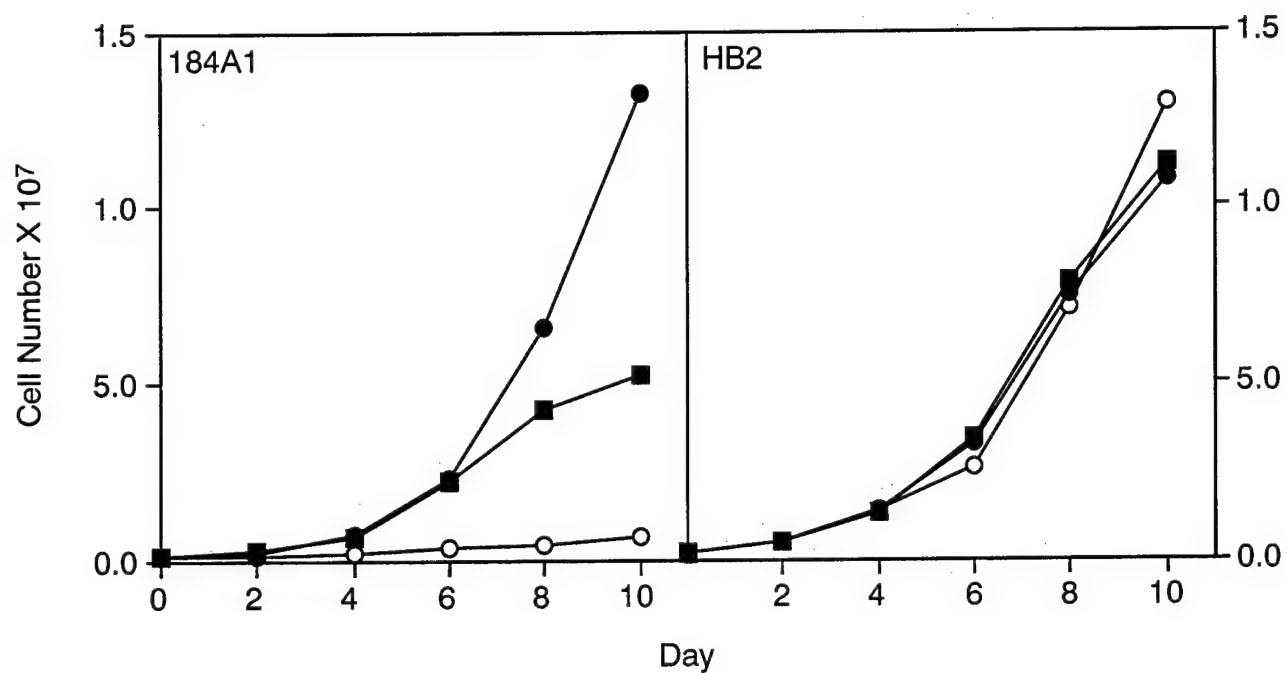
**A****B**

Figure 7

**HB2**

**184A1**

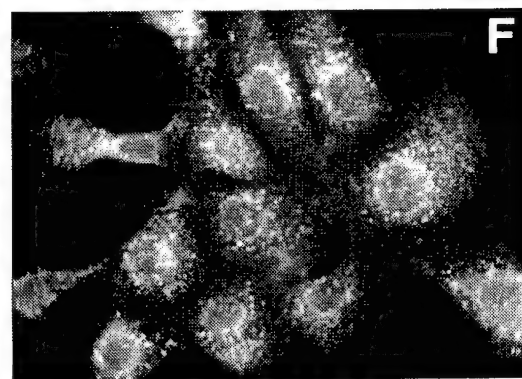
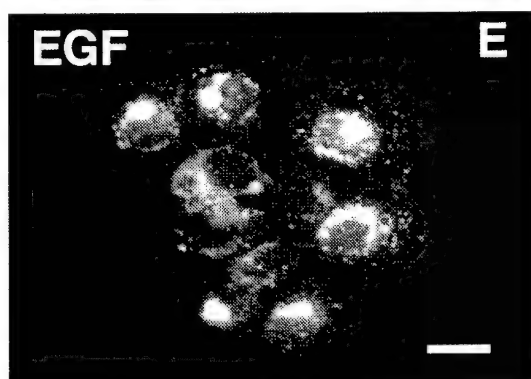
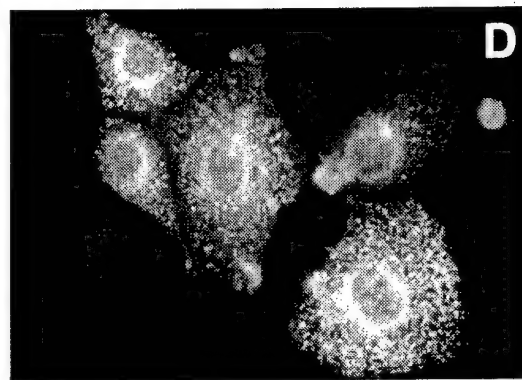
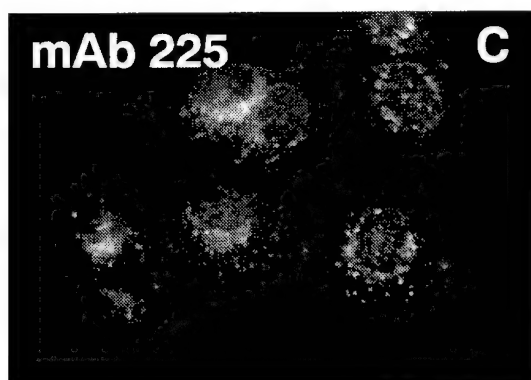
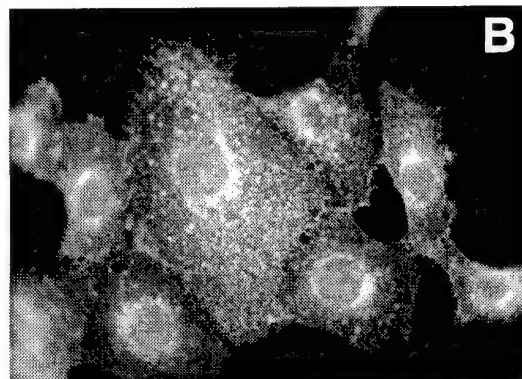
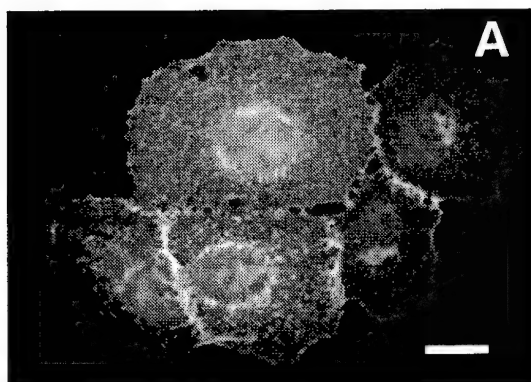


Figure 8

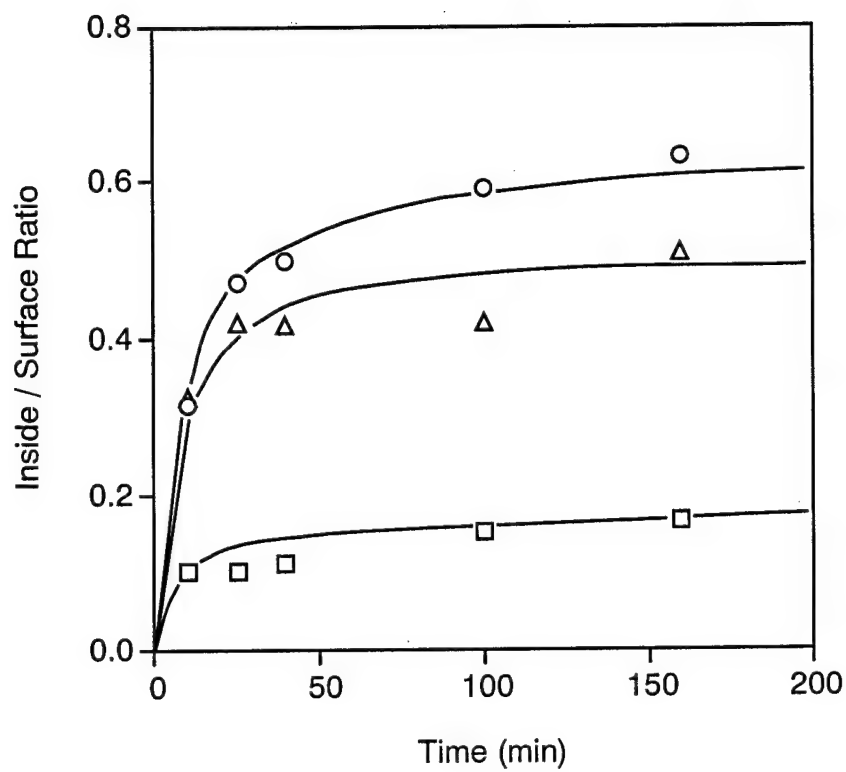
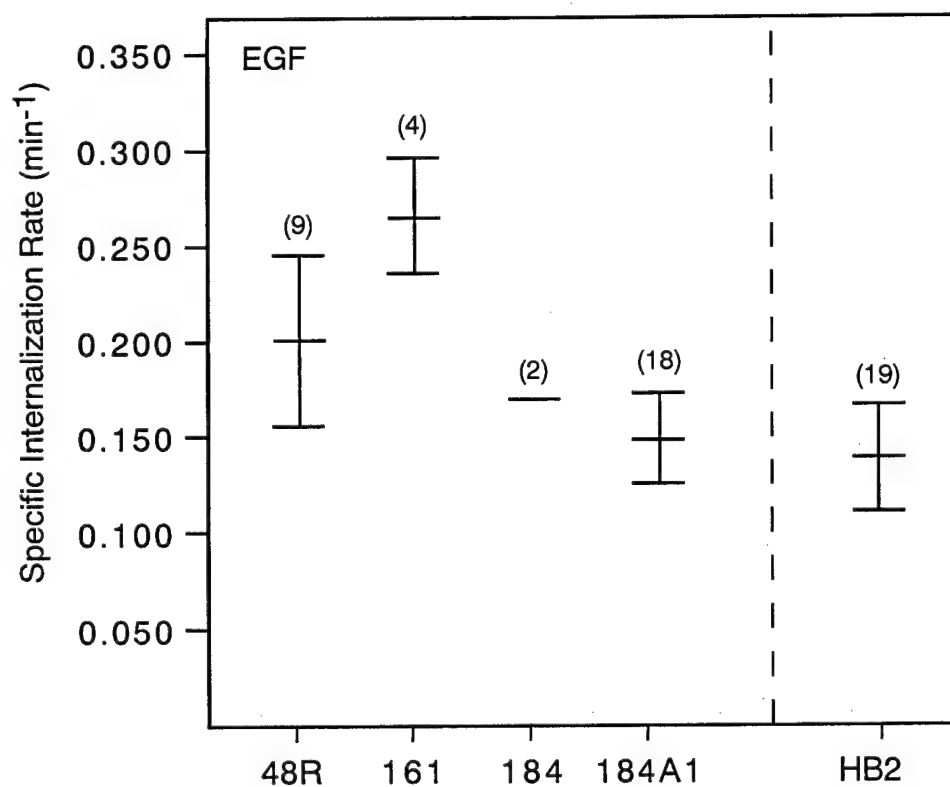
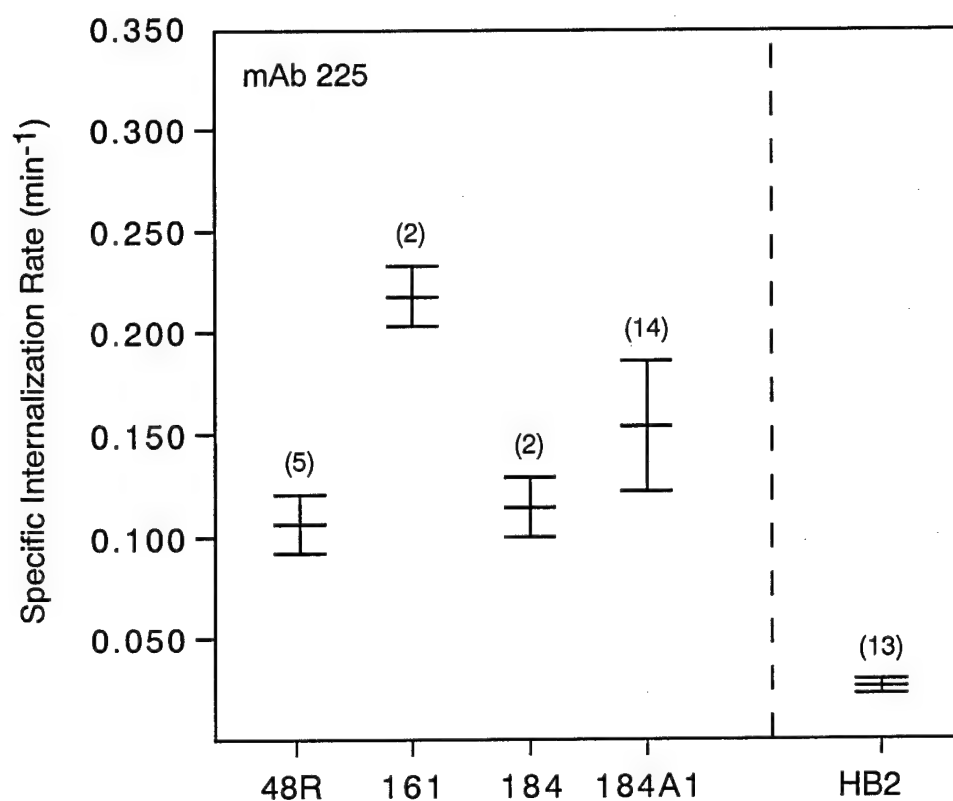


Figure 9



Mammary Epithelial Cell Line

Figure 10

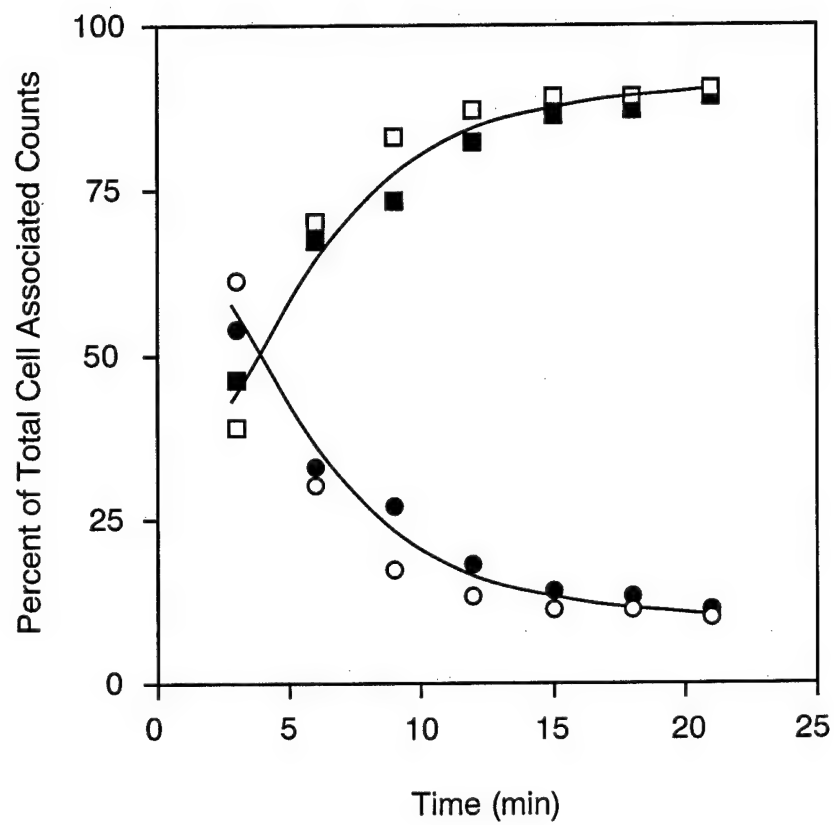




Figure 11

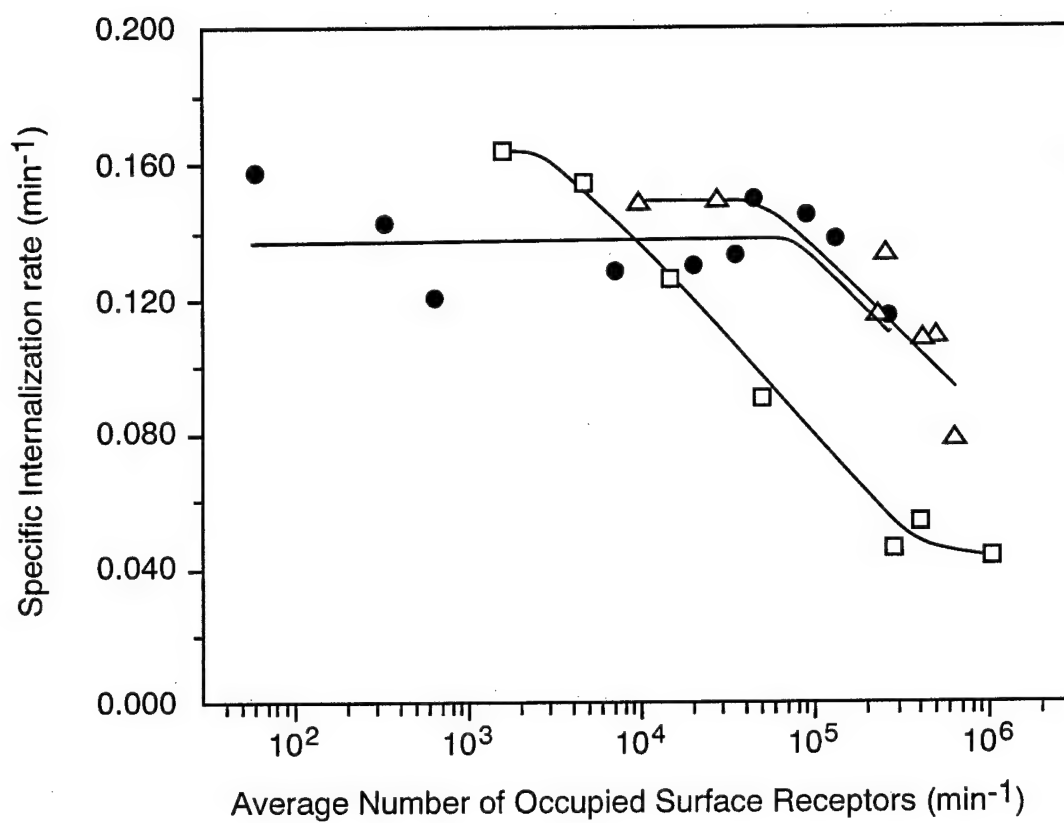


Figure 12

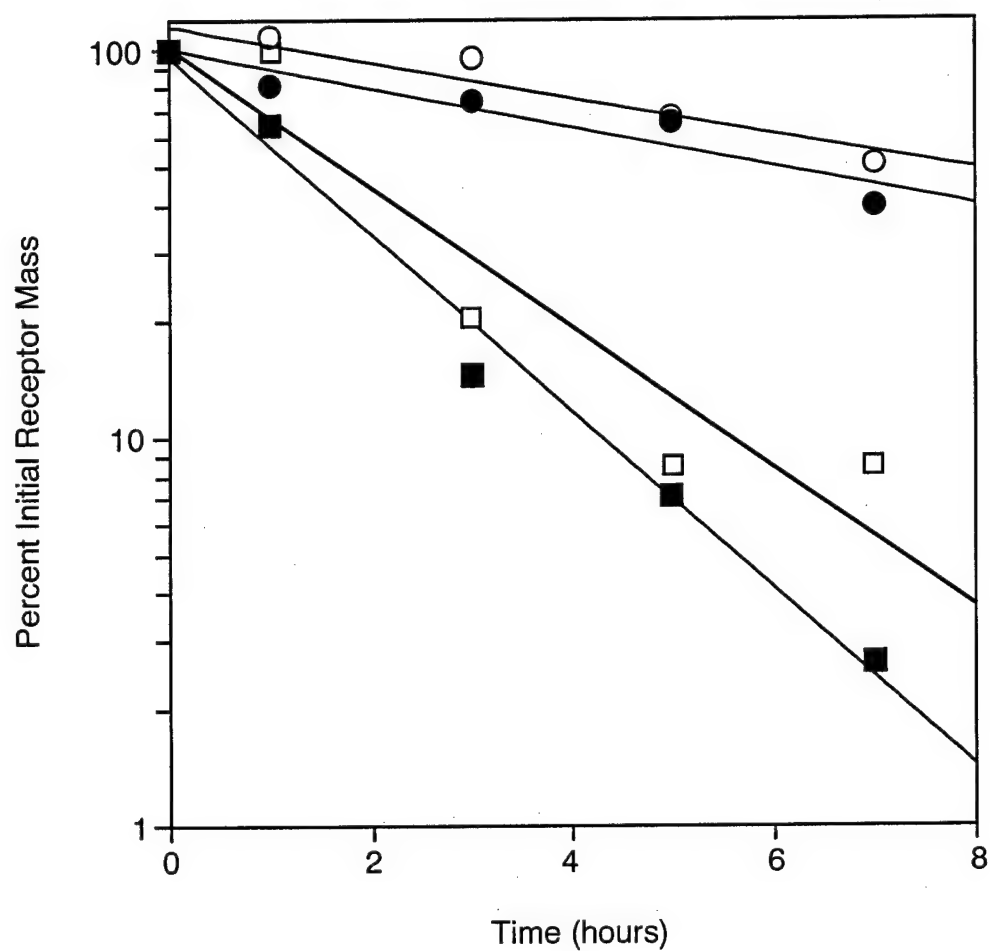
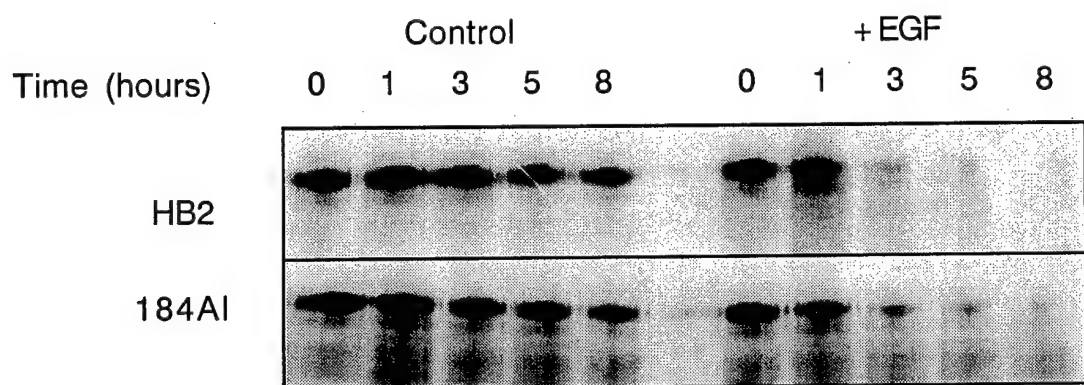


Figure 13

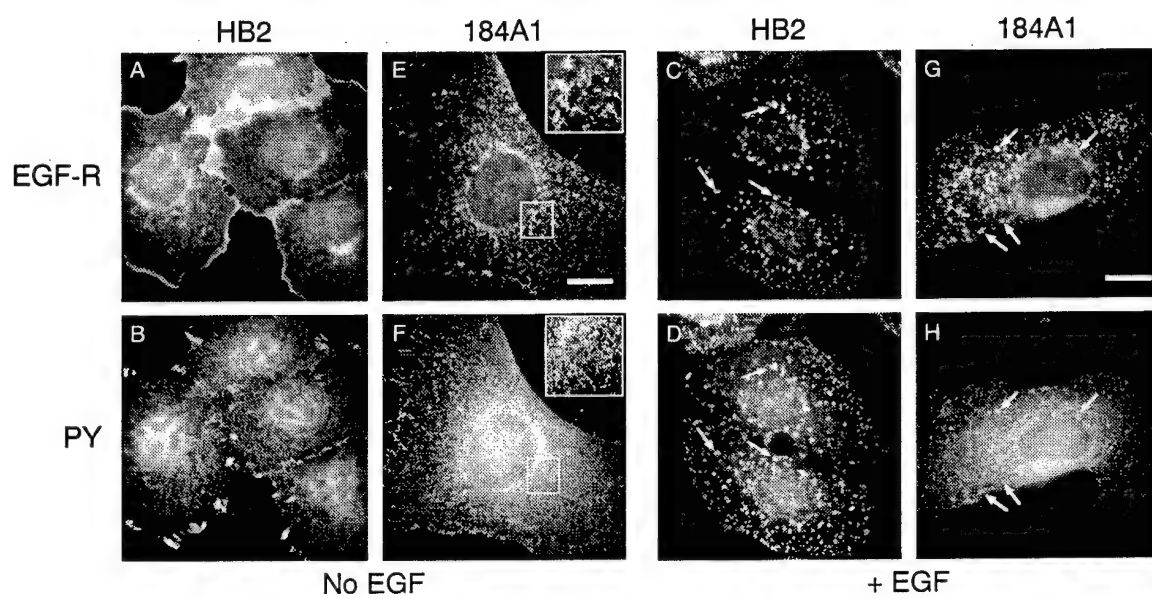
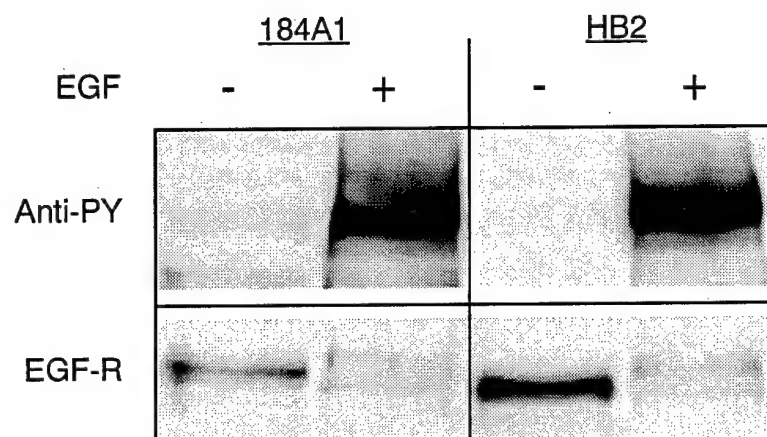


Figure 14

A



B

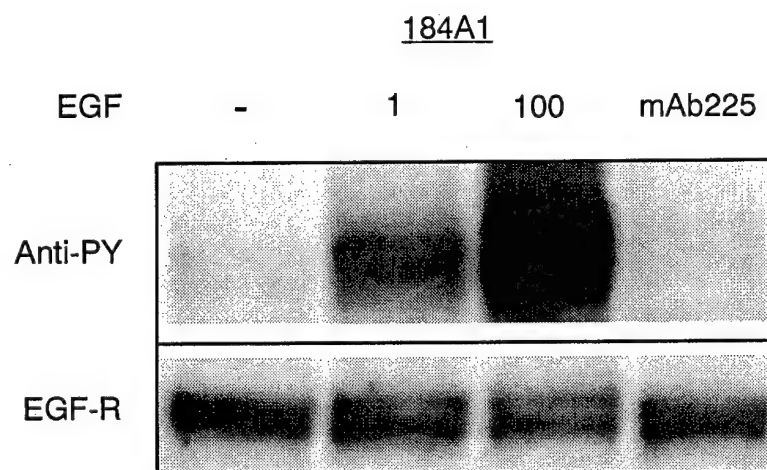


Figure 15

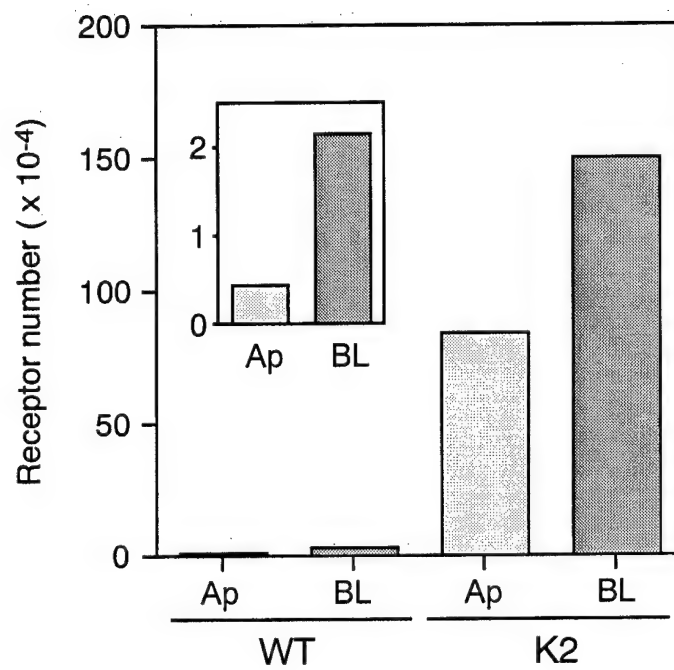




Figure 16

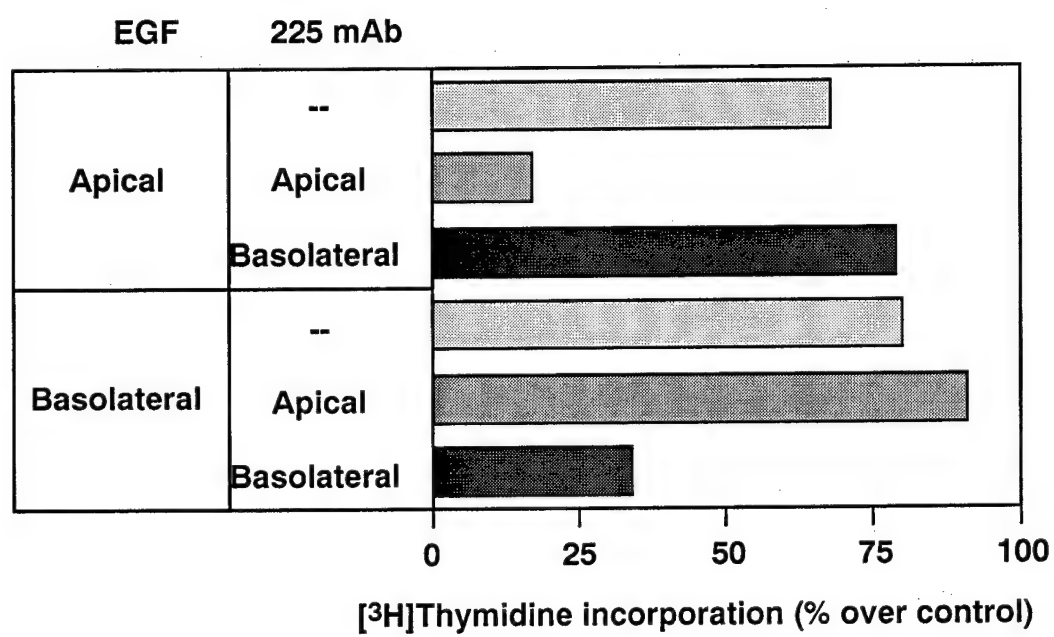


Figure 17

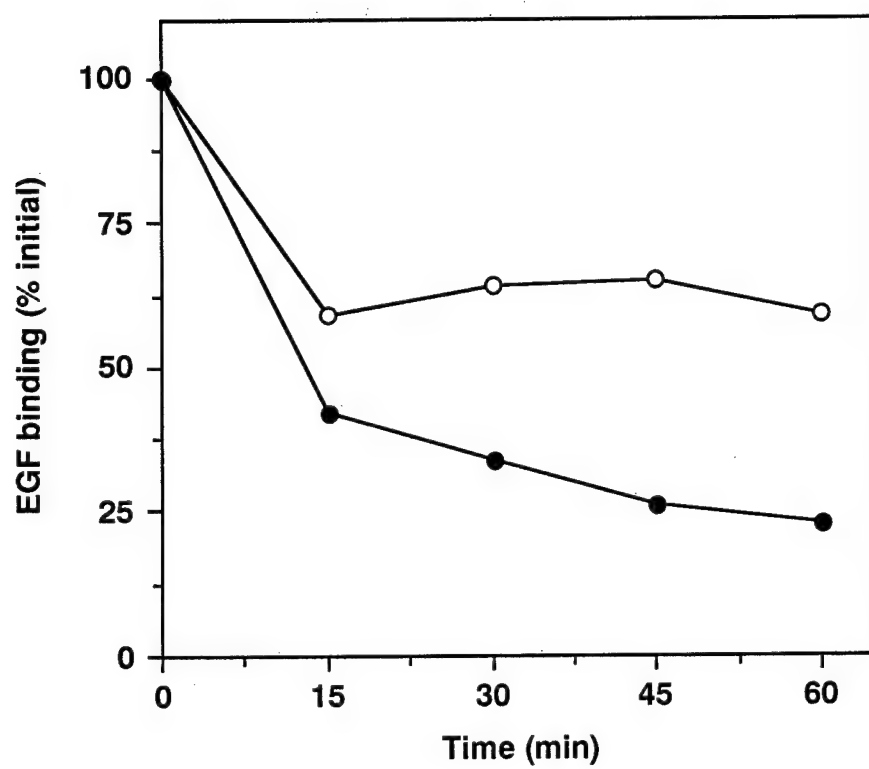


Figure 18

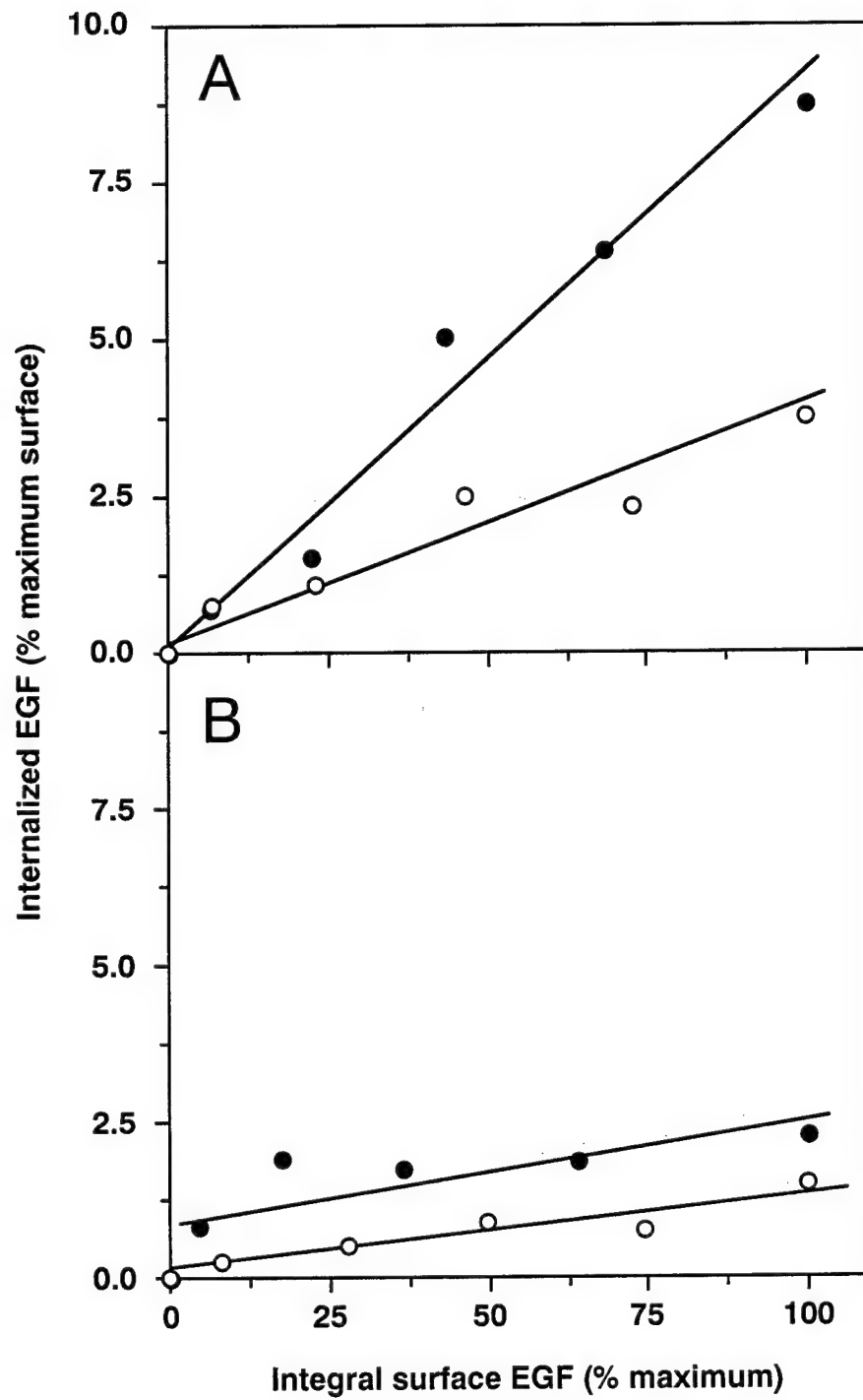


Figure 19

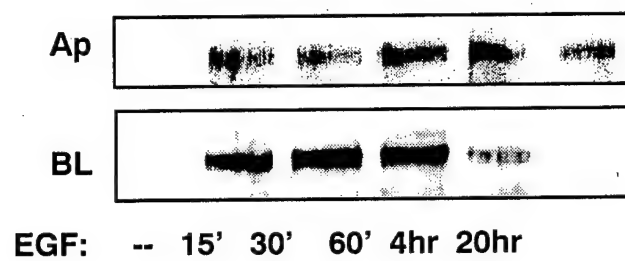


Figure 20

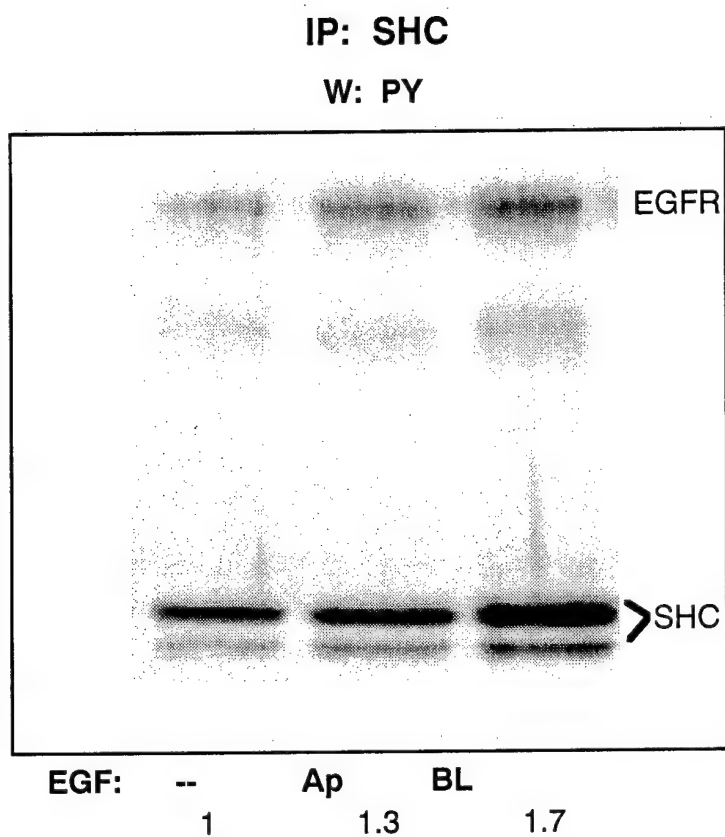




Figure 21

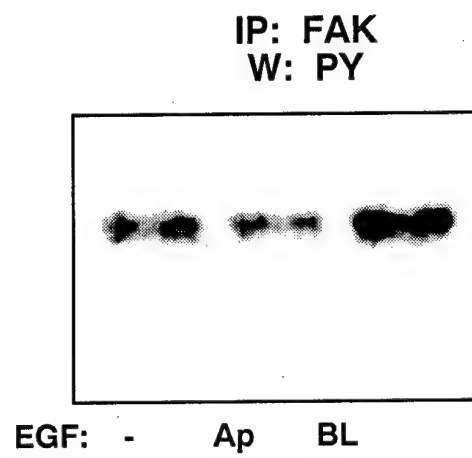


Figure 22

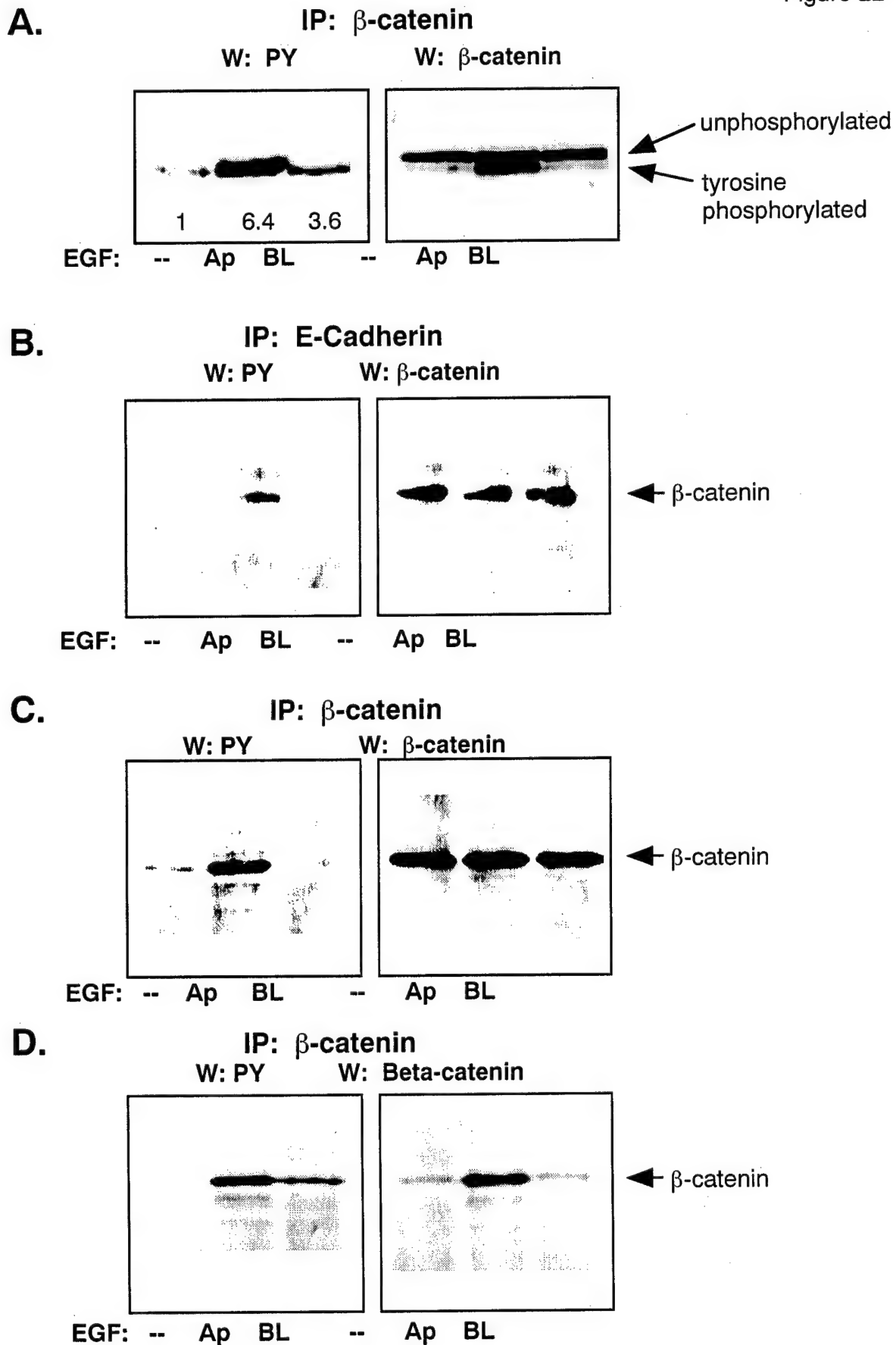
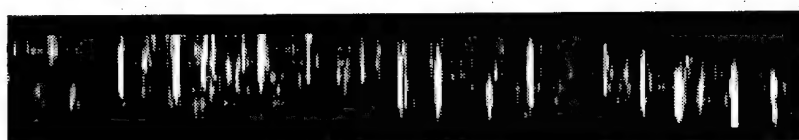


Figure 23

**A.**

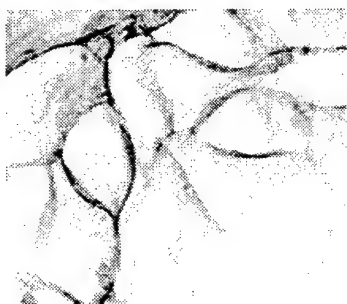


← apical  
surface

← basal  
surface

**B.**

**Anti-PY**



**Anti-beta-catenin**

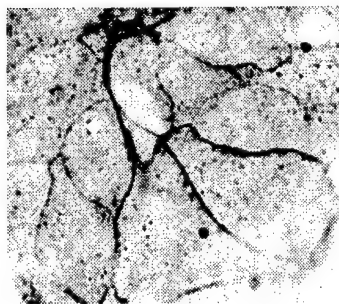


Figure 24

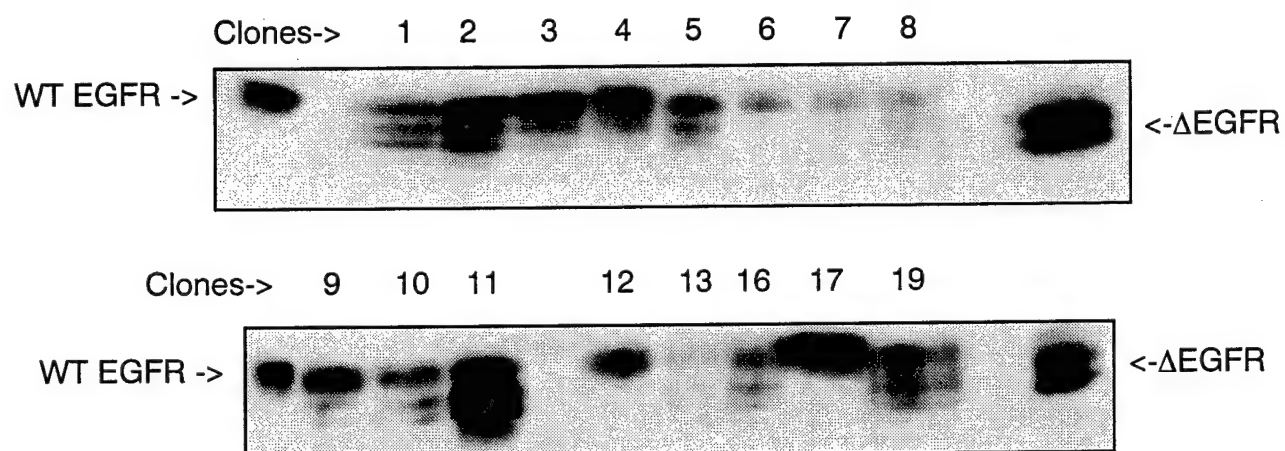
Screening HMEC clones Expressing  $\Delta$ EGFR

Figure 25

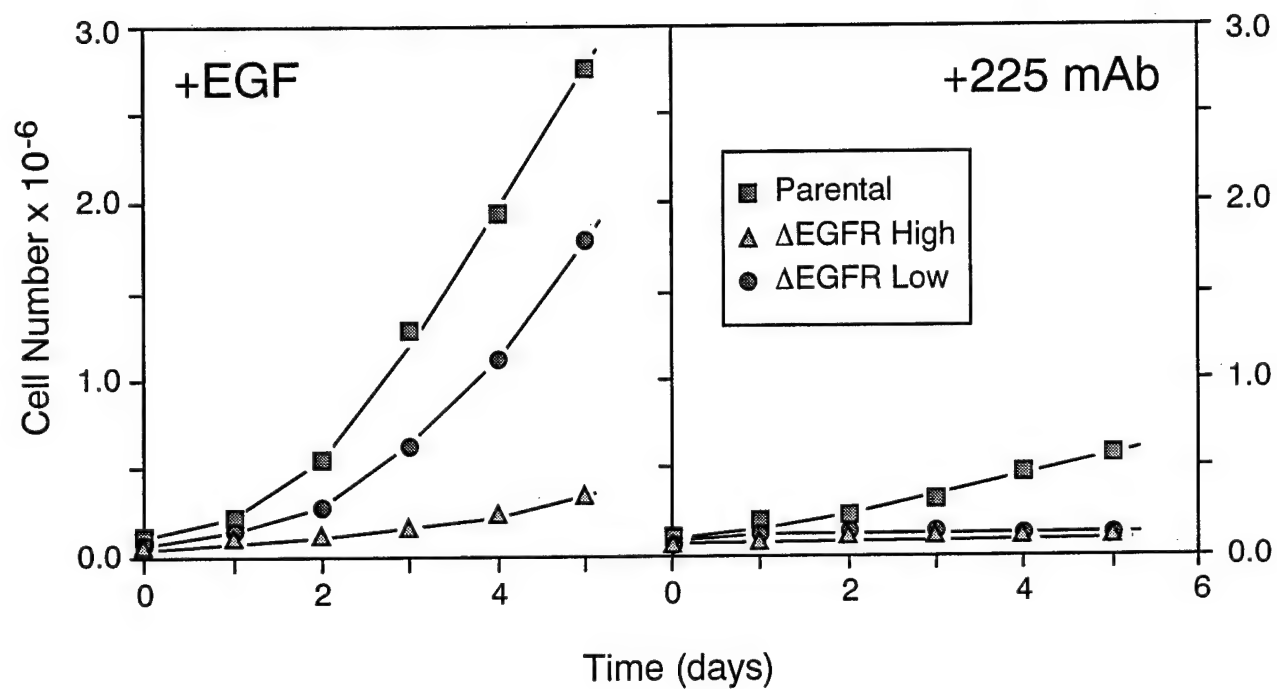




Figure 26

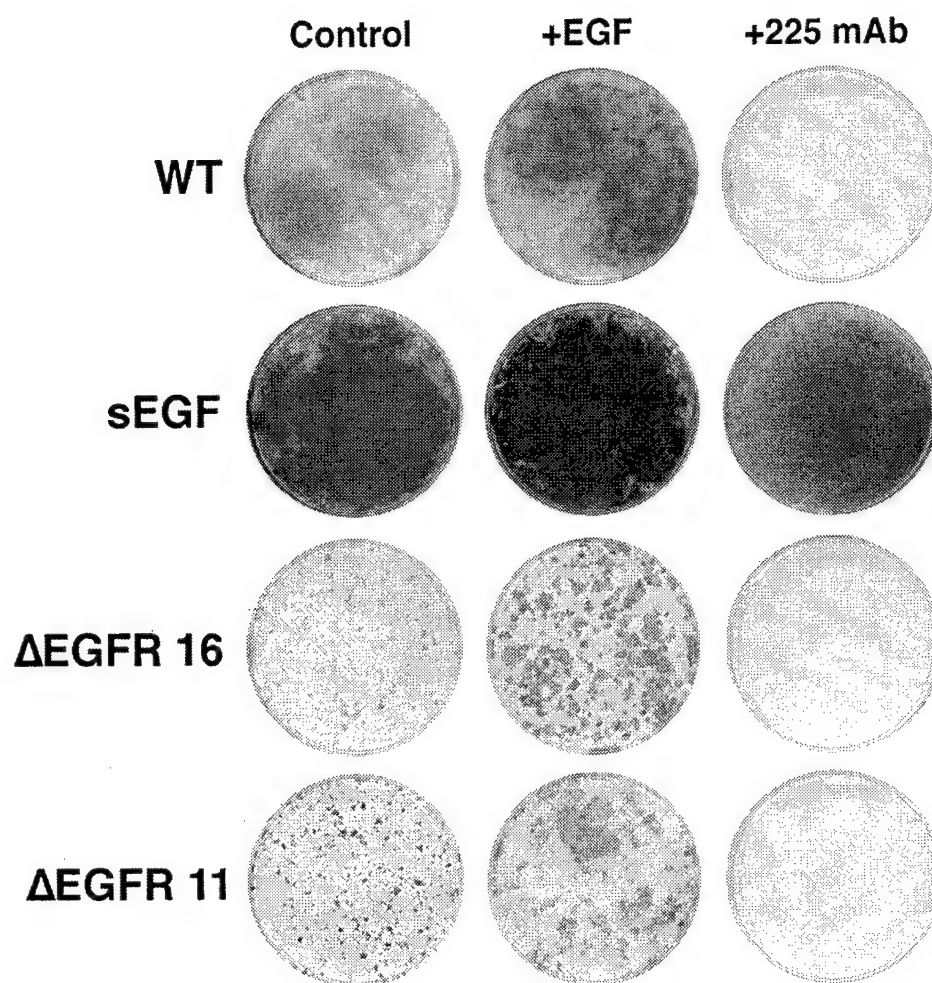


Figure 27

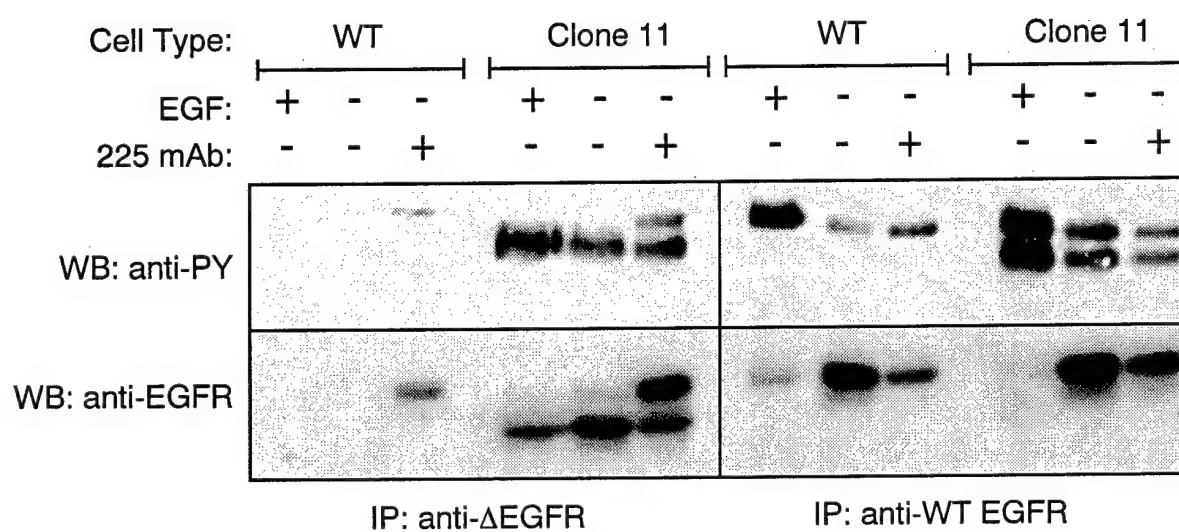


Figure 28

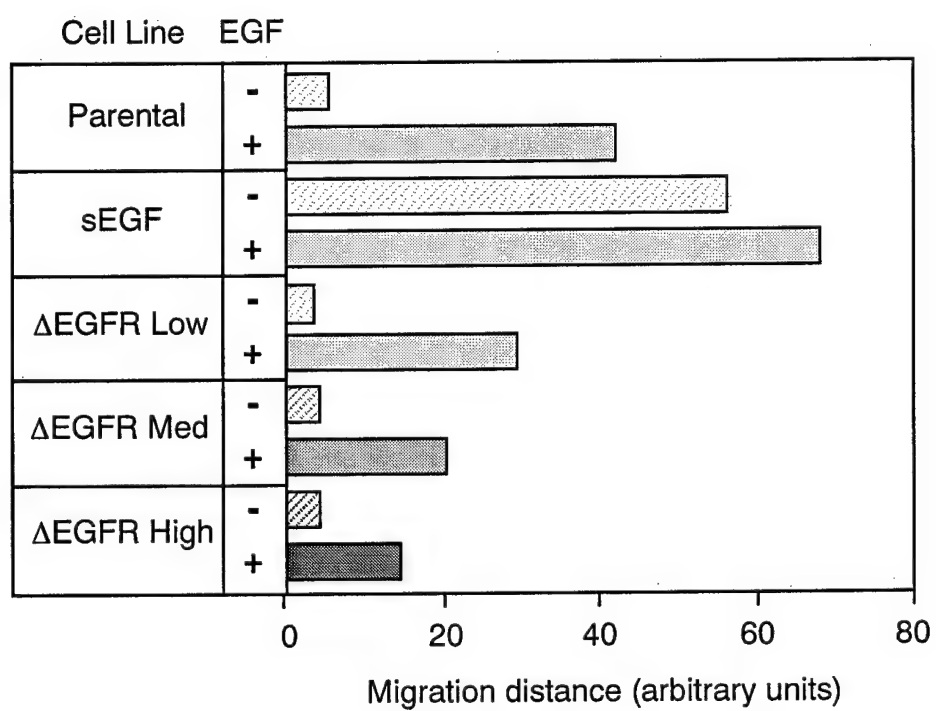


Figure 29

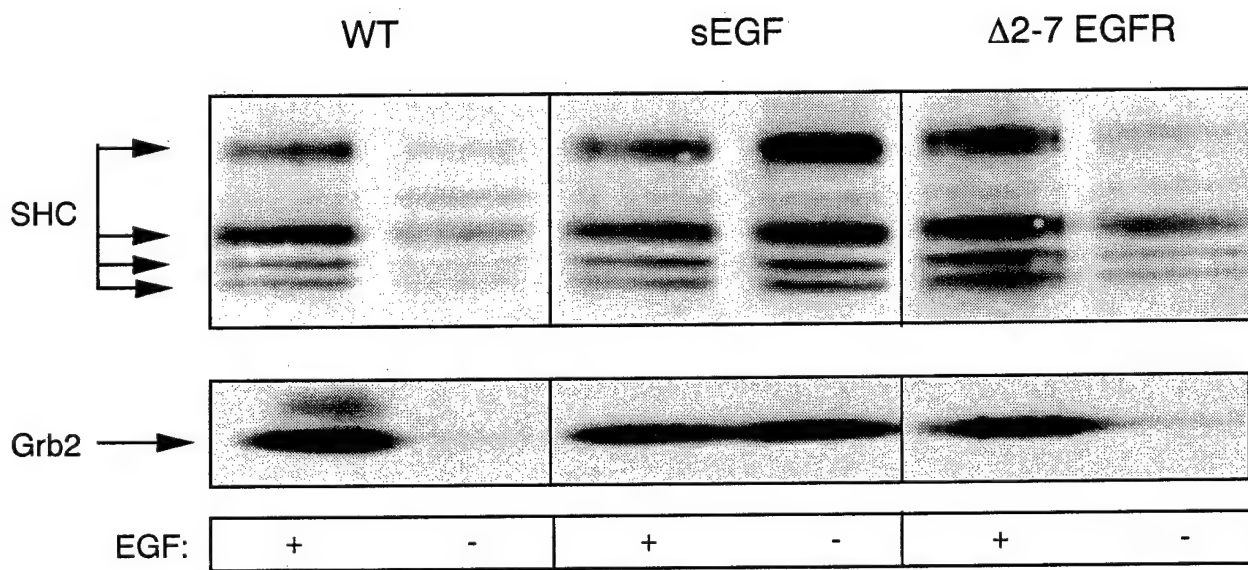


Figure 30

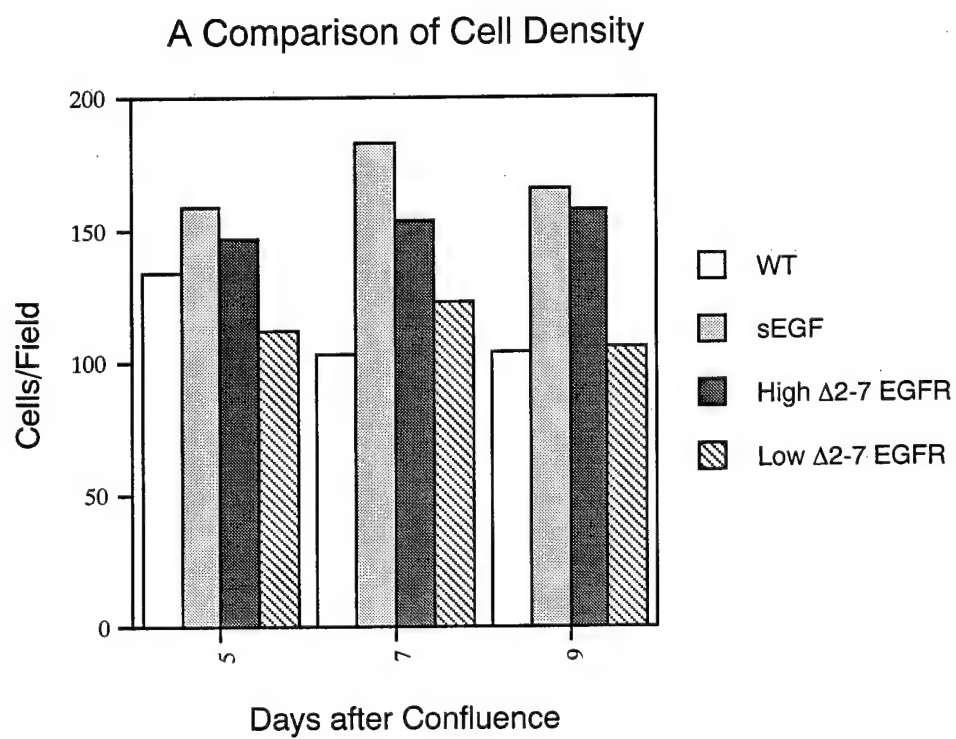




Figure 31

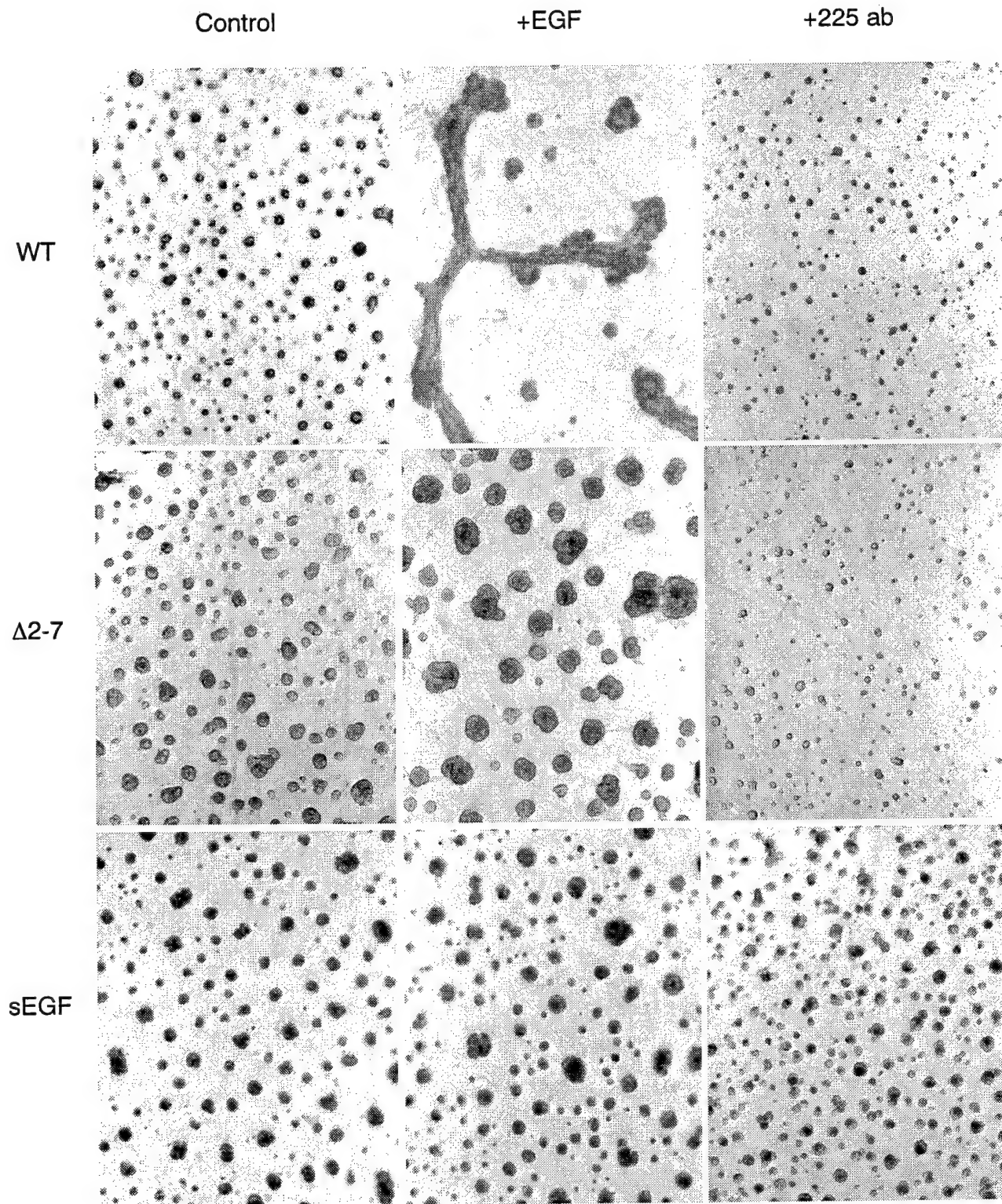


Figure 32

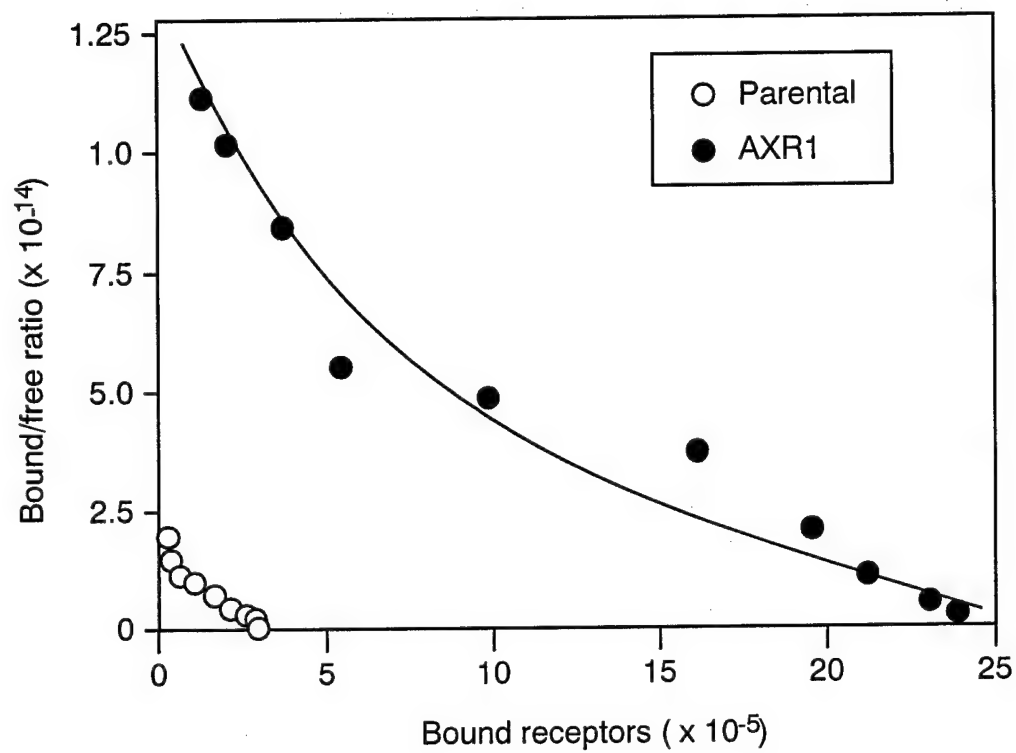


Figure 33

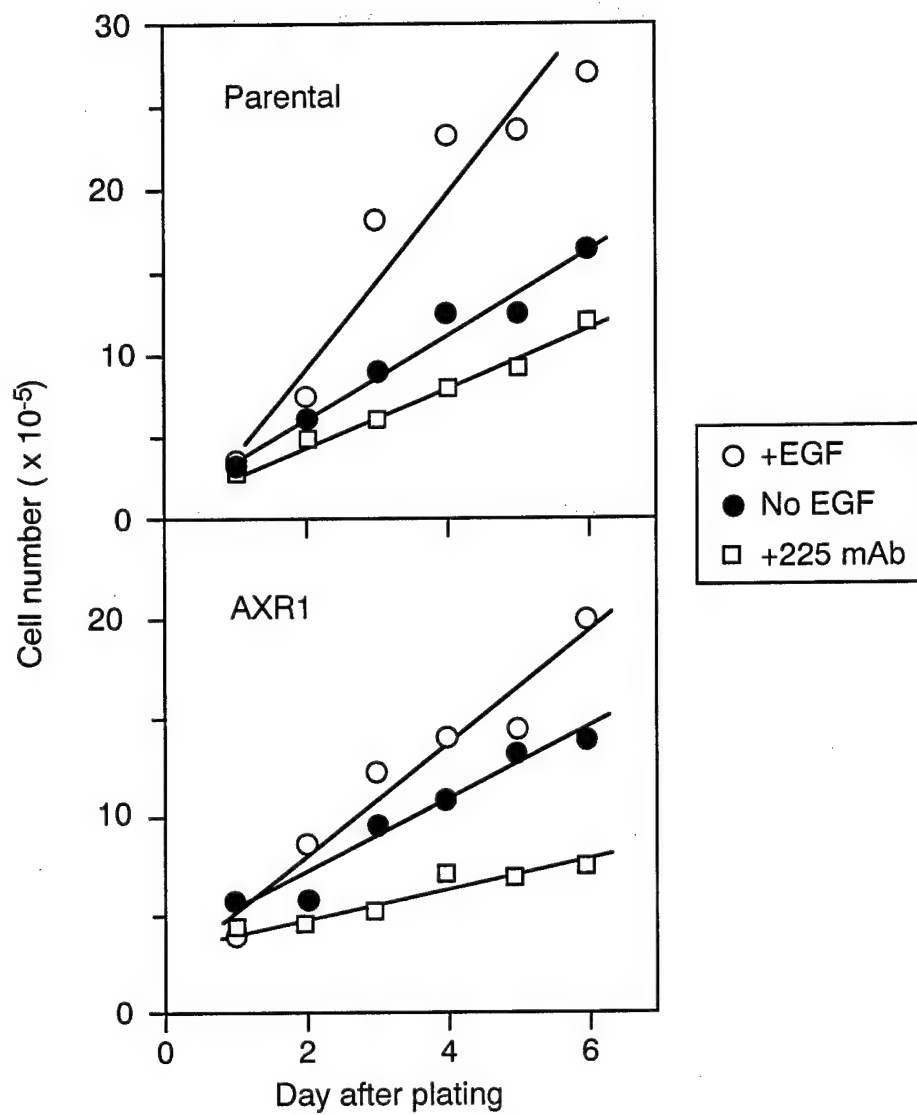


Figure 34

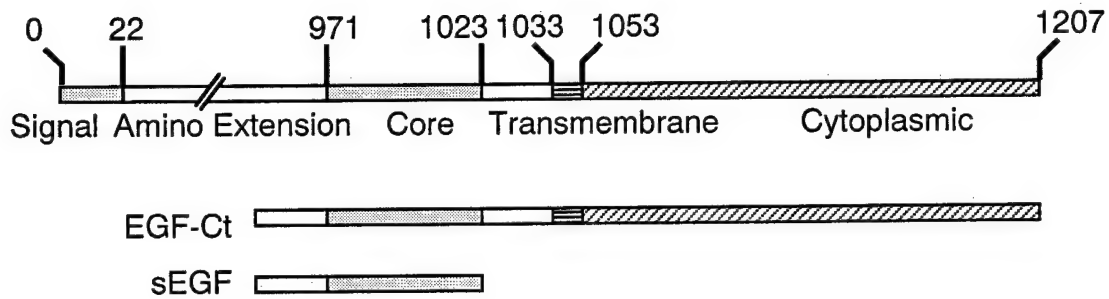
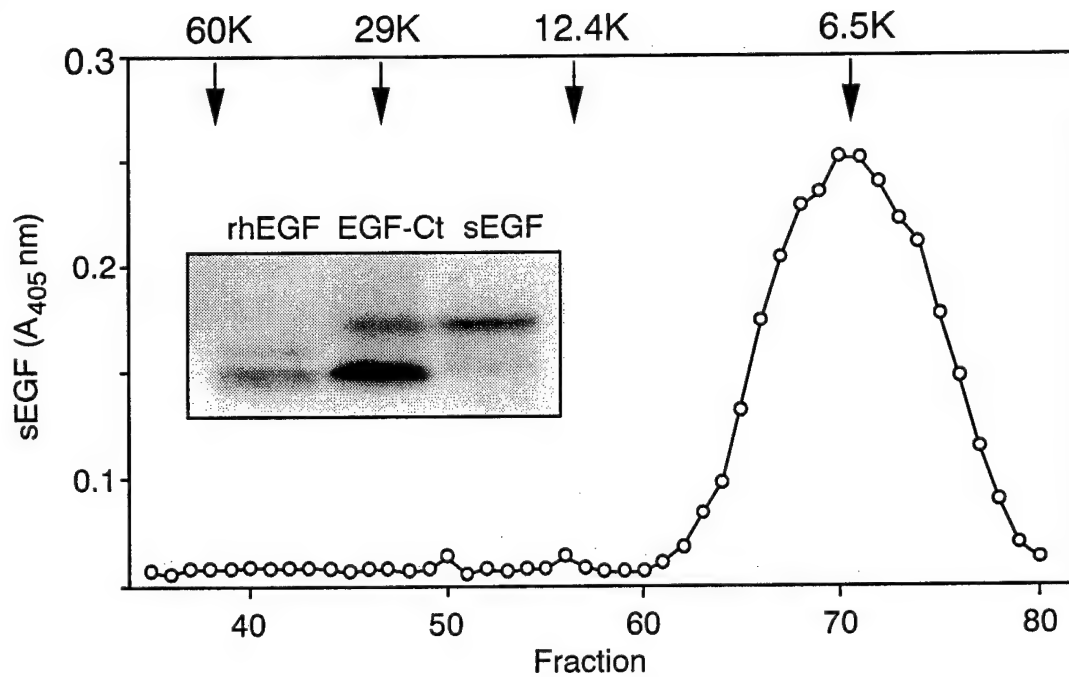
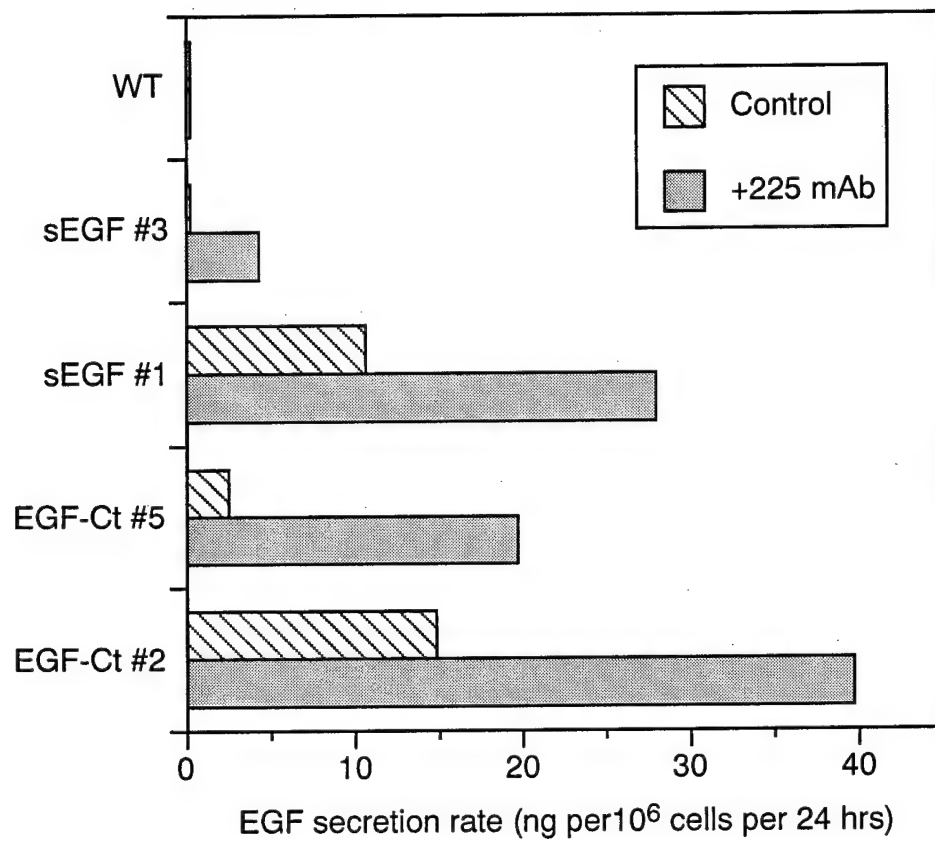
**A****B**

Figure 35

A



B

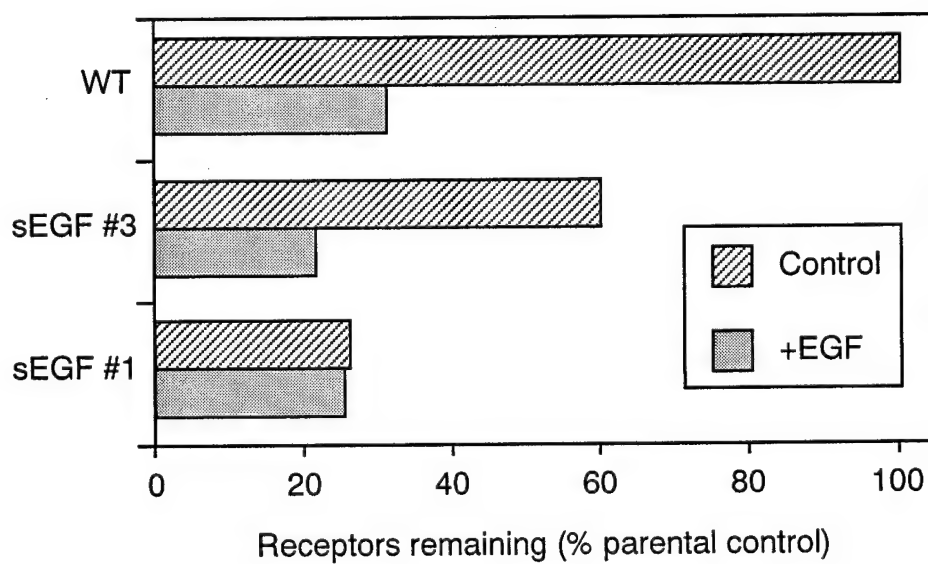


Figure 36

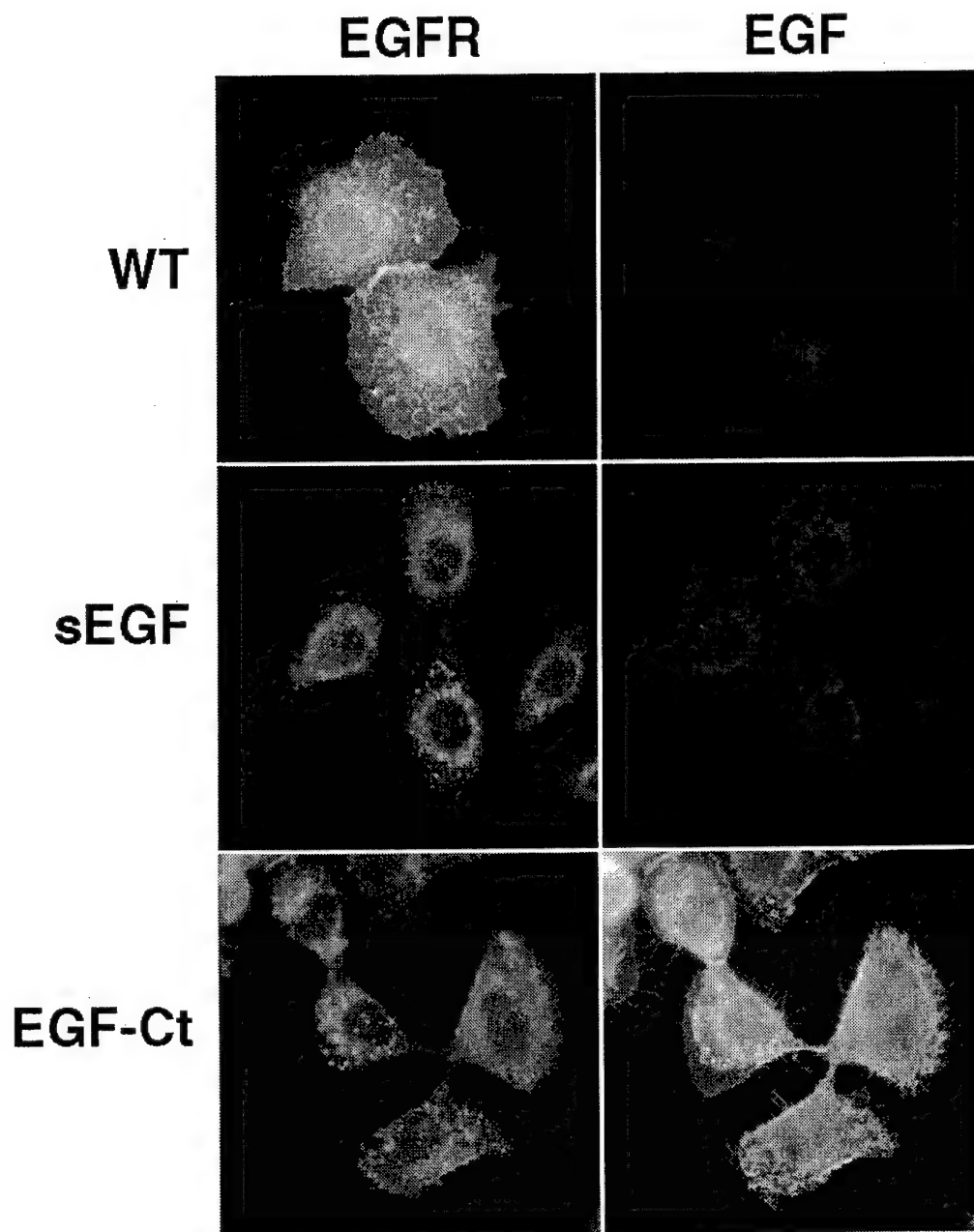




Figure 37

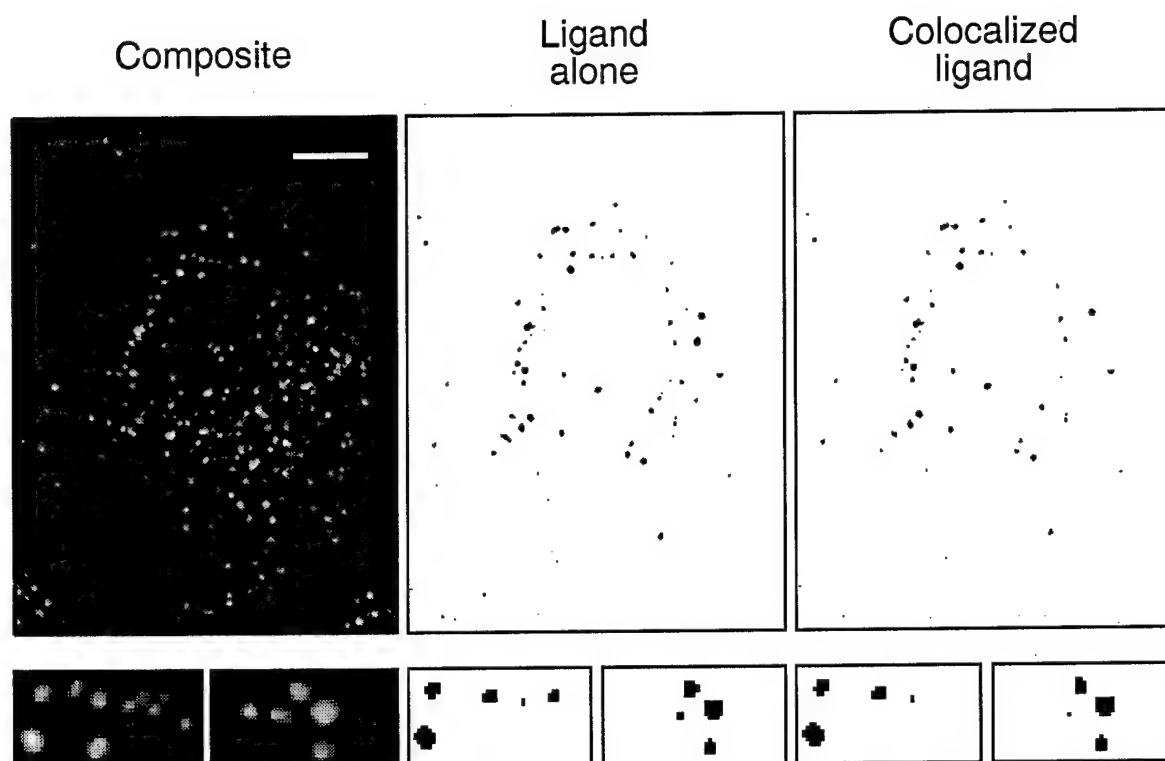


Figure 38

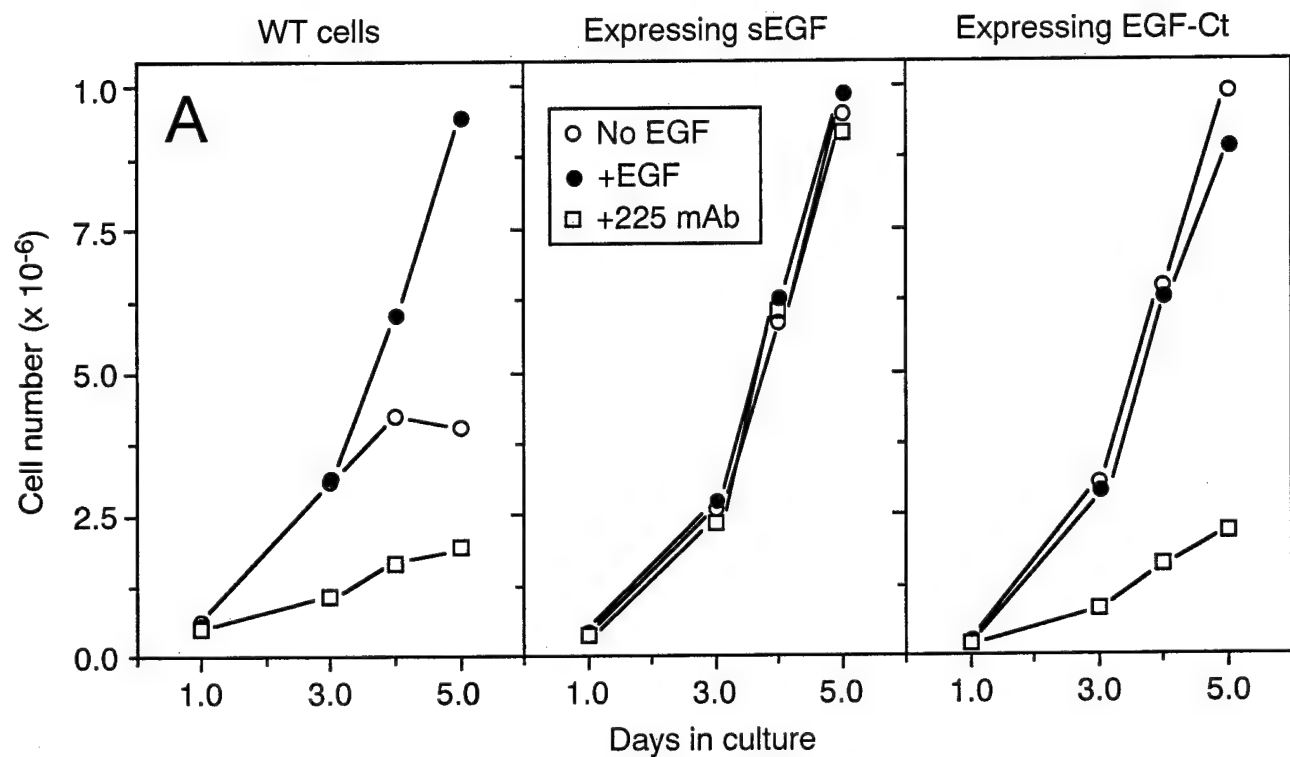
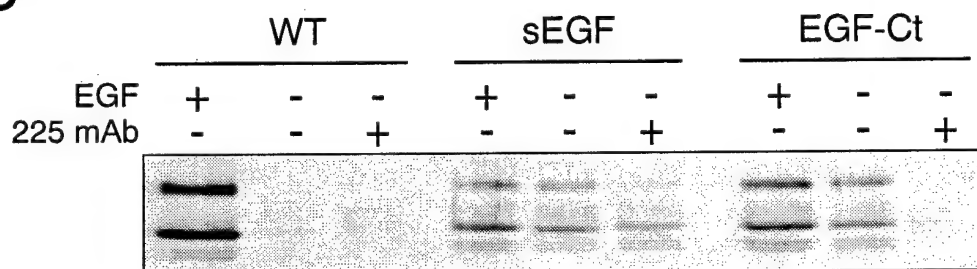
**B**

Figure 39

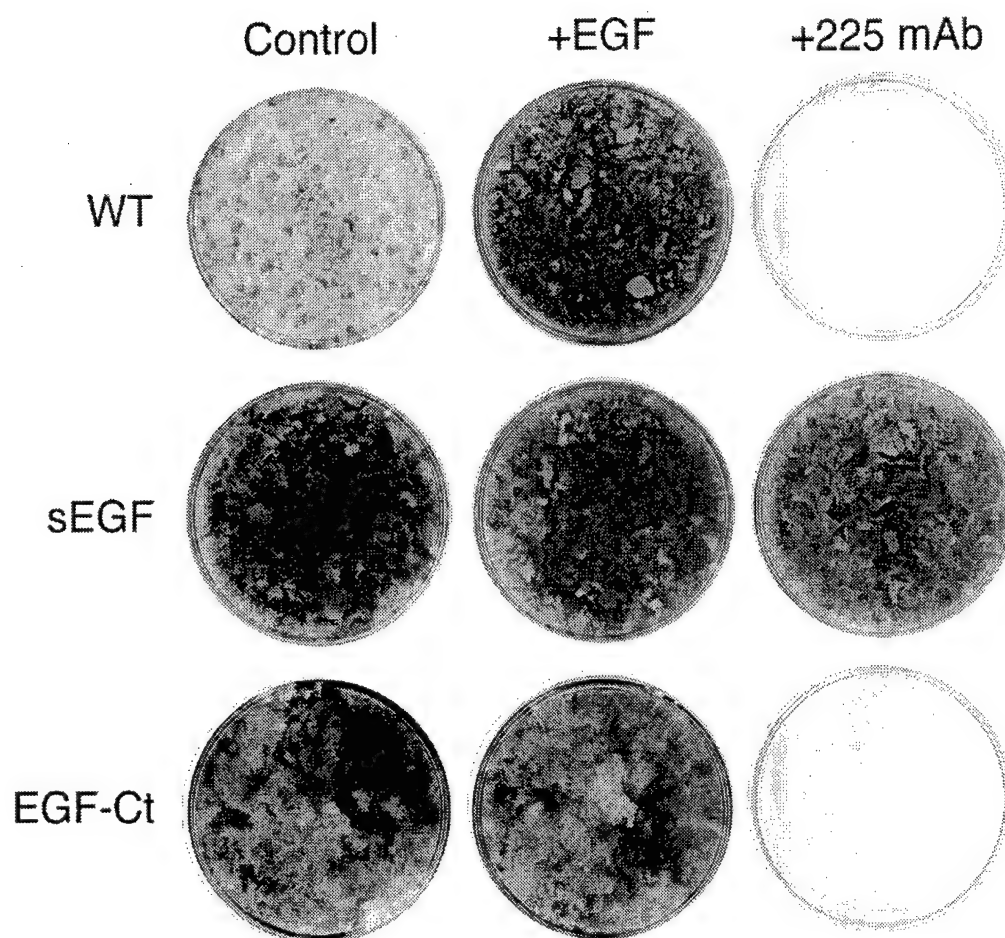


Figure 40

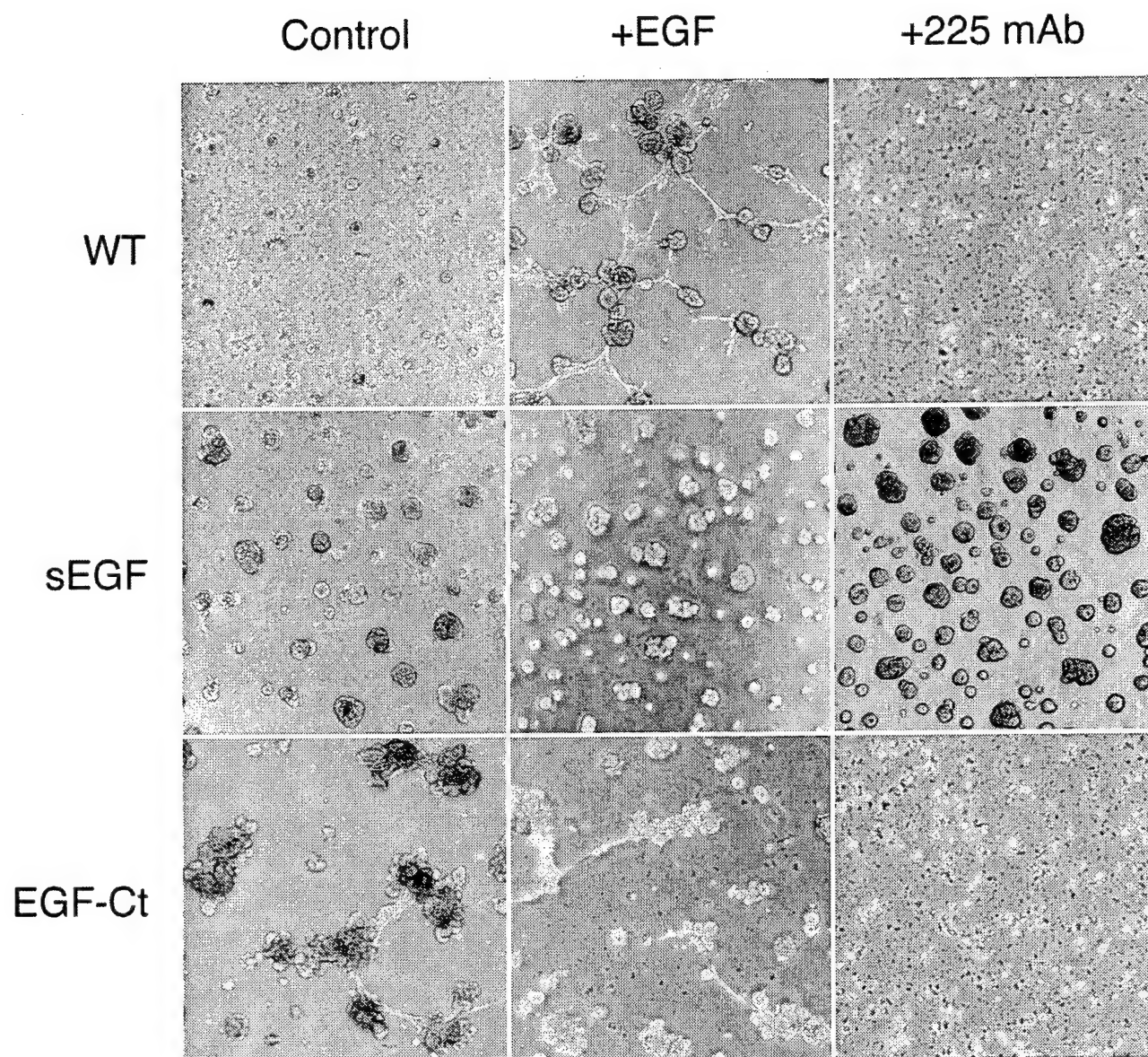


Figure 41

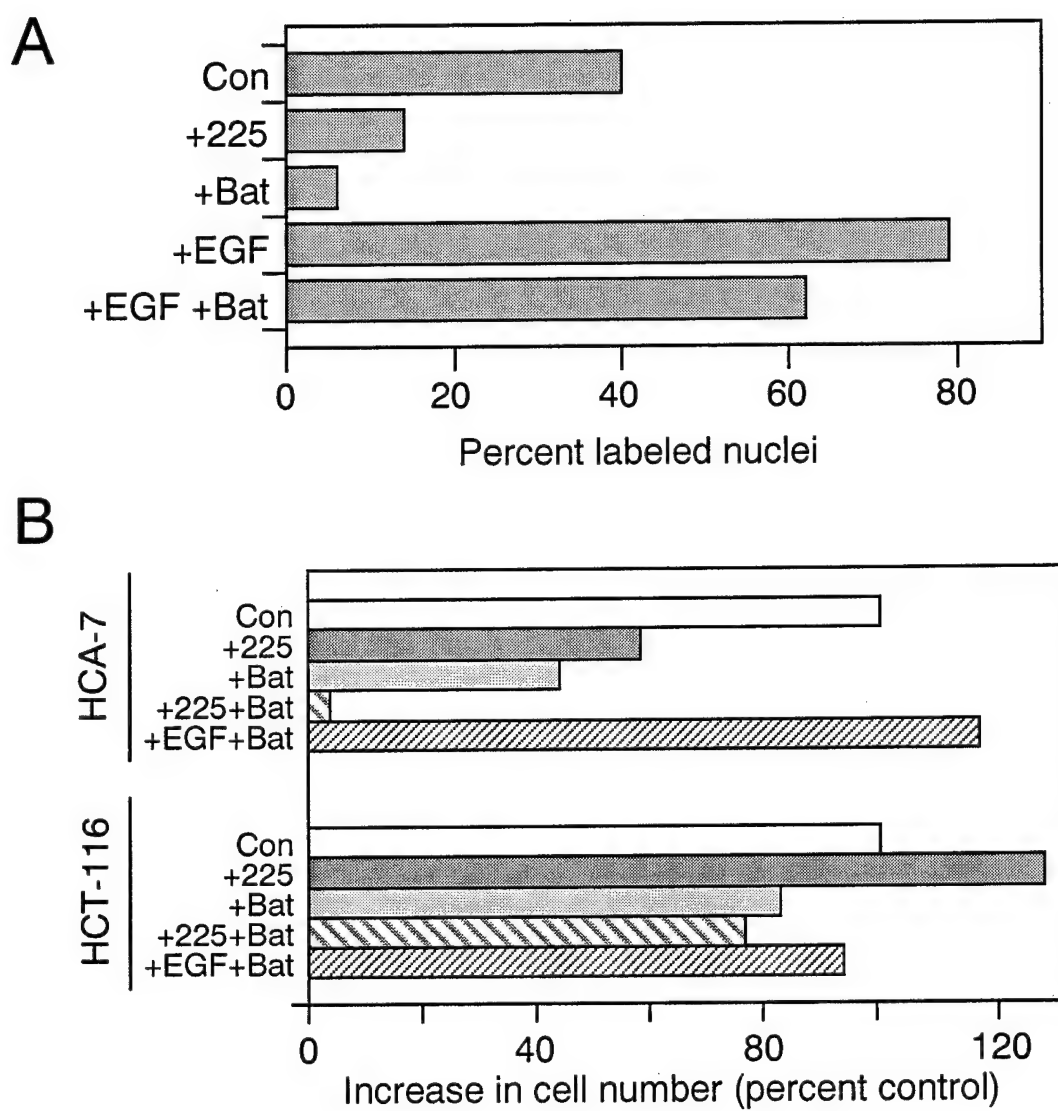


Figure 42

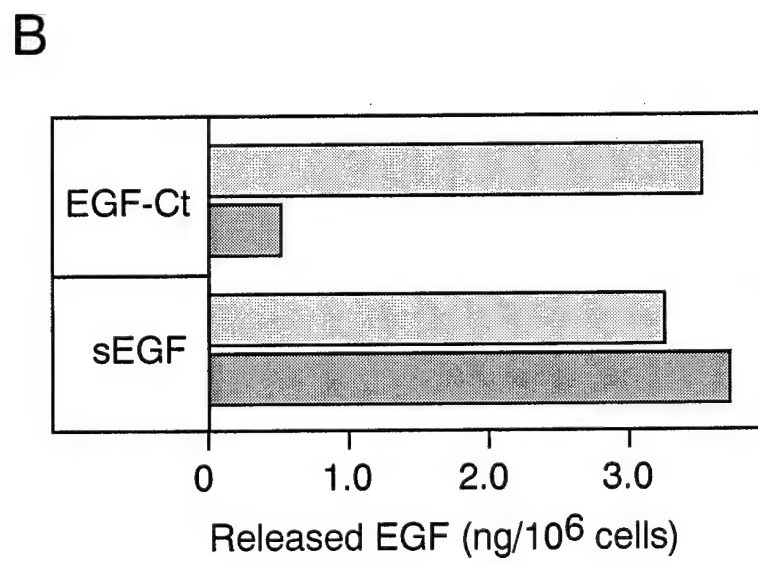
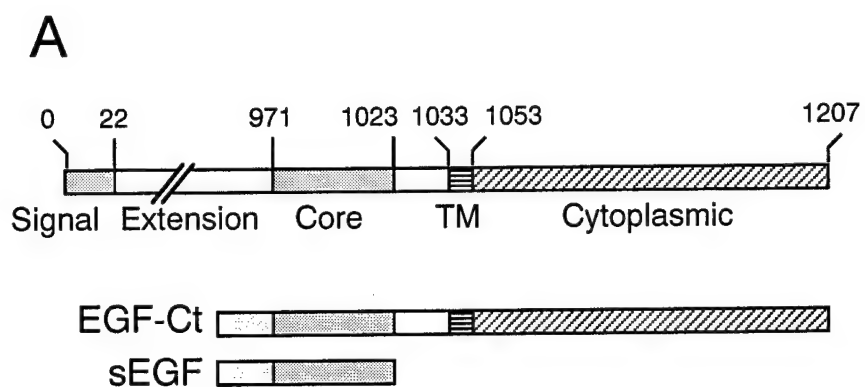




Figure 43

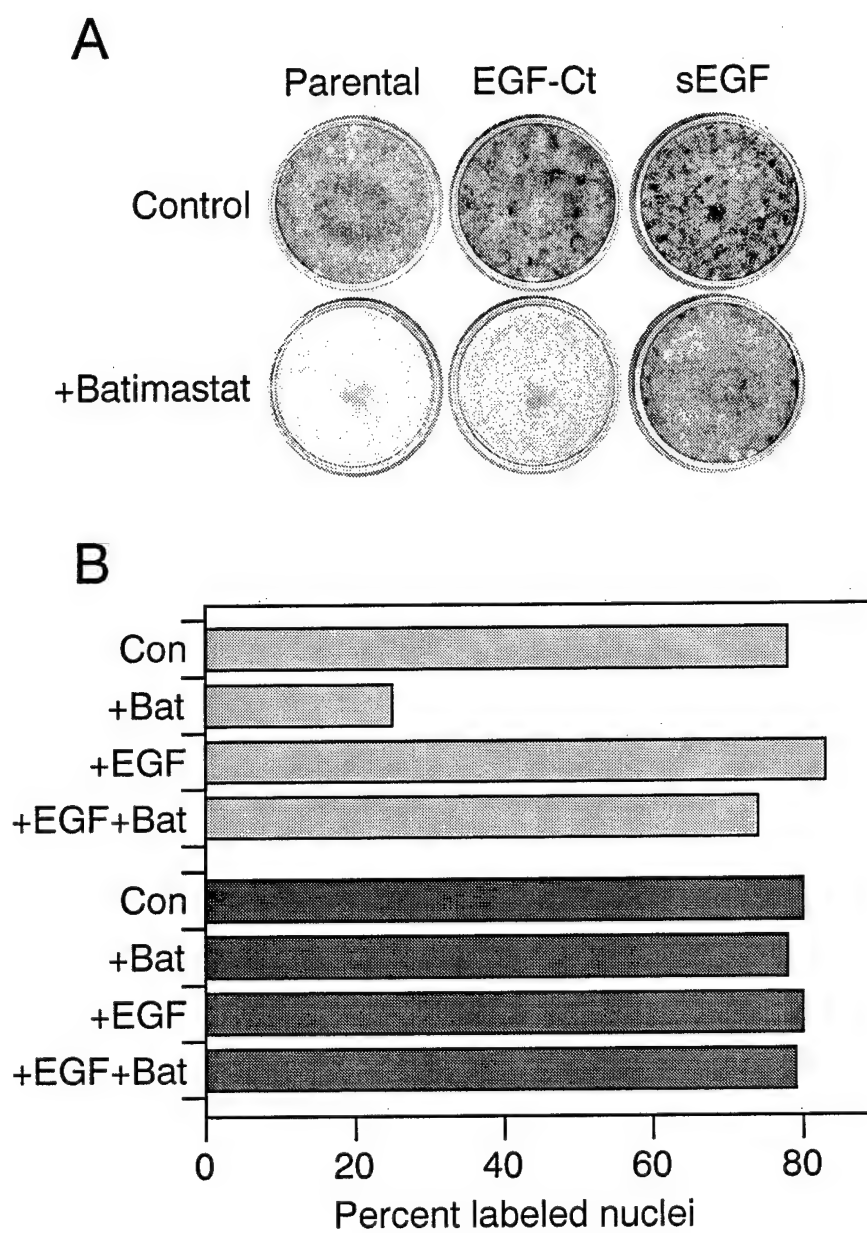


Figure 44

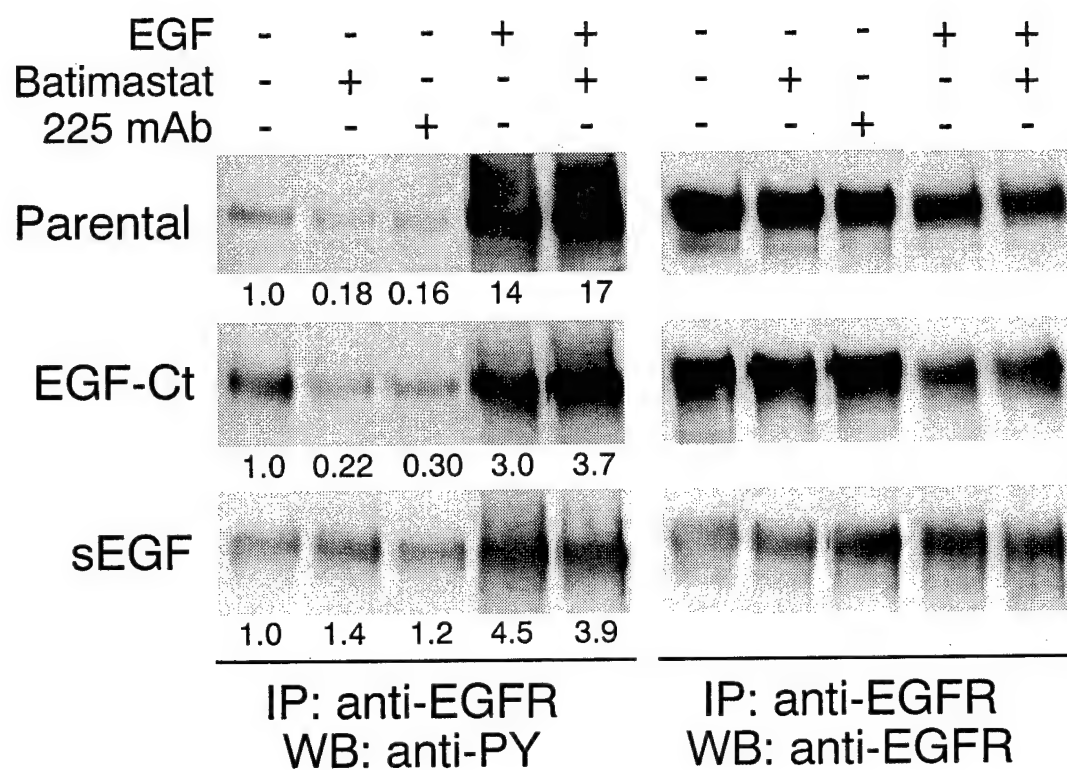


Figure 45

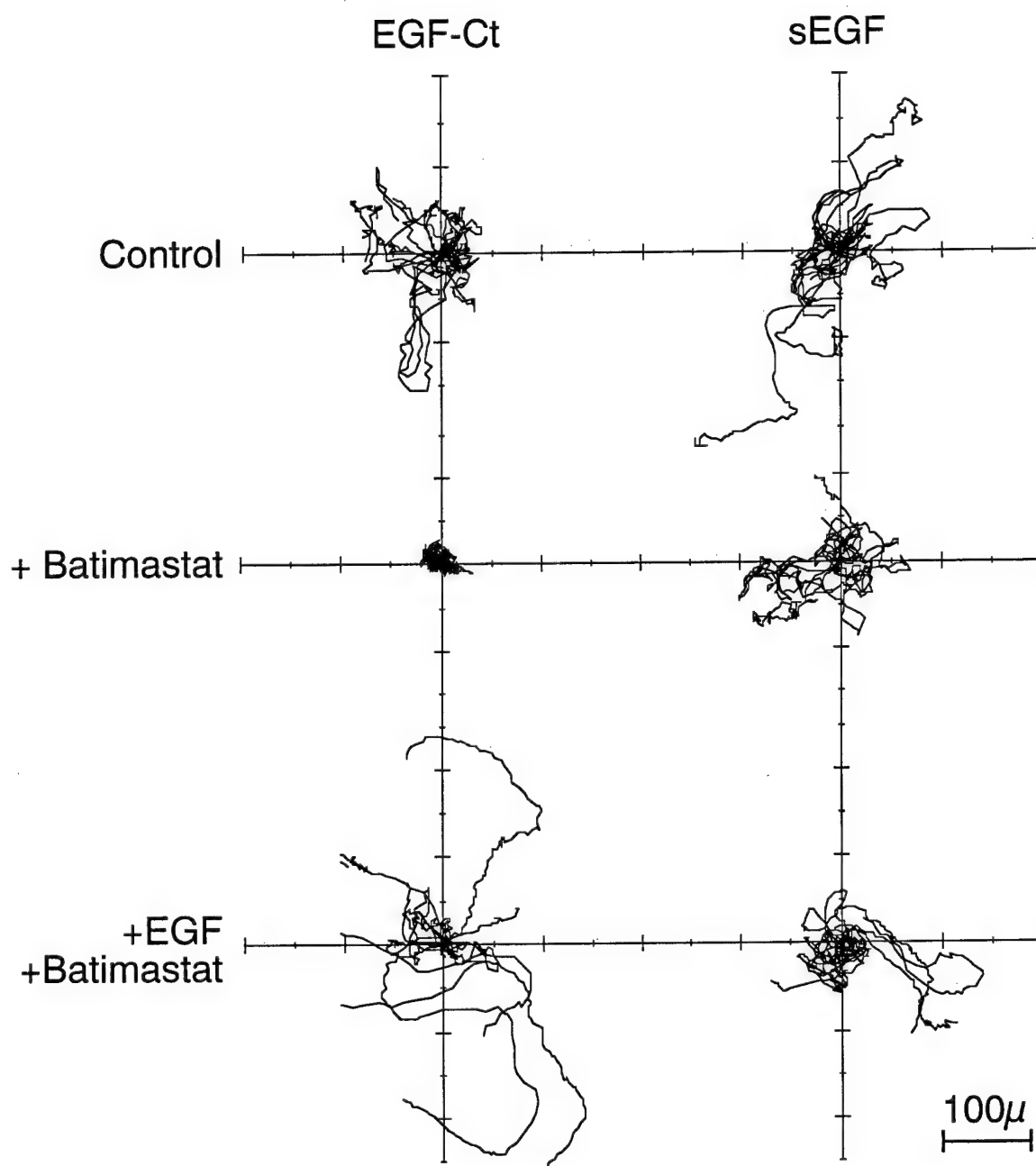


Figure 46

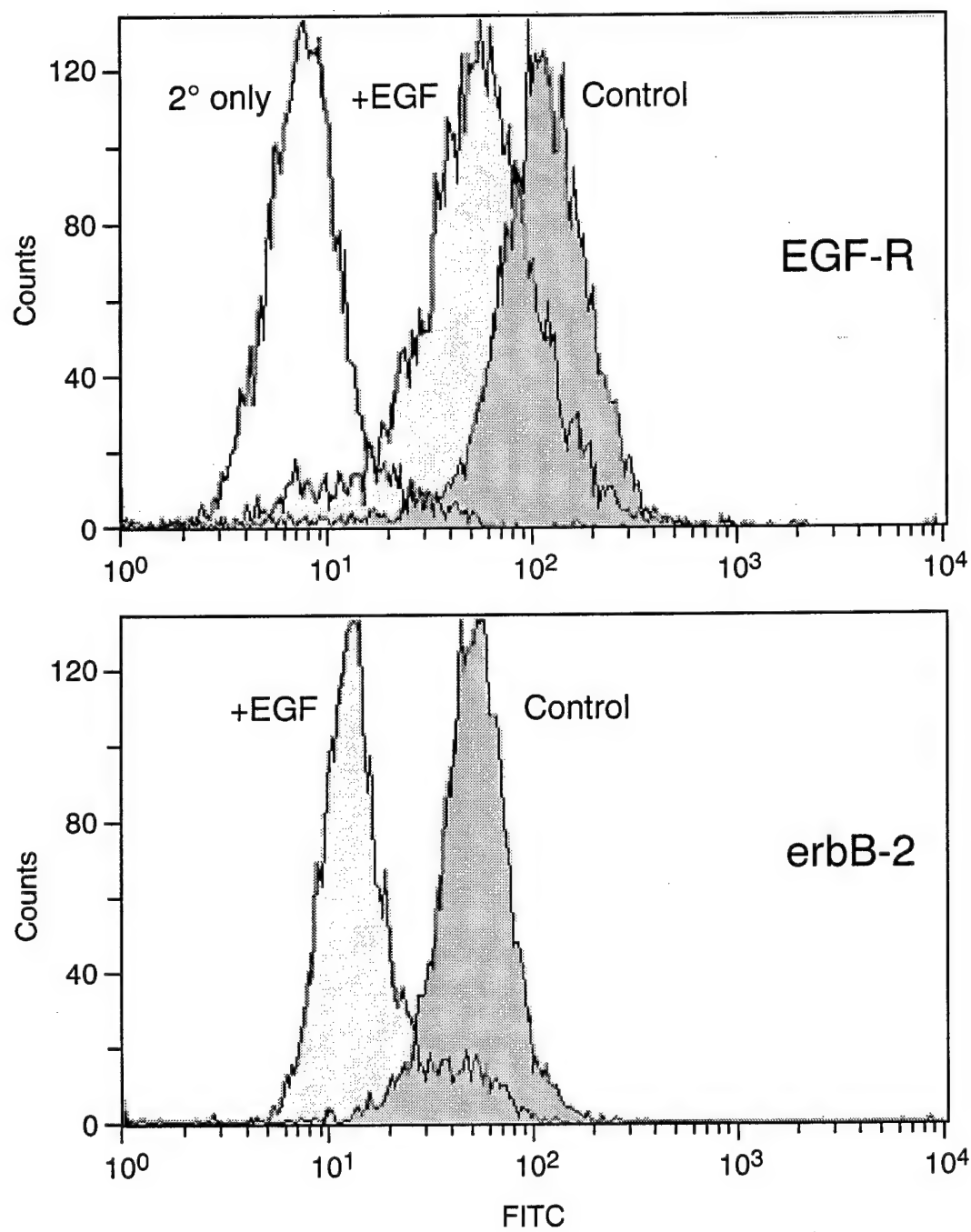


Figure 47

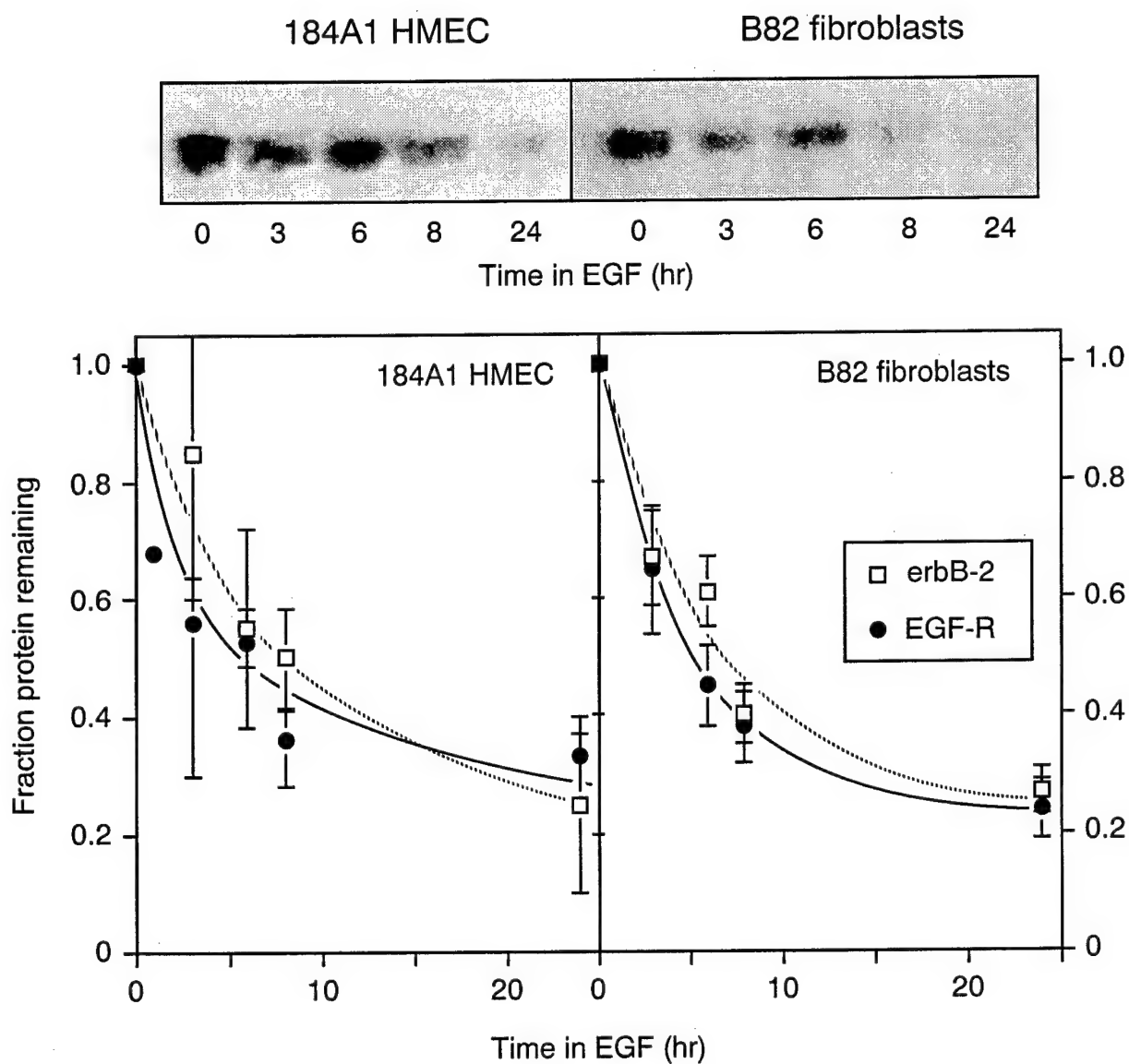


Figure 48

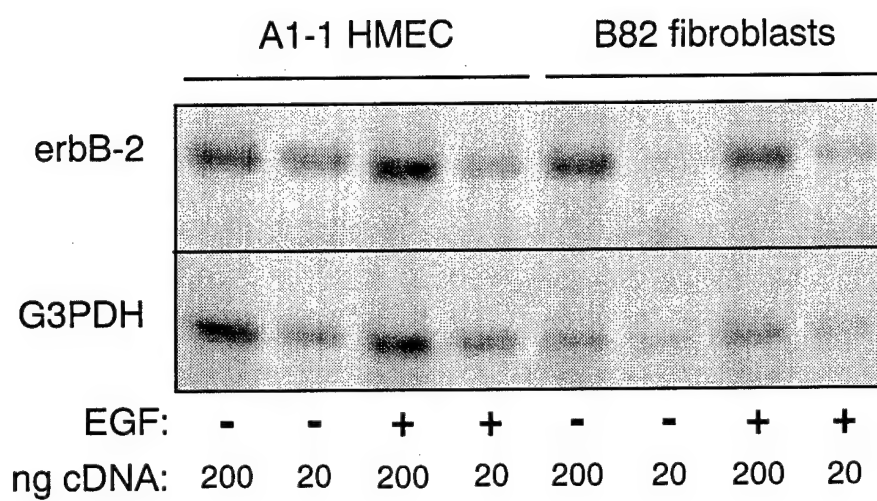




Figure 49

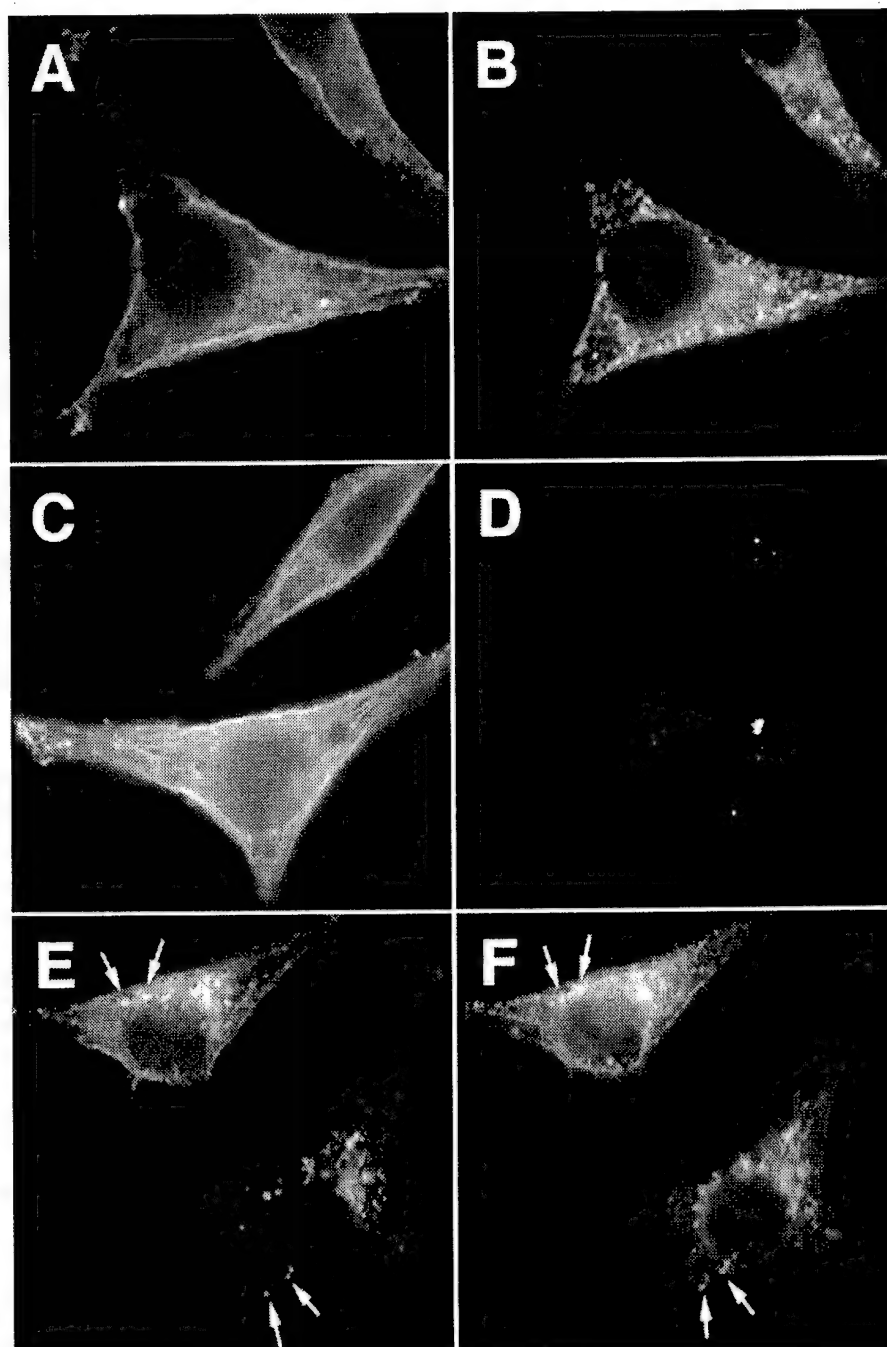


Figure 50

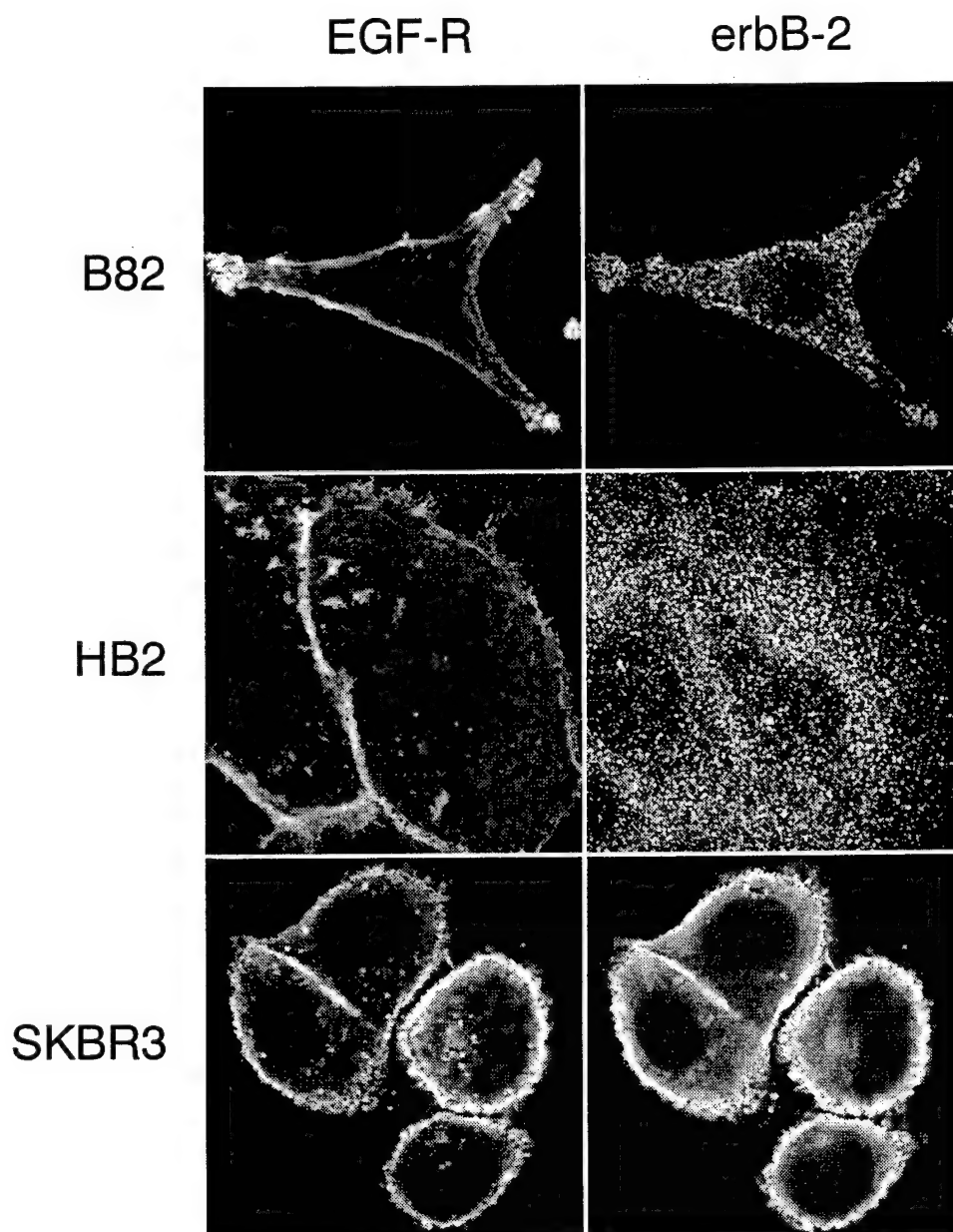


Figure 51

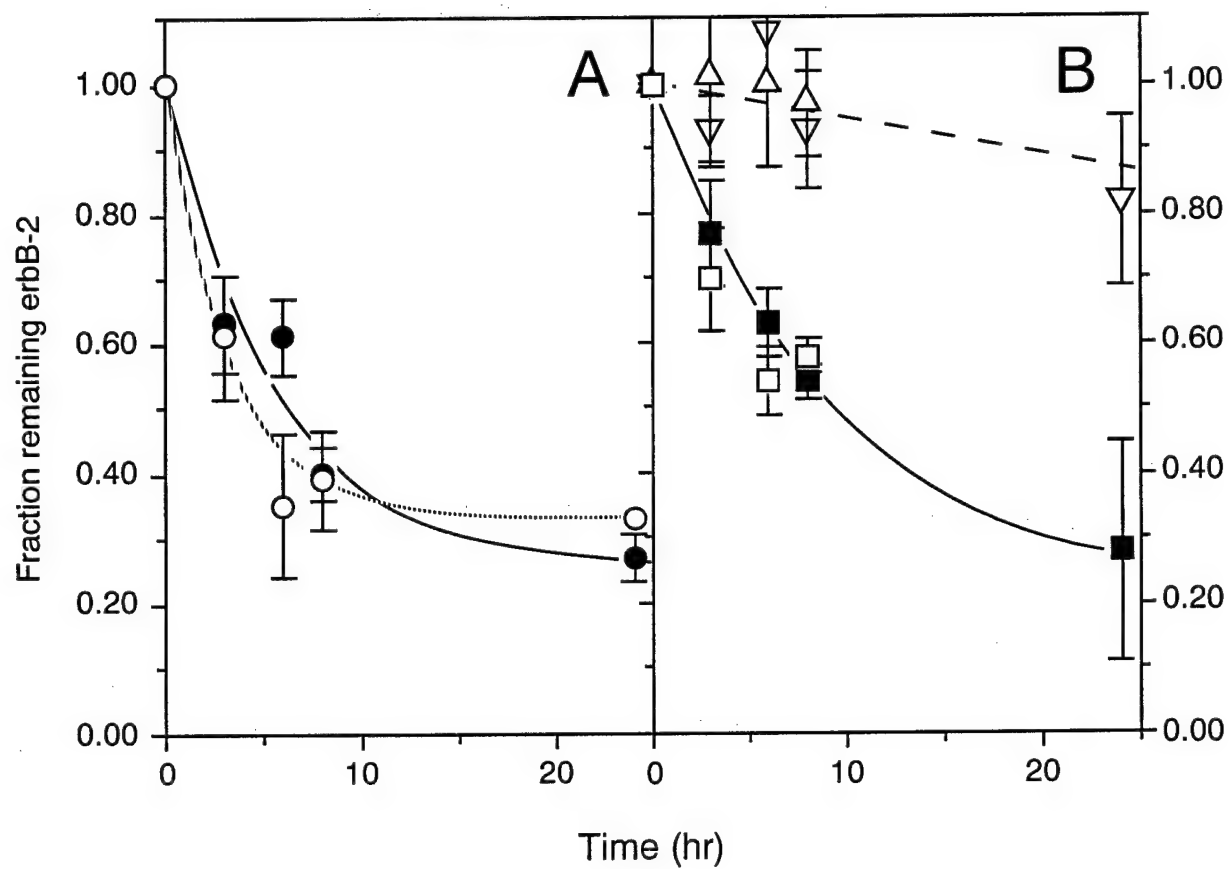


Figure 52

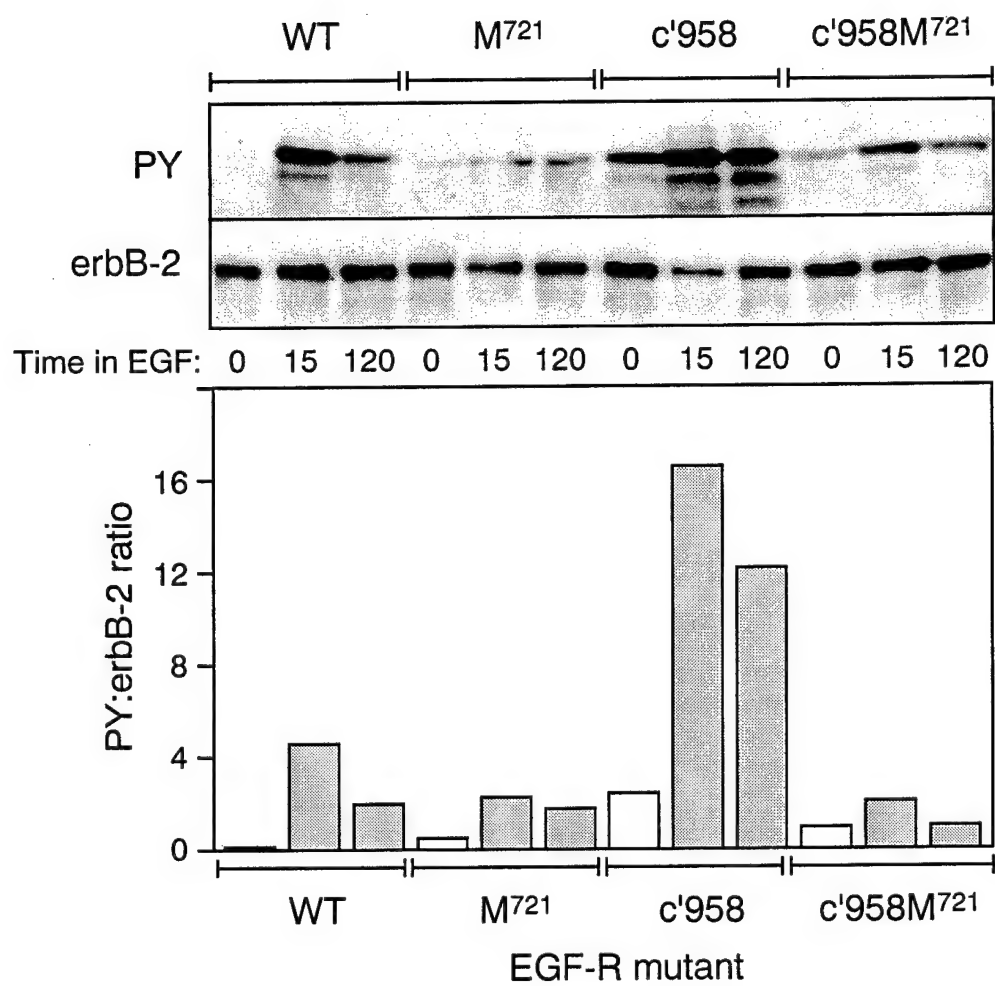


Figure 53

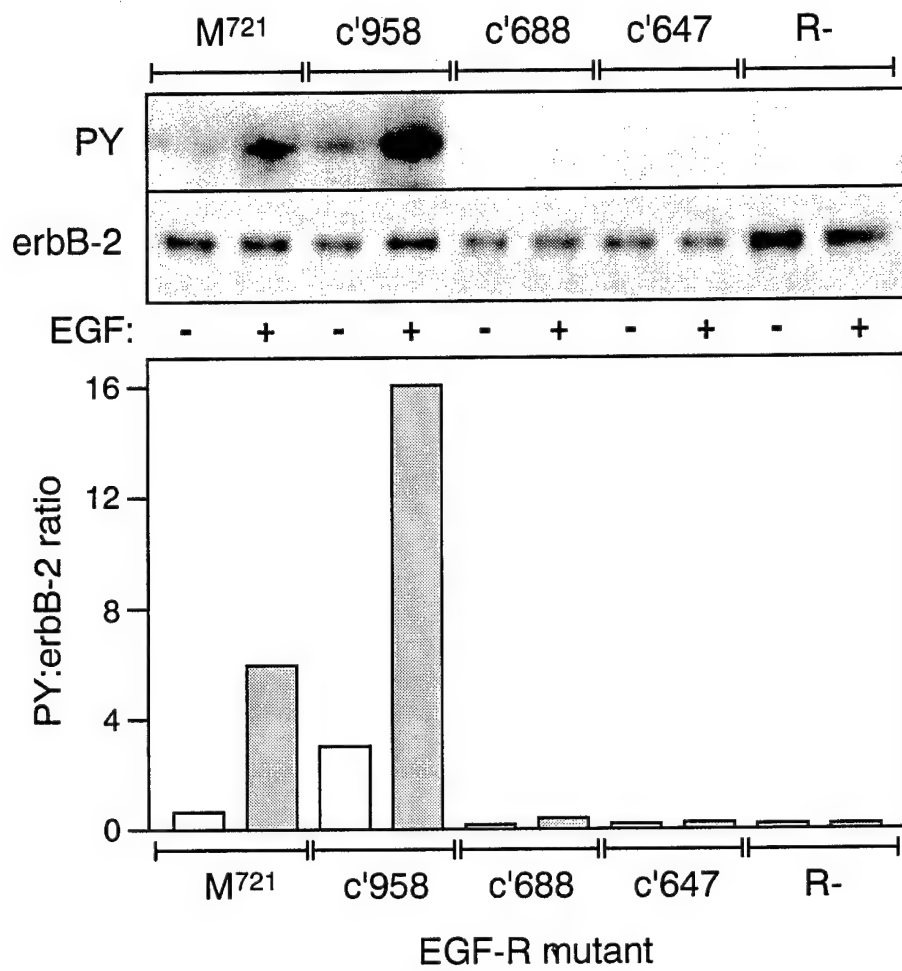


Figure 54

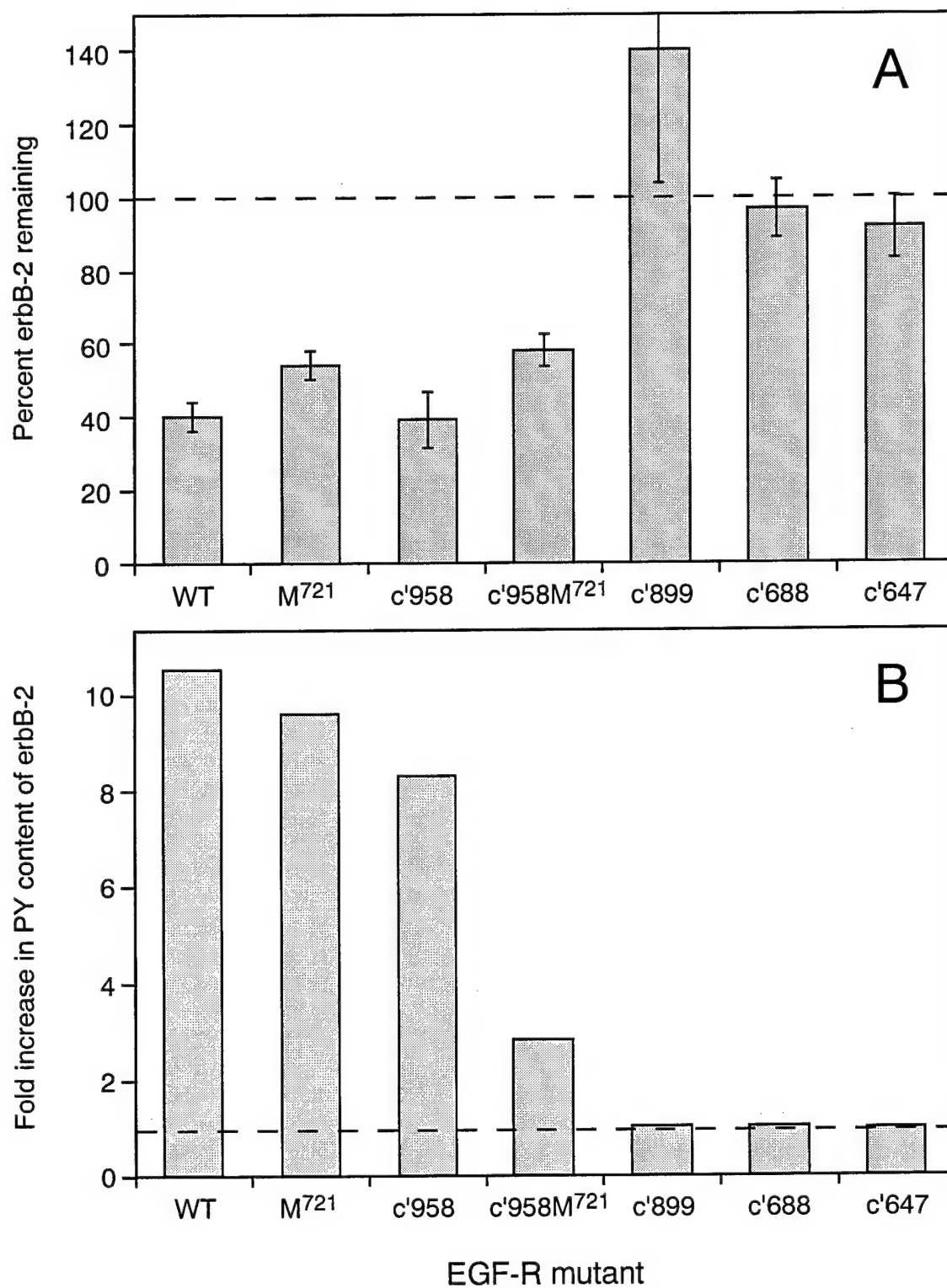
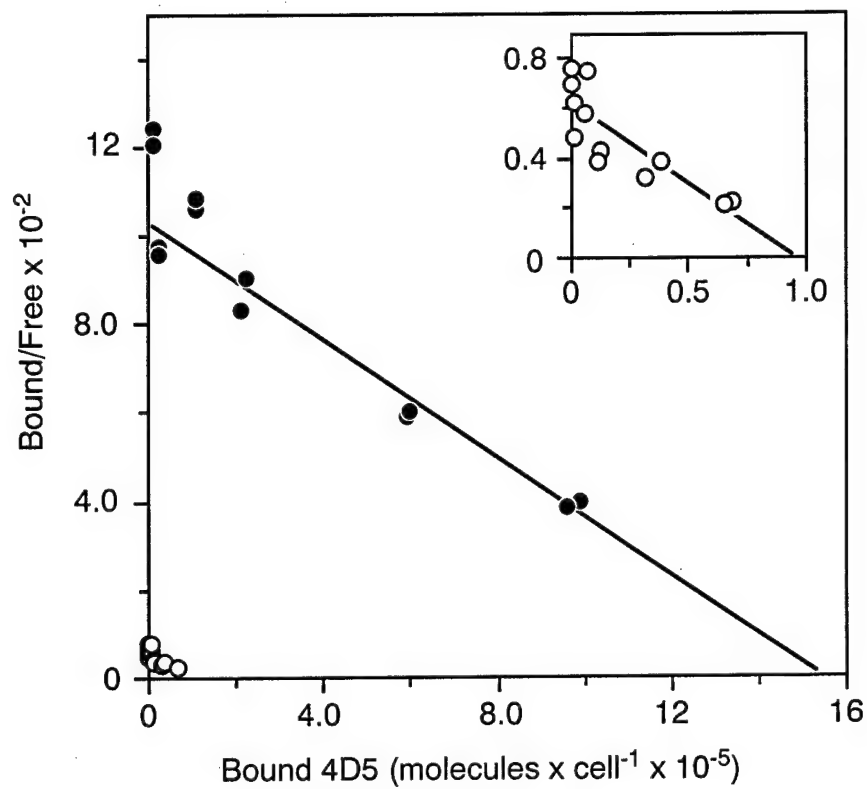




Figure 55

A



B

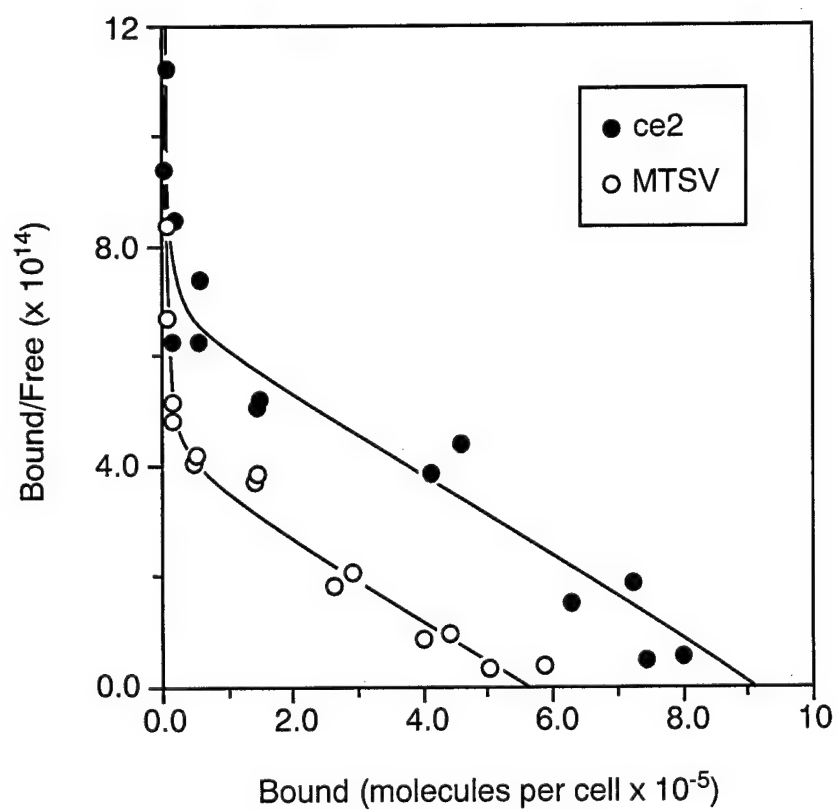


Figure 56

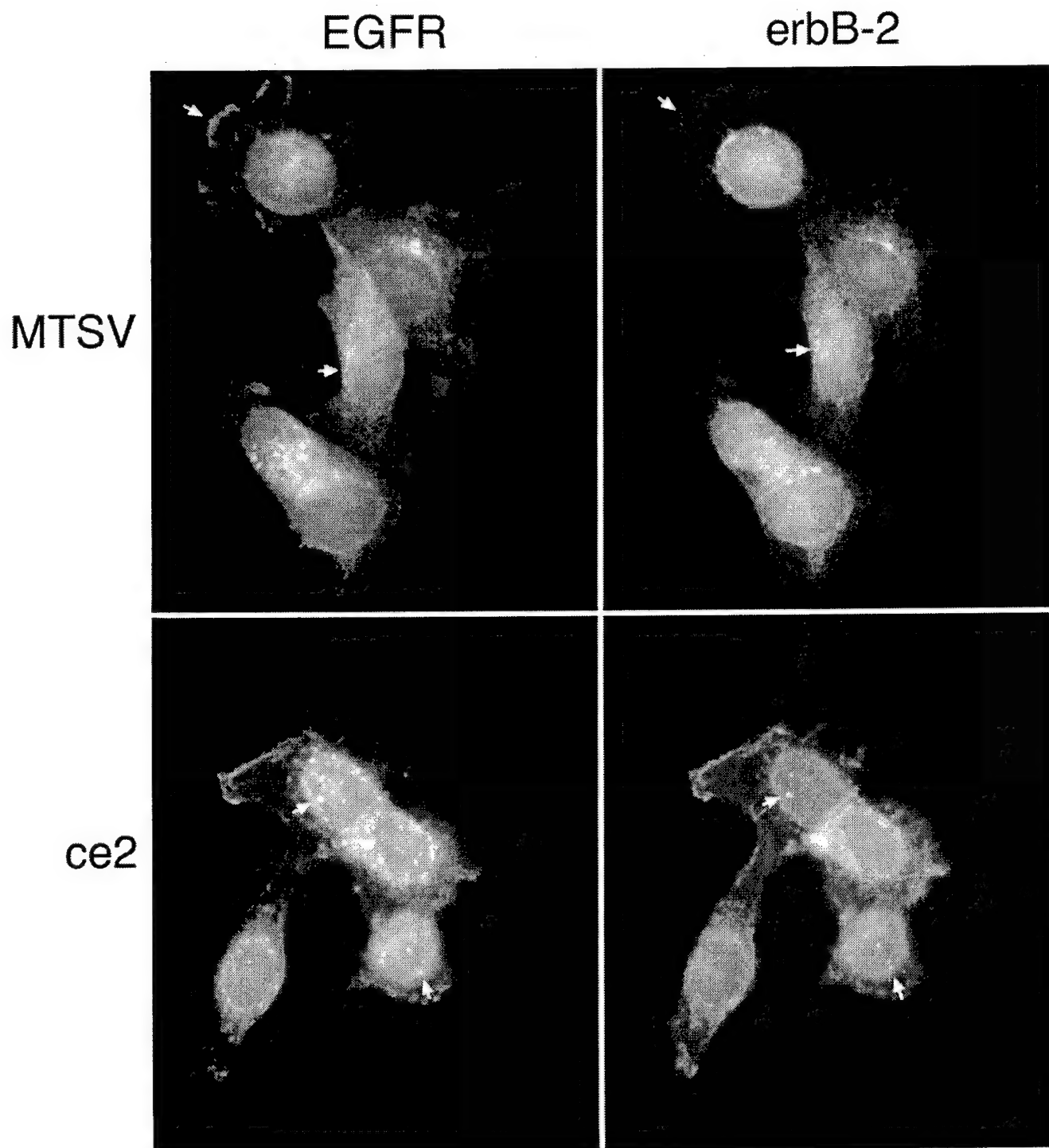


Figure 57

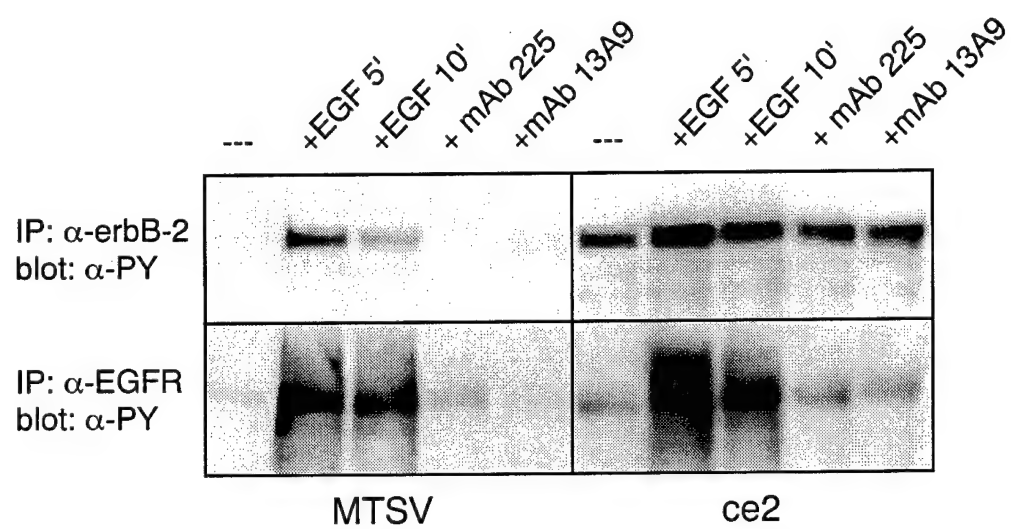


Figure 58

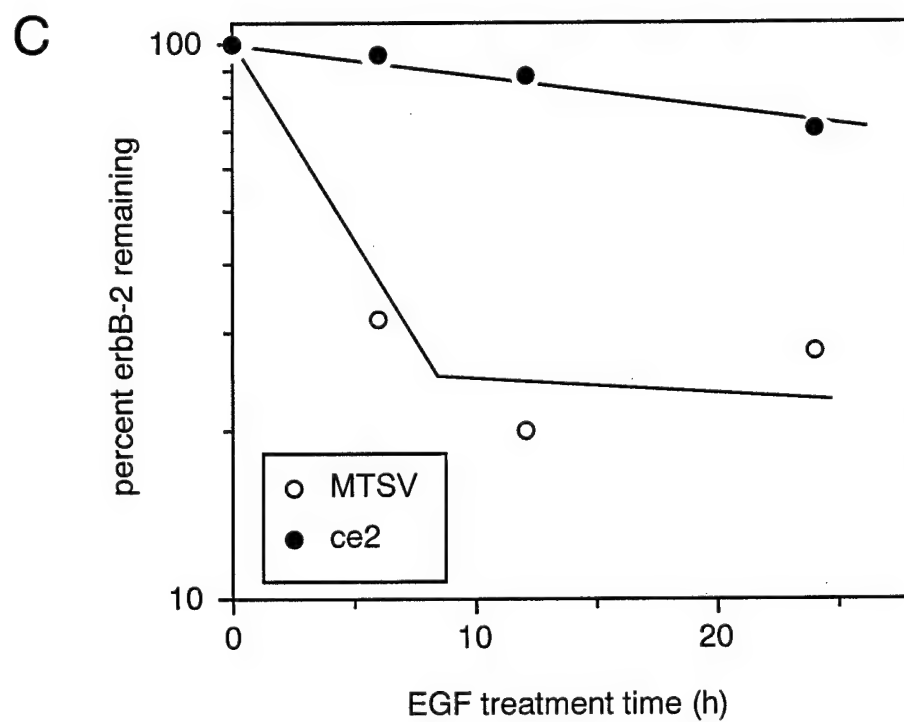
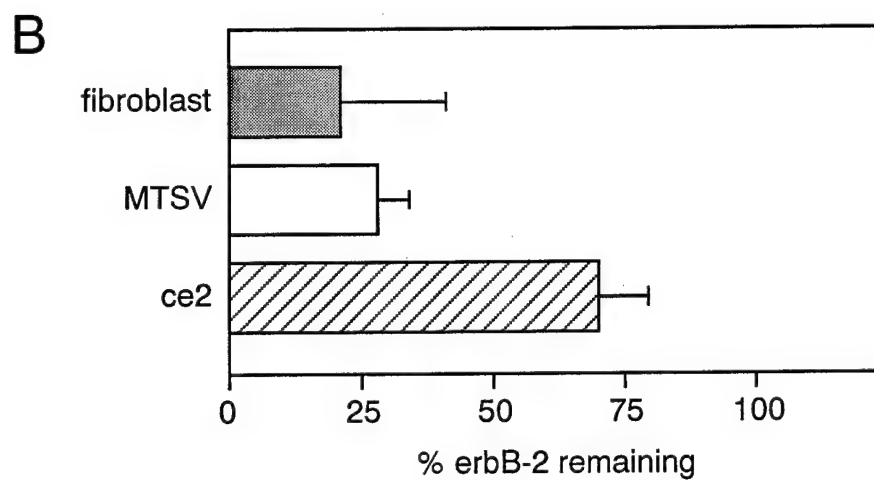
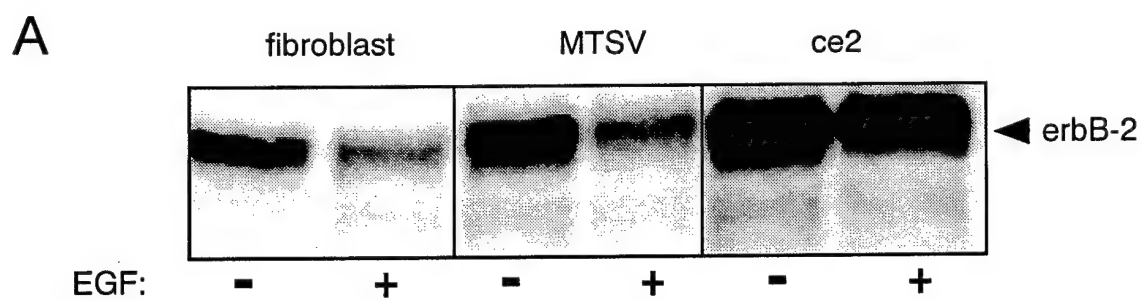


Figure 59

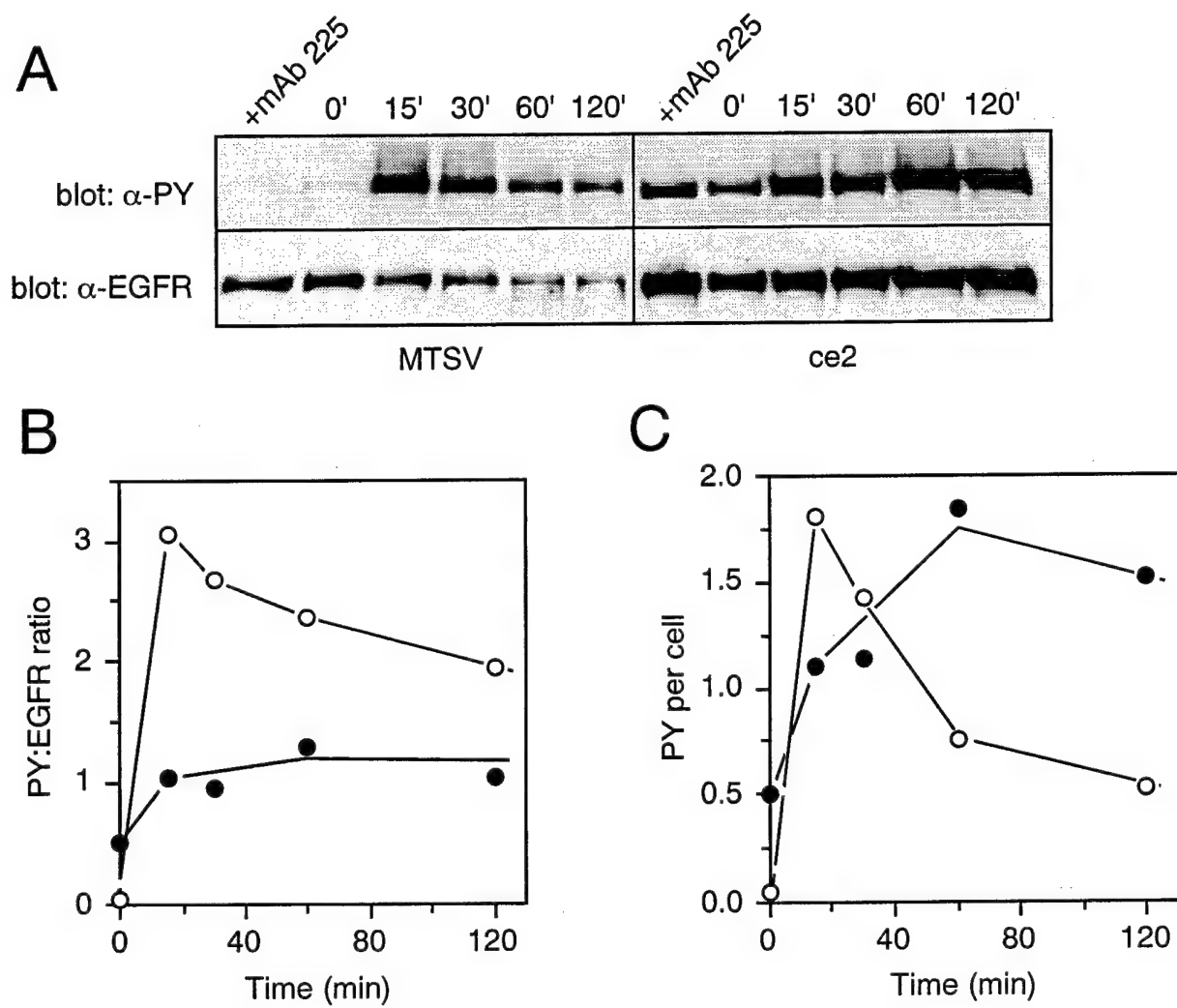


Figure 60

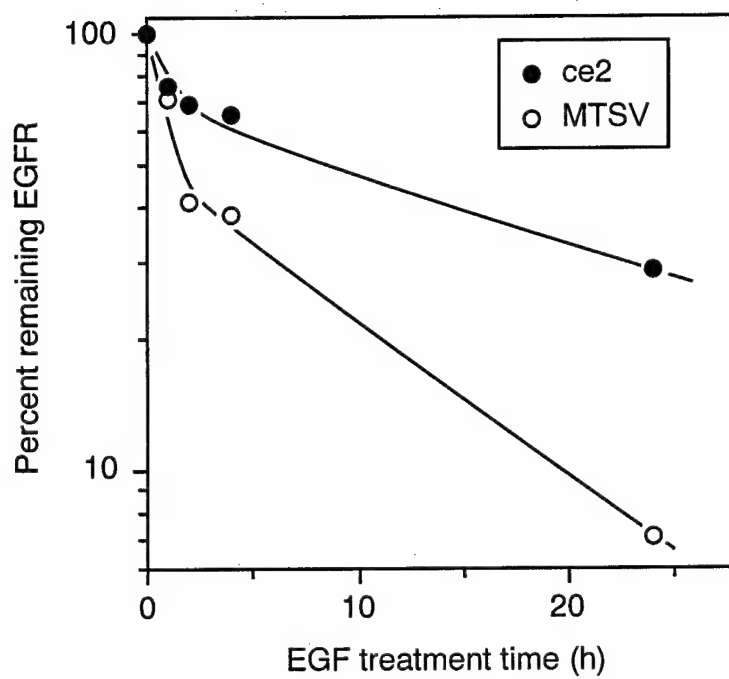




Figure 61

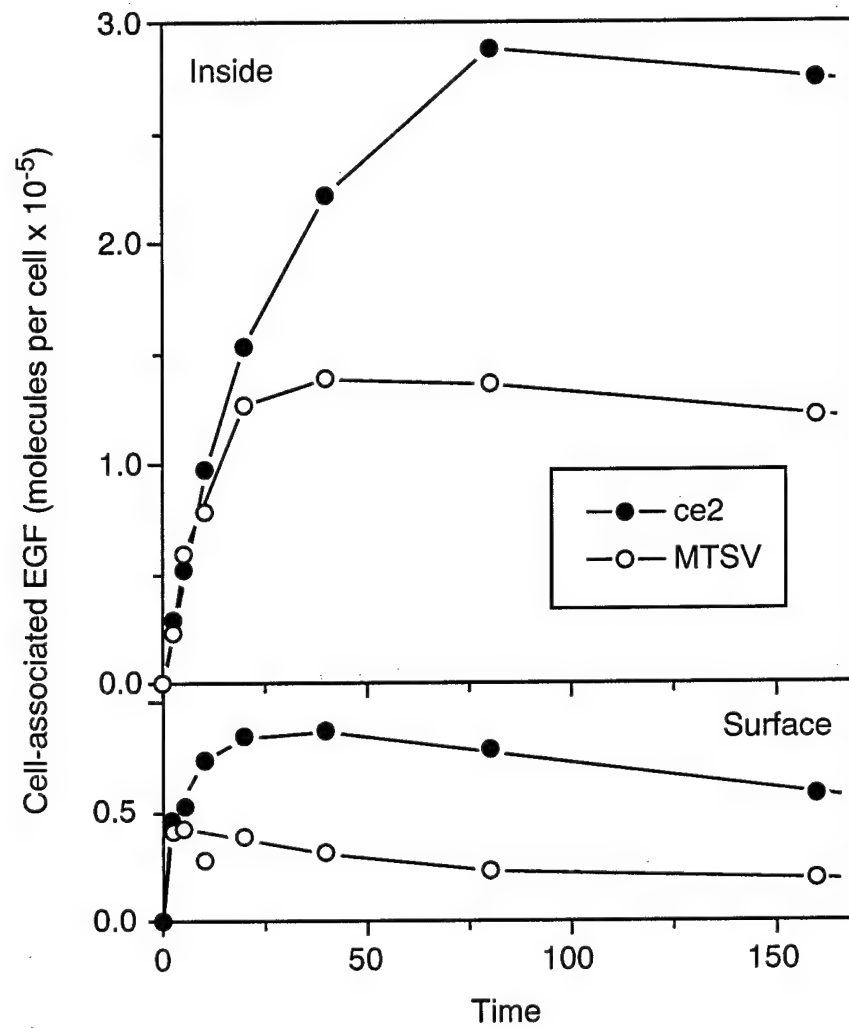


Figure 62

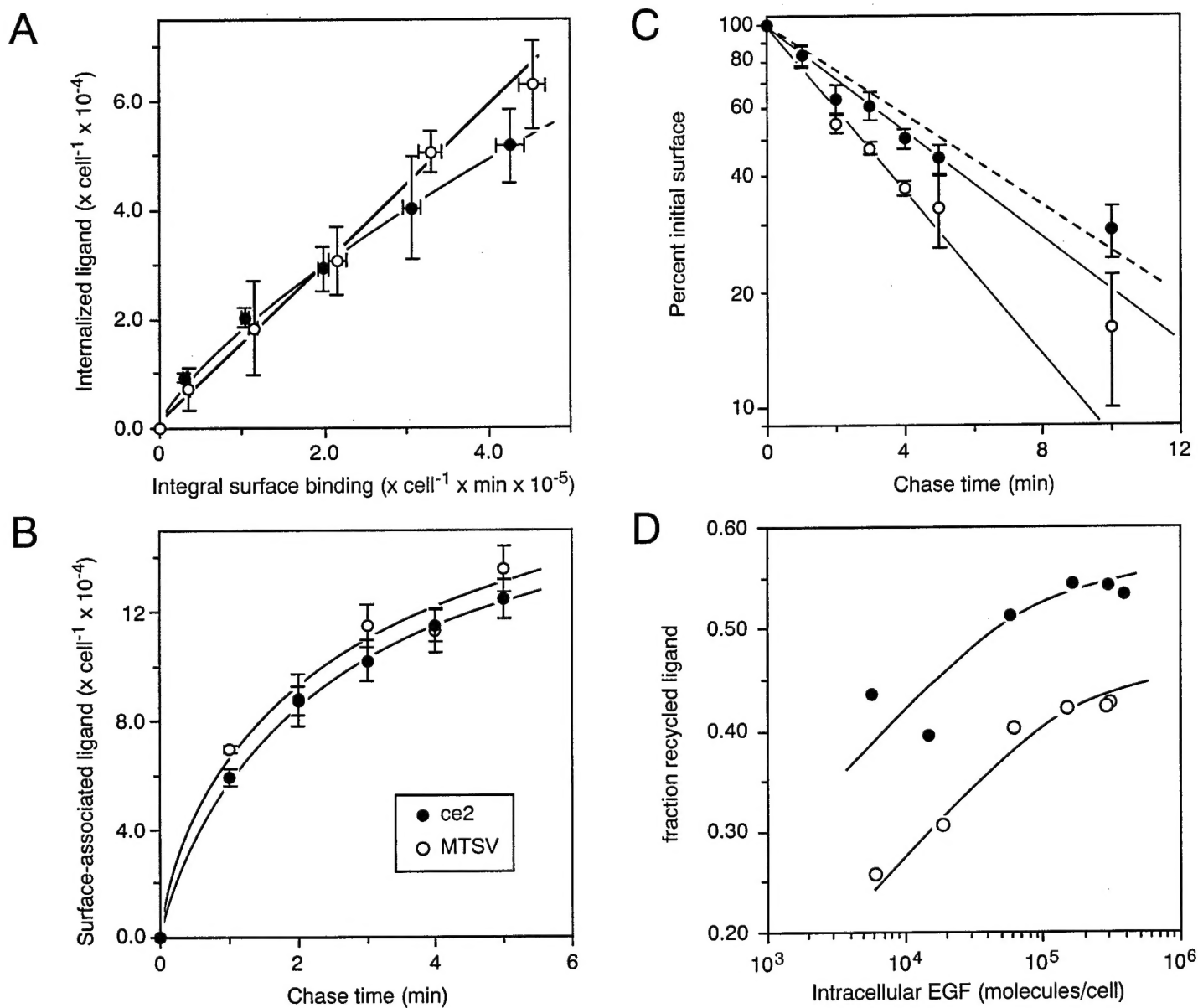
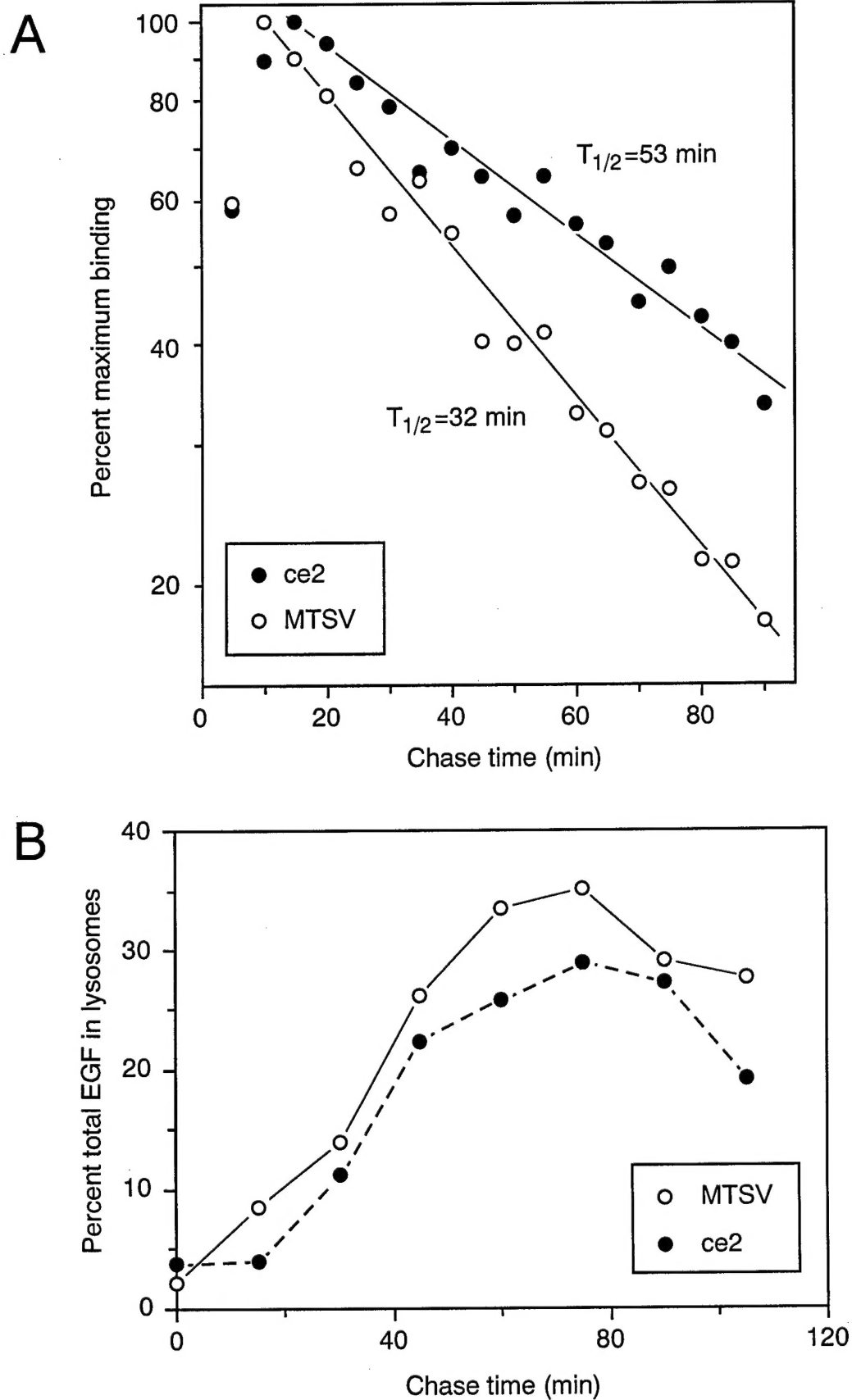


Figure 63



### **Publications resulting from this effort:**

- Opresko, L.K., Chang, C.P., Will, B.H., Burke, P.M., Gill, G.N., and Wiley, H.S. (1995) Endocytosis and lysosomal targeting of epidermal growth factor receptors are mediated by distinct sequences independent of the tyrosine kinase domain. *J. Biol. Chem.* **270**, 4325-4333.
- Nesterov, A., Wiley, H.S., and Gill, G.N. (1995) Ligand-induced endocytosis of epidermal growth factor receptors that are defective in binding adaptor proteins. *Proc. Natl. Acad. Sci. USA* **92**, 8719-8723.
- Huang, H.J.S., Nagane, M., Klingbeil, C., Lin, H., Nishikawa, R., Ji, X.D., Huang, C.M., Gill, G.N., Wiley, H.S., and Cavenee, W.K. (1997) The enhanced tumorigenic activity of a mutant epidermal growth factor receptor common in human cancers is mediated by threshold levels of constitutive tyrosine phosphorylation and unattenuated signalling. *J. Biol. Chem.* **272**, 2927-2935.
- Worthylake, R., and Wiley, H.S. (1997) Structural aspects of the epidermal growth factor receptor required for transmodulation of erbB-2/neu. *J. Biol. Chem.* **272**, 8594-8601.
- Wiley, H.S., Woolfe, M.F., Opresko, L.K., Burke, P.M., Will, B.H., Morgan, J.A., and Lauffenburger, D.A. (1998) Removal of the membrane-anchoring domain of EGF leads to intracrine signaling and disruption of mammary epithelial cell organization. *J. Cell Biol.* **143**, 1317-1328.
- Kuwada, S.K., Lund, K.A., Li, X.F., Cliften, P., Amsler, K., Opresko, L.K. and Wiley, H.S. (1998) Differential signaling and regulation of apical versus basolateral EGF receptors in polarized epithelial cells. *Am. J. Physiol.* **275**, C1419-1428.

### **Abstracts**

- Kuwada, S.K., Damstrup, L., Coffey, R.J., and Wiley, H.S. (1995) Epidermal Growth Factor receptor-mediated proliferation and binding affinity is strongly influenced by cell polarity in colonic epithelium. *In Mol. Biol. Cell* **6**, 9a
- Burke, P.M., Opresko, L.K., and Wiley, H.S. (1995) Epidermal growth factor receptor physiology in human mammary epithelial cells *in vitro*. *In Mol. Biol. Cell* **6**, 10a
- Opresko, L.K., Burke, P.M., and Wiley, H.S. (1995) Differential effect of EGF on mammary epithelial cells grown on various extracellular matrices. *In Mol. Biol. Cell* **56**, 47a
- Worthylake, B., and Wiley, H.S. (1995) Transmodulation of HER2 levels by HER1 activation. *In Mol. Biol. Cell* **6**, 237a
- Burke, P.M. and Wiley, H.S. (1996) Rapid internalization of EGF receptors is uncoupled from down-regulation in human mammary epithelial cells. *In Mol. Biol. Cell* **7**, 19a

- Worthylake, B. and Wiley, H.S. (1996) The role of the EGF receptor and HER2 trafficking in mammary epithelial cells. *In Mol. Biol. Cell* 7, 19a
- Dong, J., Will, B.H., and Wiley, H.S. (1996) Synthesis and processing of EGF/HB-EGF chimeras. *In Mol. Biol. Cell* 7, 20a
- Schooler, K.P., and Wiley, H.S. (1996) EGF receptor desensitization in breast cancer cell growth. *In Mol. Biol. Cell* 7, 20a
- Opresko, L.K. and Wiley, H.S. (1996) Oncogenic form of the EGF receptor displays altered biological activity in human mammary epithelial cells. *In Mol. Biol. Cell* 7, 25a
- Worthylake, R.A. and Wiley, H.S. (1997) Overexpression of the HER2/neu receptor tyrosine kinase inhibits its downregulation.
- Schooler, K.P. and Wiley, H.S. (1997) EGF-R amplification correlates with prolonged signaling duration, decreased rate of down regulation and increased tumorigenic potential. *In Mol. Biol. Cell* 8, 356a
- Dong, J. and Wiley, H.S. (1997) Processing of EGF and EGF/HB-EGF chimeric ligands in autocrine cells. *In Mol. Biol. Cell* 8, 356a
- Burke, P.M., Oehrtman, G.T. and Wiley, H.S. (1997) Constitutive endocytosis and efficient recycling of the EGF receptor in human mammary epithelial cells. *In Mol. Biol. Cell* 8, 357a
- Wiley, H.S., Woolfe, M.F. and Lauffenburger, D.A. (1997) Autocrine signaling as 'cell sonar'. *In Mol. Biol. Cell* 8, 359a

**Personnel receiving pay from this effort:**

H. Steven Wiley  
 Lee K. Opresko  
 Margaret Woolfe  
 Virginia Hill